Circadian characterisation of the transcription factor *Zfhx3* utilising a conditional mutagenesis approach



A thesis submitted for the degree of Doctor of Philosophy by

Ashleigh Georgina Wilcox

Word count: 35,000 (approx.)

Linacre College, University of Oxford

Mammalian Genetics Unit, Medical Research Council, Harwell

Abstract

Previous work revealed an important role for the transcription factor ZFHX3 in circadian biology. A dominant missense mutation in the gene (*Zfhx3*^{Sci}) results in a short circadian period in constant conditions and altered sleep homeostasis. However, constitutive knock-outs of this gene are embryonic lethal, limiting experimental characterisation options. In this thesis, the role of *Zfhx3* in circadian rhythm regulation throughout the lifespan of the mouse is examined using conditional mutagenesis to produce *Zfhx3* null animals.

Inducible deletion of *Zfhx3* in adult mice was achieved using a ubiquitously expressed inducible Cre line. These mice displayed significant circadian disruption, namely an acute shortening of circadian period and/or loss of rhythmicity in constant conditions. Following on from this, using SCN-enriched Cre lines driven by *Six3* and *Foxd1*, *Zfhx3* was deleted specifically in developing SCN. These animals showed a variety of sleep and circadian phenotypes when assessed. Homozygous mutants of the *Six3*-Cre line cross displayed a dramatic circadian phenotype; complete behavioural arrhythmia in all lighting conditions and an inability to entrain to a light-dark cycle. Histological examination revealed that the SCN in these mutants fails to mature, as evidenced by loss of expression of key circadian neuropeptides in this region.

This work provides evidence for the sustained importance of *Zfhx3* in circadian pacemaker function and highlights the use of conditional mutagenesis as an invaluable tool for the study circadian transcription factors. The data presented also suggests that *Zfhx3* is crucial for development of the SCN in mice.

Acknowledgements

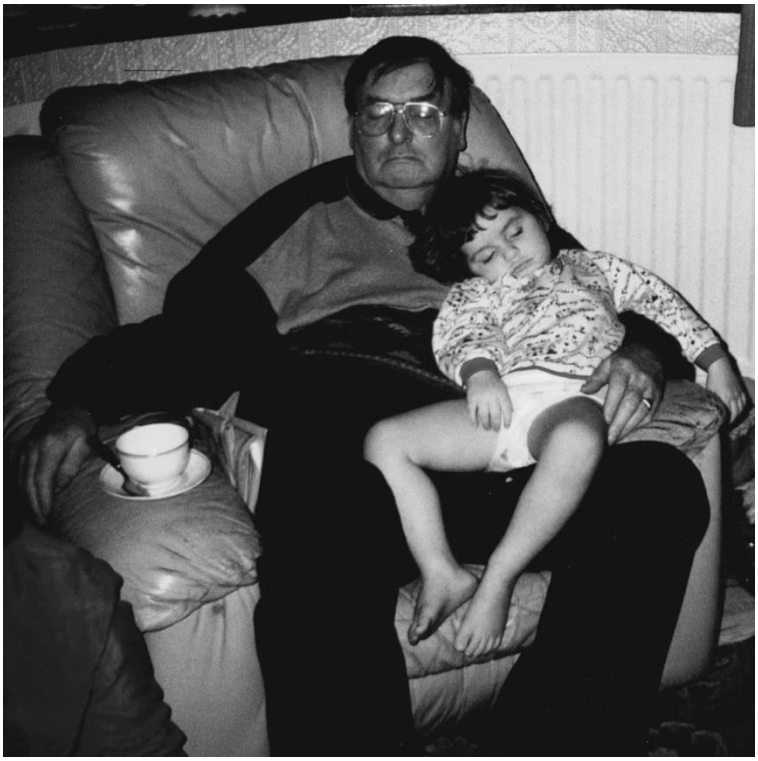
First and foremost, I'd like to thank my principal supervisor Patrick Nolan for giving me such an engaging and important project in the lab to work on. I was also incredibly lucky to have two brilliant and supportive additional supervisors: Gareth Banks and Peter Oliver, who were invaluable during my DPhil.

I could not have completed the quality of work that I have without training and guidance from some of the core staff at Harwell; in particular Adele Austin, Liz Darley and Debbie Williams. Similarly, without the likes of Greg and Rhys in the circadian suite, and Lucie, Liz and all of Ward 4, I wouldn't have been able to complete half of the mouse work I did and I hope they realise how much I appreciated them. I'd also like to thank Sara Wells, Michelle Stewart and Sonia Bains for their mouse genetics and tea making expertise respectively.

There are countless friends I have made on campus, both at MRC and elsewhere, and without their support I wouldn't have got through the final stages of my DPhil. Much to their annoyance I'm not going to list them all individually, but they know who they are and how much they've enriched my life both inside and outside of work. SQUAD.

Thank you to my Mother and Keith for looking after me when I needed it and to the rest of my family for their support even though none of them really understands what my research is about. To Murray, Kevin and Theodore for keeping me company during the early hours whilst writing. And finally, to Kightly and Kenny who are always with me in everything I do.

I'd like to end by dedicating this Thesis to my Grandad, whose pride pushed me further than I thought I could ever go myself.



Frederick John 'Roger' Woodcock

1930 - 2017

Contents

Introduction 1

Circadian rhythms 1

SCN: the master pacemaker 4

Development of the SCN 7

Peripheral oscillators and entrainment 10

Zfhx3: A novel circadian regulator 13

Sci: The original ENU mutant 14

Conditional mutagenesis: the advent of Cre-Lox 16

Thesis aims 20

Methods 22

Mice 22

Genotyping 22

Tamoxifen dosing 23

Lac Z staining of brain sections 23

Whole organ Lac Z staining 24

Embryonic Lac Z staining 25

SCN immunofluorescence 25

Intraocular injection for RHT tracing 26

Retinal Immunofluorescence 26

Measurement of locomotor activity as a circadian output 27

Wheel running: general circadian phenotyping 29

Wheel running: jet lag protocol 29

Wheel running: skeleton photoperiods 30

Wheel running: masking light pulses 30

Wheel running: feeding entrainment 30

Passive infra-red screening 31

Video-tracked sleep screening 32

Home cage monitoring 32

EEG sleep phenotyping 32

Pupillometry 33

In-situ probe generation 34

In-situ hybridisation staining 35

Nissl staining 37

H&E staining 38

qRT-PCR 38

Retinal MEA recording 39

Slit lamp 40

Optokinetic drum 41

Body composition analysis 41

Metabolic caging 42

Corticosterone analysis from urine 42

Open field 42

Light-Dark box 43

Statistics 43

Results I 45

Characterisation of a conditionally-induced knockout of Zfhx3 in adult mice 45

Introduction 46

Characterisation of Cre activity using a Lac-Z reporter 47

ZFHX3 staining is lost in adult *Zfhx3*$^{Flox/Flox}$; UBC-Cre^{+} SCN following tamoxifen treatment 50

Circadian activity is significantly altered following *Zfhx3* deletion 51

Zfhx3 adult KOs re-entrain faster to an advance in LD cycle 55

Zfhx3$^{Flox/Flox}$; UBC-Cre^{+} mice show no changes to sleep behaviour following tamoxifen treatment 59

Pupillary light reflex is significantly altered in *Zfhx3*$^{Flox/Flox}$; UBC-Cre^{+} 62

Viability issues on *Zfhx3*^{Flox} line and downstream molecular work 63

Discussion 67

Results II 70

Investigation of the Sci phenotype when expressed over an inducible Zfhx3 null allele 70

Introduction 71

Traditional circadian wheel running screening was unsuitable for characterising *Zfhx3*$^{Flox/Sci}$; UBC-Cre^{+} mice 73

PIR screening of *Zfhx3*$^{Sci/-}$ revealed further shortening of τ_{DD} and arrhythmic activity 76

Sleep parameters are unaltered in *Zfhx3*$^{Sci/-}$ mice 80

Dim light pupillary reflex is increased in *Zfhx3*$^{Sci/-}$ mice 83

Vip and *Zfhx3* expression are downregulated in *Zfhx3*$^{Sci/-}$ mice 86

Discussion 87

Results III 90

Conditional deletion of Zfhx3 using spatially enriched Cre lines 90

Introduction 91

Characterisation of Cre expression patterns using a Lac-Z reporter 92

Circadian screening of region-specific *Zfhx3* loss driven by *Six3*-Cre 96

Circadian screening of region-specific *Zfhx3* loss driven by *Foxd1*-Cre 99

Video tracked sleep screening of *Zfhx3*$^{Flox/Flox}$; *Six3*-Cre^{+} mice 109

Video tracked sleep screening of *Zfhx3*$^{Flox/Flox}$; *Foxd1*-Cre^{+} mice 111

Zfhx3$^{Flox/Flox}$; *Six3*-Cre^{+} mouse displays abnormal EEG sleep parameters .. 114

Zfhx3$^{Flox/Flox}$; *Six3*-Cre^{+} mice lack SCN identity 117

Zfhx3$^{Flox/Flox}$; *Foxd1*-Cre^{+} mice retain SCN structure 119

Discussion 120

Results IV 125

Further characterisation of an 'SCN-less' mouse 125

Introduction 126

Characterisation of visual function in *Zfhx3*$^{Flox/Flox}$; *Six3*-Cre^{+} mice 128

Zfhx3$^{Flox/Flox}$; *Six3*-Cre^{+} mice display reduced social entrainment 137

Food anticipatory activity is intact in *Zfhx3*$^{Flox/Flox}$; *Six3*-Cre^{+} mice 141

Zfhx3$^{Flox/Flox}$; *Six3*-Cre^{+} mice display a metabolic circadian rhythm 144

Corticosterone as a measure of HPA output in 'SCN-less' mice 149

Activity and anxiety-related parameters are unaffected in *Zfhx3*$^{Flox/Flox}$; *Six3*-Cre^{+} mice..... 151

Discussion..... 156

Discussion 162

References 174

Figures

Figure 1 | Canonical core clock gene loop. 3

Figure 2 | Schematic representation of the SCN. 5

Figure 3 | SCN transcription factor expression during development. 9

Figure 4 | Examples of the oscillatory capability of circadian clocks 11

Figure 5 | Schematic of ZFHX3 protein 16

Figure 6 | *Zfhx3*^{Flox} construct 18

Figure 7 | Mechanism of action for UBC-Cre line 19

Figure 1.1 | Representative X-Gal staining in E12.5 embryo and E18.5 whole brain of the tamoxifen inducible Cre line (UBC-Cre) crossed to a Lac-Z reporter line (R26R) pre tamoxifen dosing. 48

Figure 1.2 | Representative X Gal staining in heart, lungs, thorax and brain of the tamoxifen inducible Cre line (UBC-Cre) crossed to a Lac-Z reporter line (R26R). 49

Figure 1.3 | Representative ZFHX3 immunofluorescence in SCN sections of *Zfhx3*$^{Flox/Flox}$; UBC-Cre^{+} mice pre and post tamoxifen 51

Figure 1.4 | Representative double-plotted actograms for *Zfhx3*$^{Flox/Flox}$; UBC-Cre^{+} mice pre and post tamoxifen 54

Figure 1.5 | Average activity profile for *Zfhx3*$^{Flox/Flox}$; UBC-Cre^{+} and *Zfhx3*$^{Flox/Flox}$ control mice over 12:12 LD cycle post tamoxifen 55

Figure 1.6 | Representative actograms showing advance in activity onset upon release into DD for control and *Zfhx3*$^{Flox/Flox}$; UBC-Cre^{+} mice post tamoxifen. 56

Figure 1.7 | Representative actograms showing re-entrainment of wheel-running activity in response to 6-hr advance or delay in LD cycle for control (*Zfhx3*$^{Flox/Flox}$) and *Zfhx3*$^{Flox/Flox}$; UBC-Cre^{+} mice. 58

Figure 1.8 | Changes to sleep parameters measured using video tracked sleep analysis in *Zfhx3*$^{Flox/Flox}$; UBC-Cre^{+}, *Zfhx3*$^{Flox/+}$; UBC-Cre^{+}, *Zfhx3*$^{Flox/Flox}$, *Zfhx3*$^{Flox/+}$ and *Zfhx3*$^{+/+}$; UBC-Cre^{+} mice 60

Figure 1.9 | Distance travelled pre and post tamoxifen for *Zfhx3*$^{Flox/Flox}$; UBC-Cre^{+}, *Zfhx3*$^{Flox/+}$; UBC-Cre^{+} and *Zfhx3*$^{Flox/Flox}$ mice in video tracked sleep screening.. 61

Figure 1.10 | Representative images for *Zhx3*$^{Flox/Flox}$, *Zfhx3*$^{Flox/+}$; UBC-Cre^{+} and *Zfhx3*$^{Flox/Flox}$; UBC-Cre^{+} mice before and after exposure to bright and mid light intensity stimuli to measure pupillary response. 62

Figure 1.11 | Percentage pupil area at the point of maximal constriction relative to dark adapted pupil size of *Zfhx3*$^{+/+}$; UBC-Cre^{+}, *Zhx3*$^{Flox/+}$, *Zhx3*$^{Flox/Flox}$, *Zfhx3*$^{Flox/+}$; UBC-Cre^{+} and *Zfhx3*$^{Flox/Flox}$; UBC-Cre^{+}. 63

Figure 1.12 | 'short-face' phenotype observed in some *Zfhx3*$^{Flox/Flox}$ mice on congenic B6J background 64

Figure 2.1 | Wheel running actogram from a *Zfhx3*$^{Sci/Flox}$; UBC-Cre^{+} mouse demonstrating lack of wheel use 74

Figure 2.2 | Representative actograms of archive *Sci* mice compared to PIR.....75

Figure 2.3 | τ_{DD} and amplitude of all rhythmic *Zfhx3*$^{Sci/Flox}$ compound heterozygote mice screened in PIR 77

Figure 2.4 | τ_{DD} and amplitude of all mice screened pre and post tamoxifen.....78

Figure 2.5 | Actograms generated from PIR screening of a *Zfhx3*$^{Flox/Sci}$; UBC-Cre^{+} mouse pre and post tamoxifen.....78

Figure 2.6 | Data for τ_{DD} and amplitude for control groups. 79

Figure 2.7 | Sleep parameters measured in *Zfhx3*$^{Sci/Flox}$; UBC-Cre^{+}, *Zfhx3*$^{Sci/+}$; UBC-Cre^{+}, *Zfhx3*$^{Sci/Flox}$ and *Zfhx3*$^{Flox/+}$ mice prior to tamoxifen dosing and *Zfhx3*$^{Sci/-}$, *Zfhx3*$^{Sci/+}$; UBC-Cre^{+} and *Zfhx3*$^{Sci/Flox}$ mice post tamoxifen dosing. 81

Figure 2.8 | Activity over time pre tamoxifen treatment for *Zfhx3*$^{Sci/Flox}$; UBC-Cre^{+}, *Zfhx3*$^{Sci/+}$; UBC-Cre^{+}, *Zfhx3*$^{Sci/Flox}$ and *Zfhx3*$^{Flox/+}$ mice and post tamoxifen dosing for *Zfhx3*$^{Sci/-}$, *Zfhx3*$^{Sci/+}$; UBC-Cre^{+} and *Zfhx3*$^{Sci/Flox}$ mice.....82

Figure 2.9 | Representative images for *Zhx3*$^{Flox/+}$, *Zfhx3*$^{Sci/Flox}$, *Zfhx3*$^{Sci/-}$ mice before and after exposure to bright, mid and dim light stimuli to measure pupillary reflex. 84

Figure 2.10 | Percentage pupil area following bright, mid and dim light stimuli to the eyes of *Zfh*x3$^{Flox/+}$, *Zfh*x3$^{Sci/+}$; UBC-Cre^{+}, *Zfh*x3$^{Sci/Flox}$ and *Zfh*x3$^{Sci/-}$ mice. 85

Figure 2.1 | Fold change calculated for *Vip* and *Zfhx3* expression from qPCR experiments on *Zfhx3*$^{Sci/-}$ and *Zfh*x3$^{Sci/+}$; UBC-Cre^{+} control SCN tissue punches.....87

Figure 3.1 | Representative images of X-Gal staining to show Cre activity in *Foxd1*-Cre-R26R and *Six3*-Cre-R26R Lac Z expressing reporter lines.....95

Figure 3.2 | Representative images of X-Gal staining for *Six3*-Cre and *Foxd1*-Cre R26R-LacZ reporter lines in adult brain.....96

Figure 3.3 | Representative actogram for initial *Zfhx3*$^{Flox/Flox}$; *Six3*-Cre^{+} mice.....97

Figure 3.4 | Representative actograms of *Zfhx3*$^{Flox/Flox}$; *Foxd1*-Cre^{+} mice housed in LD, DD and LL conditions.....100

Figure 3.5 | Representative actograms of inconsistent wheel running behaviour in *Zfhx3*$^{Flox/Flox}$; *Foxd1*-Cre^{+} mutants.....101

Figure 3.6 | Mean values for amplitude in LD, DD and LL for all genotypes tested from the *Zfhx3-Foxd1* line. 103

Figure 3.7 | Representative actograms of behavioural response to a masking light pulse in *Zfhx3*$^{Flox/Flox}$; *Foxd1*-Cre^{+} mutants and *Zfhx3*$^{Flox/+}$ control animals 105

Figure 3.8 | Total activity counts for *Zfhx3*$^{Flox/Flox}$; *Foxd1*-Cre^{+} and control mice exposed to a 3 hour masking light pulse from ZT13-16. 106

Figure 3.9 | Circadian amplitude during entrainment to skeleton photoperiods for *Zfhx3*$^{Flox/Flox}$; *Foxd1*-Cre$^{+,}$ *Zfhx3*$^{Flox/+}$; *Foxd1*-Cre$^{+,}$ *Zfhx3*$^{Flox/Flox}$ and *Zfhx3*$^{Flox/+}$ mice.....107

Figure 3.10 | Representative actograms for control and *Zfhx3*$^{Flox/Flox}$; *Foxd1*-Cre^{+} animals undergoing a skeleton photoperiod protocol to assess entrainment.....108

Figure 3.11 | Sleep parameters measured in *Zfhx3*$^{Flox/Flox}$; *Six3*-Cre^{+}, *Zfhx3*$^{Flox/+}$; *Six3*-Cre^{+} and *Zfhx3*$^{+/+}$; *Six3*-Cre^{+} mice. 110

Figure 3.12 | Activity over time for *Zfhx3*$^{Flox/Flox}$; *Six3*-Cre^{+}, *Zfhx3*$^{Flox/+}$; *Six3*-Cre^{+} and *Zfhx3*$^{+/+}$; *Six3*-Cre^{+} mice. 111

Figure 3.13 | Sleep parameters measured in *Zfhx3*$^{Flox/Flox}$; *Foxd1*-Cre^{+} , *Zfhx3*$^{Flox/+}$; *Foxd1*-Cre^{+} and *Zfhx3*$^{+/+}$; *Foxd1*-Cre^{+} mice. 113

Figure 3.14 | Activity over time for *Zfhx3*$^{Flox/Flox}$; *Foxd1*-Cre^{+}, *Zfhx3*$^{Flox/+}$; *Foxd1*-Cre^{+} and *Zfhx3*$^{+/+}$; *Foxd1*-Cre^{+} mice.. 114

Figure 3.15 | *Zfhx3*$^{Flox/Flox}$; *Six3*-Cre^{+} mouse EEG recording: percentage time spent in wakefulness, REM and NREM sleep analysed for 48 hours prior to and after sleep deprivation.. 116

Figure 3.16 | Representative Nissl staining through the 'SCN' region of *Zfhx3*$^{Flox/Flox}$; *Six3*-Cre^{+} mutant brain and a representative immunofluorescent staining for ZFHX3 and DAPI in the central 'SCN' region of *Zfhx3*$^{Flox/Flox}$; *Six3*-Cre^{+} mutant brain. 117

Figure 3.17 | Representative in situ hybridisation of circadian neuronal markers *Vip*, *Avp* and *Rora* on sections through SCN region of *Zfhx3*$^{Flox/Flox}$; *Six3-Cre*$^{+}$, *Zfhx3*$^{Flox/+}$; *Six3-Cre*$^{+}$ and *Zfhx3*$^{Flox/Flox}$ control mice.....118

Figure 3.18 | Representative Nissl staining of a *Zfhx3*$^{Flox/+}$; *Foxd1*-Cre^{+} mutant brain and H&E staining of another *Zfhx3*$^{Flox/+}$; *Foxd1*-Cre^{+} mutant brain 119

Figure 4.1 | Optokinetic drum was used to assess the visual acuity of *Zfhx3*$^{Flox/Flox}$; *Six3*-Cre^{+}.....129

Figure 4.2 | Representative images for *Zhx3*$^{Flox/+}$, *Zfhx3*$^{Flox/+}$; *Six3*-Cre^{+} and *Zfhx3*$^{Flox/Flox}$; *Six3*-Cre^{+} mice before and after exposure to bright and dim light stimuli to measure pupillary reflex. 130

Figure 4.3 | Percentage pupil area at the point of maximal constriction (relative to dark adapted pupil size) following bright and dim light stimuli to the eyes of *Zhx3*$^{Flox/+}$, *Zfhx3*$^{Flox/+}$; *Six3*-Cre^{+} and *Zfhx3*$^{Flox/Flox}$; *Six3*-Cre^{+} mice. 132

Figure 4.4 | Representative immunofluorescent staining of retinal sections from *Six3*-Cre mice for ßGal, ZFHX3, GAD67 and Calbindin. 133

Figure 4.5 | Representative ERG recordings for *Zfhx3*$^{Flox/Flox}$; *Six3*-Cre^{+} retinas 134

Figure 4.6 | Fluorescent RHT tracing in *Zfhx3*$^{Flox/Flox}$; *Six3-Cre*$^{+}$and control mice. ...136

Figure 4.7 | Home cage activity analysis of group housed *Zfhx3*$^{Flox/Flox}$; Six3-Cre^{+} and *Zfhx3*$^{Flox/+}$; *Six3*-Cre^{+} mice.....139

Figure 4.8 | Total distance travelled between ZT4-5 and ZT11-12 for *Zfhx3*$^{Flox/Flox}$; Six3-Cre^{+}, *Zfhx3*$^{Flox/+}$; *Six3*-Cre^{+} and control mice at 4 months and 8 months of age..140

Figure 4.9 | Representative actograms for *Zfhx3*$^{Flox/Flox}$; *Six3*-Cre^{+} and control mice undergoing a timed restricted feeding protocol. 141

Figure 4.10 | Total activity counts for 3 hour time windows *Zfhx3*$^{Flox/Flox}$; *Six3*-Cre^{+}, *Zfhx3*$^{Flox/+}$; *Six3*-Cre^{+}, *Zfhx3*$^{Flox/Flox}$ and *Zfhx3*$^{Flox/+}$ mice prior and during time restricted feeding. 143

Figure 4.11 | Weight, % fat mass, % lean mass of *Zfhx3*$^{Flox/Flox}$; *Six3*-Cre^{+}, *Zfhx3*$^{Flox/+}$ and *Zfhx3*$^{+/+}$; *Six3*-Cre^{+} mice 144

Figure 4.12 | Metabolic phenotyping of *Zfhx3*$^{Flox/Flox}$; *Six3*-Cre^{+}, *Zfhx3*$^{Flox/+}$; *Six3*-Cre^{+} and *Zfhx3*$^{Flox/Flox}$ mice. 147

Figure 4.13 | *Zfhx3*$^{Flox/Flox}$; *Six3*-Cre^{+}, *Zfhx3*$^{Flox/+}$; *Six3*-Cre^{+}, *Zfhx3*$^{Flox/+}$, *Zfhx3*$^{Flox/Flox}$ and *Zfhx3*$^{+/+}$; *Six3*-Cre^{+} mice underwent body composition measurement.. 148

Figure 4.14 | Corticosterone concentration measured from urine samples of a wildtype B6J mouse and mean corticosterone concentration measured from urine samples collected at ZT0 and ZT12 from *Zfhx3*$^{Flox/Flox}$; *Six3*-Cre^{+} mice 151

Figure 4.15 | Open field parameters measured from *Zfhx3*$^{Flox/Flox}$; *Six3*-Cre^{+}, *Zfhx3*$^{Flox/+}$; *Six3*-Cre^{+} and *Zfhx3*$^{Flox/+}$ mice. 153

Figure 4.16 | Total time spent in and number of entries to dark and light compartments during light-dark box testing of *Zfhx3*$^{Flox/Flox}$; *Six3*-Cre^{+} and *Zfhx3*$^{Flox/+}$ mice.. 155

Tables

Table 1.1 | Mean (± Standard Error Mean) number of days taken to re-entrain to a 6 hour advance and a 6 hour delay in the LD cycle for all genotypes tested in the jet lag protocol. 57

Table 1.2 | Genotype distribution of litters in *Zfhx3*$^{Flox/Flox}$; UBC-Cre^{+} line 64

Table 1.3 | Genotype distribution of litters in *Zfhx3*$^{Flox/Flox}$; UBC-Cre^{+} line when bred onto mixed B6/C3H background. 65

Table 1.4 | Mean values (± Standard Error Mean) of circadian parameters for all genotypes tested pre and post tamoxifen treatment. 66

Table 3.1 | Mean values (± SEM) of circadian parameters measured for all *Zfhx3-Six3* genotypes tested 98

Table 3.2 | Mean values (± SEM) of circadian parameters measured for all *Zfhx3-Foxd1* genotypes tested 102

Abbreviations

Atbf1:	AT binding motif factor 1 (alternative name for *Zfhx3*)
Bmal1:	Brain and Muscle ARNT-Like 1
ChIP:	Chromatin immunoprecipitation
Clock:	Circadian Locomotor Output Cycles Kaput
Cry:	Cryptochrome
CSNK1D:	Casein kinase 1 delta
CSNK1E:	Casein kinase 1 epsilon
DBP:	D site of albumin promoter binding protein
DD:	Constant dark
DD_{Amp}:	Amplitude in DD
DEC1:	Deleted in esophageal cancer 1
DEC2:	Deleted in esophageal cancer 2
E(x):	Embyonic day (x)
EEG:	Electroencephalogram
EMG:	Electromyogram
ENU:	N-ethyl-N-nitrosourea
ERG:	Electroretinogram
FAA:	Food anticipatory activity
Fbxl3:	F-box/LRR-repeat protein 3
FEO:	Food entrainable oscillator
Foxd1:	Forkhead box D1
GABA:	Gamma-Aminobutyric acid
GRP:	Gastrin-releasing peptide
HPA:	Hypothalamic-pituitary-adrenal
ipRGC:	Intrinsically photosensitive retinal ganglion cells
KO:	Knock-out
LD:	Light-Dark
LD_{Amp}:	Amplitude in LD
Lhx1:	LIM homeobox 1
LL:	Constant light
LL_{Amp}:	Amplitude in LL
MEA:	Multi-electrode array
NMS:	Neuromedin-S
NREM:	Non rapid eye movement sleep
P(x):	Postnatal day (x)
Per:	Period
PER2::LUC:	Period2::Luciferase
PIR:	Passive infra-red
PROKR2:	Prokineticin Receptor 2
qRT-PCR:	Quantitative reverse transcriptase polymerase chain reaction

REM:	Rapid eye movement sleep
Rev-erba:	Nuclear receptor subfamily 1, group D, member 1
RHT:	Retinohypothalamic tract
RNAseq:	RNA sequencing
Rora:	RAR-related orphan receptor alpha
Sci:	Short circuit
SCN:	Suprachiasmatic Nucleus
SEM:	Standard error of mean
Six3:	Homeobox protein SIX3
Six6:	Homeobox protein SIX6
SNAP-25:	Synaptosomal nerve-associated protein 25
TTFL:	Transcription translation feedback loop
V1a:	Vasopressin receptor 1A
V1b:	Vasopressin receptor 1B
VIP:	Vasoactive intestinal peptide
VPAC2:	Vasoactive intestinal peptide receptor 2
Zfhx3:	Zinc finger Homeobox 3
ZT(x):	Zeitgeber time (x)
α_{DD}:	Activity in DD
α_{LD}:	Activity in LD
τ_{DD}:	Tau (free running period) in constant darkness
τ_{LL}:	Tau (free running period) in constant light
φ :	Phase angle of entrainment in LD

Introduction

Circadian rhythms

Circadian rhythms are endogenous 24 hour cycles present in all organisms studied to date (Dunlap, 1999). It is believed that the ability to entrain to the average day length on Earth conveyed an evolutionary advantage and the presence of circadian activity across all forms of life on this planet attests to this. For a rhythm to be deemed truly circadian there are three classical criteria that must be fulfilled: firstly, the oscillation must cycle with a self-sustaining period of near to 24 hours; secondly, the cycle speed must be temperature compensated; and thirdly, there must be an ability to synchronise, or entrain, the rhythm to various environmental cues (Pittendrigh, 1960). In mammals, almost every cell possesses a molecular circadian 'clock' formed by a canonical negative feedback loop of well characterised core clock genes. This in turn forms tissue and organ level clocks, which are kept in synchrony by a central circadian oscillator in the hypothalamus of the brain: the suprachiasmatic nucleus (SCN). These peripheral oscillators, as they are known, also themselves feed back to the SCN – forming what we term as a whole, the circadian system (Weaver, 1998). Entrainment of these internal circadian rhythms to an external environment by an organism is arguably the most crucial part of chronobiology. For animals the strongest entraining factor (or Zeitgeber, loosely translating to 'time giver' in German) is light, whilst others such as food availability and social cues are also worth noting (Refinetti, 2015). Desynchrony of the circadian system has been shown to have

adverse physiological effects both in animal models and humans (Jagannath et al., 2017; Roenneberg and Merrow, 2016), and is also known to be a hallmark of many psychological disorders (Banks et al., 2016; Ben-Hamo et al., 2016; Landgraf et al., 2016). In light of this, it is clear that there is still an advantage to being entrained to the environment and that circadian rhythms are still a pertinent subject worthy of further study and understanding.

Every mammalian cell possesses well known molecular circadian machinery comprised of previously characterised clock related genes (**Figure 1**). Classically, transcription and translation of genes contained in interacting negative and positive loops is what drives intrinsic circadian activity. In mammals, the negative loop consists of three period (*Per*) genes and two cryptochrome (*Cry*) genes – the proteins of which form multimeric dimers that translocate back into the nucleus and inhibit their own transcription (Takahashi, 2017). The rhythmic transcription of these genes is controlled by transcription factors CLOCK and BMAL1, which drive expression of *Cry* and *Per*. A second feedback loop comprises the regulatory element Rev-*erba*, which is a direct target of the CLOCK/BMAL1 complex; following accumulation in the cytoplasm, REV-ERBA translocates back into the nucleus and subsequently represses *Bmal1* transcription. Casein kinases (CSNK1D and CSNK1E) are also crucial in regulating periodicity as they phosphorylate PERs and CRYs, allowing PRE/CRY complexes to translocate back into the nucleus, but also leading to degradation of these proteins (depending on the particular amino acid that is phosphorylated) – thus delaying their accumulation in the cytoplasm (Lowrey and Takahashi, 2011).

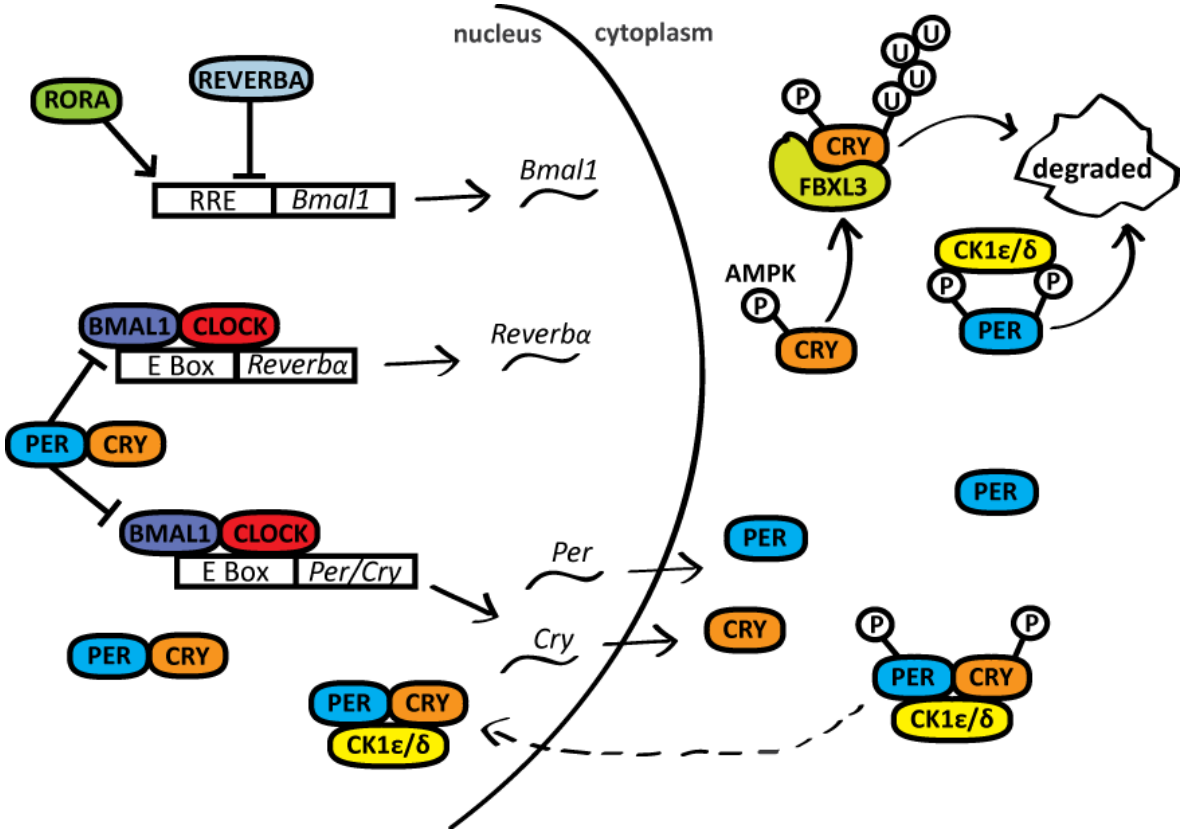


Figure 1 | Canonical core clock gene loop.

Outside of this core clock machinery, other transcription factors have been proposed to have a role in the control of circadian rhythms at the genetic level – such as DBP (Yamaguchi et al., 2000), DEC1 (Nakashima et al., 2008) and DEC2 (Honma et al., 2002). One such transcription factor, Zinc Finger Homeobox 3 (or ZFHX3), was previously identified by our lab (Parsons et al., 2015) as a key regulator of circadian rhythms through study of an ENU derived mouse mutant – *Sci* (short circuit).

The molecular clock mechanism is conserved in all organisms, despite the individual component genes being different in some instances (Hall, 1990). The first circadian mutants were generated in the early 1970s in *Drosophila melanogaster* (Konopka and Benzer, 1971), leading to the discovery of *Per* as the first circadian gene

to be identified (Hardin et al., 1990). This was soon followed by the discovery of the *Clock* mutation from mutagenesis screening in mice (Vitaterna et al., 1994), thus inspiring the identification of further key genes essential for circadian function in mammals. As well as this, studies in other models from different species: such as *Neurospora*, *Arabidopsis* and zebrafish, have all aided the understanding of the molecular basis of clock function (Loudon et al., 2000).

SCN: the master pacemaker

Located in the basal hypothalamus of the mammalian brain, the SCN is a paired bilateral structure of ~20,000 neurons responsible for co-ordinating the circadian system. The identification of the SCN as a key site for circadian rhythm generation was originally established through lesioning and heterograft transplantation studies (Ralph et al., 1990). Single neurons within the SCN exhibit their own independent rhythms in firing rate and gene expression, these are then coupled together to form a highly autonomous clock that continues to exhibit strong circadian activity indefinitely, even *ex vivo*. The SCN receives direct photic input from retinal ganglion cells via the retinal hypothalamic tract (RHT); this light signal is crucial to entrain the intrinsic circadian system to external day-night (Abrahamson and Moore, 2001). This direct photic input also induces expression of immediate early genes, such as *cFos*, in the SCN – highlighting the crucial role light has in resetting this central clock (Vosko et al., 2015). Activation of mitogen-activated protein (MAP) kinases has also been shown to cause phase resetting of the circadian system (Coogan and Piggins, 2004) in response to photic input. The SCN itself has classically been divided into 2 sub regions (**Figure 2**) characterised by neuropeptide expression: the

ventrolateral core, marked by VIP and GRP expression; and the dorsomedial shell, expressing AVP (Moore et al., 2002). It is the core region that receives retinal input and conveys this to the shell; in turn the shell directs SCN output to other brain regions (Fernandez et al., 2016; Mazuski et al., 2018). Almost all neurons in the SCN are GABAergic in nature, with GABA able to act in an excitatory or inhibitory manner in certain regions of the nuclei depending on the time of day (Albers et al., 2017). Also rising to prominence as another important class of SCN neuron are Neuromedin S-positive (NMS) cells, as it has been shown that manipulations to the TTFL in this population of cells disrupts circadian behaviour in mice (Lee et al., 2015). ZFHX3 is expressed throughout the SCN, overlapping with both VIP and AVP expression (Lein et al., 2007b; Parsons et al., 2015).

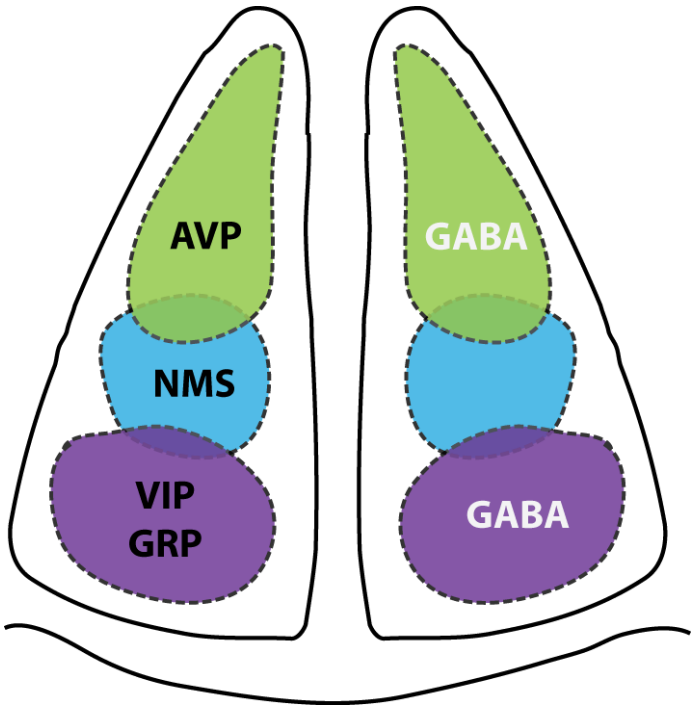


Figure 2 | Schematic representation of the neuronal subpopulations within the SCN. The shell primarily comprises AVP expressing neurons, whereas the core expresses VIP and GRP, NMS expressing neurons are dispersed throughout the central SCN. The majority of neuronal types in the SCN are also GABAergic in nature.

Oscillations produced by the SCN are much more robust than in other tissues, the SCN itself will maintain synchrony when cultured *ex vivo* for months. However, individual cells from the SCN quickly lose their rhythmicity when maintained in dispersed culture. This indicates that the strong stability of circadian rhythm generation produced by the SCN is a product of network dynamics as opposed to the individual neuronal types compromising the nuclei (Webb et al., 2009). Within the SCN, it has also been proposed by Takahashi and colleagues that there are 'coupling factors' that mediate this tight intercellular synchrony. He proposed that neuropeptides are the most likely candidates to facilitate this, but that other unknown genes may also be acting as coupling agents (Mohawk and Takahashi, 2011). VIP and its receptor VPAC2 have been shown to be key players in production of this tight synchronicity in the SCN. Mice lacking VPAC2 display abnormal activity rest patterns, and also an absence of circadian expression of the canonical core clock genes (Harmar et al., 2002; Hughes et al., 2008). Furthermore, *Vip* null mice display a loss of circadian firing in almost half of all SCN neurons and subsequent loss of synchrony between previously rhythmic neurons (Aton et al., 2005b). More recent computational work also suggests that the timing of VIP expression is crucial for synchrony of the core clock (Ananthasubramaniam et al., 2014). As well as having a role in intercellular coupling within the SCN, VIP neurons have also been suggested to directly and indirectly mediate endocrine outputs of the SCN (Vosko et al., 2007). In the absence of VIP-VPAC2 signalling, GRP was shown to confer some intracellular synchrony within the SCN (Brown et al., 2005). Thus, the VIP/GRP ventrolateral core was accepted as a key site of robust rhythm generation and the importance of neuropeptidergic signalling within the SCN was realised (Maywood et al., 2006). AVP has also been implicated in maintaining circadian stability through studies on both the gene itself

and its receptors. In voles (*Microtus arvalis*), circadian rhythmicity was shown to correlate with a number of AVP positive neurons within the SCN (Gerkema et al., 1994). Expression of the *V1a* receptor cycles in the SCN and mice lacking *V1a* have been shown to display a reduction in circadian amplitude of behavioural rhythms, indicating a reduction in synchrony within the SCN (Li et al., 2009). Moreover, mice lacking both *V1a* and *V1b* receptors have been shown to be resistant to experimental jet-lag – indicating a loss of robustness within the SCN in these animals (Yamaguchi et al., 2013). AVP synthesis has also been shown to be attenuated in *Cry* double deficient mice, leading to aperiodicity and loss of SCN tissue rhythms (Ono et al., 2016). Taken collectively, these data highlight the key role both neuronal populations have in maintaining synchrony within the master pacemaker of the SCN.

Development of the SCN

Understanding how the SCN is formed may provide essential insight into the unique self-sustaining oscillatory nature of the nuclei. The developing anterior hypothalamus divides into two developmentally distinct compartments; the ventral anterior hypothalamus and the dorsolateral subdivision. The SCN subsequently arises from the ventral anterior hypothalamus (Bedont and Blackshaw, 2015). Timing of SCN development varies between species. In mice, studies have shown that the majority of SCN cell cytogenesis occurs between E12 and E14.5; the core appears to be patterned first, with the shell developing around this region (Kabrita and Davis, 2008). Further to this it has been shown that expression of crucial developmental genes such as *Six6*, *Six3* and *Foxd1*, are required for proper SCN formation in the foetus (Clark et al., 2013; Liu and Cvekl, 2017; Newmann et al., 2018). **Figure 3**

shows an overview of the timing of expression for genes known to be involved in the development of SCN morphology. Some of these genes, such as *Six3* and *Six6*, are expressed throughout development and into adulthood, whereas others display discrete temporal windows of expression. As noted in the figure, it has recently been shown that the transcription factor LHX1 has a key role in SCN development, as well as being important in the maintenance of circadian synchrony in adult circadian rhythms (Bedont et al., 2014; Hatori et al., 2014). In mice lacking LHX1, VIP and AVP expression in the developing core and shell respectively is severely altered, however gross SCN morphology is intact (Bedont et al., 2014). This suggests that spatial development of the SCN as discrete nuclei occurs before expression of neuropeptides and that following SCN formation, genes such as *Lhx1* then regulate neuropeptide expression to confer oscillatory synchrony. The literature suggests that SCN achieves its 'adult' morphological structure by around P15, with subdomains of neuropeptide expression evident at this time (Antle et al., 2005).

Despite the majority of SCN morphology being present typically 5 days prior to birth (Kabrita and Davis, 2008), rhythmicity gradually develops during the perinatal stage as intercellular networks between the neurons begin to form (Sumova and Cecmanova, 2018). Before birth, the mouse foetal SCN is highly immature and displays a low number of synapses that eventually increase during postnatal development (Shibata and Moore, 1987). Studies on rat SCN have shown that VIP producing neurons are present in the embryo, with *Vip* mRNA being detectable using qRT-PCR (Houdek and Sumova, 2014). However, recently it has been reported that VIP and VPAC2 expression is absent prior to birth in mice despite embryonic SCN displaying rhythmicity at E15.5 (Carmona-Alcocer et al., 2018). It has also been

shown that core clock gene expression is mostly constitutive in embryonic SCN, with *Per2* expression remaining arrhythmic until after birth (Shimomura et al., 2001). Correspondingly, low protein levels for all clock genes except BMAL1 were shown to exist shortly before birth but were undetectable up until this point when analysed in mice. By P10 these protein levels were more comparable to those measured in adult SCN (Ansari et al., 2009).

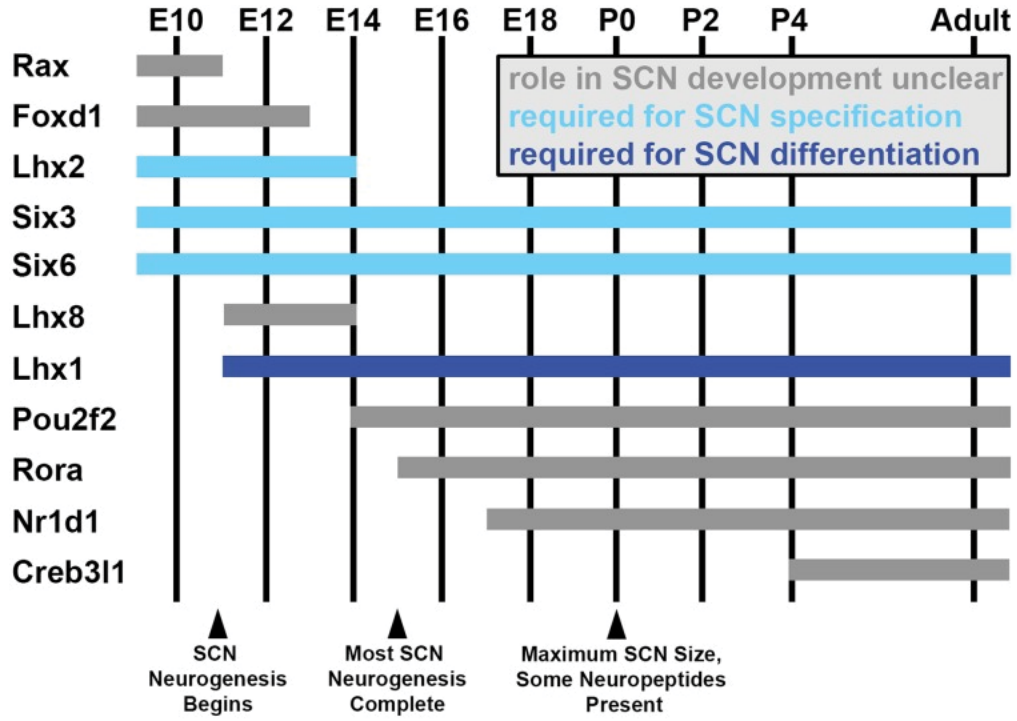


Figure 3 | SCN transcription factor expression during development. Estimated ages of expression for a subset of hypothalamus- and SCN-enriched transcription factors in the developing mouse SCN between embryonic day (E) 10 and adulthood, selected based on expression patterns and/or known developmental functions (indicated by bar colour). *Taken from (Bedont and Blackshaw, 2015).*

Early studies on rodent models showed that these immature SCNs are principally entrained by maternal signals, notably offspring of an SCN ablated mother will display desynchrony between one another when they are born (Reppert and

Schwartz, 1986). Moreover, the phase of the foetal clock has been shown to be modulated by changes to the maternal circadian system (El-Hennamy et al., 2008; Mendez et al., 2012). One study in mice has shown that, given enough time, arrhythmic explants from foetal SCN are capable of spontaneously generating rhythms (Wreschnig et al., 2014). This would suggest that the foetal clock can mature intrinsically devoid of maternal cues; however this is yet to be conclusively confirmed. The RHT, as well as intrinsically photosensitive retinal ganglion cells (ipRGCs) in the retina (Lupi et al., 2006), are functional directly after birth in mice - indicating that neonates are capable of receiving light entrainable input to the SCN from P0.

Peripheral oscillators and entrainment

All mammalian cells have been shown to display circadian activity, these cells subsequently give rise to local circadian clocks at the tissue level (Mohawk et al., 2012). Luciferase reporters, such as the *Per2::Luc* reporter driven by the *Per2* gene (Yoo et al., 2004), have been employed to demonstrate the oscillatory capacity of isolated organs (**Figure 4**). In the absence of SCN signals these explants continue to display rhythmic activity in culture, although they do not maintain as strong rhythms as the SCN (Hastings et al., 2003). Moreover, it has been shown that clock genes are expressed rhythmically in these peripheral tissues, however circadian gene expression was abolished in SCN ablated animals (Akhtar et al., 2002). The SCN co-ordinates these peripheral clocks via the autonomic nervous system (Buijs et al., 2013) and hormonal output (Balsalobre et al., 2000; LeSauter and Silver, 1998).

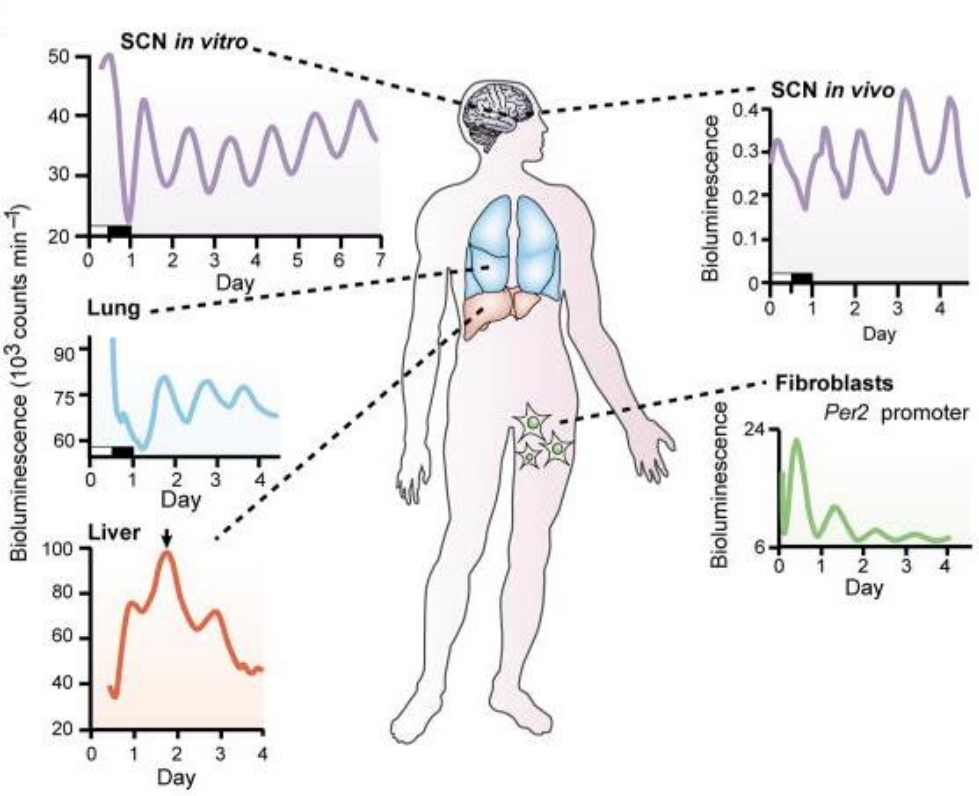


Figure 4 | Examples of the oscillatory capability of cell autonomous circadian clocks found in various organs in the mammalian circadian system. *Adapted from (Takahashi, 2017).*

Entrainment of peripheral oscillators is perhaps more intuitive in other less complex organisms – such as *Drosophila* and zebrafish, where light exposure to all parts of the body can reset and entrain the circadian system (Plautz et al., 1997; Whitmore et al., 2000). In mammals, light input to the circadian system is only conveyed by the retina to the SCN and therefore it could be assumed that this is the result of a specialised pathway of entrainment that has evolved over time (Dibner et al., 2010). However, it has become increasingly apparent that light – although the strongest, is not the only Zeitgeber of the mammalian circadian system (Refinetti, 2015). Particularly in humans, the social aspect of our lifestyles increasingly drives entrainment in modern life. In group housed animals social cues are also important

factors, with prey animals - such as mice, often conforming to the activity rest patterns of their cage mates (Mistlberger and Skene, 2004). There is also growing evidence for exercise as an entrainment factor, particularly of peripheral clocks in muscle (Tahara et al., 2017). Feeding time is possibly the most potent entrainment factor of peripheral oscillators; indeed it has been repeatedly shown to create robust changes in locomotor activity in rodents (termed food anticipatory activity, or FAA) that are independent of the light entrainable pathway and the SCN (Mistlberger, 1994). Food and water metabolism requires the recruitment of many organs, such as pancreas, gut, kidneys and skeletal muscle; with numerous peripheral oscillators involved, it is no surprise that dietary schedule is a potent Zeitgeber (Pendergast and Yamazaki, 2018; Schibler et al., 2003). Interestingly, despite other brain regions being able to adapt to altered feeding regimes, the SCN appears to be almost unresponsive to new feeding cues (Schibler et al., 2003) and FAA can occur in the absence of a functional core molecular clock (Pendergast et al., 2017). Scheduled methamphetamine dosing also causes anticipatory activity in animal models, similar to that of FAA (Tataroglu et al., 2006). Again, this 'drug entrainable oscillator' has been shown to function independently of the SCN and to be intact in clock gene mutants (Mohawk et al., 2009; Pezuk et al., 2010). Temperature has also been shown to be a strong modulator of the circadian system, with measurable changes in locomotor activity being recorded in response to temperature variations (Refinetti, 2015). The presence of, and data gathered thus far, on entrainable peripheral oscillators poses a number of interesting questions regarding the traditional hierarchical view of the circadian system.

Zfhx3: A novel circadian regulator

Originally termed *Atbf1* (AT-motif binding factor 1), ZFHX3 is a large transcription factor of ~400 kDa in size (**Figure 5**), containing four homeodomains and 23 zinc finger motifs (Yasuda et al., 1994a). *Zfhx3* is widely expressed throughout the developing brain and is upregulated during neuronal differentiation (Ishii et al., 2003; Jung et al., 2005b); following birth it is massively downregulated, due to this the gene was originally thought to be of negligible importance in the adult brain. However, relatively high expression of the gene remains in discrete nuclei of the brain throughout adulthood – alluding to the idea that ZFHX3 function could be a crucial player in other aspects of neurobiology in addition to its role in early neuronal development. Of particular interest to the field of chronobiology, high levels of ZFHX3 are detectable in adult SCN in mice (Lein et al., 2007a). It is also worth mentioning that ZFHX3 expression is found outside of the brain in a variety of adult organs – such as heart (Benjamin et al., 2009), liver (Kim et al., 2008) and lung (Zaw et al., 2017). Related to this, ZFHX3 has been implicated in numerous chronic diseases such as atrial fibrillation (Gudbjartsson et al., 2009) and cancer (Sun et al., 2015; Sun et al., 2007). Protein altering variants of ZFHX3 have also been implicated in obesity in humans (Turcot et al., 2018). However, the work presented in this thesis focusses on the neurobehavioural functions of the gene and builds on the relatively recent attribution of *Zfhx3* as a major component of the genetic basis of mammalian circadian rhythms (Parsons et al., 2015). Further to this seminal paper, there have also been studies describing a role for the gene in the control of sleep homeostasis in mice (Balzani et al., 2016) – a process related to, but outside of the canonical circadian system. Traditional null alleles of the gene are homozygous lethal during

development, heterozygote knock-outs (KOs) display pre-weaning mortality (Sun et al., 2012). Therefore, a conditional mutagenesis approach was used to further study the function of ZFHX3 in the circadian system in mice.

Sci: The original ENU mutant

N-ethyl-*N*-nitrosourea (ENU) is a potent chemical mutagen that causes single point mutations when administered to mice. These mutations occur in the germline and so breeding from these animals, typically males, results in mutant offspring for phenotyping. If any of these offspring display abnormal phenotypes when screened, subsequent breeding is undertaken to demonstrate hereditability and then positional mapping is used to determine the causative gene of the observed behaviour (Nolan et al., 1997). ENU mutagenesis can produce a range of alleles and also result in mutations to genes that would be lethal if constitutively knocked out in mice (Acevedo-Arozena et al., 2008). This method has been used to complete large scale mutagenesis screening for many genes involved in behaviour in mice. The first mammalian clock gene was discovered utilising this method (Vitaterna et al., 1994); since then, several novel circadian genes have been discovered using ENU mutagenesis.

As previously mentioned, *Zfhx3* was first attributed to have a role in circadian rhythm maintenance by studies conducted on the ENU mutant *Sci*. The *Sci* mouse displayed a shortened Tau_{DD} (τ_{DD}) that ranged from 21.4 to 23hr in initial circadian phenotyping. Candidate screening revealed this was due to a single point mutation in exon 9 of *Zfhx3*, resulting in a G to T transversion and a subsequent amino acid

change to valine from phenylalanine at position 1963. *Per2::Luc* SCN slice data from *Zfhx3*$^{Sci/+}$ mutants further confirmed shortened circadian period due to the *Sci* mutation, along with decreased amplitude in the SCN as a whole as well as in individual neurons. No changes were seen in lung slices from the same animals, indicating that despite *Zfhx3*'s expression in other tissues this mutation did not affect peripheral oscillators here. Although no significant changes to the canonical core clock genes were overserved as a result of the *Zfhx3*^{Sci} mutation, there was significantly reduced expression of certain key neuropeptides and their receptors thought to be responsible for coupling within the SCN – namely *Vip* and it's receptor *Vipr2*, and also *Prokr2*. Quantitative ChIP assays showed that ZFHX3 itself is capable of binding the promotors of key circadian neuropeptides *Avp* and *Vip*, and it is also noteworthy that ZFHX3 appeared to overlap almost completely with immunopositive AVP and VIP cells in the SCN (Parsons et al., 2015). Taken collectively, these initial studies and publications provided strong evidence that ZFHX3 is a TTFL independent regulator of the circadian system which most likely acts through regulation of a clock transcriptional axis. However, all of these previously collected data was based upon experiments on a heterozygous mutant of *Sci* (*Zfhx3*$^{Sci/+}$) as the mutation was found to be homozygous lethal. Similarly, traditional null mutants of *Zfhx3* are also lethal during development. This limits the depth that we can study in terms of gene function in the development of circadian rhythms, as we are not able to observe any phenotypes produced by a constitutive loss of function of the gene.

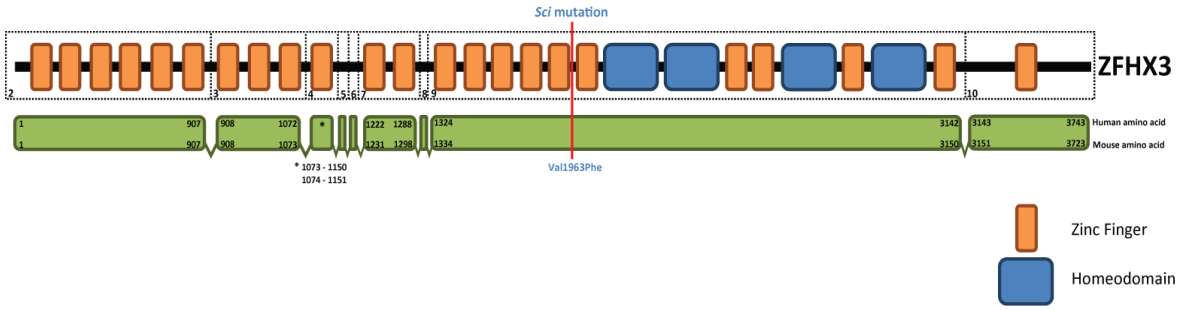


Figure 5 | Schematic of ZFHX3 protein: ZFHX3 contains 23 Zinc fingers and 4 homeodomains, also shown are coding exons and the position of the original *Sci* mutation resulting in shortened τ_{DD} in heterozygote carriers. Exon 1 is non-coding and therefore not shown. *Adapted from a figure by Paige Chandler (unpublished).*

Conditional mutagenesis: the advent of Cre-Lox

Conditional mutagenesis has been an invaluable tool for studying the genetics of various genes where null mutant alleles are homozygous lethal, and also allows the dissection of genes with pleiotropic effects. Possibly the widest used method of generating conditional mouse mutants is Cre-Lox recombination (Murray et al., 2012). In this system, a conditional allele of a target gene is created where the gene or critical exons of the gene are flanked by LoxP sites (also known as a 'floxed' allele). Upon exposure to Cre recombinase, the flanked region is excised – thus creating a conditional null allele. In mice, this is achieved via crossing mice carrying the floxed allele to a Cre driver mouse line in which Cre expression is driven by the promotor of a particular gene; allowing spatial and/or temporal deletion of the target (**Figure 6**). In recent times, this method was successfully employed to reveal a role for NMS neurons as crucial pacemaker cells within the SCN (Lee et al., 2015; Loh et al., 2015).

Despite the successes of Cre-Lox, the system itself is known to be variable amongst driver lines – with some having more off-target (or 'leaky') Cre expression than others. Because of this, it is important to characterise patterns of Cre activity

both embryonically and in adult mice. This is typically achieved using reporter lines, such as the ROSA26 line, where Lac Z or fluorescent proteins are expressed in areas where Cre activity occurs (Srinivas et al., 2001). However, it should be noted that use of these reporter lines in adults reflects the lineage of Cre activity in pre-cursor cells (if the Cre is expressed developmentally) as it is the daughter cells that will be imaged in this instance.

To generate a conditional null allele of *Zfhx3*, a floxed mouse line was used in which exons 7 and 8 are excised upon breeding to a Cre expressing mouse line. This leads to a frame shift in *Zfhx3* translation, resulting in the introduction of a stop codon and thus creating a null allele (Sun et al., 2012). By using a tamoxifen inducible Cre driver line (Ruzankina et al., 2007), an adult specific KO mouse of the gene was created to assess *Zfhx3*'s function in the generation and maintenance of adult circadian rhythms. Two spatially enriched Cre lines driven by the promotors of genes *Six3* (Furuta et al., 2000a) and *Foxd1* (Humphreys et al., 2008) were utilised to create a KO of the gene in the anterior hypothalamic region that goes on to form the SCN during development. Through subsequent breeding, homozygous mutants of all three of these lines were created for validation. As well as this, the inducible null allele was bred over the *Zfhx3*^{Sci} allele to create a compound heterozygote animal – allowing further characterisation of the *Sci* mutation. This compound heterozygote strategy has been successfully employed previously to study the nature of the ENU *Clock* mutant in circadian biology (King et al., 1997).

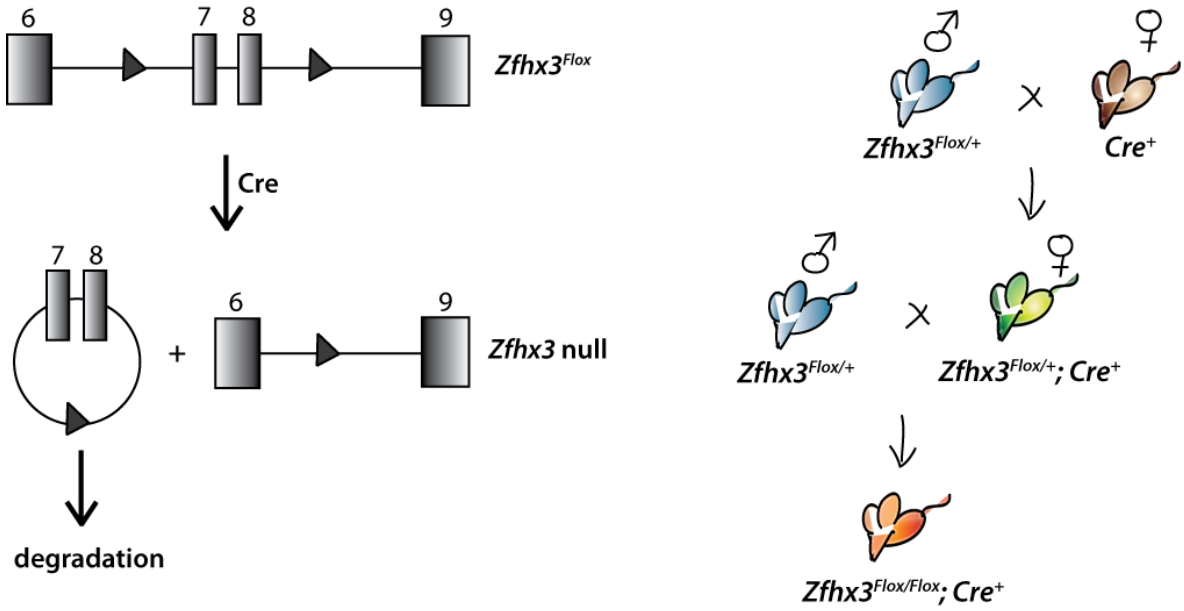


Figure 6| *Zfhx3*^{Flox} construct: exposure to Cre recombinase drives excision of critical floxed exons 7 & 8. Generic breeding scheme to achieve mutant lines: floxed mice were bred to Cre positive lines to generate both heterozygote and homozygote Cre positive floxed animals – thus creating a conditional mutant line. Male floxed mice were used, Cre was maternally inherited.

UBC-Cre was created by fusing Cre recombinase with a mutated version of the oestrogen receptor (ERT2) that is unresponsive to endogenous natural oestrogen, and is driven by the Ubiquitin C (UBC) promoter. UBC-Cre is ubiquitously expressed in all tissues; temporal deletion of the target gene is achieved via tamoxifen dosing. Tamoxifen is typically administered via intra-peritoneal injection or oral gavage, as these are the most accurate and consistent methods of dosing, but it can also be administered in chow and drinking water (Turner et al., 2011). Unlike the original version of this inducible Cre line (Jaisser, 2000), ERT2 was developed to be more sensitive to tamoxifen induction and generate more specific Cre expression. Prior to tamoxifen dosing, Cre-ERT2 is confined to the cytoplasm of cells and therefore expression of the target gene remains stable. Upon exposure to tamoxifen Cre-ERT2

translocates to the nucleus, where recombination occurs and thus deletion of the target gene is achieved (**Figure 7**).

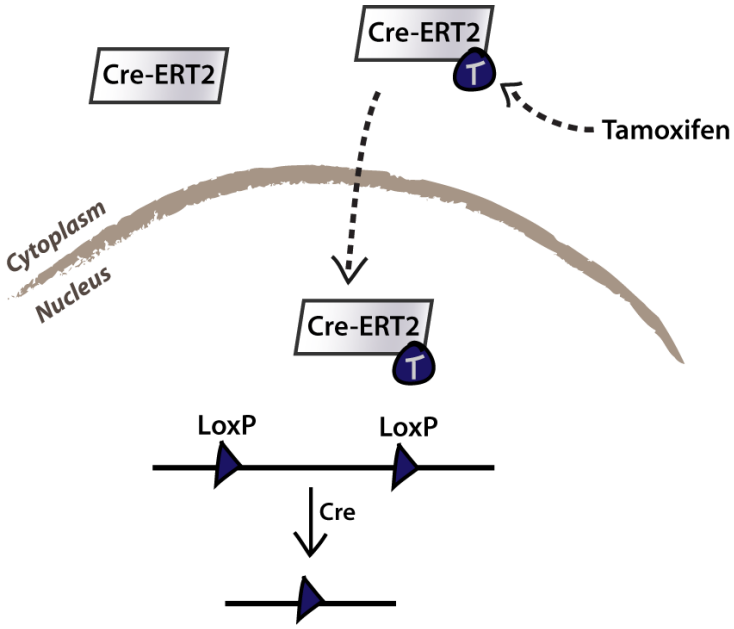


Figure 7 | Mechanism of action for UBC-Cre line. Cre is fused to a modified ERT2 receptor, upon exposure to tamoxifen Cre is translocated into the nucleus where it causes recombination of the target gene region flanked by LoxP sites causing gene deletion.

The *Six3*-Cre line was created via insertion of a Cre expressing transgene, containing a nuclear localisation sequence, into the first coding exon of the *Six3* gene. Following development, the line was crossed to a reporter line to assess establish pattern of Cre activity. This data showed that the Cre line displayed robust retinal and ventral forebrain expression by E9 in embryos. Cre expression was also shown to be more spatially restricted than native *Six3* expression (Furuta et al., 2000a). As noted previously *Six3* itself is an important gene in the development of the SCN, and so this Cre line has been used to drive deletion of target genes in the cells that go on to form the SCN during embryonic neurogenesis. Notably, the transcription factor LHX1

was identified as a regulator of circadian rhythms and crucial for terminal differentiation of the SCN via use of this *Six3*-Cre (Bedont et al., 2014).

Foxd1-Cre was originally developed to study gene expression in the kidney, due to the strong expression of native *Foxd1* in this region (Levinson et al., 2005). However, *Foxd1* has also been implicated in development of the retina, optic chiasm and, most recently, the SCN (Carreres et al., 2011; Herrera et al., 2004; Newmann et al., 2018). The *Foxd1*-Cre line was created via targetted insertion of a Cre protein coding region into the 5' untranslated region of *Foxd1* (Humphreys et al., 2010). Despite *Foxd1* being recently implicated in SCN development, there are no publications currently available (as far as the author is aware) on use of the *Foxd1*-Cre line to drive gene deletion in the SCN region.

Thesis aims

The overall main aim of this thesis was to build on previously ascribed circadian functions of *Zfhx3* from studies of the $Zfhx3^{Sci/+}$ mutant. Three major hypotheses were explored relating to this, all of which employed conditional mutagenesis approaches in the mouse to study the effects of *Zfhx3* loss.

The first hypothesis was that *Zfhx3* is a key regulator of adult circadian rhythms. This was studied through the use of a ubiquitously expressed adult inducible Cre line (UBC-Cre); some of these results of have been already published (Wilcox et al., 2017), the rest are presented in Results I. The second hypothesis was that when $Zfhx3^{Sci}$ is bred over an adult inducible null to create a compound heterozygote mutant ($Zfhx3^{Sci/-}$), the true nature of the *Sci* mutation would be revealed. This was achieved

through inter-breeding of the aforementioned adult inducible knock-out of *Zfhx3* and the previously characterised *Zfhx3*^{Sci} mutant. And finally, the third hypothesis was that loss of *Zfhx3* in the SCN region during development would significantly alter circadian function in adult mice. This was examined through study of the circadian behaviour and SCN structure of two different mutants, one driven by *Six3*-Cre and the other by *Foxd1*-Cre.

Methods

Mice

All animal studies were performed under the guidance issued by the Medical Research Council in Responsibility in the Use of Animals for Medical Research (July 1993) and Home Office Project License 30/3206, with local ethical approval. When not being tested, mice were group housed in individually ventilated cages under 12:12 h light/dark conditions with food and water available *ad libitum*. *Zfhx3*$^{Flox/+}$ mice (Sun et al., 2012) were obtained from Dr Jin-Tang Dong (Emory University). An inducible Cre line expressing UBC-cre (B6.Cg-Tg(UBC-cre/ERT2)1Ejb/J) was obtained from the Jackson Laboratory (Ruzankina et al., 2007). The Tg(Six3-cre)69Frty line was created by Dr Yas Furuta (Furuta et al., 2000b) and imported from Joseph Bedont (John Hopkins University). The B6;129S4-Foxd1tm1(GFP/cre)Amc/J line (Humphreys et al., 2010) was also imported from Dr Bedont.

Genotyping

Mice were genotyped using a qPCR copy count Taqman assay in which progress of the qPCR assay is measured using a Taqman probe to detect different levels of fluorescence based on the amount of gene product amplified.

WT *Zfhx3* primers:	AAGAAGCGATAAGCTAACACCAGG
	ACGCCAAAGGTTGAGGAGAATG
Probe sequence:	TTAAAGGAATTCACGGGGTTAGGGC

Mutant *Zfhx3* primers:	GCCATAACTTCGTATAATGTATGCTATACG
	ACGCCAAAGGTTGAGGAGAATG
Probe sequence:	TTATAAGCTTACGGGGTTAGGGCTGT
Sci primers:	TCCACGCATTGCTTCAGATG
	TGTGCCTTCTGCTTGTTCTCA
Probe sequence:	CTTTGAGCTCGTCATT
UBC-Cre primers:	GGGCTGCAGGTCGACTCT
	TCGTTGCATCGACCGGTAATG
Probe sequence:	AGAGGATCCAGTTAACCTCGAGGGC
Foxd1-Cre primers:	CGCAAGAACCTGATGGACATG
	ACCGGCAAACGGACAGAA
Probe sequence:	TTCAGGGATCGCCAGGCGTTT
Six3-Cre primers:	CCATGGCTCCCAAGAAGAAGAG
	CCTGGCGATCCCTGAACATG
Probe sequence:	TGTCCAATTTACTGACCGTACACCAA

Tamoxifen dosing

Tamoxifen was administered via oral gavage for 5 days with a 7 day recovery period allowed before further testing. A stock concentration of 20 mg/ml Tamoxifen solution was prepared by dissolving Tamoxifen (Cambridge Bioscience, UK) in 1% Ethanol then Corn Oil (MP Biomedicals, UK). Mice were dosed at 8 weeks of age according to their weights to give a total dose over the 5 days of 1 g/kg.

Lac Z staining of brain sections

Brains were collected and fresh frozen in OCT Compound (VWR International Ltd, UK) compound on dry ice. Frozen blocks were then stored at -70°C until sectioning using a cryostat. 30 µM sections were collected on slides and slides were subsequently stored at -20°C until staining. X-gal staining solution (2 mM $MgCl_2 \cdot 6H_20$, 0.02%

IGEPAL, 5 mM Potassium Ferrocyanide, 5 mM Potassium Ferricyanide, 4°C 1X PBS pH 8.0, 10% Sodium Deoxycholate, 0.1% 1 mg/ml X-Gal in DMF) was made fresh on the day of staining and filtered before use. Slides were incubated in 4% PFA on ice then washed three times with pH 8.0 PBS solution before incubation in X-gal staining solution at 37°C for ~48 hours. After staining, slides were rinsed in PBS and post-fixed in 4% PFA before washing in PBS and then dH20. Slides were dehydrated by two 1 minute incubations in 70% IMS (Industrial Methylated Spirit), then one 1 minute incubation in 100% IMS and left in Xylene until coverslipping. Slides were mounted using DPX (Sigma-Aldrich, UK) mountant and left to dry before imaging. Slides were scanned at 20X using a NanoZoomer-RS (Hamamatsu Photonics, Japan) and images acquired using NDP.View 2.4.26 (Hamamatsu Photonics K.K.).

Whole organ Lac Z staining

A lethal dose of Euthatal (200 mg/ml) was given via intraperitoneal injection to allow animals to undergo perfusion for fixation. Mice were transcardially perfused with heparinised PBS followed by 4% PFA to fix all tissues; fixed organs were then dissected out and incubated in X gal staining solution at 4°C for up to 48 hours. Following this, organs were washed with PBS at pH 8.0 and then post fixed in 4% PFA at pH 8.0 overnight at 4°C. Organs were then cleared with 50% glycerol overnight at 4°C and a final clearing step of 70% glycerol at 4°C was performed before they were stored in this solution at 4°C until imaging.

Embryonic Lac Z staining

Embryos were taken at specified time points and removed from their yolk sacs into ice cold pH 8.0 PBS on an agitating platform until they were clean of any residual blood. Once clean, embryos were fixed in 4% PFA on ice for 20 minutes and then washed three times with PBS on ice. Embryos were then incubated in X gal staining solution at room temperature for up to 48 hours. Once stained, two 1 hour PBS washes were performed on ice before post fixing at 4°C overnight in 4% PFA. A final PBS wash was used to remove any residual PFA after post fixing, and embryos were then imaged.

SCN immunofluorescence

Brains were dissected at ZT3 and immediately embedded in moulds containing OCT compound (VWR international, USA), moulds were then floated in isopentane on dry ice to freeze the samples. 12 µM sections were cut on a cryostat and collected onto slides. Slides were fixed in 4% paraformaldehyde for four hours at 4°C, washed in PBS, then incubated in 3% Hydrogen Peroxide in Methanol for 30 mins at 4°C before washing with PBS again and then blocking in 5% normal goat serum made up in 0.5% PBS-Triton. Anti-ZFHX3 raised in Rabbit (Parsons et al., 2015) was diluted 1:1000 in the blocking solution and primary incubation was 24 hours at 4°C. Anti-Rabbit 488 raised in goat (Abcam, UK) was diluted 1:200 in PBS and secondary incubation was 2 hours at room temperature, following a PBS wash. Slides were coverslipped using ProLong Gold Antifade mountant with DAPI (Life Technologies, UK). Sections were imaged using an inverted confocal microscope running Zen software; settings were re-used between images and the 'best fit' function applied to all captured images.

Intraocular injection for RHT tracing

Mice were anaesthetised via intraperitoneal injection of Dormitor (1 mg/kg) and Ketamine (60 mg/kg). Syringes for intraocular injection were first cleaned with ddH20/PBS before loading with fluorescently tagged Cholera Toxin 488 (Alexa Fluor, C34775) and 594 (Alexa Fluor, C34777). 0.2 µl air plus 2 µl liquid for injection was taken up into the syringe. 488 was injected into the left eye of the mouse, 594 was used for injection into the right eye (488 reconstituted with 80 µl sterile saline = 6.25 µg/ml; 594 reconstituted with 100 µl = 5 µg/µl). Tropicamide was placed on the eyes and left to cover the eye for ~2 minutes followed by phenylephrine hydrochloride drops prior to injection. Visotears eye drops were then applied before using notched forceps to grip the eye muscle. Toxin was injected past the ring muscle above the eye and the needle held in place for 5 seconds following injection. Following this, this forceps were released and the injection needle released. More viscotears and proxymetacaine were then applied to the eye. Antisedan (5 mg/kg) was then injected intraperitoneally to revive the animal and the animal was monitored every 15 minutes during recovery, chloramphenicol eye drops were used during this time. Syringes for injection were cleaned five times using ddH20 between animals. After 72 hours, mice were culled and brains dissected into 4% PFA for 8 hours at 4°C before being transferred to 20% sucrose solution overnight. Brains were sectioned at 40 µM and sections processed for imaging as previous.

Retinal Immunofluorescence

Whole eyes were dissected and immediately fixed in 4% PFA at 4°C overnight then left in PBS under sectioning. Primary antibodies were incubated for 24–72 hours at

4 °C. Secondary antibodies were incubated 1:200 for 2 hours at 22 °C. All secondary antibodies were raised in donkey and conjugated with Alexa dyes (Life Technologies). For retinal sections, all antibodies were diluted in PBS with 2.5% donkey serum and 0.2% Triton-X. All wash steps were performed using PBS with 0.05% Tween-20. Samples were mounted in Prolong Gold anti-fade media containing DAPI (Life Technologies). Fluorescent images were collected using a LSM 710 laser scanning confocal microscope and Zen 2009 image acquisition software (Zeiss). Individual channels were collected sequentially. Laser lines for excitation were 405 nm, 488 nm, 561 nm and 633 nm. Emissions were collected between 440–480, 505–550, 580–625 and 650–700 nm for blue, green, red and far-red fluorescence respectively. For all images, global enhancement of brightness and contrast was performed using Zen Lite 2011 image analysis software (Zeiss). For direct quantitative comparisons (where stated), all images were acquired and processed under identical conditions. Primary antibodies used were: 1:1000 ß-gal Chicken polyclonal (ab9361, Abcam), 1:1000 Calbindin rabbit polyclonal (ab11426, Abcam), 1:1000 GAD67 Mouse monoclonal, 1:1000 (MAB5406, Millipore).

Measurement of locomotor activity as a circadian output

For many years, the principal measure of circadian output has been that of locomotor activity. In mice this has classically been achieved via single housing of animals with free access to a running wheel, running wheel revolutions are then recorded as a measurement of circadian activity (Banks and Nolan, 2011; Siepka and Takahashi, 2005). Utilising this technique, mice can be exposed to many different lighting conditions to assess the function of the light entrainable oscillator within the

SCN. Wheel running has also been employed to assess the state of peripheral oscillators, such as the food entrainable oscillator (FEO), through data collection on anticipatory activity (Carneiro and Araujo, 2012).

Currently, the most common alternatives to wheel running employ passive infra-red screening technology to record movement. An example of this type of technology is the Continuous Open Mouse Phenotyping of Activity and Sleep Status (COMPASS) system (Brown et al., 2016), which has been used for circadian characterisation of some mutant lines in this thesis. This method uses a passive infra-red (PIR) sensor above the cage to detect movement, from this data activity rest patterns can be established and used to create circadian actograms for analysis. In addition to this, periods of immobility can be used to record sleep bouts that have been shown to correlate with EEG sleep data (Fisher et al., 2012): thus maximising the amount of data available from one screening procedure. Whether robust anticipatory activity, such as FAA, is recordable using this system is yet to be assessed.

Both passive infra-red and wheel running screening require animals to be singly housed in order to reliably collect individual circadian data. As noted earlier, social aspects are one of the hallmarks of human circadian entrainment in the modern world. Also, cohousing of animal models has also been shown to affect circadian behaviour, leading to the proposal of a socially entrainable clock (Mistlberger and Skene, 2004). Therefore, the ability to monitor circadian activity of group housed animals provides an attractive proposition for the study of social influences on circadian rhythms. Recently data has been published on a caging system that facilitates this through video tracked analysis of mice in the home cage, combined with radio-frequency identification (RFID) microchip data on individual mice (Bains et

al., 2016). The fact that mice are kept in the home cage for recording also negates any stress effects on the circadian system of screening of single housing and screening in a potentially novel environment. Validation of this system has shown that individual circadian parameters can be reliably collected from group housed mice. Also, the data collected suggests that wheel running circadian screening may underestimate activity during the light phase and differences between background strains of mice (Bains et al., 2016; Bains et al., 2018).

Wheel running: general circadian phenotyping

Adult mice (>6 weeks) were individually housed with free access to a running wheel and *ad libitum* food; these cages were placed in light controlled chambers and wheel running activity monitored via ClockLab software (Actimetrics). Initial circadian screens were composed of seven days in a 12 hour LD cycle (100 lux light intensity) and then twelve days in constant darkness. Measures for τ_{DD}, α_{LD}, α_{DD}, amplitude and activity in light phase were taken. More involved circadian screens were undertaken depending on whether a circadian phenotype was observed in these initial screens.

Wheel running: jet lag protocol

A jet-lag simulation was undertaken to assess re-entrain to advancing and delaying of LD cycle. Mice were maintained for 3 days in standard LD conditions after which the LD cycle was advanced by 6 hours and the new LD schedule maintained for 14 days. Subsequently, the LD cycle was delayed by 6 hours and mice were again maintained for 14 days under these new conditions. The number of days taken to re-entrain to the

new LD cycle was assessed by measuring the difference between lights off and activity onset. 100 lux light intensity was used during lights on throughout the screen.

Wheel running: skeleton photoperiods

Skeleton photoperiods were used to assess entrainment in mutants and eliminate effects of light on masking of behaviour. Mice were individually housed with free access to a running wheel on a standard 12:12 LD cycle for 7 days before being released into DD for 9 days. Following this mice were transferred onto a skeleton photoperiod consisting of lights on for 15 minutes at ZT0 and ZT12 for 14 days and entrainment assessed during this period. τ_{LD} and corresponding amplitude was measured to assess entrainment to skeleton photoperiods.

Wheel running: masking light pulses

Masking light pulses were undertaken to assess masking behaviour to light in mutants. Mice were maintained on a 12:12 LD cycle for 3 days before a masking light pulse was given for 3 hours between ZT13-16. Total activity was measured for the 3 hours during the light pulse and compared to average total activity for ZT13-16 for the 2 days prior to the light pulse.

Wheel running: feeding entrainment

A scheduled feeding paradigm was undertaken to assess whether mutants could entrain to feeding times, thereby assessing whether the food entrainable oscillator

was in-tact in these animals. Mice were housed in constant darkness with access to food *ad libitum* for 5 days to allow them to dissociate from entrainment to an LD cycle before starting the feeding entrainment paradigm. On day 1 of the feeding protocol, food was taken away at 8pm and returned at 8am the following morning; the mice then went on to only have access to food for 12 hours for 3 days, this was reduced to 8 hours for the following 3 days, and then 6 hours for the remainder of the screen. Following this, mice were then placed on *ad libitum* feeding again. Anticipatory activity was calculated by recording total activity counts for 3 hours prior to food availability and averaged for the total time under 6 hour restricted feeding. The corresponding 3 hour time period in days prior to food restriction, when mice were on *ad libitum* food, was taken and averaged for comparison.

Passive infra-red screening

Passive infra-red screening was used to undertake standard circadian screening on mutant mice that did not run well on running wheels. Mice were analysed for circadian activity and immobility defined sleep via the COMPASS system as described in Brown *et al.* (Brown *et al.*, 2016). Mice were individually housed and data captured for 5 days in a 12:12 LD cycle, followed by 9 days in constant darkness. Data analysis was performed using custom python scripts and excel sheets, developed in house (Banks et al, in preparation). Circadian analysis was performed on ActogramJ software (University of Wuerzburg, Germany). Measures for τ_{DD}, amplitude, total sleep in LD and % sleep in the light phase in LD were taken.

Video-tracked sleep screening

Mice were singly housed and analysed for immobility defined sleep using video tracking analysis. Data was recorded using AnyMaze software (Version 4.5, Stoelting, USA), each >40 second period of immobility was defined as sleep, as described in Banks *et al*. 2015 and Fisher *et al*. 2012.

Home cage monitoring

Group housed mice were tagged with RFID microchips inserted into the abdominal cavity and left to recover for three days in the home cage. Chipped mice were then placed in the Home Cage Analysis system (Actual Analytics, Edinburgh). Video data was captured as well as location tracking using RFID co-ordinates using a gridded array of RFID sensors beneath the cage base (Bains *et al.*, 2016). Mice were recorded for 72 hours at 4 months and 8 months of age and movement data for either the light or dark period was summed over the 72 hours. Transitionary activity was validated by summing total distance travelled for 2 hours between ZT11-12 (an hour before and after lights off) and compared to total distance travelled for 2 hours between ZT4-5 (during the inactive phase).

EEG sleep phenotyping

One *Zfhx3*$^{Flox/Flox}$; *Six3*-Cre^{+} and two *Zfhx3*$^{Flox/Flox}$ littermate controls aged between 4-6 months underwent surgery for EEG sleep phenotyping. Mice were anaesthetised with isofluorane and implanted with a transmitter that measures electroencephalography (EEG) and electromyography (EMG) (Data Sciences, HD-X02). Leads from the

transmitter were led, subcutaneously, to the skull, where holes were drilled to implant EEG-screw electrodes, the screws were then covered with dental acrylic. EMG electrodes were attached to the muscle in the nape of the neck. Animals were able to freely move while assessed in their home-cage environment. Dataquest Ponemah Core software (version 6.40, DSI) was used to acquire the EEG/EMG data. Electrical activities were sampled at 500 Hz, with a bandwidth applied to acquire data between 0.5-80 Hz and a humbug filter that cut out 50 Hz noise. Following surgery, 5-7 days recovery was allowed before recording. At the end of the recovery period, baseline sleep recording was carried out for 2 days prior to 6 hours sleep deprivation and then 2 days further recording undertaken to monitor recovery. Sleep deprivation was achieved via manual methods such as air puffs and light cage manipulation to keep the animal awake. EEG and EMG signals were continuously acquired through all protocol conditions, except the 6 hours of sleep deprivation. EEG data was imported into NeuroScore software (DSI systems) for sleep staging and analysis. Vigilance states were analysed in 10 second epochs and identified based on the combination of EMG data and EEG power spectra. Epochs with artefacts were excluded from analysis. Percentage time spent in wakefulness, REM and NREM sleep was calculated for both light and dark phases.

Pupillometry

Mice were dark adapted for 1–2 hours prior to testing. A xenon arc lamp (150 W solar simulator, Lot Oriel, UK) was used to produce a light intensity of 14.6 log quanta/cm^2/s (173 lW/cm^2/s) for bright light, 11.6 log quanta/cm^2/s (0.17 lW/cm^2/s) for mid light and 10.4 log quanta/cm^2/s (0.1 lW/cm^2/s). Light was transmitted to the eye via

a liquid light pipe as an irradiant light stimulus using a two inch integrating sphere (Pro-lite Technology, UK). Images of the consensual pupillary light response were collected with a Prosilica near infrared sensitive charge couple device video camera (BRSL) at a rate of 10 frames / s. The camera was positioned perpendicular to the contra-lateral eye, which was illuminated by infra-red light emitting diodes (850 nm, 10 nm half-bandwidth). In this way, consensual pupil responses could be measured in response to an irradiant light stimulus. Animals remained un-anaesthetized during the procedure but were temporarily restrained by "scruffing", using normal husbandry techniques for the duration of the recording (29 secs). After brief baseline measurements of the dark-adapted pupil (2 secs), the left eye was exposed to the light stimulus for 10 secs. The stimulated eye was not dilated using Tropicamide. Recovery data were collected for a post-stimulus period of 17 secs. Each animal was tested on multiple occasions to minimise any artefacts due to handling. Images were analysed using MB-Ruler to measure pupil diameter and pupil area calculated (Markus Bader, Germany).

In-situ probe generation

Constructs for *in situ* hybridisation were amplified by PCR from genomic DNA. Primers: *Avp* (1–490 bp of accession number NM_009732.1), *Vip* (191–715 bp of NM_011702.1), *Rora* (Forward: TGACTGGCGTAGCTTTTCCT, Reverse: ACATGGTTTAAGCCCACAGC). The PCR product was then processed using Qiagen Quick PCR clean up kit as per manufacturer's instructions. The clean PCR fragment was then cloned using a TOPO TA Cloning Kit for Sequencing (Invitrogen, Life Technologies) as per manufacturer's instructions, the pCR 4-TOPO vector and 2 µl

PCR product was used in the cloning reaction. A subsequent 4 µl of the cloning reaction was used to transform α-select competent cells (Bioline, Meridian Bioscience) as per manufacturer's instructions. Cells were streaked onto Ampicillin containing agar plates and incubated overnight to select colonies containing cloned fragment. Single colonies were picked used a pipette tip and added to 5 ml LD media + 100 µg/ml ampicillin, this was then incubated at 37°C overnight in a shaking incubator at 220 rpm. Plasmid purification was performed using a QIAGEN mini prep kit as per manufacturer's instructions and plasmid DNA eluted in a final volume of 30 µl. This was then sequenced using stock primers for T3 at Source Biosciences (Oxford, UK). Clones containing the fragment in the desired orientation were linearised by restriction digest using 2 µl PstI enzyme in a 30 µl reaction, this was then ran out on an agarose gel and the correct size band excised. The excised fragment was purified using a QIAGEN gel purification kit as per manufacturer's instructions. 250-500 ng linearised DNA was incubated for 90 minutes at 37°C with 2 µl 10x DIG labelling mix, 2 µl 10x polymerase buffer, 1 µl RNasin, 2 µl RNA polymerase and H_2O up to a final volume of 20 µl. The probe was then purified using a Roche QuickSpin RNA column kit (Roche Life Science, US).

In-situ hybridisation staining

Brains were collected at ZT3 and frozen in OCT compound on dry ice then stored at -80°C until sectioning. Brains were sectioned on a cryostat at 15 µM and collected onto slides then stored at -80°C until staining. The procedure was carried out under RNAse free conditions. All glassware was baked prior to use and all solutions were made using DEPC-treated H_2O and then autoclaved. Surfaces and apparatus were regularly

cleaned with RNAse-Zap (Sigma-Aldrich, UK) and rinsed with DEPC treated H_2O and filter tips were used throughout. Prior to in *situ* hybridisation, slides were brought to RT for 1 hour. Slides were then fixed in 4% PFA in PBS at RT for 15 minutes followed by three 3 minute washes in PBS. The slides were then placed into acetylation mix (442 ml DEPC H_2O, 5.69 ml Triethanolamine, 780 µl concentrated Hydrochloric Acid) and 1 ml acetic anhydride added dropwise over 4 minutes before being left to incubate for a further 6 minutes. Slides then underwent three 5 minute PBS washes. The back of the slides were then wiped and left on a slide rack for 1 minute and the sections were outlined with a PAP pen. 500 µl hybridisation solution (2.5 ml Deionisied Formamide 100%, 100 µl *E. Coli* tRNA (10 mg/ml), 100 µl 1X Denhardts50 X, 0.5 g Dextran sulphate, 0.175 g NaCl, 0.012 g SDS, 10 µl 0.5M EDTA pH 8.0, DEPC H_2O up to 5ml) was added to each slide and left to incubate for 1 hour at RT. During the incubation, 80 ng of probe was added to 200 µl of hybridisation solution (this was multiplied by the number of slides being processed) and left to mix by rotating at RT for 1 hour. The slides were then drained onto tissue and 200 µl of the probe-hybridisation mix was added to each slide. Parafilm was then placed over each slide before transferring to the *in situ* chamber with 20 ml 5X SSC, 50% formamide in the bottom of the chamber. This was then incubated for 16-20 hours at 60°C. Each slide was placed into a 50 ml Falcon tube containing 30 ml 5 X SSC. The Falcon tubes were then left to incubate for 5 minutes at 70°C or until the parafilm started to detach from the slides. The parafilm was removed and the slides were incubated in 0.2 X SSC at 70°C for 1 hour. The slides were then placed in fresh 0.2 X SSC and incubated for 5 minutes at RT followed by another 5 minute incubation in buffer B1 (30 ml 5M NaCl, 100 ml 1M Tris-HCl pH 7.6) at RT. The backs of the slides were then wiped and 500 µl blocking solution was added to each slide and left to incubate for 1 hour at RT. During

this incubation, anti-DIG antibody was diluted 1:5000 in blocking reagent and left to mix at 4°C on a rotator for 1 hour prior to use. After the blocking incubation, the slides were drained and 500 µl anti-DIG solution added to each slide and incubated overnight at 4°C. The following day, slides were washed 3 X 5 minutes in buffer B1 at RT. The slides were then left to incubate in buffer B2 (10 ml 5M NaCl, 50 ml 1M Tris-HCl pH 9.5, 25 ml 1M $MgCl_2$) for 5 minutes at RT. In a dark-room, the slides were drained and 500 µl detection mix (100 ul NBT/BCIP per 5 ml of B2 buffer) was added to each slide. The slides were then placed in an incubation chamber, humidified with water and left for 12 – 48 hours in the dark at RT until the colour development was complete. Following this, slides were washed twice for 5 minutes in PBS before visualising.

Nissl staining

Brains were collected at ZT3 and frozen in OCT compound on dry ice then stored at -80°C until sectioning. Brains were sectioned on a cryostat at 15 µM and collected onto slides then stored at -80°C until staining. Slides were thawed and briefly washed in PBS before fixation in 4% ice cold PFA for 10 mins, then washed with PBS again. Following this sections were stained in 0.1% Cresyl Violet solution for ~15 minutes until staining had visually developed. Sections were then rinsed with dH20 and washed in 70% ethanol before being dehydrated via two 3 min incubations in 100% ethanol. Slides were then incubated in Xylene until mounting to clear the sections and coverslipped using DPX mountant.

H&E staining

Brains were collected at ZT3 and frozen in OCT compound on dry ice then stored at -80°C until sectioning. Brains were sectioned on a cryostat at 30 µM and collected onto slides then stored at -80°C until staining. On the day of staining, slides were thawed for at least 30 minutes at RT then fixed in 4% ice cold PFA for 10 mins and washed with PBS. Slides were then placed in racks and stained using Gills III haematoxylin and counterstained with Eosin on a Sakura Automatic Stainer (Sakura Finetec). Slides were then coverslipped using clearium mounting media (Leica Biosystems).

qRT-PCR

Brains were removed and placed into a brain matrix (Kent Scientific, Torrington CT, USA). A skin graft blade (Swann-Morton, Sheffield, UK) was positioned at Bregma −0.10 mm. A second blade was placed 1 mm (Bregma −1.10) caudal from the first, and a 1 mm thick brain slice was dissected. SCN punches were taken using a sample corer (1 mm internal diameter, Fine Science Tools GmbH, Heidelberg, Germany) from the brain slice, fresh frozen on dry ice and stored at −80°C prior to RNA extraction. RNA was extracted from SCN tissue punches using the Maxwell 16 Instrument (Promega, UK) using the Maxwell LEV simplyRNA tissue kit (Promega, UK) as per instructions. The sample was homogenised in 250 µl of homogenisation solution in homogenisation bead tubes (1.5 mm beads, Sigma Aldrich, UK) using the Fast Prep FP120 instrument (Thermo Scientific, UK) set at speed 6.5 for 20 sec. Maxwell 16 cartridges were set up following manufacturer's instructions. RNA was eluted in 40 µl water. cDNA synthesis was performed using the High Capacity cDNA RT kit (ThermoFisher

Scientific) starting with 2 µg of total RNA. cDNA for qRT-PCR amplification was used at a final concentration of 10 ng per well. Technical replicates were ran for all samples. Fast Sybr Green mastermix (ThermoFisher Scientific) was used with a final volume of 20 µl. Primers were used at a final concentration of 360 nM. Fold changes were calculated using the $\Delta\Delta C_t$ method using the 7500 Software v2.0.6 and normalised using actin as a housekeeping control gene (Livak and Schmittgen, 2001).

Retinal MEA recording

Multielectrode arrays were used to record from *Zfhx3*$^{Flox/Flox}$; *Six3*-Cre^{+} retinas as previously described (Hughes et al., 2016). Mice were culled by cervical dislocation at ZT6–8, followed immediately by enucleation and dissection of retinae under dim red light conditions (>610 nm) in AMES media (Sigma) bubbled with 95% O_2 5% CO_2 (pH 7.4). Retina were then placed ganglion cell side down onto glass bottomed MEA chambers containing 60 electrodes each 30 µm in diameter and spaced 200 µm apart (Multi Channel Systems) and anchored in place with glass coated metal harps (ALA Scientific Instruments). MEA chambers were placed into the MEA recording device (MEA1060-Inv, Multi-Channel Systems), fitted with a gas permeable perfusion manifold (ALA Scientific Instruments), and mounted onto the stage of an inverted Olympus IX71 microscope so that the recording electrodes were positioned in the microscope light path. Retinae were continuously perfused at 2 ml/minute with AMES media bubbled with 95% O_2 5% CO_2 (pH 7.4) and maintained at 34 °C using a combination of water bath heater (36 °C), in-line perfusion heater (35 °C), and base plate heater incorporated into the MEA system (34 °C) to minimise temperature fluctuations in the sample chamber. Recorded signals were collected, amplified and

digitized at 25 KHz using MC Rack software (Multi Channel Systems). Retinae were perfused in the dark for 60 minutes prior to recording of light responses. For all recordings baseline activity was recorded for 30–60 s prior to light stimulation. For recording of flash ERG type responses retina were stimulated with 500 ms flashes of light. Retinae were dark adapted for 20 minutes between bouts of recordings. For blockade of input from rod and cone photoreceptors a cocktail of synaptic blockers was added to the media containing 100 µM L(+)-2-amino-4-phosphonobutyrate (L-AP4) (group III metabotropic glutamate receptor agonist), 40µm 6,7-dinitroquinoxaline-2,3-dione (DNQX) (AMPA/kainate receptor antagonist), and 30 µM d-2-amino-5-phosphonovalerate (d-AP5) (NMDA receptor antagonist) (all from Tocris, Bristol, UK). Monochromatic light stimuli (360 nm and 500 nm, bandwidth 20 nm) were generated by a Xenon arc light source with a slit monochromator (Cairn Optoscan) and delivered via a 10x microscope objective beneath the MEA chamber. Duration and wavelength of light stimuli were controlled via Metafluor software (Molecular Devices). Intensity of light stimuli were adjusted using neutral density filters (0 to 4 log units, Thor Labs) and controlled via an automated filter wheel (Prior Scientific) placed into the microscope light path. The power of light stimuli (µW/cm^2/s) was measured at the sample focal plane using an in-line power meter (PM160T, Thor Labs), with power measurements converted to irradiance (photons/cm^2/s) using an irradiance conversion toolbox.

Slit lamp

The anterior segment, including lens and cornea was assessed using a slit lamp as described in (Thaung et al., 2002). Mice were restrained by light scruffing and held up

to the slit lamp, where the light is centered onto the mouse's eye. The procedure was performed in a dark room with the light of the slit lamp being slowly brightened to ensure pupil constriction.

Optokinetic drum

Mice were acclimatised for 30 minutes to the phenotyping room prior to starting the test. Mice were then individually placed onto a raised circular platform of 8 cm diameter in the centre of four screens each displaying the same black and white vertical bar pattern. The mouse was allowed to settle for 30 seconds before starting the test. The frequencies of the stripes used were 0.25 cycles / degree (subtending an angle of 2° when viewed from the centre of the drum), 0.125 cycles / degree (4°), or 0.0625 cycles / degree (8°). The pattern was rotated anticlockwise for 30 seconds at a rotation speed of two revolutions per minute (12°/sec) to assess right eye ability and repeated clockwise to assess left eye ability. During the rotations, the mouse was observed for its head tracking response. The test started with the 2° stripe and if no head tracking response was observed, the stripe was increased to 4° and 8°.

Body composition analysis

Body mass was measured on scales calibrated to 0.01 g. Analysis of body composition was performed either by DEXA using the Lunar PIXImus Mouse Densitometer (Wipro GE Healthcare, Madison, WI) or using an Echo MRI whole body composition analyzer (Echo Medical System, USA). Percentage fat and lean mass were recorded.

Metabolic caging

Mice were individually housed in PhenoMaster cages (TSE Systems, Bad Homburg, Germany) for 3 days, collection of energy intake/expenditure related data was carried out during the final 24 hours of this time. The cage system includes a photobeam-based activity monitoring system that records ambulatory movements in the horizontal and vertical planes. Food and water were available *ad libitum* throughout testing. Measures for activity/distance travelled, O_2 consumption, CO_2 production and energy expenditure were taken.

Corticosterone analysis from urine

Mice were singly housed on a 12:12 LD cycle. Urine was collected from mice at every 4 hours across the LD cycle by scruffing and collection of voluntary urination into an Eppendorf tube, urine was then kept at -20°C until use. Corticosterone levels were analysed using an AssayMax ELISA kit (AssayPro, St Charles USA) as per manufacturer's instructions.

Open field

Four square arenas (44x44 cm) were set up in a square in a small testing room with a video camera overhead. Lighting in arenas was set at 150-200 lux. A minimum of two and a maximum of four mice were tested at one time, one mouse per arena. Arenas were cleaned with 70% ethanol before and after each trial. Each mouse was placed in the arena and recorded using video tracking software (Ethovision, Noldus, Netherlands) for 20 minutes. All open field testing was carried out in the morning,

between 8am and 12am. Videos were analysed using Ethovision software. Each arena was divided into three zones, periphery (8 cm from the edge of the arena), centre (an 11x11 cm box in the centre of the arena), and the remaining intermediate zone. Parameters measured for each zone were; total distance moved, frequency of zone entries and duration in zones.

Light-Dark box

The test arena consisted of a high sided Perspex box split into two areas, one third with black walls and a black lid, enclosed except for a small opening that led to the light side, and two thirds consisting of clear walls, a white floor and no lid. Light levels in the open side of the light dark box were set at 100 lux. One mouse at a time was placed in the open side of the box facing away from the door. Video tracking was started. After 5 minutes the mouse was removed and placed back into its home cage. The light dark box was cleaned before each run with 70% alcohol. Video tracking was analysed using Ethovision software and parameters analysed included duration in light side, duration in dark side and number of crosses between light and dark zones.

Statistics

Statistical analyses were performed using In-Vivo Stat (v3.7) and GraphPad Prism Software (v7). Shapiro-Wilk testing was used to test for normality of data to decide whether parametric or non-parametric analysis was to be conducted. If data was deemed normally distributed then regular ANOVA or student's t-test was used where applicable. If data was deemed to be not normally distributed then Kruskal-Wallis

ANOVA or non-parametric t-test was used where applicable. Following ANOVA, Tukey and Dunn's multiple comparison testing was performed for parametric and non-parametric data respectively.

Results I

Characterisation of a conditionally-induced knockout of Zfhx3 in adult mice

Introduction

Previous work on *Zfhx3* has highlighted its crucial role in cell cycle arrest (Jung et al., 2005b) and neuronal differentiation (Ishii et al., 2003; Miura et al., 1995). Aberrant *Zfhx3* function has also been attributed in the development of various cancers (Cho et al., 2007; Sun et al., 2015; Sun et al., 2007) and atrial fibrillation (Benjamin et al., 2009; Gudbjartsson et al., 2009). ZFHX3 is highly expressed in the embryonic brain before undergoing significant downregulation post birth, whereby expression is restricted to a number of localised nuclei (Watanabe et al., 1996). One such area that retains high ZFHX3 expression in the adult brain is the SCN (Lein et al., 2007b), which suggests a key role for the transcription factor in this brain region. Constitutive knock-out (KO) of *Zfhx3* results in pre-weaning sub lethality in heterozygote mutants (Sun et al., 2012), and the ENU mutant $Zfhx3^{Sci}$ was shown to be homozygous perinatal lethal (Parsons et al., 2015). Subsequent studies on heterozygous *Sci* mutants revealed that *Zfhx3* function is necessary during development to maintain stable circadian rhythms, and also identified a role for *Zfhx3* in sleep interval timing in mice (Balzani et al., 2016; Parsons et al., 2015). However, all of these previous studies were conducted on mutants where developmental functions of *Zfhx3* are disrupted. Considering the pleiotropic nature of this gene, it was of paramount importance to study the role of *Zfhx3* in the adult mouse – irrespective of its developmental functions. To achieve this, a tamoxifen inducible Cre line (Ruzankina et al., 2007) was employed, allowing gene expression to be unaltered during development and then abolished in adulthood. Conditional mutagenesis approaches have been previously successful in characterising dual functions of circadian related genes, such as LHX1 (Hatori et al., 2014) and *Bmal1* (Yang et al.,

2016). By studying the effects of this adult specific *Zfhx3* KO mouse, an adult specific function of *Zfhx3* in circadian biology could be investigated.

Characterisation of Cre activity using a Lac-Z reporter

In order to delete *Zfhx3* in the adult mouse, a ubiquitously expressed inducible Cre line was employed: UBC-Cre, which is driven under the modified oestrogen receptor ERT2 (Ruzankina et al., 2007). UBC-Cre is a ubiquitously expressed Cre driver line, in which recombinase activity is triggered following dosing of the mutant mouse with tamoxifen. The UBC-Cre line was initially crossed to a ubiquitously expressed *Rosa26* reporter to map evidence of Cre activity in adult brain and other tissues, both before and after tamoxifen administration. In this reporter line, lac-Z is flanked by LoxP sites; upon exposure to Cre recombinase, lac-Z can be detected using X-Gal staining – thus providing a proxy for the pattern of Cre activity in the Cre line being tested. Before any tamoxifen dosing was used, embryos were harvested from this line to establish whether leaky Cre was evident during development (**Figure 1**). There was no detectable staining in E12.5 whole embryos when the Cre was paternally inherited, although some faint scattered staining was apparent in the cortex of E18.5 brains. Adult mice (~2.5 months of age) produced from this UBC-Cre-R26R cross were dosed using the same method that would be used for dosing mutant animals (see Methods). Tamoxifen was administered daily for 5 days via oral gavage; mice were then left to recover for 1 week before tissues were harvested and stained. Substantial X-Gal staining was present across a variety of tissues post tamoxifen dosing, indicating the Cre line to be sufficient to induce recombination in the experimental mutant line (**Figure 1.2**). Some very sparse staining was also observed

pre tamoxifen in the cortex of adult brain, however this was not reflected by an equivalent protein loss in the experimental mutant lines (**Figure 1.3**).

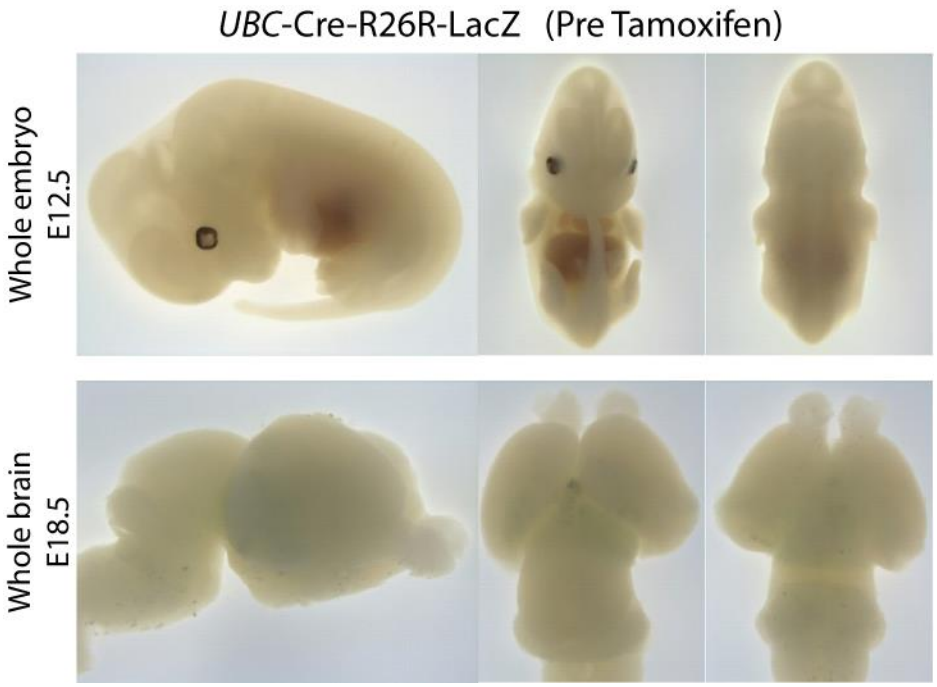


Figure 1.1 | Representative X-Gal staining in E12.5 embryo and E18.5 whole brain of the tamoxifen inducible Cre line (UBC-Cre) crossed to a Lac-Z reporter line (R26R) pre tamoxifen dosing. Blue staining indicates areas where Cre is active.

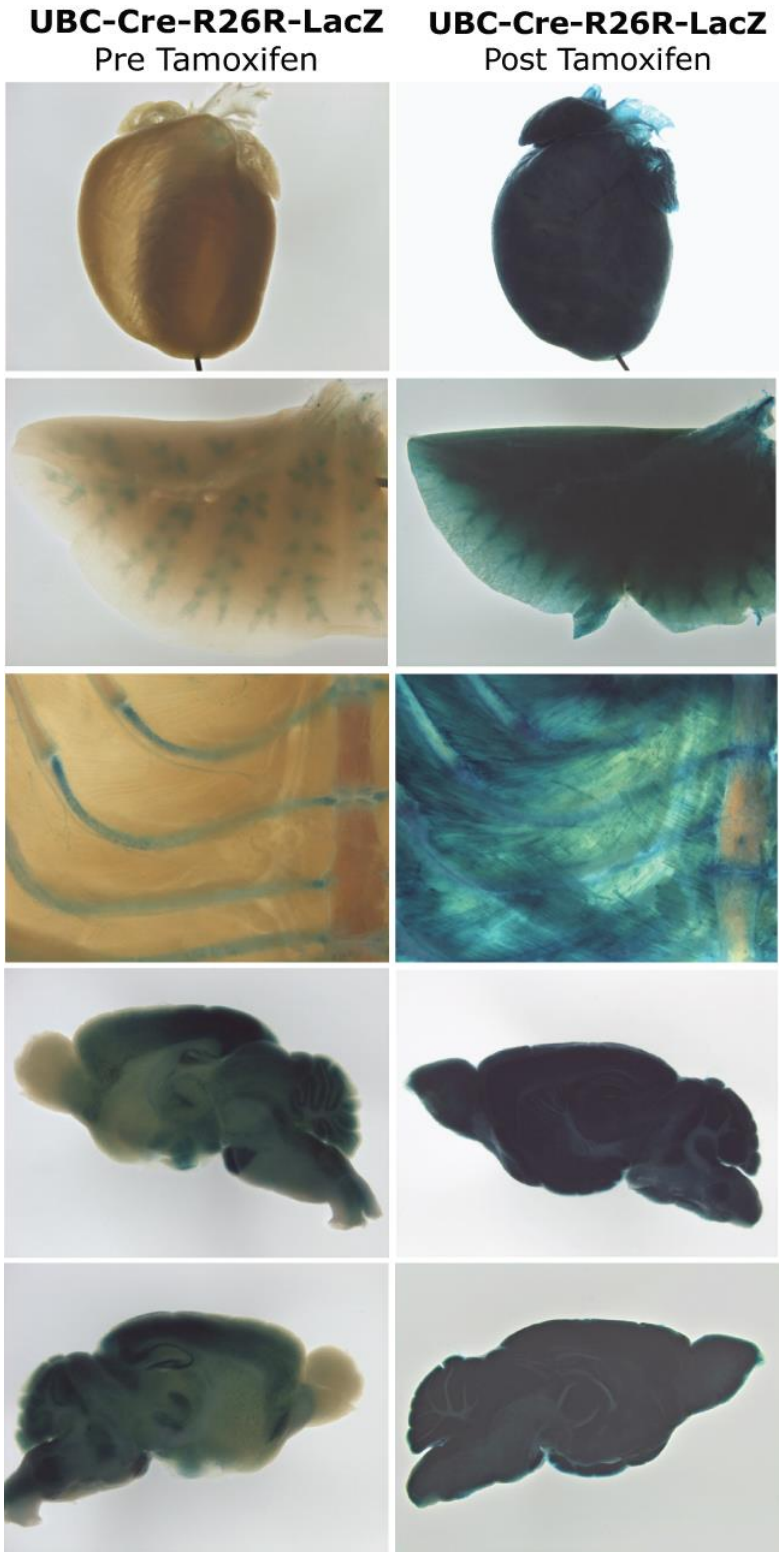


Figure 1.2 | Representative X Gal staining in heart, lungs, thorax and brain of the tamoxifen inducible Cre line (UBC-Cre) crossed to a Lac-Z reporter line (R26R). Blue staining indicates areas where Cre is active pre/post tamoxifen dosing.

ZFHX3 staining is lost in adult *Zfhx3*$^{Flox/Flox}$; UBC-Cre^{+} SCN following tamoxifen treatment

Once the UBC-Cre line had been validated using the R26R reporter line, the Cre driver mice were crossed to a *Zfhx3*^{Flox} line (Sun et al., 2012) to generate inducible *Zfhx3* KO mice. As discussed previously (see general Introduction chapter), an initial cohort of *Zfhx3*$^{Flox/+}$; UBC-Cre^{+} mice were generated that were then crossed to *Zfhx3*$^{Flox/+}$ mice to generate the experimental cohorts for circadian characterisation. The following control genotypes were produced from this cross: *Zfhx3*$^{+/+}$, *Zfhx3*$^{Flox/+}$, *Zfhx3*$^{Flox/Flox}$ and *Zfhx3*$^{+/+}$; UBC-Cre^{+}. *Zfhx3*$^{Flox/+}$; UBC-Cre^{+} and *Zfhx3*$^{Flox/Flox}$; UBC-Cre^{+} mice were also produced; these would form the heterozygote and homozygote mutant cohorts respectively, following tamoxifen dosing.

Immunofluorescence was undertaken on SCN sections from these animals to investigate the extent of protein loss following tamoxifen treatment, and also to ensure that there was no loss of ZFHX3 prior to tamoxifen dosing due to leaky Cre expression. Prior to tamoxifen treatment, there was no obvious reduction in ZFHX3 staining in *Zfhx3*$^{Flox/Flox}$; UBC-Cre^{+} mice compared to control SCN from a *Zfhx3*$^{Flox/+}$ mouse. Following treatment, however, ZFHX3 staining is effectively absent in the SCN of *Zfhx3*$^{Flox/Flox}$; UBC-Cre^{+} brain. SCN sections from control genotypes show no evident decrease in ZFHX3 staining following tamoxifen treatment (**Figure 1.3)**. This result confirmed that UBC-Cre was a suitable driver Cre to delete ZFHX3 in adult SCN, where *Zfhx3* is highly expressed, and therefore the *Zfhx3*$^{Flox/Flox}$; UBC-Cre^{+} line could be considered a true inducible KO of *Zfhx3* for circadian characterisation.

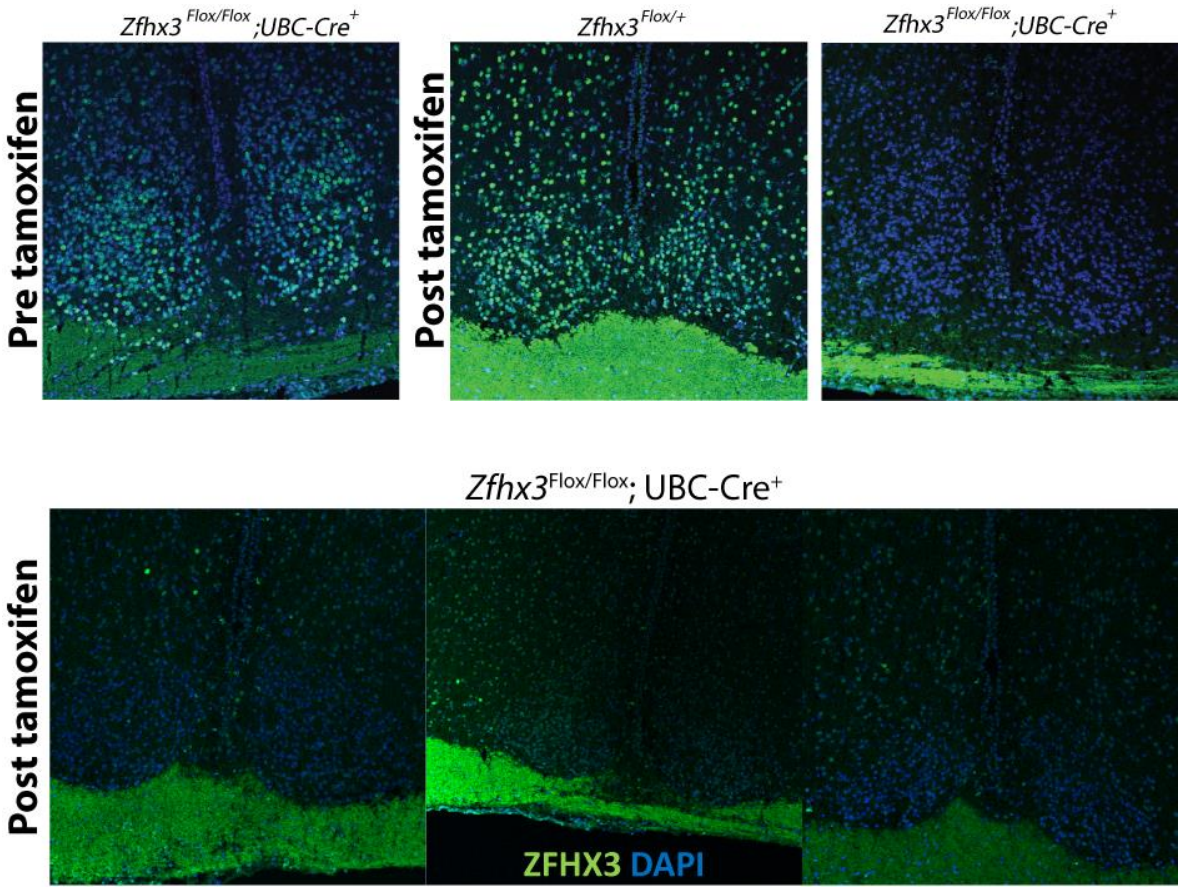


Figure 1.3 | Above: Representative ZFHX3 immunofluorescence in SCN sections of *Zfhx3*$^{Flox/Flox}$; UBC-Cre^{+} mice pre and post tamoxifen, and of *Zfhx3*$^{Flox/+}$ control mice post tamoxifen. **Below**: Three more examples of individual *Zfhx3*$^{Flox/Flox}$; UBC-Cre^{+} SCN sections following tamoxifen treatment. ZFHX3 immunopositive cells were undetectable following tamoxifen dosing in *Zfhx3*$^{Flox/Flox}$; UBC-Cre^{+} mice while staining remains robust in *Zfhx3*$^{Flox/+}$ SCN. Blue: DAPI, Green: ZFHX3.

Circadian activity is significantly altered following *Zfhx3* deletion

All genotypes generated underwent circadian analysis (data shown in **Table 1.4**). However, for uniformity and clarity, *Zfhx3*$^{Flox/Flox}$; UBC-Cre^{-} mice have been used as the representative control group in figures, as no significant differences were found between control groups. A cohort of *Zfhx3*$^{Flox/Flox}$; UBC-Cre^{+} mice [n=10] and all controls were screened for changes in circadian parameters both before and after

tamoxifen treatment using wheel running to collect activity data (Banks and Nolan, 2011). Reassuringly, there were no significant group differences in any circadian parameters analysed prior to tamoxifen treatment (**Table 1.4**). Following tamoxifen treatment seven out of ten *Zfhx3*$^{Flox/Flox}$; UBC-Cre^{+} mice displayed a significant shortening of τ_{DD} [$F(4,41)=28.4$; $p<0.0001$]. Subsequent between group comparisons confirmed that this shortening of τ_{DD} was significantly different to all other genotypes analysed; this was corrected using Bonferroni adjustment to confirm statistical significance (adjusted p values all $p<0.005$ for *Zfhx3*$^{Flox/Flox}$; UBC-Cre^{+} vs all other genotypes). In addition to this, three *Zfhx3*$^{Flox/Flox}$; UBC-Cre^{+} mice became arrhythmic in DD following tamoxifen treatment (**Figure 1.4**). A comparison of Chi-squared periodograms in these animals pre- and post-tamoxifen showed a loss of significant peak amplitude following tamoxifen treatment (**Figure 1.4C**).

Amplitude was also decreased in *Zfhx3*$^{Flox/Flox}$; UBC-Cre^{+} animals post tamoxifen [$p=0.0034$], however this did not remain statistically significant following multiple testing correction. Direct comparison of pre and post tamoxifen values for φ (phase angle of entrainment) and α_{DD} (activity time in DD) in *Zfhx3*$^{Flox/Flox}$; UBC-Cre^{+} revealed a decrease in both values that did not survive multiple testing correction. Despite that, these results confirmed that a complete loss of adult *Zfhx3* significantly disrupts normal circadian behaviour. *Zfhx3*$^{Flox/+}$; UBC-Cre^{+} mutant mice showed no changes to the circadian parameters measured following tamoxifen dosing, this was also the case for all control genotypes (**Table 1.4**). Therefore, it appears that one functional *Zfhx3* allele is sufficient for normal circadian behaviour in the adult mouse.

When studying the actograms produced by *Zfhx3*$^{Flox/Flox}$; UBC-Cre^{+} mice post tamoxifen, mice appeared to display more activity in the light phase than before

tamoxifen dosing. To analyse whether the daily pattern of activity over 24 hours differed in tamoxifen treated *Zfhx3*$^{Flox/Flox}$; UBC-Cre^{+} animals compared to controls (*Zfhx3*$^{Flox/Flox}$ mice), average wheel running activity was measured in 6 minute time bins over the 24 hour LD cycle. Following tamoxifen treatment, all *Zfhx3*$^{Flox/Flox}$; UBC-Cre^{+} mice showed an increased proportion of activity in the light phase of a standard 12:12 LD cycle. The interaction between this and tamoxifen treatment was found to be significant [$F(4,446)=3.91$; $p=0.0081$], however significant changes did not survive multiple testing correction. Investigation of total activity over 24 hours (**Figure 1.5**) revealed that tamoxifen treated *Zfhx3*$^{Flox/Flox}$; UBC-Cre^{+} animals showed a significantly different average pattern of activity compared to controls [$F(240,4079)=2.03$; $p=0.0001$]. This difference was clear at two stages of the dark phase: firstly, during the early period of the dark phase *Zfhx3*$^{Flox/Flox}$; UBC-Cre^{+} animals showed elevated activity compared to controls and secondly, during the late period of the dark phase *Zfhx3*$^{Flox/Flox}$; UBC-Cre^{+} animals showed decreased activity compared to controls. Moreover, *Zfhx3*$^{Flox/Flox}$; UBC-Cre^{+} mutants appeared to show an increase in activity prior to the onset of the dark phase when compared to control mice.

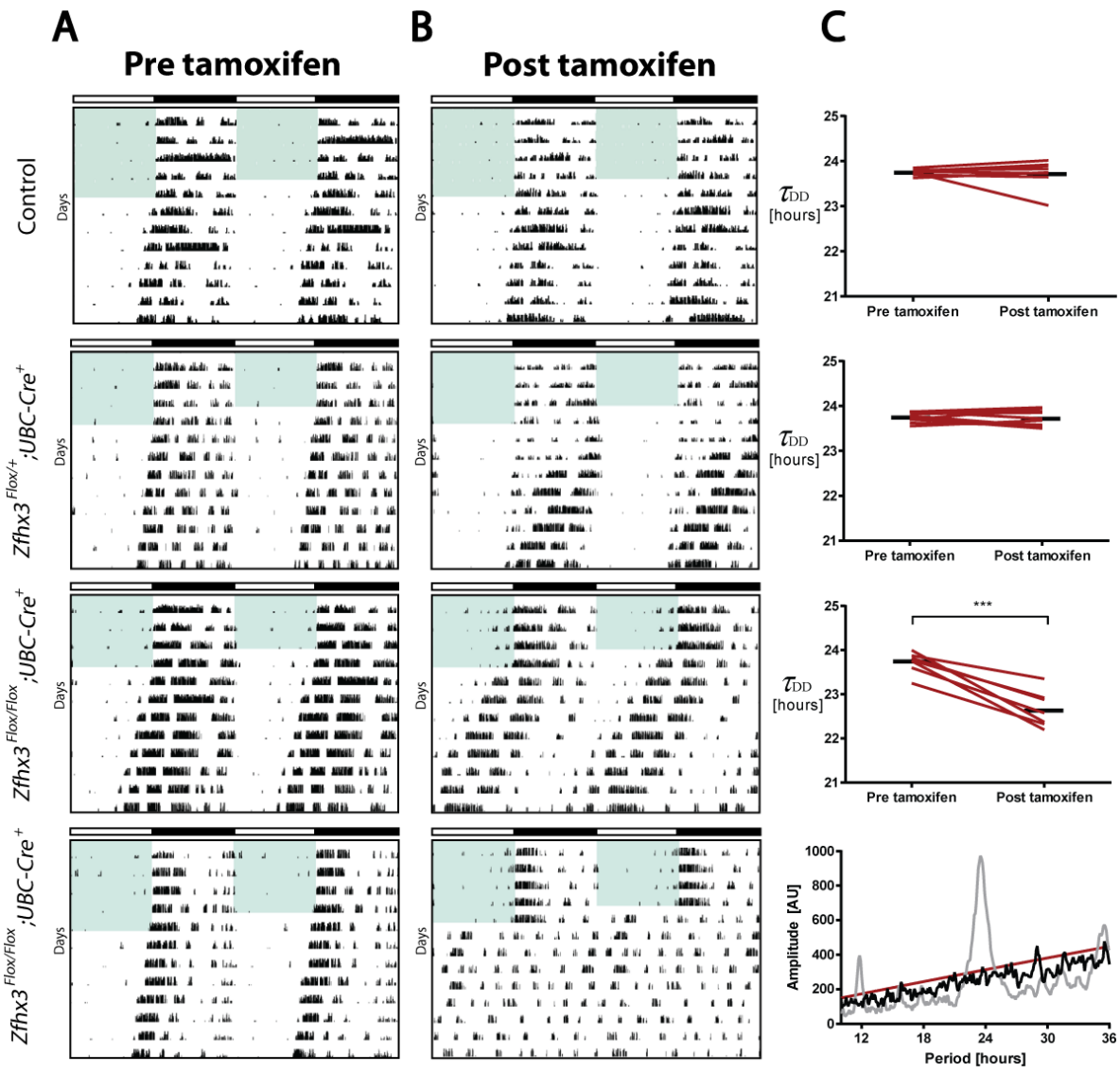


Figure 1.4 | Representative double-plotted actograms for *Zfhx3*$^{Flox/Flox}$; UBC-Cre^{+} [n=7], *Zfhx3*$^{Flox/+}$; UBC-Cre^{+} [n=11] and control (*Zfhx3*$^{Flox/Flox}$) mice [n=8] pre (**A**) and post tamoxifen (**B**). **C**: Change in period in constant darkness following tamoxifen treatment for genotypes shown; ***denotes significance at $p<0.001$. A representative chi-squared periodogram in constant darkness is shown for *Zfhx3*$^{Flox/Flox}$; UBC-Cre^{+} mice that became arrhythmic following tamoxifen treatment [n=3], grey line denotes periodogram pre tamoxifen, black line denotes periodogram post tamoxifen, red line denotes chi-squared line of significance.

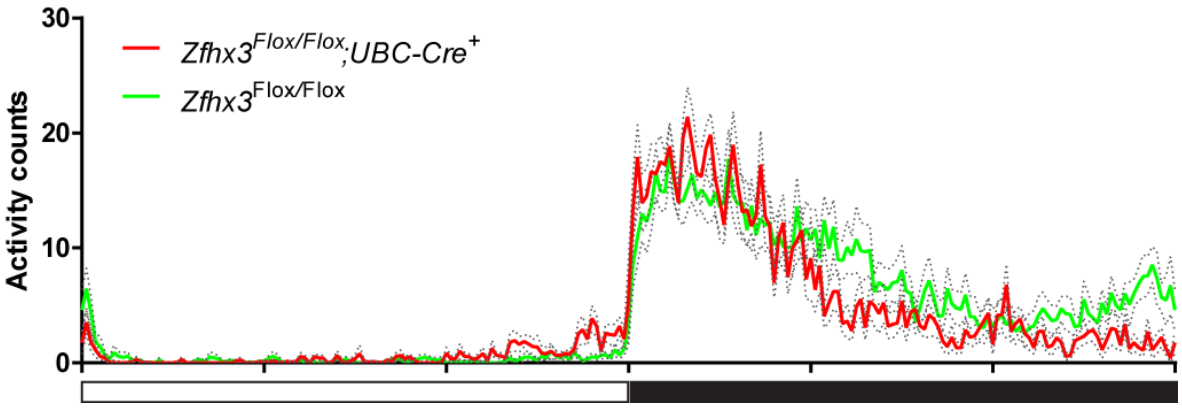


Figure 1.5 | Average activity profile for *Zfhx3*$^{Flox/Flox}$; UBC-Cre^{+} and *Zfhx3*$^{Flox/Flox}$ control mice over 12:12 LD cycle post tamoxifen [n=10]. Grey dashed lines denote SEM of data points; LD indicated underneath graph.

Zfhx3 adult KOs re-entrain faster to an advance in LD cycle

Upon release into DD, all tamoxifen-treated *Zfhx3*$^{Flox/Flox}$; UBC-Cre^{+} mice that maintained stable rhythms (i.e. did not become arrhythmic in DD) showed an initial advance in activity onset compared with this measurement prior to tamoxifen treatment [p=0.01] or in controls [p=0.002]. This advance in activity was, on average, around four hours greater than the modest advances typically seen upon release into DD from LD in controls (**Figure 1.6**). This apparent strong advance in activity onset prompted investigation into the behaviour of these mutants in jet-lag protocols. As well as this, previous work on vasopressin receptor KO mice (Yamaguchi et al., 2013) revealed a jet lag resistance phenotype, and as AVP was found to be altered in *Sci* mice (Parsons et al., 2015), this further encouraged investigation of jet-lag activity in these animals. To analyse re-entrainment to a shift in the LD cycle, animals were subjected to an abrupt six hour advance, and also delay, in the LD cycle. The number of days taken to re-entrain to the new LD cycle was measured for all groups following tamoxifen treatment (data shown in **Table 1.1**). Since a defective clock may cause

entrainment effects which are difficult to interpret, *Zfhx3*$^{Flox/Flox}$; UBC-Cre^{+} mice that were arrhythmic in DD were excluded from this analysis. However it is notable that when tested, these arrhythmic animals did resynchronise to the new LD cycle in a similar manner to rhythmic animals [number of days to re-entrain: rhythmic animals = 3.0 ±0.52; arrhythmic animals = 2.0 ±0.57; p=0.28].

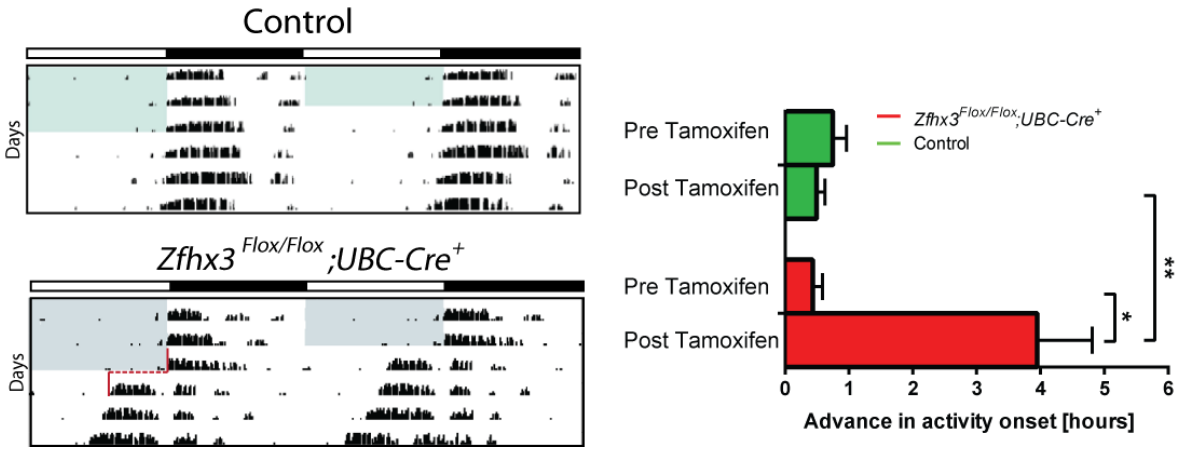


Figure 1.6 | Left: Representative actograms showing advance in activity onset upon release into DD for control and *Zfhx3*$^{Flox/Flox}$; UBC-Cre^{+} mice post tamoxifen. Right: Advance in activity onset upon release into DD. Difference in activity onset from last day of LD pre (upper bars) and post (lower bars) tamoxifen for *Zfhx3*$^{Flox/Flox}$; UBC-Cre^{+} mice (red) [n=7] and control mice (green) [n=6]. ** denotes significance at p<0.01, *denotes significance at p<0.05.

There was no significant difference in response to a 6 hour delay in the LD cycle between genotypes [F(4,214)=0.37; p=0.825]. However, there was a marked significant difference between *Zfhx3*$^{Flox/Flox}$; UBC-Cre^{+} mice and controls in response to a six hour advance in LD [F(4,39)=3.94; p=0.0088], with mutants re-entraining on average twice as fast as control mice (**Figure 1.7**). Average activity onsets in these mice advanced by around four hours on day 1 and then by almost a further two hours on day 2. Pairwise comparisons following multiple test correction demonstrated *Zfhx3*$^{Flox/Flox}$; UBC-Cre^{+} animals had an earlier onset of activity for the first two days

following the phase advance [$p<0.05$ and $p<0.01$ for *Zfhx3*$^{Flox/Flox}$; UBC-Cre^{+} for days 1 and 2 respectively following phase advance]. There were no other significant differences between genotypes throughout the time course of the experiment (**Table 1.1**).

As noted previously, *Zfhx3*$^{Flox/Flox}$; UBC-Cre^{+} animals displayed a large increase in activity onset time when first released into DD (**Figure 1.6**) and therefore the faster re-entrainment time to an advance in LD seen in these animals could be due to this. To validate whether this was the case, the advances in activity onsets that occurred on the first two days of release into DD were compared with those that occurred on the first two days of the advancing LD protocol. These advances were comparable in *Zfhx3*$^{Flox/Flox}$; UBC-Cre^{+} animals, suggesting that the effects of negative masking upon release into DD plus a faster clock accounted for differences in re-entrainment in the phase advance protocol.

Genotype	n	Days to re-entrain to advance	*p* value
Zfhx3$^{Flox/Flox}$; UBC-Cre^{+}	6	3.0 (±0.5)	n/a
Zfhx3$^{Flox/+}$; UBC-Cre^{+}	10	5.6 (±0.5)	0.0471
Zfhx3$^{Flox/Flox}$	9	4.9 (±0.7)	0.0970
Zfhx3$^{Flox/+}$	10	6.6 (±0.5)	0.0109
Zfhx3$^{+/+}$; UBC-Cre^{+}	10	6.3 (±0.7)	0.0146

Genotype	n	Days to re-entrain to delay	*p* value
Zfhx3$^{Flox/Flox}$; UBC-Cre^{+}	5	3.0 (±0.8)	n/a
Zfhx3$^{Flox/+}$; UBC-Cre^{+}	6	2.8 (±0.2)	1.0000
Zfhx3$^{Flox/Flox}$	4	3.8 (±0.6)	1.0000
Zfhx3$^{Flox/+}$	8	3.1 (±0.3)	1.0000
Zfhx3$^{+/+}$; UBC-Cre^{+}	4	3.3 (±0.5)	1.0000

Table 1.1 | Mean (± Standard Error Mean) number of days taken to re-entrain to a 6 hour advance and a 6 hour delay in the LD cycle for all genotypes tested in the jet lag protocol. All data shown is for animals post tamoxifen treatment. P values shown are for that genotype compared to *Zfhx3*$^{Flox/Flox}$; UBC-Cre+ and Bonferroni corrected for multiple comparison.

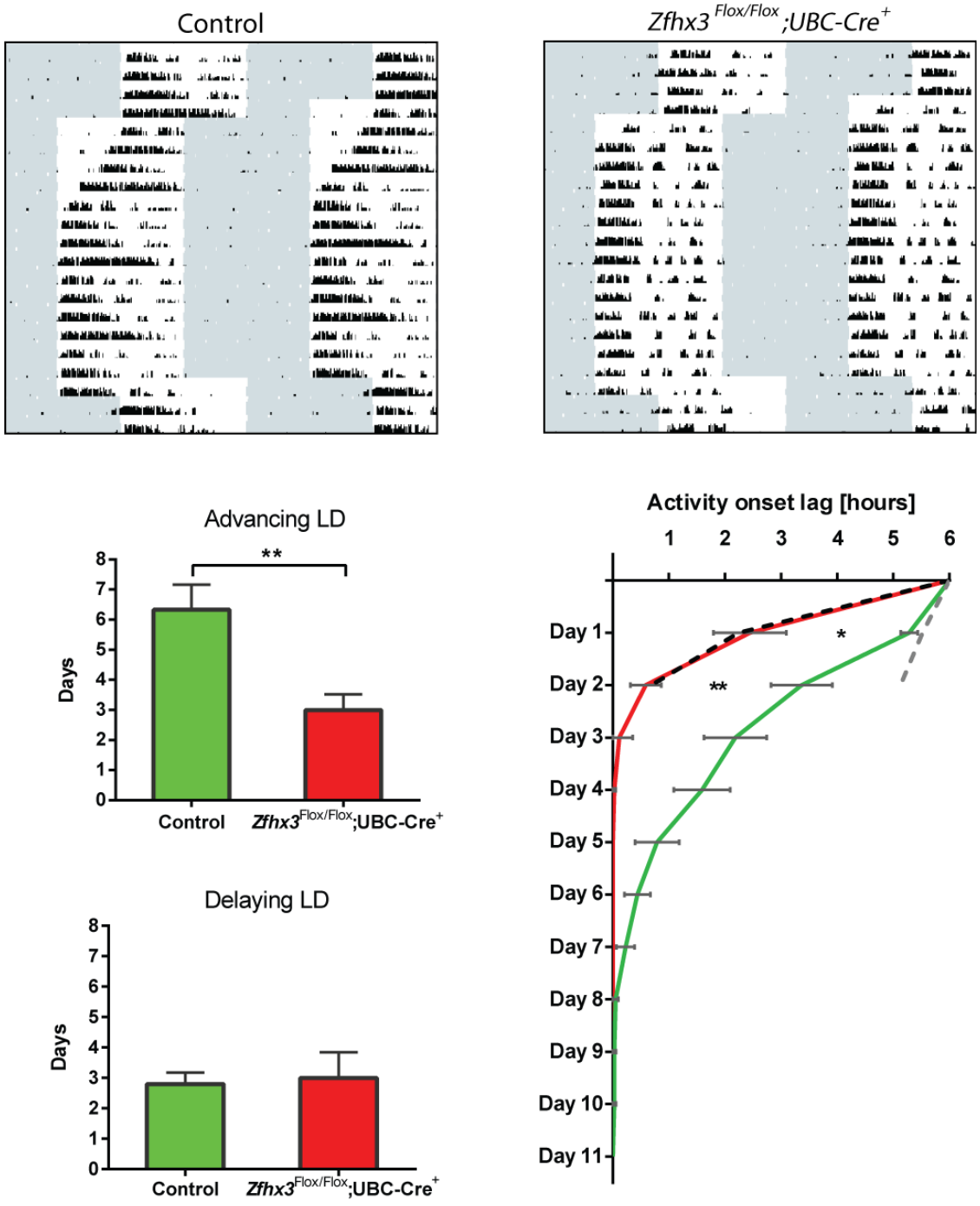


Figure 1.7 | Representative actograms showing re-entrainment of wheel-running activity in response to 6 hour advance or delay in LD cycle for control (*Zfhx3*$^{Flox/Flox}$) and *Zfhx3*$^{Flox/Flox}$; UBC-Cre^{+} mice. Average number of days taken for control and *Zfhx3*$^{Flox/Flox}$; UBC-Cre^{+} mice to re-entrain to a 6 hour advance in LD and a 6 hour delay in LD is also shown. Average activity onset lag graph shows time of onset respective to lights on for control [green, n=9] and *Zfhx3*$^{Flox/Flox}$; UBC-Cre^{+} [red, n=6] mice following an advance in LD cycle of 6 hours. All jet lag experiments were undertaken post tamoxifen treatment. For reference, dashed lines show respective advances in activity onset over the first two days following release into DD for control (grey) and mutant (black) mice. * denotes significance at $p<0.05$, ** denotes significance at $p<0.01$, error bars denote SEM of data.

Zfhx3$^{Flox/Flox}$; UBC-Cre^{+} mice show no changes to sleep behaviour following tamoxifen treatment

Zfhx3$^{Flox/Flox}$; UBC-Cre^{+}, *Zfhx3*$^{Flox/+}$; UBC-Cre^{+} and control mice underwent video tracked sleep screening to determine whether any changes to sleep behaviour were altered following tamoxifen dosing to delete ZFHX3 in mutant lines. In this screening method, periods of immobility over a 24 hour period under standard 12:12 LD conditions were used to define sleep bouts – this methodology has been shown to correlate well with EEG sleep analysis in previous evaluation studies (Fisher et al., 2012). Collected data was analysed using repeat measures ANOVA and Sidak's multiple comparison test used to compare between genotypes pre tamoxifen and post tamoxifen, as well as directly between pre/post tamoxifen within genotypes. There were no changes to the distance travelled in the light [$F(4,29)=1.096$, $p=0.3773$] and dark [$F(4,29)=0.5404$, $p=0.7072$] phase between groups. There were also no significant changes found to total time spent immobile (time asleep) in the light [$F(4,29)=1.695$, $p=0.1781$] and dark phases [$F(4,29)=0.9978$, $p=0.4246$] of the LD cycle. Average number of immobile episodes in light [$F(4,29)=0.4964$, $p=0.7384$] and dark [$F(4,29)=1.278$, $p=0.3015$] also showed no significant change following tamoxifen treatment between genotypes (**Figure 1.8**). In addition to these parameter totals, activity over time was also analysed before and after tamoxifen dosing. **Figure 1.9** shows the average distance travelled over a 24 hour time period for *Zfhx3*$^{Flox/Flox}$; UBC-Cre^{+}, *Zfhx3*$^{Flox/+}$ and UBC-Cre^{+} mutant mice, *Zfhx3*$^{Flox/Flox}$ is shown as a representative control group for clarity. There was a slight reduction in average distance travelled during the dark phase of the LD cycle for all groups following tamoxifen treatment, however this was not significant when analysed [$F(207, 1334)=1.144$, $p=0.0939$].

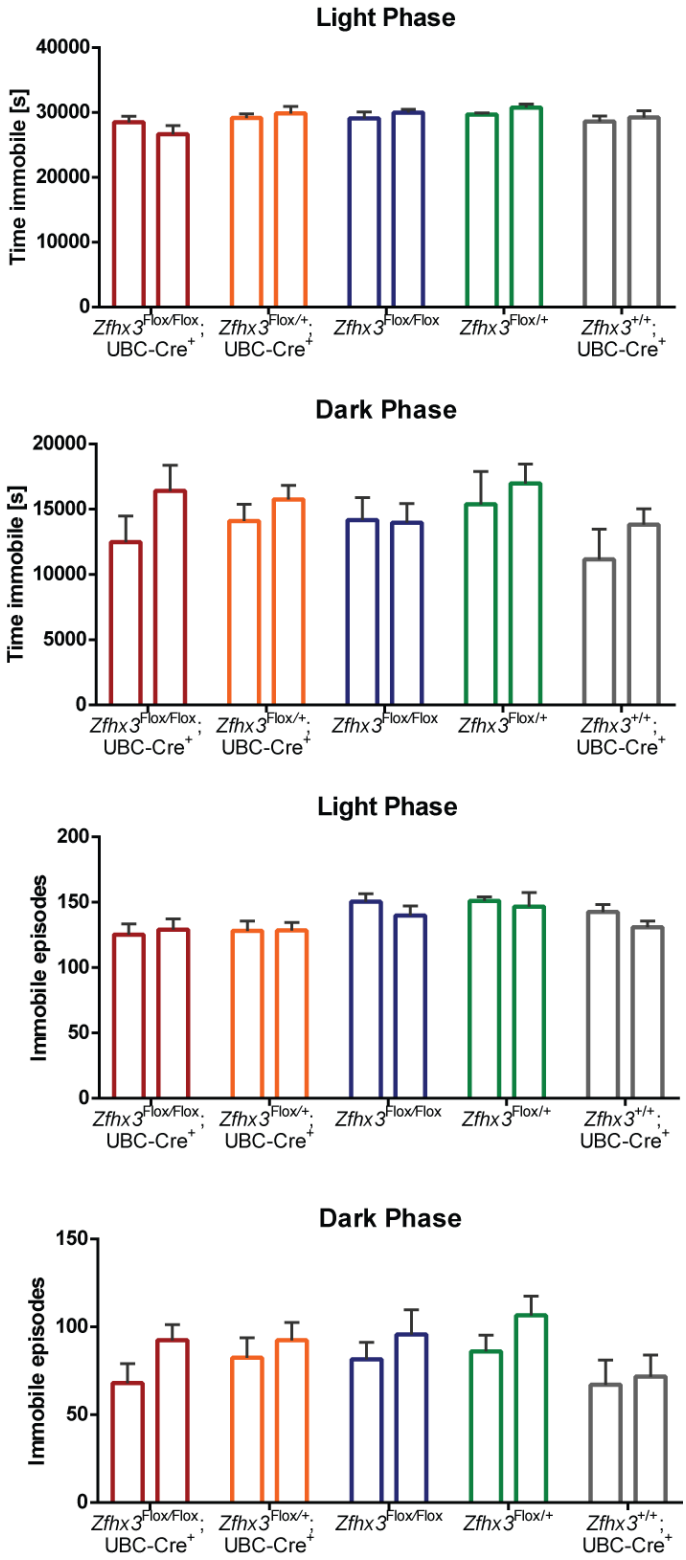


Figure 1.8 | Changes to sleep parameters measured using video tracked sleep analysis in *Zfhx3*$^{Flox/Flox}$; UBC-Cre^{+}, *Zfhx3*$^{Flox/+}$; UBC-Cre^{+}, *Zfhx3*$^{Flox/Flox}$, *Zfhx3*$^{Flox/+}$ and *Zfhx3*$^{+/+}$; UBC-Cre^{+} mice pre (left bars) and post (right bars) tamoxifen treatment. Error bars denote SEM of data sets.

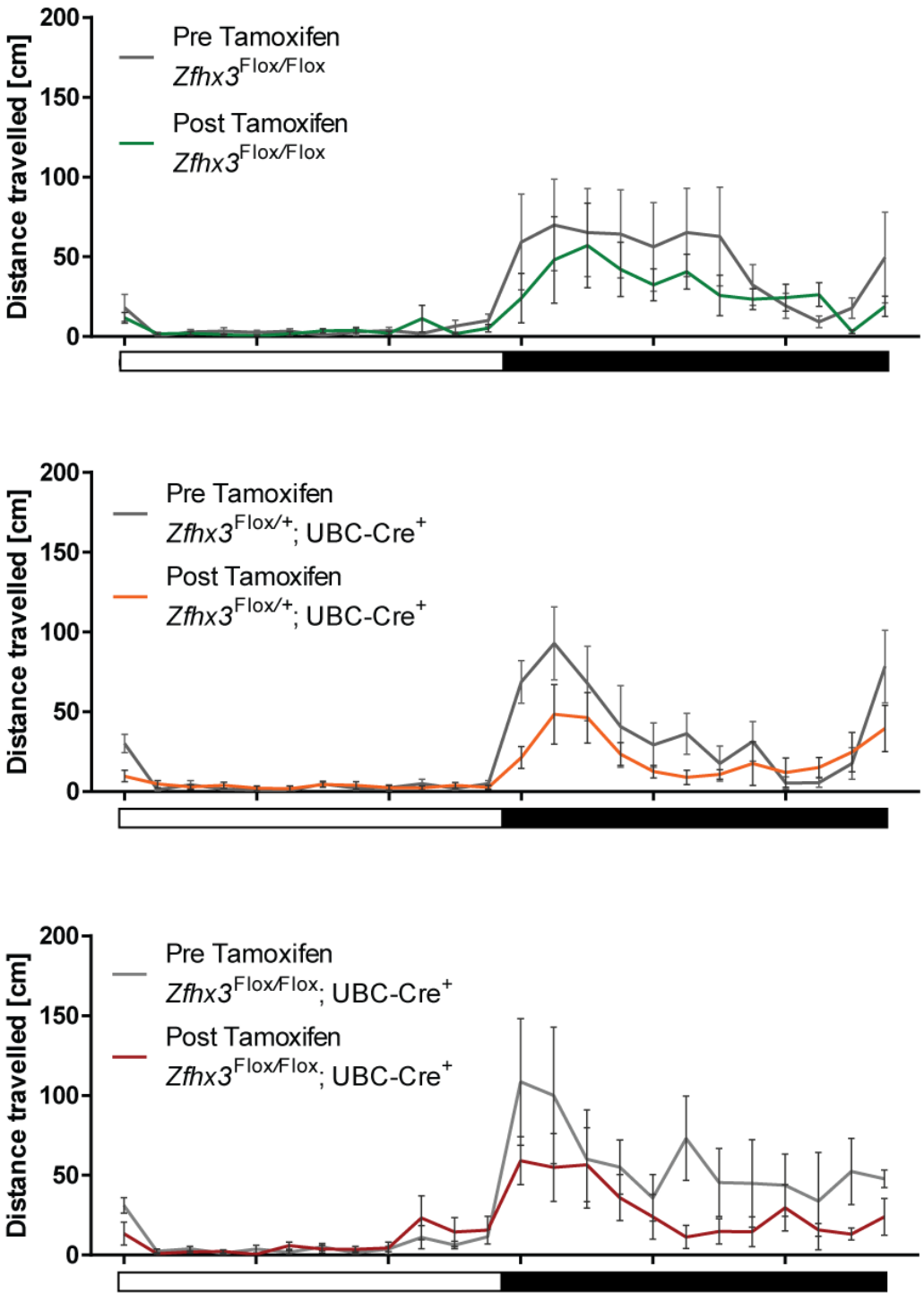


Figure 1.9 | Distance travelled pre and post tamoxifen for *Zfhx3*$^{Flox/Flox}$; UBC-Cre^{+}, *Zfhx3*$^{Flox/+}$; UBC-Cre^{+} and *Zfhx3*$^{Flox/Flox}$ mice in video tracked sleep screening, collected in hourly time bins. Error bars denote SEM of data; pre/post tamoxifen indicated on graphs; black/white bars denote LD cycle.

Pupillary light reflex is significantly altered in *Zfhx3*$^{Flox/Flox}$; UBC-Cre^{+}

Unpublished data from Hughes et al has demonstrated that *Zfhx3* is expressed in some retinal cells and may play a role in the pupillary light reflex. Therefore, it was pertinent to assess pupillary light reflex in *Zfhx3*$^{Flox/Flox}$; UBC-Cre^{+} mice to observe whether ZFHX3 has a role in the adult retina. Following tamoxifen dosing, *Zfhx3*$^{Flox/Flox}$; UBC-Cre^{+}, *Zfhx3*$^{Flox/+}$; UBC-Cre^{+} and mice from all control groups underwent pupillometry to measure pupillary reflex in response to bright (100 lux/13.4 log quanta) and mid (1 lux/11.1 log quanta) intensity . Measurements were taken at the point of maximal pupil constriction under both light conditions; representative images are shown in **Figure 1.10.** ANOVA analysis revealed that *Zfhx3*$^{Flox/Flox}$; UBC-Cre^{+} mice were found to have a significantly attenuated pupillary reflex response under both bright [$F(4,24)=10.13$, $p<0.0001$] and mid [$F(4,23)=5.933$, $p<0.0020$] light conditions. Tukey multiple comparison testing confirmed that this was significantly different between *Zfhx3*$^{Flox/Flox}$; UBC-Cre^{+} mice and all other genotypes tested. In contrast, *Zfhx3*$^{Flox/+}$; UBC-Cre^{+} mutants showed comparable pupillary reflex responses to control animals (**Figure 1.11**).

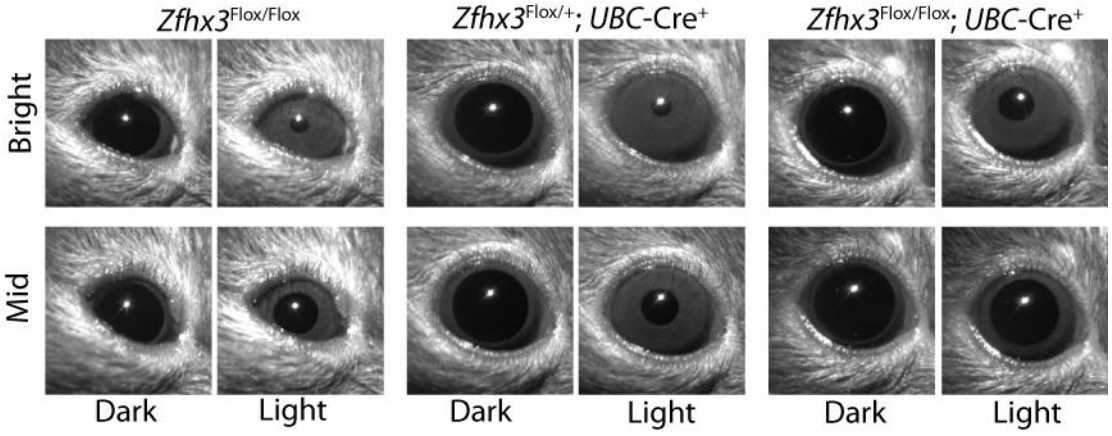


Figure 1.10 | Representative images for *Zhx3*$^{Flox/Flox}$, *Zfhx3*$^{Flox/+}$; UBC-Cre^{+} and *Zfhx3*$^{Flox/Flox}$; UBC-Cre^{+} mice before and after exposure to bright (100 lux/13.4 log quanta) and mid (1 lux/11.1 log quanta) light intensity stimuli to measure pupillary response.

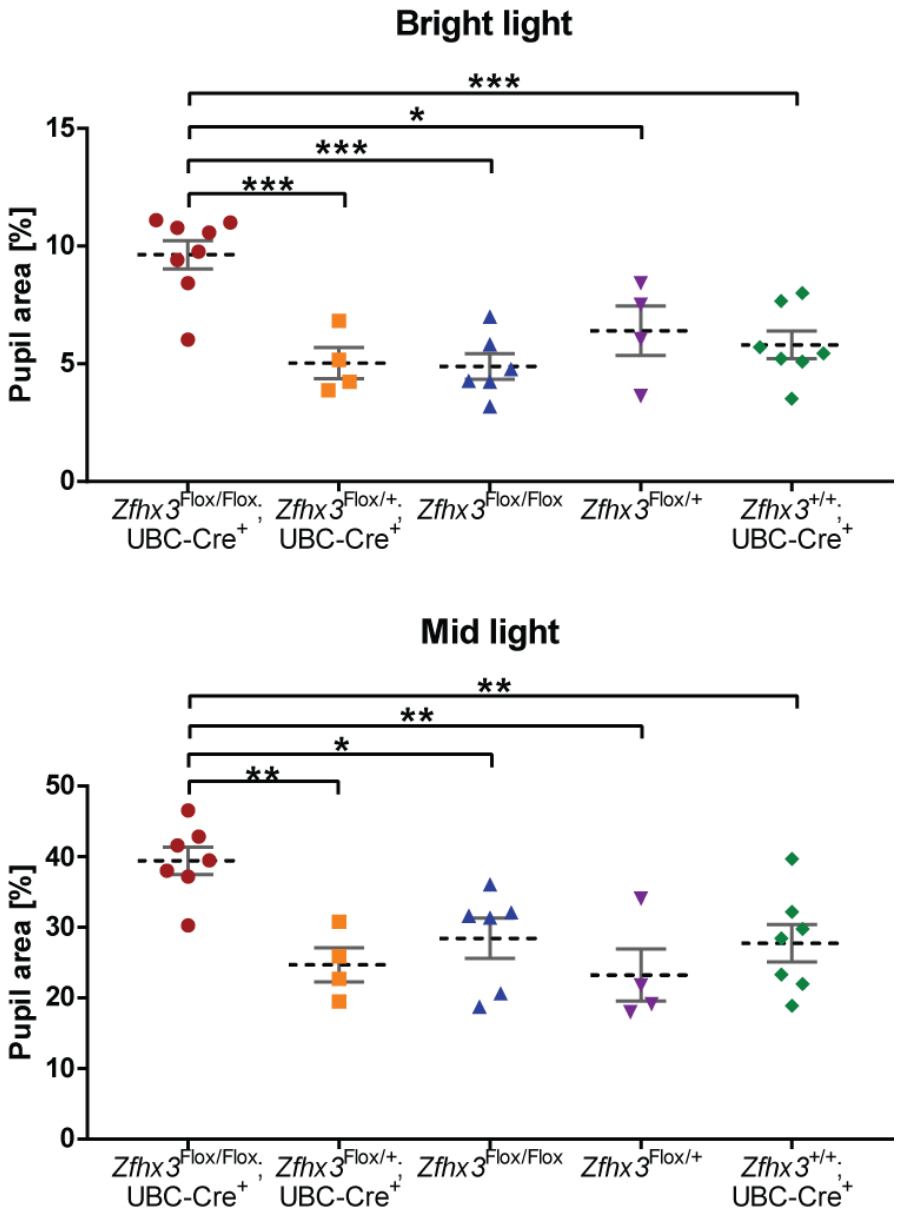


Figure 1.11 | Percentage pupil area at the point of maximal constriction relative to dark adapted pupil size, following bright (100 lux) and mid (1 lux) light stimuli to the eyes of *Zfhx3*$^{+/+}$; UBC-Cre^{+}, *Zhx3*$^{Flox/+}$, *Zhx3*$^{Flox/Flox}$, *Zfhx3*$^{Flox/+}$; UBC-Cre^{+} and *Zfhx3*$^{Flox/Flox}$; UBC-Cre^{+}. Dashed black line denotes mean of data, error bars denote SEM of group data. Tukey multiple comparison testing was used to determine significant differences between groups. * denotes significance at $p<0.05$, ** denotes significance at $p<0.01$, *** denotes significance at $p<0.001$.

Viability issues on *Zfhx3*^{Flox} line and downstream molecular work

When the first progeny of the intercross breeding to produce this line were genotyped, there was a very evident underrepresentation of mice homozygous for the

floxed allele. **Table 1.2** shows the outcome of *Zfhx3*^{Flox} distribution from initial crosses on this line; a chi-square test confirmed that the distribution of genotypes was significantly different to expected [X^2 (2, n=289) = 20.79, p<0.0001]. A subsequent binomial test showed that this loss of homozygotes does not segregate with Cre expression [p=0.108] and therefore the viability is an issue with the floxed line alone and not a combination effect of carrying both floxed and Cre alleles. In addition to this loss of *Zfhx3*$^{Flox/Flox}$ mice, craniofacial abnormalities were also observed in some *Zfhx3*$^{Flox/Flox}$ animals. Visual inspection of these mice revealed abnormally shorter faces, as shown in **Figure 1.12**. It is unknown whether this contributed to the decreased viability of *Zfhx3*$^{Flox/Flox}$ animals, however later in adult life many of these 'short-faced' mice did suffer from malocclusion.

Flox Genotype	Expected #	Observed #	Expected %	Observed %
Wildtype	72.25	79	25.00	27.34
Heterozygous	144.5	171	50.00	59.17
Homozygous	72.25	39	25.00	13.49
TOTAL	289.0	289.0	100.0	100.00

Table 1.2 | Genotype distribution of litters in *Zfhx3*$^{Flox/Flox}$; UBC-Cre^{+} line. Chi-square analysis confirmed that the distribution is significantly different to that of the expected genotype distribution [X^2 (2, n=289)=20.79, p<0.0001].

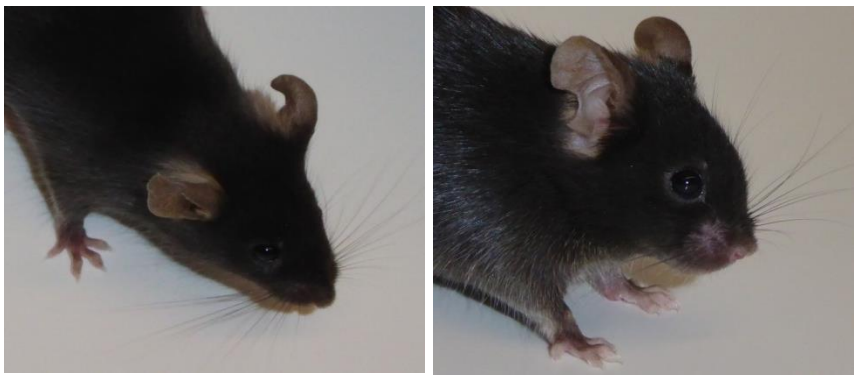


Figure 1.12 | Right image shows 'short-face' phenotype observed in some *Zfhx3*$^{Flox/Flox}$ mice on congenic B6J background, this craniofacial abnormality was irrespective of whether a Cre allele was present or not. Left image shows a *Zfhx3*$^{Flox/Flox}$ mouse with regular craniofacial appearance.

This created some difficulty when attempting to breed large cohorts; in an attempt to improve the viability of *Zfhx3*$^{Flox/Flox}$ animals, the line was outcrossed to C3H and maintained on a mixed background of 75% B6 and 25% C3H. To achieve this *Zfhx3*$^{Flox/+}$; Cre^{+} B6 mice were first bred to inbred C3H mice to produce *Zfhx3*$^{Flox/+}$; Cre^{+} animals that were 50% B6 and 50% C3H, these were then subsequently bred to *Zfhx3*$^{Flox/+}$ B6 mice to produce both Cre positive and negative *Zfhx3*$^{Flox/Flox}$ animals. As is shown in **Table 1.3**, this improved viability of the *Zfhx3*^{Flox} allele, allowing more Cre positive and negative *Zfhx3*$^{Flox/Flox}$ animals to be produced for molecular analysis. These experimental animals were dosed with tamoxifen and used for SCN tissue punch collections at circadian time-points every 6 hours, along with pre tamoxifen controls; this tissue has been used for RNAseq – the results of which are currently being analysed by bioinformatics collaborators.

Flox Genotype	Expected #	Observed #	Expected %	Observed %
Wildtype	124	96	25.00	19.35
Heterozygous	248	258	50.00	52.02
Homozygous	124	142	25.00	28.63
TOTAL	496	496	100.0	100.00

Table 1.3 | Genotype distribution of litters in *Zfhx3*$^{Flox/Flox}$; UBC-Cre^{+} line when bred onto mixed B6/C3H background.

Genotype	n	τDD [hours] Pre Tamoxifen	τDD [hours] Post Tamoxifen	*p* value	Adjusted *p* value
Zfhx3$^{Flox/Flox}$; UBC-Cre^{+}	7	23.72 (±0.09)	22.66 (±0.15)	0.0001	0.0045
Zfhx3$^{Flox/+}$; UBC-Cre^{+}	11	23.76 (±0.03)	23.74 (±0.05)	0.7968	1.0000
Zfhx3$^{Flox/Flox}$; UBC-Cre^{-}	8	23.75 (±0.02)	23.73 (±0.11)	0.8102	1.0000
Zfhx3$^{Flox/+}$; UBC-Cre^{-}	10	23.76 (±0.04)	23.78 (±0.04)	0.8155	1.0000
Zfhx3$^{+/+}$; UBC-Cre^{+}	10	23.69 (±0.09)	23.74 (±0.04)	0.4852	1.0000

Genotype	n	Amplitude [AU] Pre Tamoxifen	Amplitude [AU] Post Tamoxifen	*p* value	Adjusted *p* value
Zfhx3$^{Flox/Flox}$; UBC-Cre^{+}	7	5272 (±636)	3658 (±646)	0.0034	0.1530
Zfhx3$^{Flox/+}$; UBC-Cre^{+}	11	5284 (±361)	5568 (±541)	0.4964	1.0000
Zfhx3$^{Flox/Flox}$; UBC-Cre^{-}	8	5405 (±517)	6165 (±614)	0.1459	1.0000
Zfhx3$^{Flox/+}$; UBC-Cre^{-}	10	4218 (±320)	4830 (±320)	0.1666	1.0000
Zfhx3$^{+/+}$; UBC-Cre^{+}	10	4571 (±423)	5789 (±656)	0.0076	0.3420

Genotype	n	Activity in light phase [%] Pre Tamoxifen	Activity in light phase [%] Post Tamoxifen	*p* value	Adjusted *p* value
Zfhx3$^{Flox/Flox}$; UBC-Cre^{+}	10	6.79 (±1.02)	11.32 (±2.01)	0.0135	0.6075
Zfhx3$^{Flox/+}$; UBC-Cre^{+}	11	4.51 (±1.04)	5.25 (±1.50)	0.8215	1.0000
Zfhx3$^{Flox/Flox}$; UBC-Cre^{-}	10	8.81 (±1.99)	5.98 (±1.67)	0.1141	1.0000
Zfhx3$^{Flox/+}$; UBC-Cre^{-}	10	10.17 (±1.99)	6.10 (±1.03)	0.0253	1.0000
Zfhx3$^{+/+}$; UBC-Cre^{+}	10	6.46 (±1.32)	3.69 (±0.98)	0.1236	1.0000

Genotype	n	ψ [°] Pre Tamoxifen	ψ [°] Post Tamoxifen	*p* value	Adjusted *p* value
Zfhx3$^{Flox/Flox}$; UBC-Cre^{+}	10	179 (±0.9)	169 (±7.1)	0.0055	0.2475
Zfhx3$^{Flox/+}$; UBC-Cre^{+}	11	175 (±3.7)	172 (±7.5)	0.3587	1.0000
Zfhx3$^{Flox/Flox}$; UBC-Cre^{-}	9	175 (±5.1)	176 (±4.0)	0.9868	1.0000
Zfhx3$^{Flox/+}$; UBC-Cre^{-}	10	179 (±0.7)	181 (±0.5)	0.6193	1.0000
Zfhx3$^{+/+}$; UBC-Cre^{+}	10	180 (±0.7)	181 (±0.6)	0.8466	1.0000

Genotype	n	α_{LD} [hours] Pre Tamoxifen	α_{LD} [hours] Post Tamoxifen	*p* value	Adjusted *p* value
Zfhx3$^{Flox/Flox}$; UBC-Cre^{+}	10	12.09 (±0.14)	11.59 (±0.52)	0.0796	1.0000
Zfhx3$^{Flox/+}$; UBC-Cre^{+}	11	12.10 (±0.16)	11.85 (±0.14)	0.3470	1.0000
Zfhx3$^{Flox/Flox}$; UBC-Cre^{-}	9	12.22 (±0.22)	12.03 (±0.13)	0.4906	1.0000
Zfhx3$^{Flox/+}$; UBC-Cre^{-}	10	12.11 (±0.17)	12.07 (±0.09)	0.8707	1.0000
Zfhx3$^{+/+}$; UBC-Cre^{+}	10	11.93 (±0.12)	11.86 (±0.10)	0.8508	1.0000

Genotype	n	α_{DD} [hours] Pre Tamoxifen	α_{DD} [hours] Post Tamoxifen	*p* value	Adjusted *p* value
Zfhx3$^{Flox/Flox}$; UBC-Cre^{+}	10	12.20 (±0.82)	10.73 (±1.26)	0.0229	1.0000
Zfhx3$^{Flox/+}$; UBC-Cre^{+}	11	12.84 (±0.27)	13.22 (±0.23)	0.5089	1.0000
Zfhx3$^{Flox/Flox}$; UBC-Cre^{-}	8	13.64 (±0.39)	13.08 (±0.39)	0.5556	1.0000
Zfhx3$^{Flox/+}$; UBC-Cre^{-}	10	12.67 (±0.24)	12.77 (±0.21)	0.8686	1.0000
Zfhx3$^{+/+}$; UBC-Cre^{+}	10	12.68 (±0.19)	12.27 (±0.18)	0.4978	1.0000

Table 1.4 | Mean values (± Standard Error Mean) of circadian parameters for all genotypes tested pre and post tamoxifen treatment. Both un-adjusted and adjusted *p*-values are shown for pairwise comparisons of group data pre/post tamoxifen; Bonferroni adjustment was used for correction of multiple comparisons.

Discussion

Many important transcription factors have critical roles during development; this makes it difficult to study adult specific roles of the gene but also to generate constitutive null mutants for experimental analysis as many are embryonic lethal. By utilising a temporal conditional mutagenesis approach, the developmental functions of *Zfhx3* were circumvented, allowing the study of purely adult-related functions of the gene. The data presented in this chapter confirms a role for *Zfhx3* in the adult circadian system distinct from any previously ascribed roles in the development of the circadian system and therefore confirms that the gene is necessary for normal circadian function throughout the lifespan of the mouse. Moreover, by utilising an inducible Cre line, the same animal was able to be used for data collection before and after tamoxifen treatment – thus eliminating some of the natural variability usually observed between animals when measuring circadian parameters.

Despite viability issues when breeding *Zfhx3*$^{Flox/Flox}$ animals, suitable cohort numbers for circadian and sleep phenotyping were generated. It is important to note that these animals were deemed suitable for use, despite reduced initial viability, as they showed no circadian phenotype prior to tamoxifen treatment and were indistinguishable from their control counterparts at this point. Equally, the craniofacial abnormalities seen in some animals did not interfere with recording of nor did they alter circadian behaviour. Attempts were made to breed this phenotype out of the line, but as the cause was unknown and emergence of the phenotype sporadic, this proved incredibly difficult. Equally, attempts were made to improve the viability of *Zfhx3*$^{Flox/Flox}$ animals in an effort to reduce breeding numbers; this was achieved by maintaining the line on a mixed B6/C3H background – these mice will form the basis

for any future experiments on the *Zfhx3*$^{Flox/Flox}$; UBC-Cre^{+} line. The abnormalities associated with *Zfhx3*$^{Flox/Flox}$ animals may be due to disruption of regulatory elements in intronic regions of the gene when the *Zfhx3*^{Flox} allele was created; however there were no viability issues originally reported with the *Zfhx3*^{Flox} allele alone during generation (Sun et al., 2012). Although unlikely, a linked random mutation could have been generated upon re-derivation of the line at Harwell. To confirm this, whole genome sequencing could be undertaken on the *Zfhx3*^{Flox} line. However, a more desirable approach would be to generate a new Floxed allele or continue to maintain the line on a mixed background – as previously mentioned.

There was an interesting split of circadian phenotypes observed in *Zfhx3*$^{Flox/Flox}$; UBC-Cre^{+} mice upon release into DD, with some mice displaying a shortening of circadian period and others displaying arrhythmic activity. However, all mice appeared to be entrained to the LD cycle. This could perhaps be a 'false' entrainment though, when considering the data presented on rapid re-entrainment to an advancing LD cycle – which appears to show evidence for negative masking in *Zfhx3*$^{Flox/Flox}$; UBC-Cre^{+} animals. Indeed, negative masking would account for the rapid initial increase in activity onset when *Zfhx3*$^{Flox/Flox}$; UBC-Cre^{+} mice are first released into DD, as this could be due to a faster running internal clock that is being suppressed by the light cycle. The differences in activity could possibly also be due to differential Cre recombinase activity between mutants, but this seems unlikely given that all SCNs assessed so far displayed a lack of ZFHX3 staining – however, the mice used for histological analysis had not undergone circadian screening and so their phenotype cannot be directly associated. It is perhaps more likely that deletion of ZFHX3 has affected intracellular clocks within the brain, and even peripheral oscillators, thus

altering their robustness. This in turn could alter phase coherence of oscillators (Schibler et al., 2015) slightly differently in different mutants, therefore producing a scale of severity in terms of circadian locomotor phenotype. It should be noted that differences in circadian phenotype within the same line are not uncommon and have been shown to occur in both *Lhx1* and *Vip* mutants (Aton et al., 2005a; Bedont et al., 2014; Colwell et al., 2003). However, single gene knock-outs that induce arrhythmic activity are relatively uncommon (Baggs et al., 2009a) as, prior to this data, only *Bmal1* knock-out mice have been shown to display arrhythmia under DD conditions (Bunger et al., 2000): reinforcing the notability of *Zfhx3* as a key circadian pacemaker gene.

Results II

Investigation of the Sci phenotype when expressed over an inducible Zfhx3 null allele

Introduction

ENU mutagenesis has been invaluable in the discovery of circadian and behavioural related genes (Oliver and Davies, 2012). In 1994, Takashi and colleagues discovered the first mammalian clock gene utilising this method in mice (Vitaterna et al., 1994). Since then several novel circadian genes have been discovered using this mutagenesis approach, such as *Fbxl3* (Godinho et al., 2007), SNAP-25 (Oliver et al., 2012) and, of course, *Zfhx3* (Bacon et al., 2004).

ENU (or *N*-ethyl-*N*-nitrosourea) is a powerful mutagen that causes random single point mutations in the genome when administered at a controlled dose. Typically, ENU is given to male mice to produce germline mutations that are subsequently passed on to progeny when these males are mated with wildtype females. The resulting mutant offspring are screened for behavioural abnormalities and positional cloning used to identify the causative mutation of an observed phenotype (Rinchik, 1991). This method of mutagenesis screening provides an unbiased approach to screening for novel genes and can also result in a range of mutations altering gene function. These include: hyper- and hypo-morphic mutations, which increase or reduce the amount of gene product, respectively; neomorphic mutations, which convey a new function for a gene; antimorphic mutations, which produces a gene product which antagonises the original gene function; and also loss of function mutations, which effectively abolish gene function (Oliver and Davies, 2012; Wilkie, 1994). A single point mutation can also result in viable progeny in cases where a constitutive null allele would be lethal, allowing characterisation of the gene that otherwise would not have been possible (Acevedo-Arozena et al., 2008).

Many circadian genes are semidominant (Hall, 1990), meaning heterozygous mutants display a dominantly inherited phenotype that is less severe than homozygous mutants; this was the case for both mammalian *Clock* (Vitaterna et al., 1994) and *Zfhx3* (Parsons et al., 2015). However, the presence of a wildtype allele can sometimes be confounding when attempting to validate mutants. Therefore, assessing the true nature of these mutations produced by ENU can be difficult. To further investigate the nature of the *Clock* mutation in mice, complementation studies were performed to generate compound heterozygotes. To achieve this, the *Clock* mutant was crossed to a null allele to create a compound heterozygote for phenotypic assessment. From these studies it was concluded that *Clock* was an antimorphic mutation, thus aiding to further understanding of how this mutant fitted into what was known about the molecular control of mammalian circadian rhythms (King et al., 1997).

Similarly, the *Sci* mutation was a single point mutation in *Zfhx3* that was homozygous lethal; due to this lethality only heterozygote mutants were available for characterisation and therefore all analysis could potentially be confounded by the presence of an intact wildtype *Zfhx3* allele. A constitutive null allele was not available for intercrossing to produce a traditional compound heterozygote. Therefore, the UBC-Cre driven inducible *Zfhx3* KO mouse (described in Results I) was used to create a compound heterozygote mutant, which could be used to study the *Sci* mutation in isolation in adult mice. This would hopefully allow us to characterise the nature of *Sci* and further aid in our understanding of its function in the genetics of mammalian chronobiology.

Traditional circadian wheel running screening was unsuitable for characterising *Zfhx3*$^{Flox/Sci}$; UBC-Cre^{+} mice

Zfhx3$^{Sci/-}$ mice were bred to *Zfhx3*$^{Flox/+}$; UBC-Cre^{+} mice to obtain a *Zfhx3*$^{Sci/Flox}$; UBC-Cre^{+} experimental cohort for circadian characterisation. Prior to tamoxifen dosing, animals should behave as *Zfhx3*$^{Sci/+}$ mice whereas following tamoxifen dosing, the floxed allele would be converted to a null allele in these mice, rendering them effectively as *Zfhx3*$^{Sci/-}$ animals (see Results I for information on UBC-Cre and tamoxifen dosing). As well as these animals, mice with the following genotypes that resulted from this cross were also run for comparison: *Zfhx3*$^{Sci/+}$; UBC-Cre^{+}, *Zfhx3*$^{Sci/Flox}$ and *Zfhx3*$^{Flox/+}$. Due to cage space and costs, the additional *Zfhx3*$^{+/+}$ control group was not used. In order to functionally compare these different genotypes, mice were then initially screened using traditional wheel running experiments both pre and post tamoxifen treatment. However, analysis of the subsequent actograms indicated that all mice containing the *Sci* allele did not run robustly on wheels; as a result there was insufficient data to effectively compare circadian parameters in all experimental groups (an example actogram is shown in **Figure 2.1**). This was also noted in the original publication describing the *Sci* mutation (Bacon et al., 2004).

This led us to the consider using passive infra-red (PIR) screening (see Methods for more detail) as an alternative method of circadian data collection as it does not rely on a running wheel to collect data (Brown et al., 2016). As PIR screening was a relatively untested procedure at the time, it was necessary to establish the similarity in circadian parameters calculated using both methods prior to screening compound mutants carrying complex conditionally-targeted alleles. In order to investigate this, *Zfhx3*$^{Sci/+}$ mice (i.e. heterozygous ENU mutants) underwent an initial

screening test to establish whether PIR would accurately reflect the full spectrum of circadian phenotypes first observed using wheel running when the mutant line was initially described (Bacon et al., 2004). In the original study, a variety of circadian phenotypes were observed: arrhythmia in DD, shortened τ_{DD} with robust wheel-running, fragmented running activity and significant bouts of wheel-running during the light phase. In these initial PIR screens, examples of all of these equivalent phenotypes were detectable in the *Zfhx3*$^{Sci/+}$ mice (**Figure 2.2**). *Zfhx3*$^{Sci/+}$ mice [n=8] displayed an average τ_{DD} of 23.29 hr, which was significantly shortened compared to wildtype *Zfhx3*$^{+/+}$ [n=6] mice [Mann-Whitney U=6.5, p=0.02]. Therefore PIR was deemed a reliable method of circadian screening for *Zfhx3*$^{Sci/Flox}$ mice.

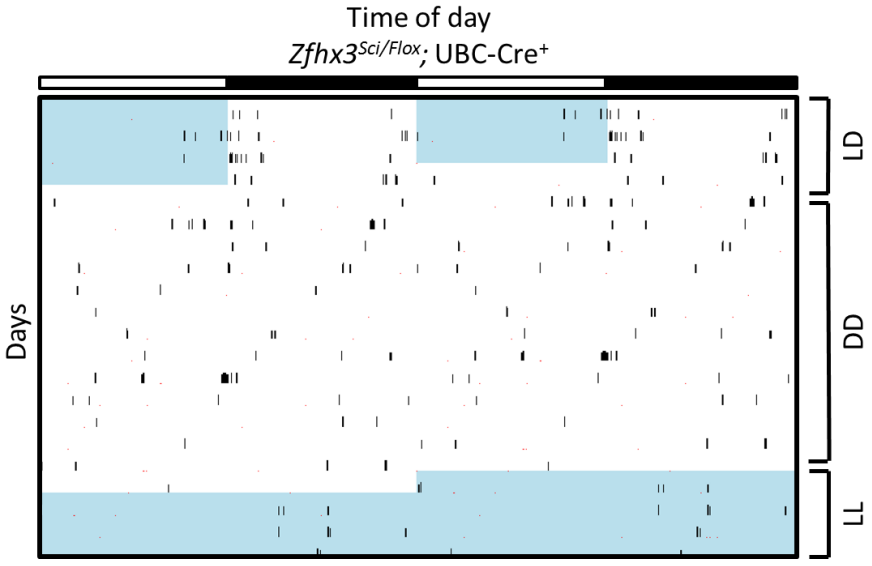


Figure 2.1 | Wheel running actogram from a *Zfhx3*$^{Sci/Flox}$; UBC-Cre^{+} mouse demonstrating lack of wheel use, making this method an unreliable data source to measure all circadian parameters.

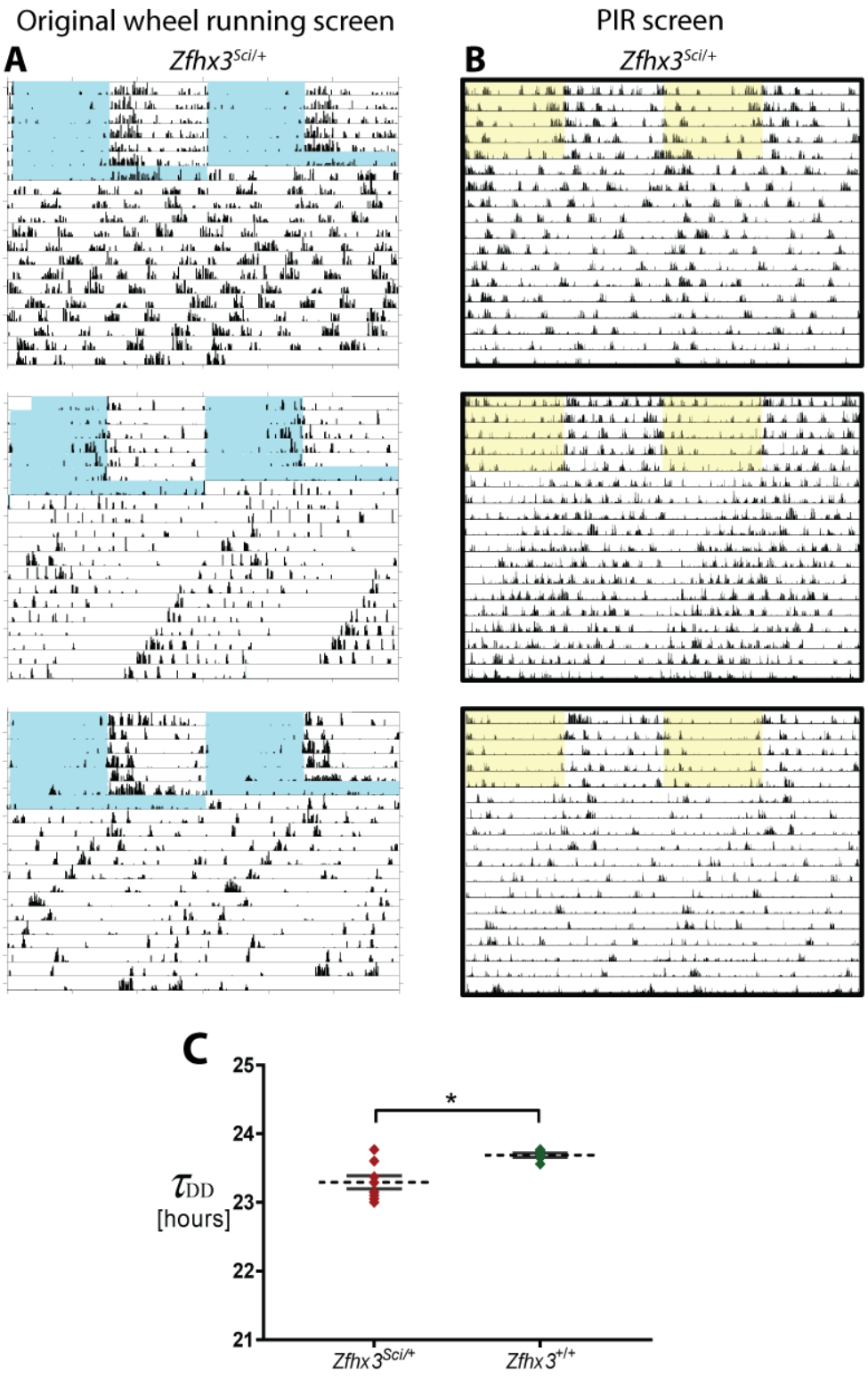


Figure 2.2 | A Representative actograms of archive *Sci* mice (taken from (Bacon et al., 2004)); **B** actograms generated from PIR screening of *Sci* mice, showing comparable circadian behaviours to those first captured with wheel running assays; **C** τ_{DD} is shown to be significantly shorter than wildtype controls when measurements are taken from PIR screening. * denotes significance at $p<0.05$

PIR screening of *Zfhx3*$^{Sci/-}$ revealed further shortening of τ_{DD} and arrhythmic activity

Unfortunately, PIR screening data was unavailable both pre and post tamoxifen for all mutants screened as some had already been dosed with tamoxifen for wheel running screening before the need for a different method of data collection was realised. Because of this, pre and post tamoxifen data was analysed in independent groups and not as repeated measures in the same mice (as was the case for mutants in Results I). Prior to tamoxifen dosing, all mice containing the *Sci* allele displayed a characteristic shortened τ_{DD} (as discussed previously); *Zfhx3*$^{Flox/+}$ mice displayed a mean τ_{DD} of 23.76hr [SEM: 0.077]. As expected due to the presence of mice containing the *Sci* mutation, values for τ_{DD} were found to be statistically different among genotypes [$F(3,28)=6.164$, $p=0.0024$] prior to tamoxifen treatment (**Figure 2.3**); this was also the case for amplitude [$H=11.08$, $p=0.0113$].

Following tamoxifen dosing to produce *Zfhx3*$^{Sci/-}$ mice, five animals were arrhythmic in PIR screening – leaving only two with a measureable τ_{DD} and amplitude. The mean τ_{DD} of these two animals was shorter than the pre tamoxifen group (22.2hr vs 23.2hr), and this was deemed statistically significant [$t(8)=2.811$, $p=0.0228$] – however more n numbers would be required to increase the reliability of this test (**Figure 2.3**). Amplitude was unchanged in *Zfhx3*$^{Sci/-}$ mice compared to *Zfhx3*$^{Sci/Flox}$; UBC-Cre^{+} mice [$t(5)=0.2235$, $p=0.8320$]. Statistical comparison of τ_{DD} for all groups post tamoxifen revealed a significant interaction effect [$F(3,12)=5.752$, $p=0.0114$], this was also the case for amplitude (**Figure 2.4**). When directly comparing pre and post tamoxifen data for controls, τ_{DD} was unaltered in *Zfhx3*$^{Sci/+}$; UBC-Cre^{+} [$U=9$, $p=0.6303$], *Zfhx3*$^{Sci/Flox}$ [$t(17)=0.05096$, $p=0.9600$] and *Zfhx3*$^{Flox/+}$ [$t(6)=0.02735$,

p=0.9791] mice. In addition to this, amplitude was also unchanged in *Zfhx3*$^{Sci/+}$; UBC-Cre^{+} [U=5, p=1939], *Zfhx3*$^{Sci/Flox}$ [t(13)=0.1264, p=0.9013] and *Zfhx3*$^{Flox/+}$ [U=6, p=0.7857] mice (**Figure 2.6**). This confirms that the presence of Cre and tamoxifen treatment did not alter circadian phenotype in control animals.

In spite of low n numbers for statistical analysis, the fact that the majority of *Zfhx3*$^{Sci/-}$ mice were arrhythmic confirms that the *Sci* mutation produces a more severe circadian phenotype when expressed over a null allele. Actograms for one of the few mice that were able to be screened both pre and post tamoxifen are shown in **Figure 2.5** to illustrate this effect.

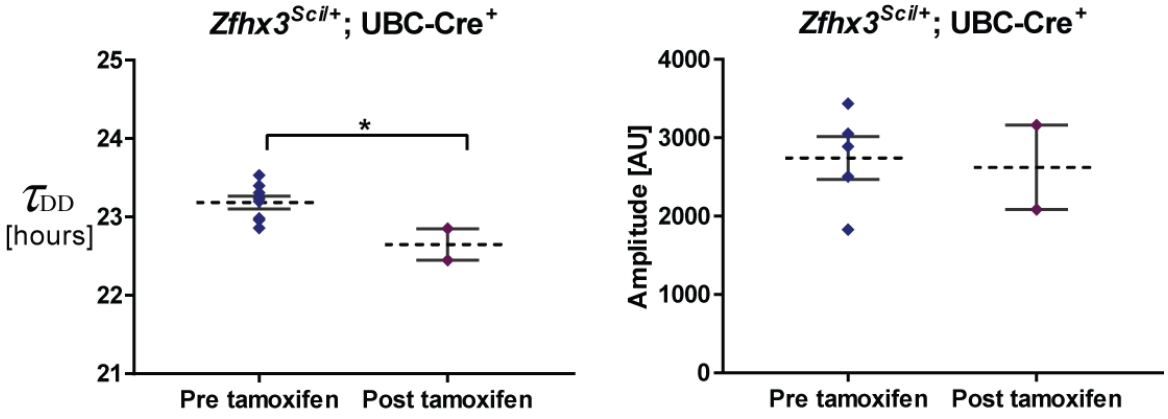


Figure 2.3 | τ_{DD} and amplitude of all rhythmic *Zfhx3*$^{Sci/Flox}$ compound heterozygote mice screened in PIR, pre tamoxifen mice are those of genotype *Zfhx3*$^{Sci/Flox}$; UBC-Cre^{+} and therefore display an initial Sci shortening, post tamoxifen mice are of genotype *Zfhx3*$^{Sci/-}$ and are essentially mice with *Sci* over a null allele of *Zfhx3*. Dashed line denotes mean of each group, grey error bars denote SEM of both datasets.

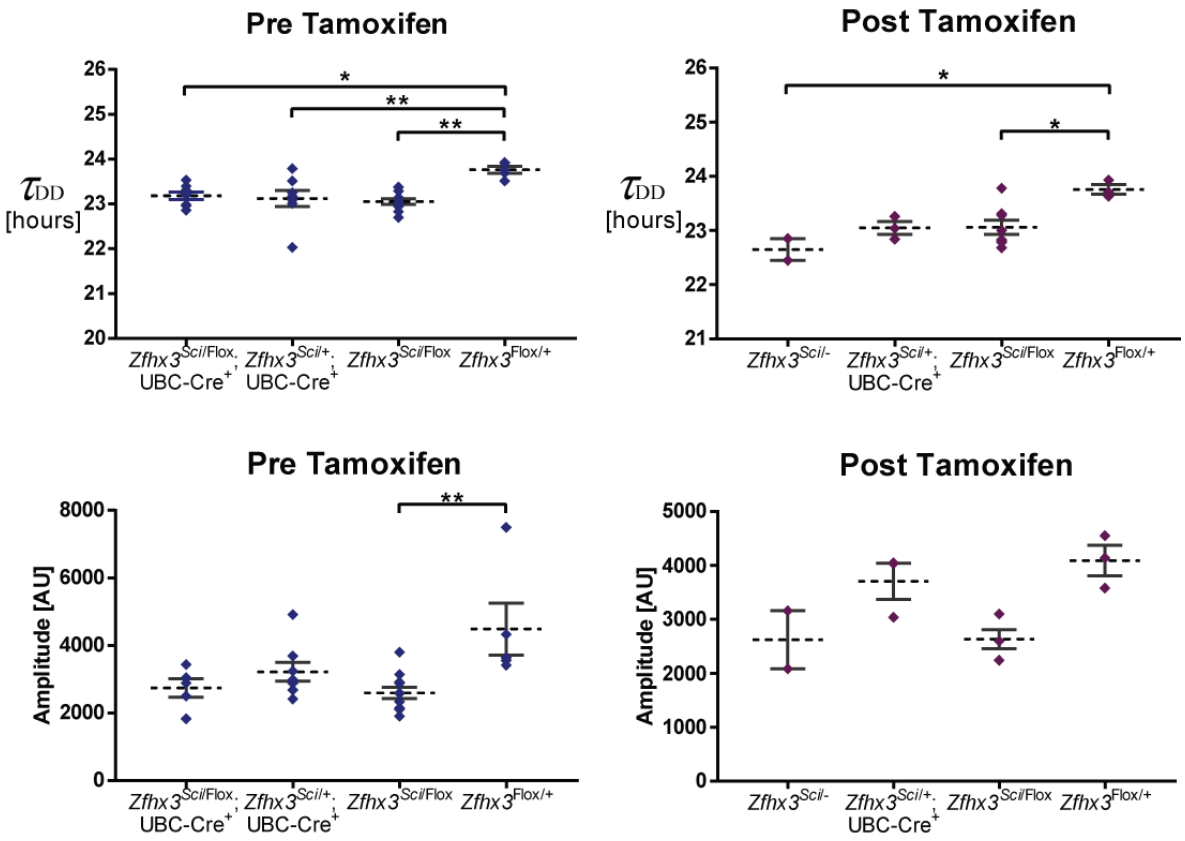


Figure 2.4 | τ_{DD} and amplitude of all mice screened pre and post tamoxifen (genotypes indicated on graph), multiple comparison testing was used to assess corrected significance between genotypes. Dashed lines denote mean of data set, error bars indicate SEM of data. * denotes significance at $p<0.05$, ** denotes significance at $p<0.01$.

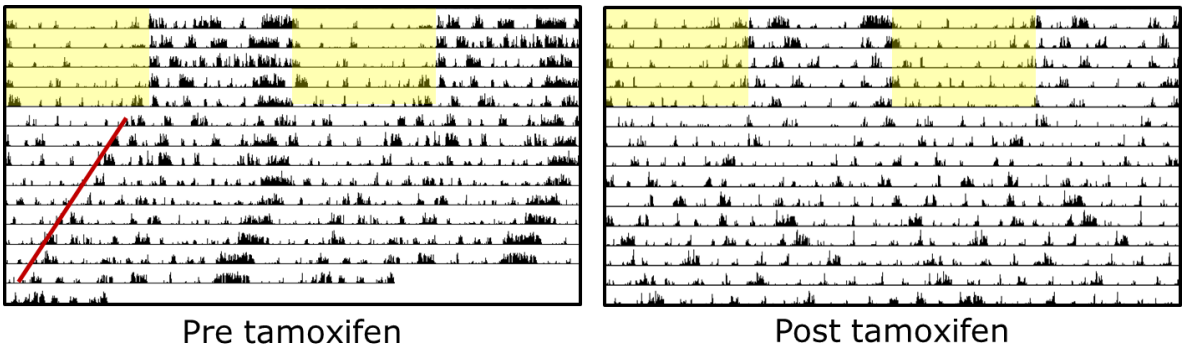


Figure 2.5 | Actograms generated from PIR screening of a *Zfhx3*$^{Sci/Flox}$; UBC-Cre^{+} mouse pre and post tamoxifen, showing arrhythmic activity in DD following tamoxifen dosing to produce *Zfhx3*$^{Sci/-}$ mice. Yellow shading denotes lights on, red line highlights best fit through activity to measure τ_{DD}.

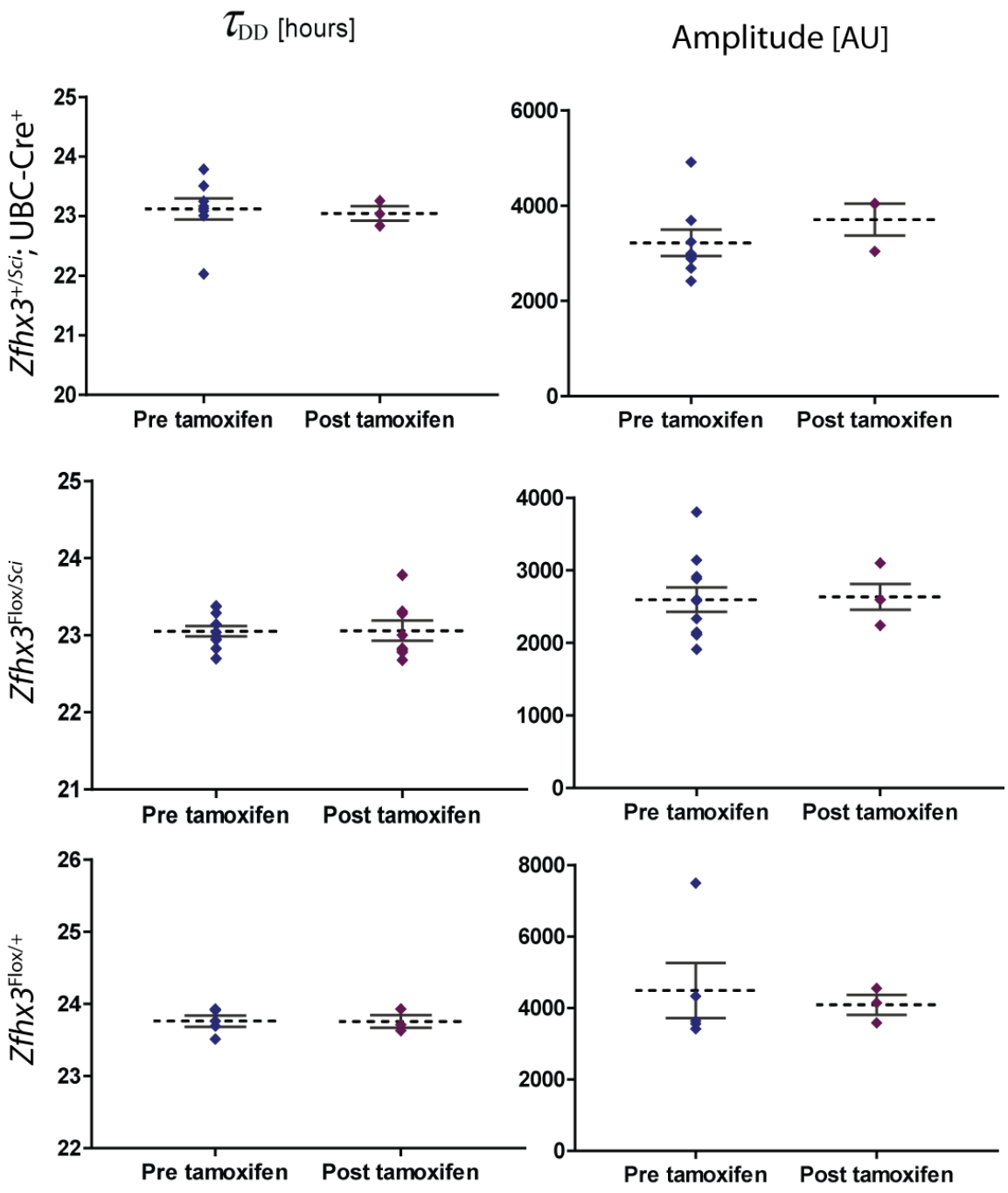


Figure 2.6 | Data for τ_{DD} and amplitude for control groups (genotypes are indicated on the graphs), data is shown for mice pre and post tamoxifen dosing. Dashed lines denote mean of data set, error bars indicate SEM of data.

Sleep parameters are unaltered in *Zfhx3*$^{Sci/-}$ mice

Data on sleep was extracted from PIR analysis using a similar method to that described in Results I, where periods of immobility are defined as sleep bouts. Due to the fact that pre and post tamoxifen data was not available for all mice, as mentioned previously, data collected for pre and post tamoxifen was treated as separate for genotypes. For pre tamoxifen, *Zfhx3*$^{Flox/+}$ data was also available as an extra control group for a non *Sci* containing comparison (**Figure 2.7**). When comparing groups before tamoxifen dosing, all mice with the *Sci* mutation had a higher amount of total sleep across the LD cycle than *Zfhx3*$^{Flox/+}$ animals, however this was not statistically significant [$F(3,32)=2.336$, $p=0.0924$]. The proportion of this sleep that was in the light phase of the LD cycle was not different between groups [$F(3,32)=2.188$, $p=0.1086$]. When the activity over 24 hours was analysed for all genotypes pre tamoxifen using 2 way ANOVA, there was a significant interaction effect between genotype and time [$F(141,1504)=1.919$, $p<0.0001$]. As evidenced in **Figure 2.8** this was due to *Zfhx3*$^{Flox/+}$ mice travelling more throughout the dark phase, and also showing a greater increase in activity around ZT12. All mice containing *Sci* showed comparable activity patterns across the LD cycle prior to the tamoxifen treatment. Following tamoxifen treatment, there were no differences between *Zfhx3*$^{Sci/-}$ and control groups in total sleep [$F(2,14)=0.6664$, $p=0.5291$] or percentage sleep in the light phase [$F(2,14)=0.5715$, $p=0.5773$]. Activity over the LD cycle was also statistically comparable between groups [$F(94,658)=1.188$, $p=0.1221$], despite *Zfhx3*$^{Sci/-}$ mice displaying a reduction in activity compared to *Zfhx3*$^{Sci/Flox}$; UBC-Cre^{+} counterparts. Unpaired t-tests were also conducted to directly compare values for *Zfhx3*$^{Sci/Flox}$; UBC-Cre^{+} (pre tamoxifen) and *Zfhx3*$^{Sci/-}$ (post tamoxifen) mutant mice. This analysis also confirmed that there were

no significant changes to total sleep [t(5.965)=1.251, p=0.2577] or percentage sleep in the light phase [t(13)=1.312, p=0.2121] following tamoxifen treatment.

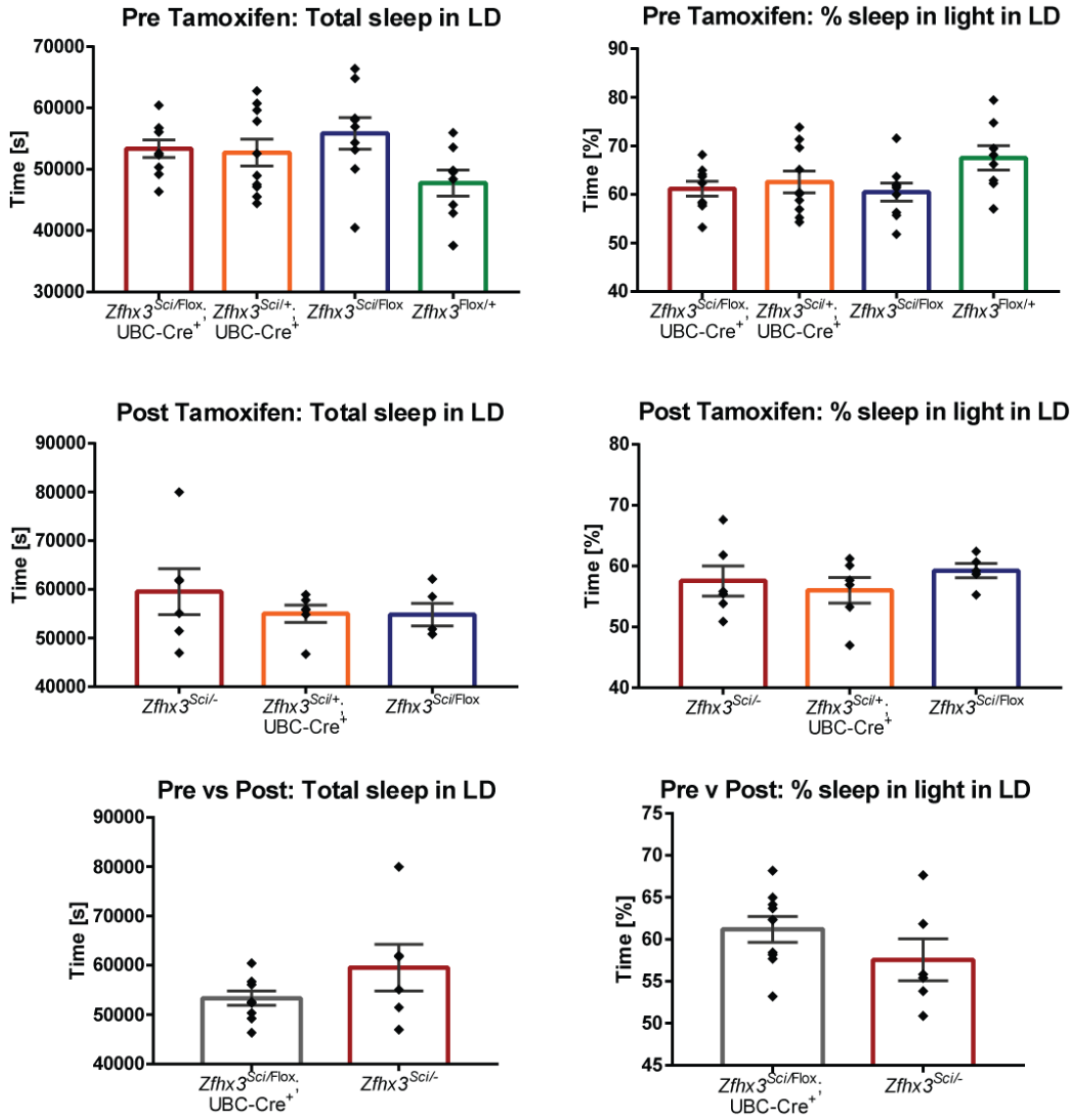


Figure 2.7 | Sleep parameters measured in *Zfhx3*$^{Sci/Flox}$; UBC-Cre^{+} [n=9], *Zfhx3*$^{Sci/+}$; UBC-Cre^{+} [n=10], *Zfhx3*$^{Sci/Flox}$ [n=9] and *Zfhx3*$^{Flox/+}$ [n=8] mice prior to tamoxifen dosing and *Zfhx3*$^{Sci/-}$ [n=6], *Zfhx3*$^{Sci/+}$; UBC-Cre^{+} [n=6] and *Zfhx3*$^{Sci/Flox}$ [n=5] mice post tamoxifen dosing. All measurements were over a 24 hour period of a standard 12:12 LD cycle. Error bars denote SEM of mean for group data.

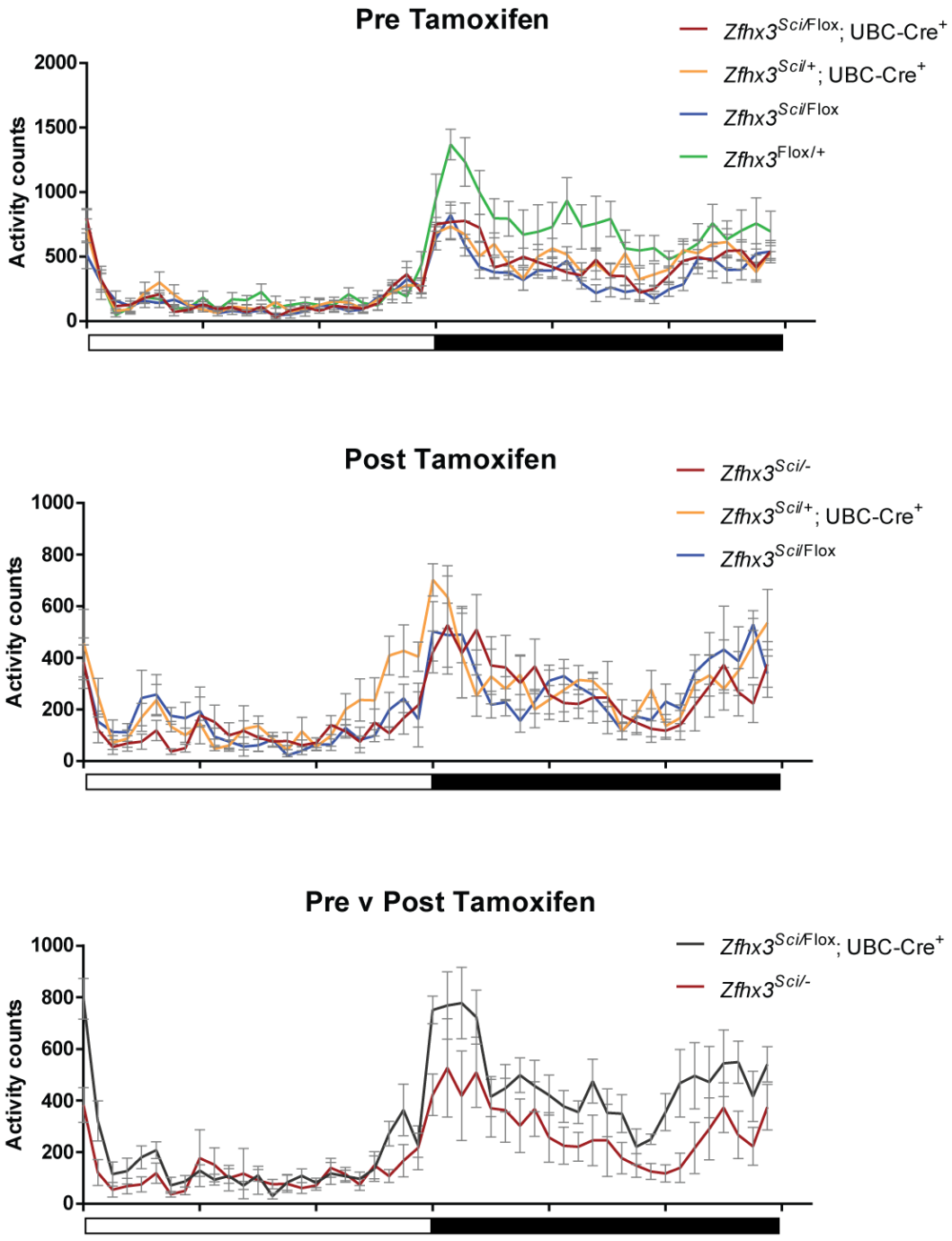


Figure 2.8 | Activity over time pre tamoxifen treatment for *Zfhx3*$^{Sci/Flox}$; UBC-Cre^{+} [n=9], *Zfhx3*$^{Sci/+}$; UBC-Cre^{+} [n=10], *Zfhx3*$^{Sci/Flox}$ [n=9] and *Zfhx3*$^{Flox/+}$ [n=8] mice and post tamoxifen dosing for *Zfhx3*$^{Sci/-}$ [n=6], *Zfhx3*$^{Sci/+}$; UBC-Cre^{+} [n=6] and *Zfhx3*$^{Sci/Flox}$ [n=5] mice. Lines denote average data for each genotype; error bars denote SEM of mean for group data; LD cycle indicated below graphs.

Dim light pupillary reflex is increased in *Zfhx3*$^{Sci/-}$ mice

Previous unpublished data on *Sci* mice (Jess Edwards, DPhil thesis) has shown that mutants have an enhanced pupillary reflex to a dimmer light stimulus (11.6 log quanta /cm^2 / s (0.17 lW/ cm^2 / s) than their control littermates. The pupil response to bright light (14.6 log quanta / cm^2 / s or 173 lW/ cm^2 / s) however was comparable to wildtype mice. This data suggested that the *Sci* mutation may cause a novel gain of function attribute in the retina – where *Zfhx3* is expressed (Hughes *et al*, unpublished data). To further investigate this hypothesis, pupillometry was carried out on *Zfhx3*$^{Sci/-}$ mice to examine the pupillary reflex in mice that would be lacking any possible compensatory effect from an intact *Zfhx3* allele. Mice were dark adapted then restrained and one eye exposed to a bright and mid light stimulus for 10 seconds (as conducted in pupillometry section of Results I). However, an additional light intensity (0.1 lux or 10.4 log quanta) was also used to investigate possible sensitivity to dim light. Pupil diameter was measured from the resulting images and pupil area calculated at the point of maximal constriction.

Representative images for *Zfhx3*$^{Sci/-}$ eyes measured following exposure to bright, mid and dim light stimuli are shown in **Figure 2.9**, along with images for post tamoxifen control genotypes *Zfhx3*$^{Sci/Flox}$ and *Zfhx3*$^{Flox/+}$.

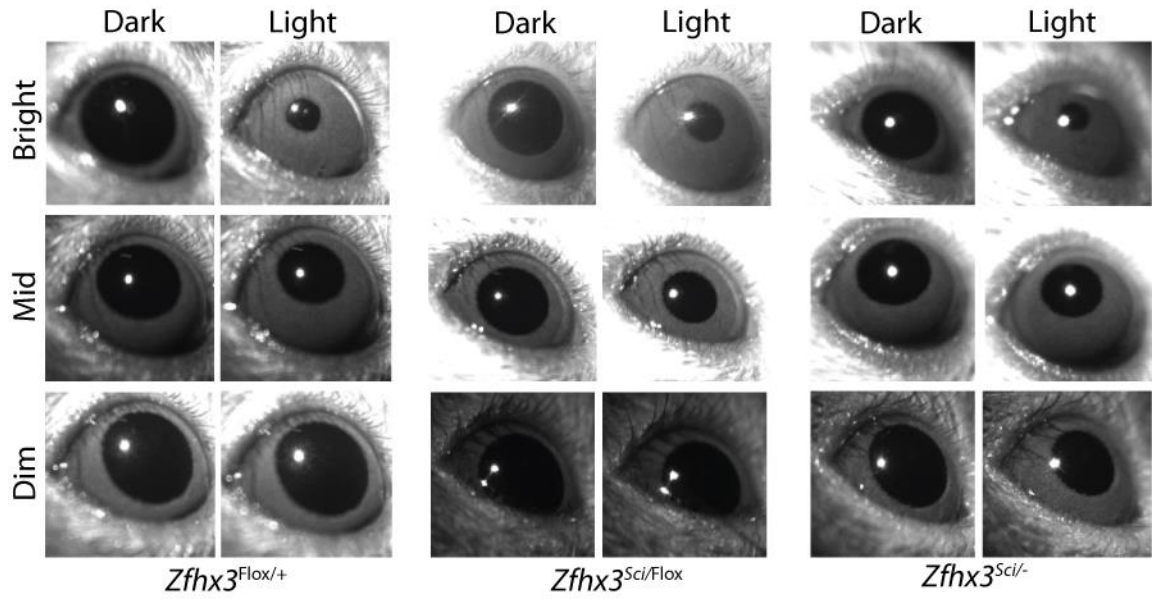


Figure 2.9 | Representative images for *Zhx3*$^{Flox/+}$, *Zfhx3*$^{Sci/Flox}$, *Zfhx3*$^{Sci/-}$ mice before and after exposure to bright, mid and dim light stimuli to measure pupillary reflex. All pupillometry screening was carried out post tamoxifen dosing.

Four different genotypes were analysed: two *Sci* positive controls – *Zfhx3*$^{Sci/+}$; UBC-Cre^{+} and *Zfhx3*$^{Sci/Flox}$, one *Sci* negative control group – *Zfhx3*$^{Flox/+}$, and the compound mutant *Zfhx3*$^{Sci/-}$. Under bright (100 lux or 13.4 log quanta) light, there were no differences in the pupillary reflex between the groups analysed; this was also the case for mid (1 lux or 11.1 log quanta) light. Although under this mid light condition, mean pupil area was reduced for *Zfhx3*$^{Sci/+}$; UBC-Cre^{+} and *Zfhx3*$^{Sci/Flox}$ controls, as well as *Zfhx3*$^{Sci/-}$; the lack of statistical significance is likely due to the spread of data observed in the *Zfhx3*$^{Flox/+}$ control group. A significant change in pupillary reflex was observed when *Zfhx3*$^{Sci/-}$ mice were measured under dim (0.1 lux or 10.4 log quanta) light, when compared with *Zfhx3*$^{Flox/+}$ (**Figure 2.10**). The percentage pupil area in dim light was also lower than *Zfhx3*$^{Sci/+}$; UBC-Cre^{+} and *Zfhx3*$^{Sci/Flox}$ animals, indicating a more pronounced phenotype due to the *Sci* mutation when examined over a null allele.

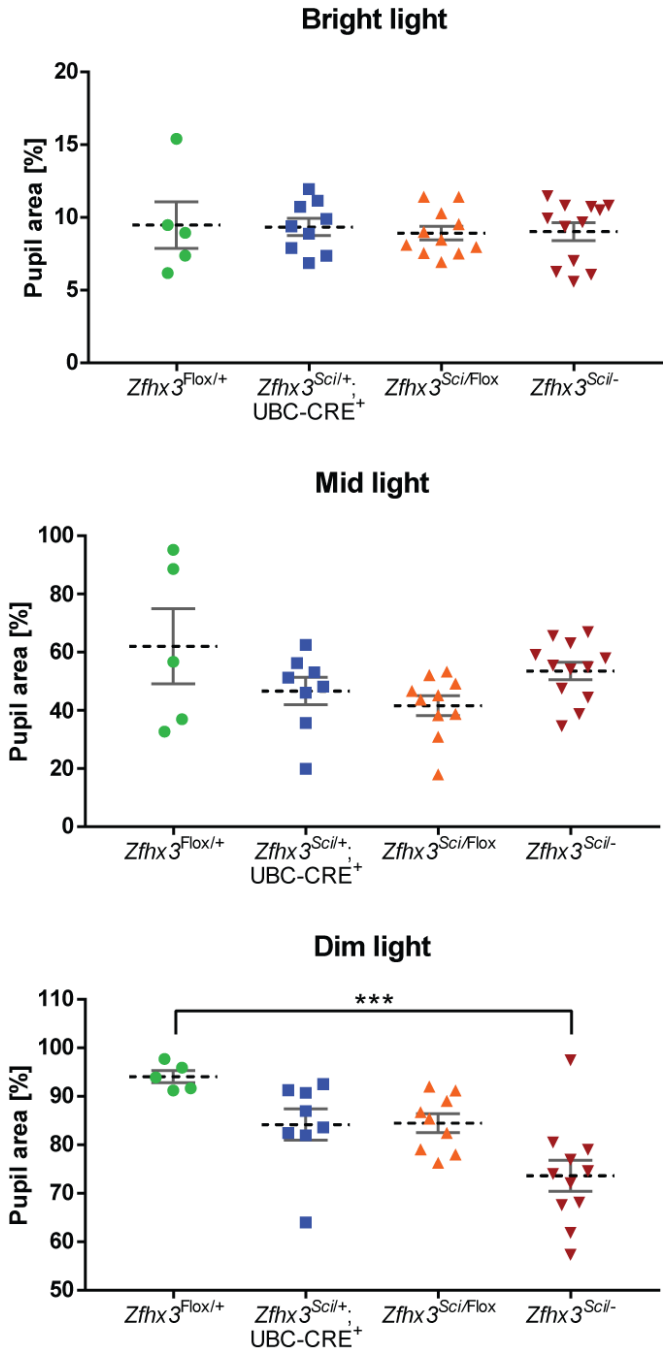


Figure 2.10 | Percentage pupil area following bright (100 lux), mid (1 lux) and dim (0.1 lux) light stimuli to the eyes of *Zfh*x3$^{Flox/+}$, *Zfh*x3$^{Sci/+}$; UBC-Cre^{+}, *Zfh*x3$^{Sci/Flox}$ and *Zfh*x3^{Scil-} mice. Dashed black line denotes mean of data, grey lines denote SEM of data points. *** denotes p=0.0007 in Tukey multiple comparison test of groups.

Vip and *Zfhx3* expression are downregulated in *Zfhx3*$^{Sci/-}$ mice

SCN punches were taken at ZT6 and ZT18 from the brains of *Zfhx3*$^{Sci/-}$ and *Zfh*x3$^{Sci/+}$; UBC-Cre^{+} controls post tamoxifen treatment. These were used for qPCR experiments (**Figure 2.11**) to validate loss of *Zfhx3* and also assess any changes to the circadian neuropeptide *Vip* – as this gene was shown to be downregulated in *Zfhx3*$^{Sci/+}$ previously (Parsons et al., 2015). Primers were designed to target 2 sites of *Zfhx3*: across exons 5-6, upstream of the floxed exons in *Zfhx*3^{Flox} and across exons 9-10, downstream of the floxed exons in *Zfhx*3^{Flox}. Expression of all targets was found to be downregulated in *Zfhx3*$^{Sci/-}$ compared to *Zfh*x3$^{Sci/+}$; UBC-Cre^{+} controls. Expression of *Zfhx3* upstream of the flox site in *Zfhx3*$^{Sci/-}$ showed a 0.47 fold change at ZT6 and a 0.58 fold change at ZT18 compared to *Zfh*x3$^{Sci/+}$; UBC-Cre^{+}; downstream floxed region expression showed a 0.62 and 0.67 fold change at ZT6 and ZT18 respectively. *Vip* expression was also downregulated at both time-points in *Zfhx3*$^{Sci/-}$ mice: 0.15 at ZT6 and 0.70 at ZT18. The decrease in *Zfhx3* exons5-6 expression at ZT6 was also statistically significant at p=0.0148, all other changes were found to be non-significant (unfortunately, no non-*Sci* control tissues were available for comparison).

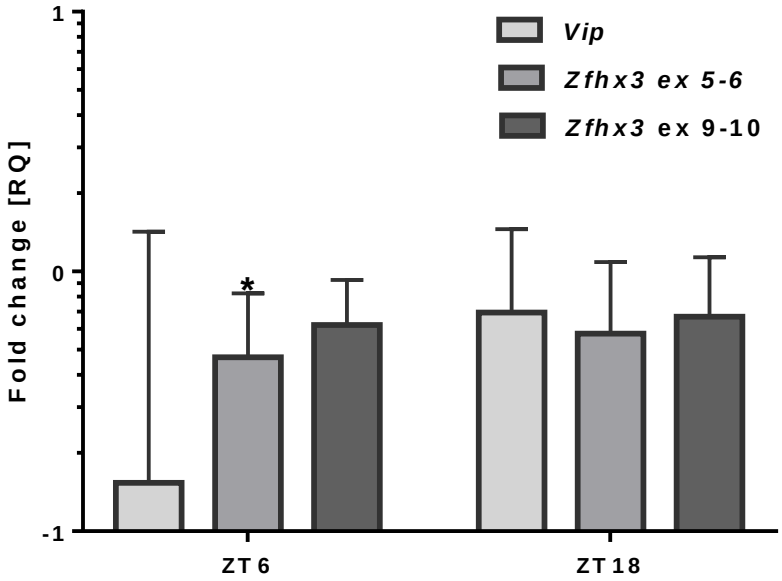


Figure 2.11 | Fold change calculated for *Vip* and *Zfhx3* expression from qPCR experiments on *Zfhx3*$^{Sci/-}$ and *Zfh*x3$^{Sci/+}$; UBC-Cre^{+} control SCN tissue punches, relative gene expression levels compared to the housekeeping gene *Actin*. Fold change was calculated using the $2^{(-\Delta\Delta Ct)}$ method. * denotes $p<0.05$.

Discussion

As the results of the previous chapter (Results I) showed, *Zfh*x3$^{Flox/+}$; UBC-Cre^{+} mice do not display a circadian period phenotype. This is the first indication that the *Sci* mutation is not a complete loss of function as *Zfhx3*$^{Sci/+}$ mice have a pronounced circadian period phenotype and therefore if this were a loss of function, the same would be expected in *Zfh*x3$^{Flox/+}$; UBC-Cre^{+} animals. Of course, this discrepancy could have been due to a developmental deficit in *Zfhx3*$^{Sci/+}$ mice as opposed to the heterozygote adult inducible mutants. *Zfhx3*$^{Sci/-}$ animals were shown to either have a further shortening of τ_{DD} or become arrhythmic in DD, compared to *Zfhx3*$^{Sci/+}$; *Zfhx3* and *Vip* expression was also downregulated in *Zfhx3*$^{Sci/-}$ SCN tissue compared to *Zfhx3*$^{Sci/+}$, indicating further molecular disruption to the circadian system.

Unfortunately no wildtype tissue was available for comparison in these qPCR studies, however previous data has demonstrated that *Zfhx3* and *Vip* are already downregulated in *Zfhx3*$^{Sci/+}$ animals (Parsons et al., 2015).

What is evident from this study and previous experiments (Parsons et al., 2015) is that there is most likely some loss of function effect on *Zfhx3,* as evidenced by reduction in gene expression of *Zfhx3* itself and various circadian related neuropeptides. However, other previous data (Hughes et al, unpublished) has shown that *Zfhx3*$^{Sci/+}$ mice display increased sensitivity under dim light conditions. Data presented in this chapter shows that *Zfhx3*$^{Sci/-}$ mice have an even further increase in pupillary light reflex under dim light conditions: this suggests a possible gain of function effect in the retina. It is reasonable to posit that given the complexity of ENU mutants, the *Sci* mutation contains a variety of hypo- and hypermorphic mutational functions in differing systems. However, with reference to a retinal phenotype in the *Zfhx3*$^{Sci/-}$ mouse, it should be noted that both *Zfhx3*$^{Sci/+}$ and *Zfhx3*$^{Sci/-}$ mice are maintained on a mixed genetic background that contains C3H – which has been shown to be a natural carrier of a mutation leading to retinal degeneration (Chang et al., 2002). Recently, pupil control has been shown to be modulated by both cone cell types in the retina, as well as melanopsin (Hayter and Brown, 2018). In light of this, *Zfhx3*$^{Sci/-}$ mice should be genotyped to ensure that they do not contain any retinal degeneration mutations that could confound the pupillometry data presented here and thus the attribution of any gain of function effects in *Sci*. However, this is unlikely as animals with degenerate retinae should constrict less in response to light stimulus – which is the opposite of what is described here in *Zfhx3*$^{Sci/-}$ animals.

It also cannot be ruled out that *Sci* may be an antimorphic mutation, similar to the original *Clock* mutant (King et al., 1997; Vitaterna et al., 2006), as this would also explain an exaggerated phenotype over a null allele. In this instance, the *Sci* mutation would be producing a gene product that competes with wildtype *Zfhx3* gene function; upon removal of the wildtype *Zfhx3* allele, the competing gene product would be able to fully assert its effects. Again, as previously stated, due to the pleiotropic nature of *Zfhx3*, the *Sci* mutation most likely contains elements of two or more classic mutational classifications – depending on the system studied.

Results III

Conditional deletion of Zfhx3 using spatially enriched Cre lines

Introduction

Zfhx3 is highly expressed in the developing brain before undergoing rapid downregulation in the majority of regions following birth (Ishii et al., 2003). Expression remains high in a small number of discrete nuclei, one being the SCN – where gene expression remains strikingly prevalent. Given previous data published on *Zfhx3*'s role in chronobiology (Balzani et al., 2016; Parsons et al., 2015), it is perhaps unsurprising that ZFHX3 is expressed throughout life in this key circadian pacemaker. In both studies, a dominant ENU-induced missense mutation resulted in significant circadian and sleep deficits. Following on from this, *Zfhx3* was then confirmed to be a critical gene necessary for the maintenance of functional circadian behaviour in adulthood – irrespective of any developmental role the gene has (Wilcox et al., 2017). However, both the ENU and tamoxifen-inducible mouse mutants resulted in *Zfhx3* disruption/loss in all tissues and brain regions of the mouse. This makes it somewhat difficult to disentangle a key area of circadian disruption, or a key area in which gene expression is needed to maintain a functional circadian system, as the role of other central and peripheral oscillators that may also express ZFHX3 cannot be excluded. Also, as *Zfhx3* is known to be involved in neurogenesis (Jung et al., 2005b), the transcription factor is a likely regulator of many neurodevelopmental processes throughout the brain (including the SCN). Therefore, it became pertinent to explore a possible role for *Zfhx3* in the developing SCN and assess whether Cre-mediated deletion of the gene in this area from an early developmental stage would affect circadian rhythm generation. To evaluate this, two conditional mouse mutants were generated – driven by the promoters of two genes known to have a role in SCN development: *Six3* and *Foxd1*. The resulting mutants from these crosses would lack

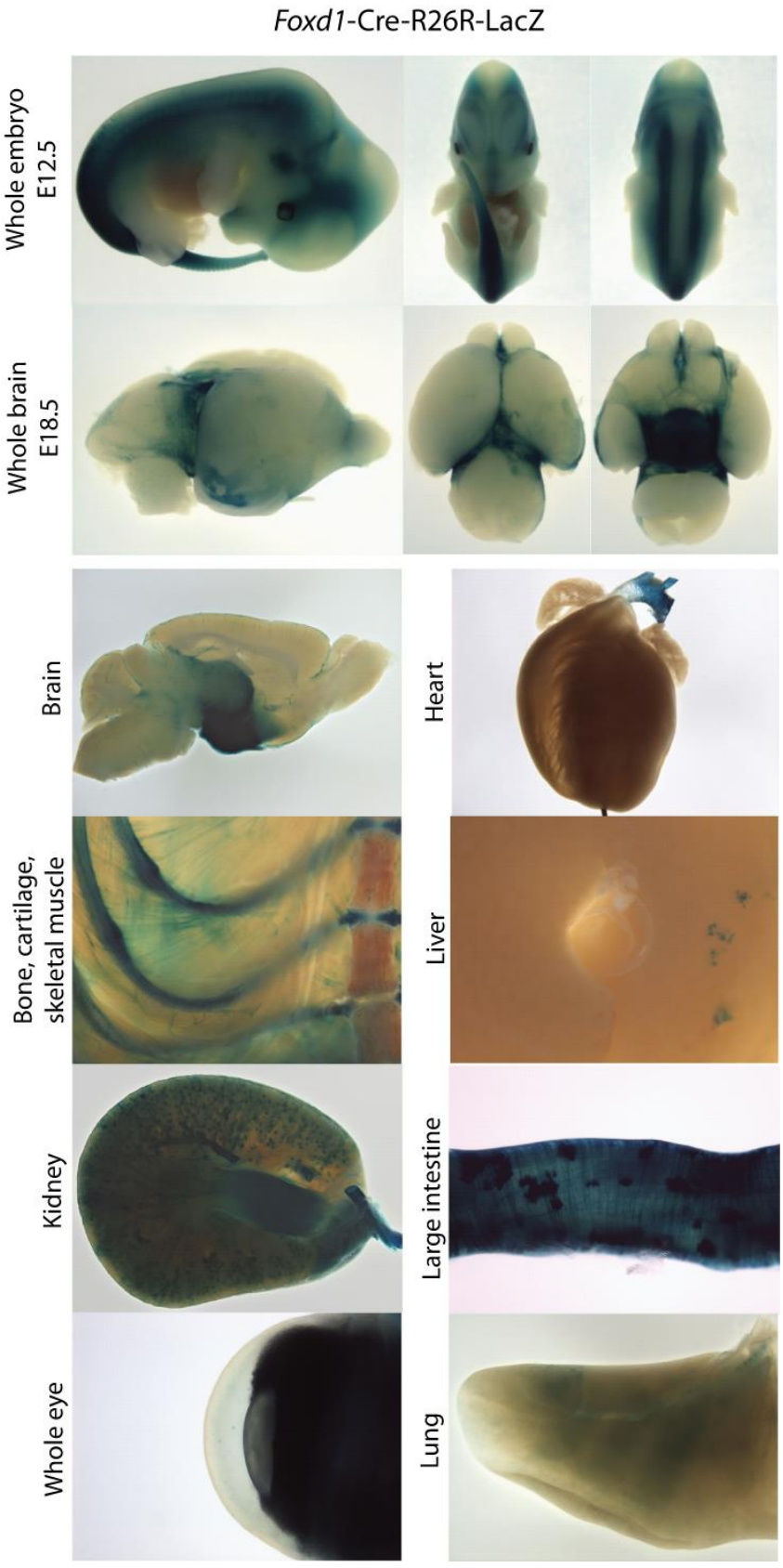
ZFHX3 in the SCN region from midgestation onwards, providing a unique opportunity to study what role the transcription factor has in development of the major pacemaker of the circadian system.

Characterisation of Cre expression patterns using a Lac-Z reporter

Utilising the same breeding strategy as previously described for generating conditional Cre-Lox mutants, mouse lines were generated that were homozygous or heterozygous for the *Zfhx3*^{Flox} allele and hemizygous for the Cre allele as well as controls. These mice are effectively heterozygous and homozygous mutants of *Zfhx3* loss in SCN. It should be noted that deletion of *Zfhx3* would only be relevant in regions where either *Six3* or *Foxd1* were expressed as well as *Zfhx3*; therefore deletion would not completely mirror areas of Cre activity shown with reporter lines.

To establish where/when Cre activity occurs in these lines and assess their suitability, both were crossed to an R26R Lac-Z expressing reporter and images taken to confirm patterns of Cre expression. In the *Foxd1*-Cre-R626R line, staining was observed throughout the spinal column of the embryo at E12.5 and strong Cre expression was apparent in the basal hypothalamic region of the brain at E18.5. Staining persists in the hypothalamus of the adult brain, as well as being apparent the eye, intestine and kidney. Weak staining also emerged in the adult lung and liver. The *Six3*-Cre-R626R line had much more localised expression in the forebrain of the embryo at E12.5, which continued into the E18.5 brain. In the adult, strong staining was apparent in the basal hypothalamus of the brain, as well as in the eye and optic nerves. Considering both reporter lines in parallel; *Foxd1* was found to have staining

in a greater number of peripheral organs in addition to the brain (**Figure 3.1**), as well as more widespread expression in the 18.5dpc embryo. This indicated that this Cre line might not produce as tight spatial deletion of *Zfhx3* as the *Six3*-Cre line would. However, expression in the developing hypothalamus was robust in both lines and consistent staining patterns were observed between littermates. In addition to this whole organ staining, adult brains were coronally sectioned and images taken to confirm that Cre activity was evident in the SCN region – as this was the primary target for deletion. In both lines, this was indeed the case and so they were both deemed suitable lines to drive deletion of *Zfhx3* in cells that go on to form the adult SCN in mice. Staining appeared notably stronger in images of the adult SCN from *Six3*-Cre-R26R line (**Figure 3.2**). Some scattered cortical staining was observed in both lines; off target Cre expression is a common occurrence and so this was not unexpected, however these areas did not appear to overlap with *Zfhx3* expression and so fortunately would not lead to off target deletion of *Zfhx3*.


Foxd1-Cre-R26R-LacZ
Whole embryo E12.5
Whole brain E18.5
Brain
Heart
Bone, cartilage, skeletal muscle
Liver
Kidney
Large intestine
Whole eye
Lung

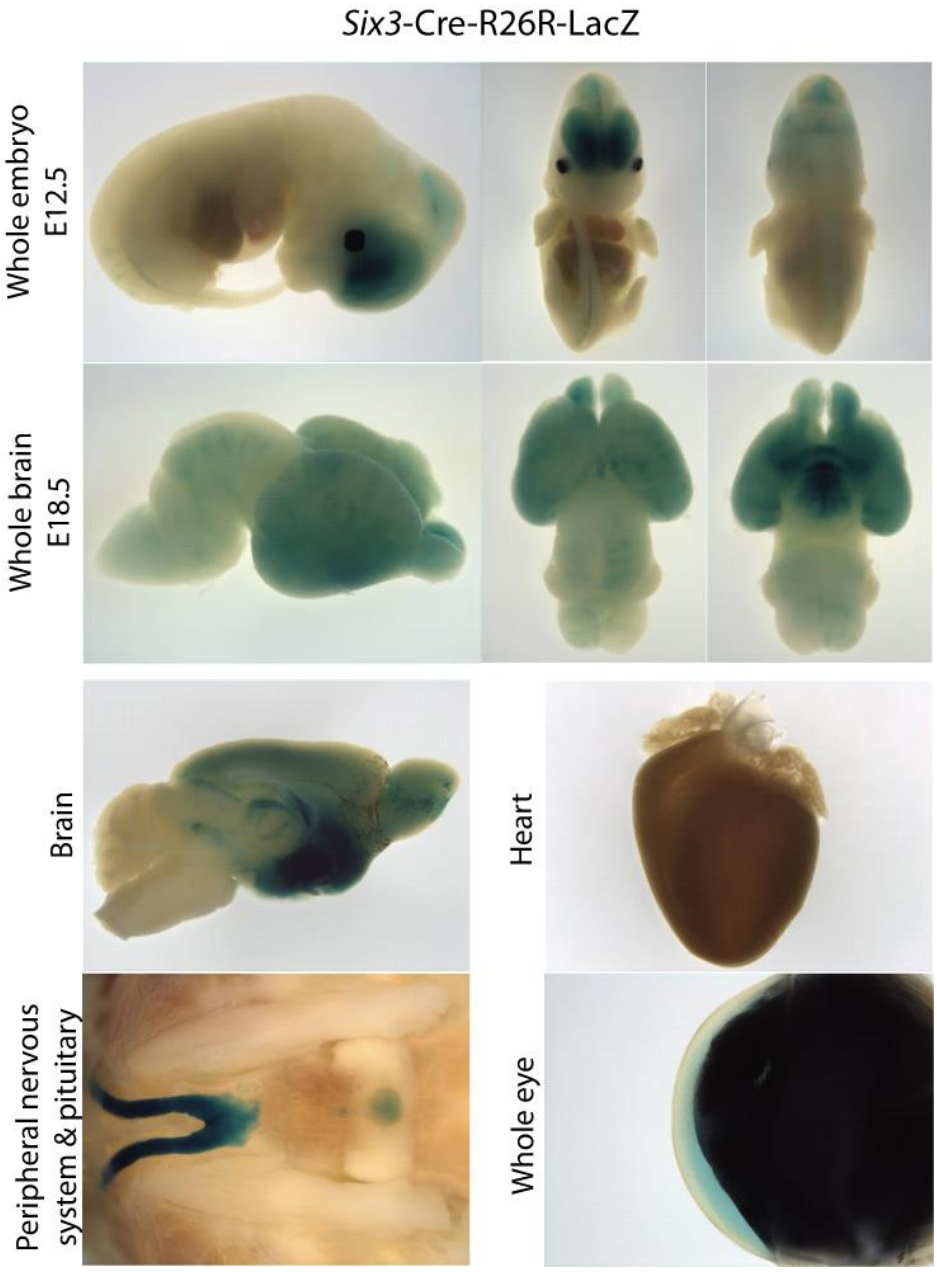


Figure 3.1 | Representative images of X-Gal staining to show Cre activity in *Foxd1*-Cre-R26R and *Six3*-Cre-R26R Lac Z expressing reporter lines. Images shown are for organs where staining was detected for each line.

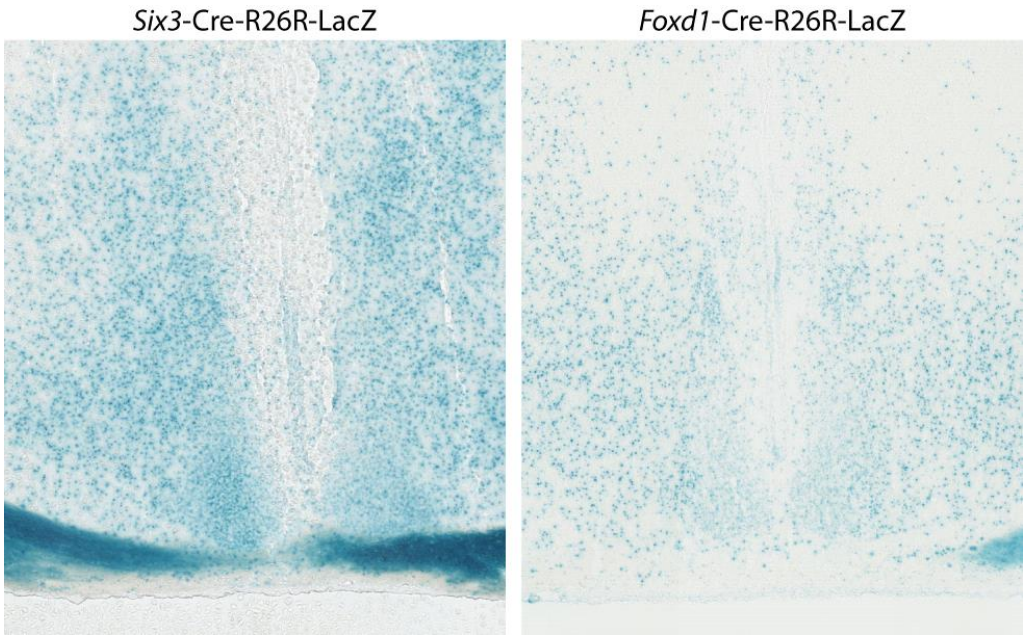


Figure 3.2 | Representative images of X-Gal staining for *Six3*-Cre and *Foxd1*-Cre R26R-LacZ reporter lines in adult brain; sections are shown for central SCN region. Magnification 5x for both images.

Circadian screening of region-specific *Zfhx3* loss driven by *Six3*-Cre

Following characterisation of Cre activity using the R26R reporter line, both Cre lines were crossed to the *Zfhx3*^{Flox} line to create region-specific KO mutants of *Zfhx3*. The first of these lines to be discussed will be *Zfhx3*$^{Flox/Flox}$; *Six3*-Cre^{+}. As with previous conditional *Zfhx3* mutants (see circadian screening in Results I), the primary circadian phenotyping these mice underwent was standard wheel running to assess their locomotor rhythms in LD, DD and LL. This initial screening revealed a striking phenotype in *Zfhx3*$^{Flox/Flox}$; *Six3*-Cre^{+} animals; these mice were behaviourally arrhythmic in DD and LL, but also appeared to show a complete absence of masking behaviour in LD – arguably the most severe circadian phenotype observable (**Figure 3.3**). This lack of response to light in a circadian context limited the breadth of traditional circadian phenotyping available to utilise on this mutant. Despite this, the

complete arrhythmia in all lighting conditions was a striking phenotype alone. In contrast, *Zfhx3*$^{Flox/+}$; *Six3*-Cre^{+} mice showed a potential subtle change in circadian locomotor activity; on first analysis the only parameter displaying change was α_{DD} (**Table 3.1**). The heterozygote mutants appeared to be active for longer in DD compared to controls when analysed using ANOVA [$F(4, 35)=3.875$, $p=0.0104$]. Tukey multiple testing between groups revealed that *Zfhx3*$^{Flox/+}$; *Six3*-Cre^{+} mice were shown to have a significantly higher α_{DD} compared to *Zfhx3*$^{Flox/Flox}$; *Six3*-Cre^{-} mice [$p=0.0260$], but no significant difference was found when comparing *Zfhx3*$^{Flox/+}$; *Six3*-Cre^{+} to any other control groups. Therefore, the biological relevance of this is most likely minimal as any true difference in circadian activity should yield a significant change in mutants compared to all control groups.

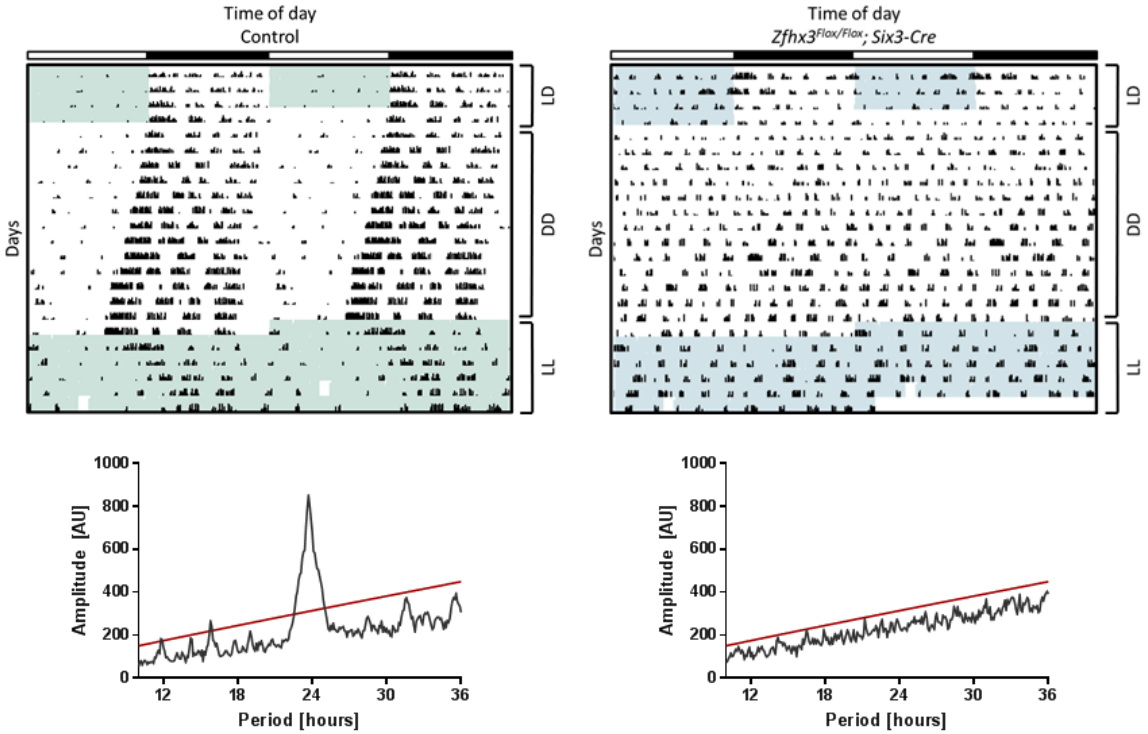


Figure 3.3 | Representative actogram for initial *Zfhx3*$^{Flox/Flox}$; *Six3*-Cre^{+} mice [n=10] screened using wheel running assay (right); a representative actogram for *Zfhx3*$^{Flox/Flox}$; *Six3*-Cre^{-} control mice is shown on the left for comparison. Beneath are periodograms generated from the DD portion of each actogram, showing the amplitude of the τ_{DD} measured – confirming that there is no circadian rhythm evident in *Zfhx3*$^{Flox/Flox}$; *Six3*-Cre^{+} mice.

Genotype	n	αLD	LD_{Amp}
Zfhx3$^{Flox/+}$; *Six3*-Cre^{+}	15	11.41 (±0.16)	2621 (±158.7)
Zfhx3$^{Flox/Flox}$	6	11.62 (±0.25)	2787 (±214.5)
Zfhx3$^{Flox/+}$	6	11.95 (±0.27)	2342 (±122.2)
Zfhx3$^{+/+}$; *Six3*-Cre^{+}	7	11.58 (±0.14)	3096 (±329.5)
Zfhx3$^{+/+}$	6	11.98 (±0.21)	2652 (±277.0)
Significance		F(4,35)=1.511, *p*=0.2201	F(4,35)=1.263, *p*=0.3028

Genotype	n	τDD	αDD	DD_{Amp}
Zfhx3$^{Flox/+}$; *Six3*-Cre^{+}	15	23.73 (±0.05)	13.65 (±0.43)	4417 (±561.2)
Zfhx3$^{Flox/Flox}$	6	23.83 (±0.02)	11.85 (±0.28)	5020 (±792.6)
Zfhx3$^{Flox/+}$	6	23.89 (±0.04)	12.13 (±0.32)	3309 (±314.9)
Zfhx3$^{+/+}$; UBC-Cre^{+}	7	23.77 (±0.05)	12.56 (±0.28)	5137 (±634.2)
Zfhx3$^{+/+}$	6	23.87 (±0.07)	12.16 (±0.28)	4686 (±702.4)
Significance		F(4, 35)=1.571, *p*=0.2036	F(4,35)=3.875, *p*=0.0104	F(4,35)=0.9712, *p*=0.4356

Genotype	n	τLL	LL_{Amp}
Zfhx3$^{Flox/+}$; *Six3*-Cre^{+}	11	24.96 (±0.13)	3425 (±382.6)
Zfhx3$^{Flox/Flox}$	5	25.24 (±0.13)	4200 (±889.9)
Zfhx3$^{Flox/+}$	6	25.48 (±0.15)	4289 (±341.9)
Zfhx3$^{+/+}$; UBC-Cre^{+}	5	25.09 (±0.08)	3536 (±449.3)
Zfhx3$^{+/+}$	5	25.24 (±0.04)	4691 (±797.0)
Significance		F(4,27)=2.626, *p*=0.0566	F(4,28)=10.82, *p*=0.3845

Table 3.1 | Mean values (± SEM) of circadian parameters measured for all *Zfhx3-Six3* genotypes tested. D'Agostino & Pearson test for normality was conducted on data to test for Gaussian distribution before one way ANOVAs were conducted to assess significance (α=0.05). Not all mice underwent LL screening due to timing issues, which accounts for the change in n number for LL data.

Circadian screening of region-specific *Zfhx3* loss driven by *Foxd1*-Cre

Zfhx3$^{Flox/Flox}$; *Foxd1*-Cre^{+} animals, and controls, also underwent initial wheel running circadian screens in LD, DD and LL conditions. These mutants showed a variety of different wheel running phenotypes, making this a challenging line to assess phenotypically. As shown in **Figure 3.4**, wheel running activity in DD was inconsistent in certain animals – with period appearing to change part way through constant conditions. Others displayed stronger offsets than onsets of activity or long periods of activity, which can lead to inconsistent identification of activity onset. In addition to this, some mutant mice did not run particularly well on wheels, again making data collection quite challenging (example actograms shown in **Figure 3.5**). However despite these differences in behaviour, all mutants appeared to entrain to the LD cycle and there was no difference in τDD when compared to controls – unlike what was observed in *Zfhx3*$^{Flox/Flox}$; *Six3*-Cre^{+} mice. **Table 3.2** summarises the data collected on circadian parameters for the *Zfhx3*$^{Flox/Flox}$; *Foxd1*-Cre^{+} line; amplitude was the only parameter significantly different between genotypes, this was a consistent finding in LD [H=12.55, p=0.0137], DD [F(4,38)=9.103, p<0.0001] and LL [H=14.6, p=0.0056] and the data showed that mutants had a much lower amplitude throughout screening (**Figure 3.6**). For LD and LL, Dunn's test was used for multiple comparisons between the genotypes. The results of this showed that significant differences were found between *Zfhx3*$^{+/+}$ controls and *Zfhx3*$^{Flox/Flox}$; *Foxd1*-Cre^{+} and *Zfhx3*$^{Flox/+}$; *Foxd1*-Cre^{+} mice in LD [p=0.0212 and p=0.0317, respectively], and the same groups were also found to be different in LL [p=0.0070 and p=0.0294, respectively]. For DD, Tukey multiple comparison testing was used following an initial ANOVA. This revealed that *Zfhx3*$^{Flox/Flox}$; *Foxd1*-Cre^{+} mice had a significantly

lower DD_{Amp} than *Zfhx3*$^{Flox/Flox}$ [p=0.0192], *Zfhx3*$^{Flox/+}$ [p=0.0263] and *Zfhx3*$^{+/+}$ [p<0.0001] mice; *Zfhx3*$^{Flox/+}$; *Foxd1*-Cre^{+} mice were found to be only significantly different to *Zfhx3*$^{+/+}$ mice [p=0.0027]. This consistently lower amplitude throughout screening perhaps explains the inconsistency observed in locomotor behaviour between *Zfhx3*$^{Flox/Flox}$; *Foxd1*-Cre^{+} animals, as low amplitude indicates a less robust circadian rhythm and therefore this could cause aberrant wheel running activity.

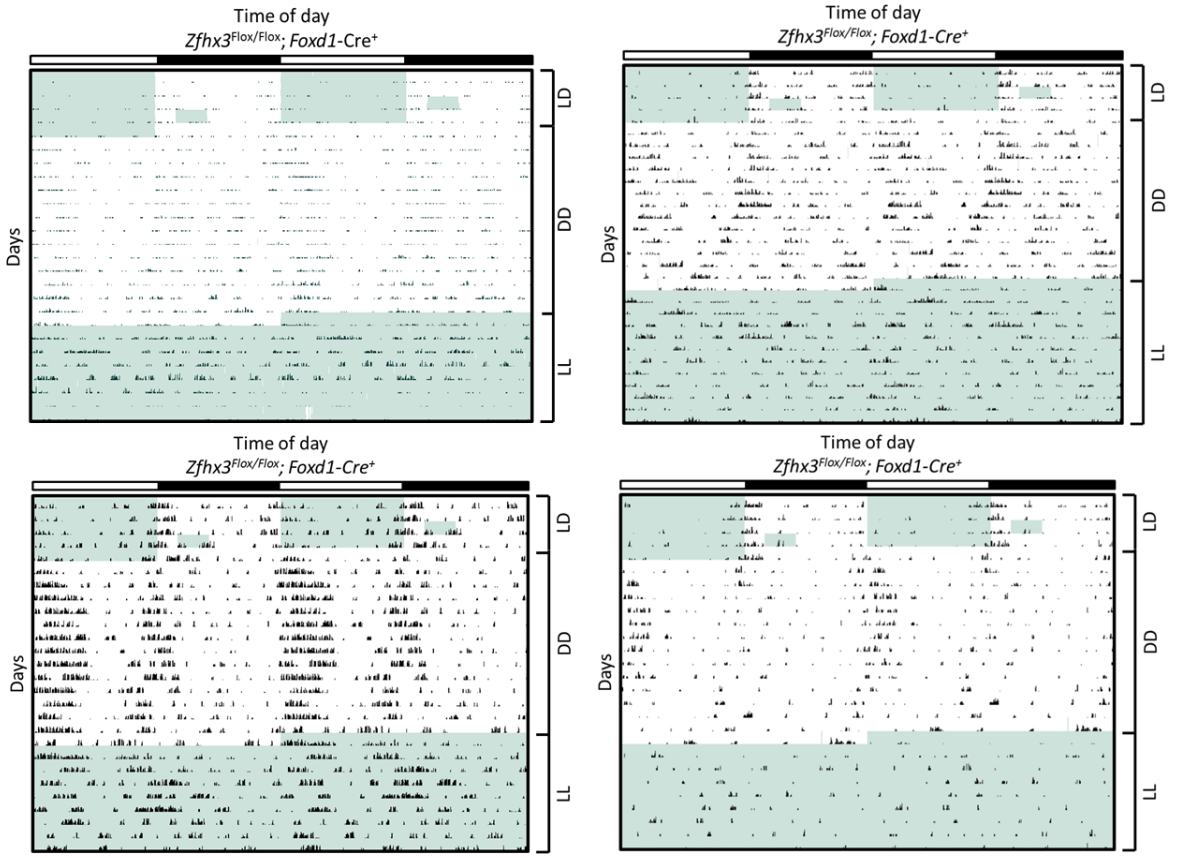


Figure 3.4 | Representative actograms of *Zfhx3*$^{Flox/Flox}$; *Foxd1*-Cre^{+} mice housed in LD, DD and LL conditions. A variety of phenotypes were observed, with some mice having stronger offsets than onsets and others not utilising the running wheel consistently. A masking light pulse was conducted in the early portion of the dark phase of LD day 4 on these actograms.

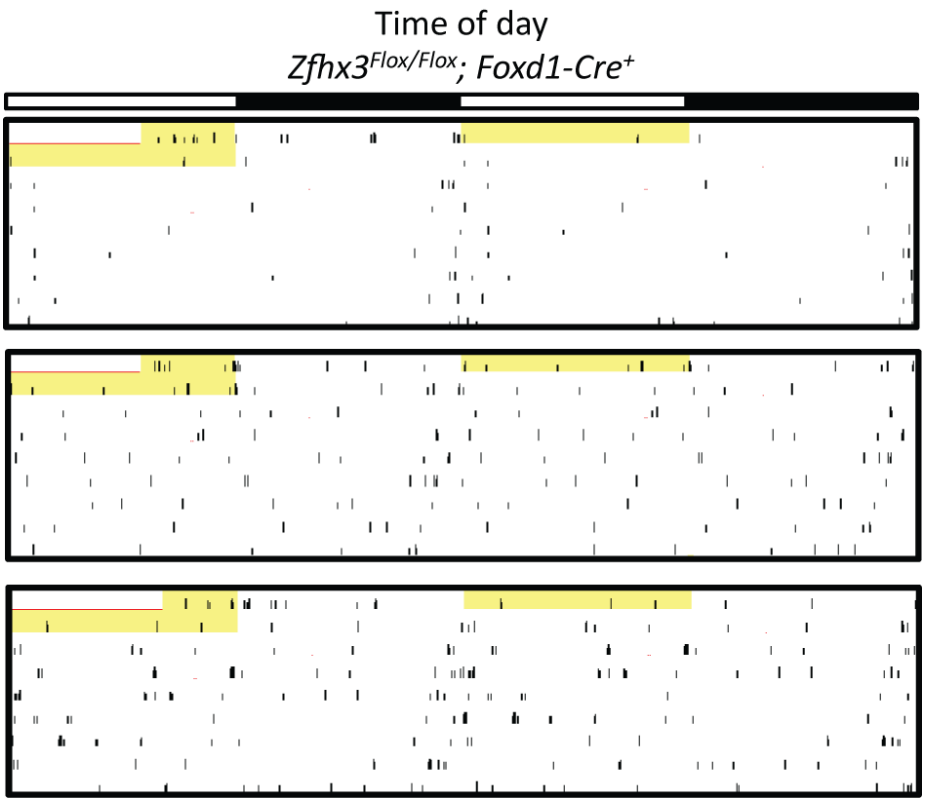


Figure 3.5 | Representative actograms of inconsistent wheel running behaviour in *Zfhx3*$^{Flox/Flox}$; *Foxd1*-Cre^{+} mutants. Yellow shading denotes lights on.

Genotype	n	αLD	n	LD_{Amp}
Zfhx3$^{Flox/Flox}$; *Foxd1*-Cre^{+}	12	12.3 (±0.32)	10	2150 (±28.4)
Zfhx3$^{Flox/+}$; *Foxd1*-Cre^{+}	10	11.1 (±0.28)	10	2218 (±180.7)
Zfhx3$^{Flox/Flox}$	6	11.8 (±0.28)	5	2836 (±451.3)
Zfhx3$^{Flox/+}$	8	11.6 (±0.26)	8	2328 (±174.8)
Zfhx3$^{+/+}$	7	11.8 (±0.12)	7	2958 (±96.8)
Significance		H=9.237, *p*=0.0554		H=12.55, *p*=0.0137

Genotype	n	τDD	n	αDD	n	DD_{Amp}
Zfhx3$^{Flox/Flox}$; *Foxd1*-Cre^{+}	11	23.79 (±0.07)	11	11.48 (±1.72)	11	2500 (±155.4)
Zfhx3$^{Flox/+}$; *Foxd1*-Cre^{+}	10	23.71 (±0.05)	10	12.16 (±0.40)	10	3528 (±421.5)
Zfhx3$^{Flox/Flox}$	7	23.77 (±0.10)	7	11.67 (±0.52)	7	4432 (±394.9)
Zfhx3$^{Flox/+}$	8	23.85 (±0.04)	8	11.81 (±0.24)	8	4286 (±608.3)
Zfhx3$^{+/+}$	7	23.88 (±0.05)	7	11.86 (±0.18)	7	5934 (±522.9)
Significance		H=4.348, *p*=0.3609		F(4,38)=0.6897, *p*=0.9909		F(4,38)=9.103, *p*<0.0001

Genotype	n	τLL	n	LL_{Amp}
Zfhx3$^{Flox/Flox}$; *Foxd1*-Cre^{+}	6	24.66 (±0.38)	4	2334 (±353.4)
Zfhx3$^{Flox/+}$; *Foxd1*-Cre^{+}	10	24.82 (±0.12)	10	3283 (±417.9)
Zfhx3$^{Flox/Flox}$	7	25.1 (±0.04)	7	4207 (±140.7)
Zfhx3$^{Flox/+}$	8	24.99 (±0.07)	8	4215 (±724.3)
Zfhx3$^{+/+}$	7	25.16 (±0.07)	7	6340 (±649.8)
Significance		F(4,33)=1.527, *p*=0.2170		H=14.6, *p*=0.0056

Table 3.2 | Mean values (± SEM) of circadian parameters measured for all *Zfhx3-Foxd1* genotypes tested. D'Agostino & Pearson or Shapiro-Wilk test for normality was conducted on data to test for Gaussian distribution before one way ANOVAs or Kruskal-Wallis analysis were conducted to assess significance (α=0.05).; numbers [n] vary amongst parameters measured due to unreliable wheel running in certain parts of the screening for some animals.

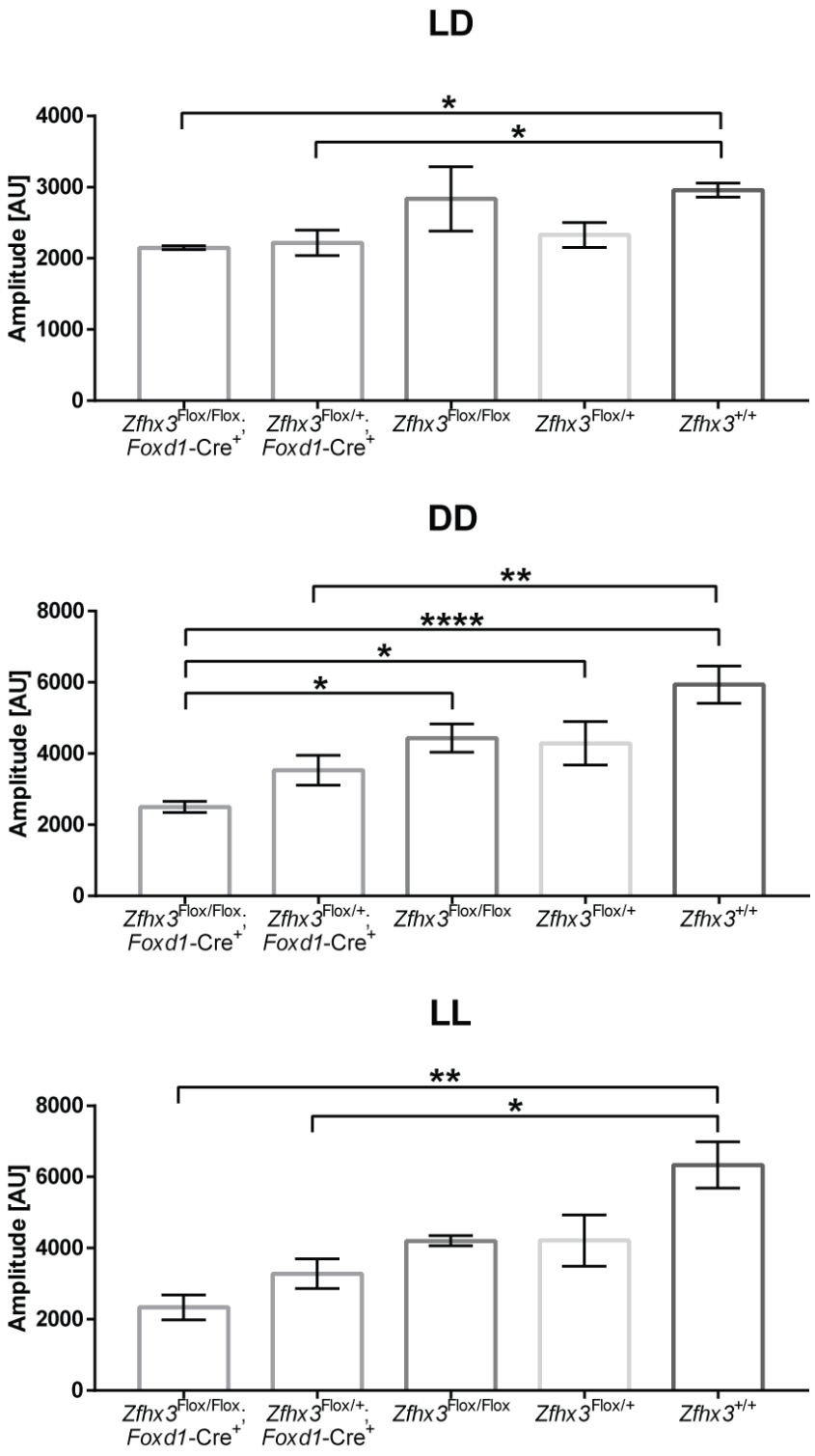


Figure 3.6 | Mean values for amplitude in LD, DD and LL for all genotypes tested from the *Zfhx3-Foxd1* line. Dunn's multiple testing was used to assess LD and LL amplitude, Tukey multiple comparison test was used to assess DD amplitude. Significance level is indicated on the graphs; * denotes $p<0.05$, ** denotes $p<0.01$, *** denotes $p<0.001$ and **** denotes $p<0.0001$.

As *Zfhx3*$^{Flox/Flox}$; *Foxd1*-Cre^{+} mice appeared to entrain to the LD cycle, despite expressing a range of wheel running characteristics in DD and LL, the next step was to confirm whether this was true entrainment or masking behaviour. The first step to study this was to introduce a masking light pulse in one of the circadian screens being conducted; this was a 3 hour light pulse at ZT13-16 during LD. Light at this time should suppress circadian locomotor activity compared to the previous day's activity, **Figure 3.7** shows an example of how this appears on control actogram (*Zfhx3*$^{Flox/+}$ was used for this example) in contrast to a *Zfhx3*$^{Flox/Flox}$; *Foxd1*-Cre^{+} mutant. This was assessed by comparing activity in this time window to that recorded on the previous two days. **Figure 3.4** shows actograms taken from this screen that include a masking light pulse; it is evident from just these three examples that *Zfhx3*$^{Flox/Flox}$; *Foxd1*-Cre^{+} mice displayed differing reactions to the light, with activity being suppressed to different extents among individuals. Again, analysis of this data was hampered by the significantly reduced levels of wheel running activity observed in certain individuals – meaning there was no measurable activity regardless of the light pulse. A total of five *Zfhx3*$^{Flox/Flox}$; *Foxd1*-Cre^{+} mice that were assessed in the screen containing the light pulse resulted in enough measurable activity data to analyse, along with two *Zfhx3*$^{Flox/Flox}$ and three *Zfhx3*$^{+/+}$ control mice. For analysis purposes, data from the two control groups was pooled to enable an appropriate comparison using equal numbers of animals. Total activity counts were measured for the 3 hour time period during the light pulse; this was then compared to an average of the activity for the same 3 hour time period on the previous 2 days prior to the pulse (**Figure 3.8**). The data shows that not only did *Zfhx3*$^{Flox/Flox}$; *Foxd1*-Cre^{+} mice not display a suppression of locomotor activity, the mean activity counts increased from an average of 59(±23) to 151(±69). In

contrast control mice exhibited a decrease in average activity counts from 928(±167) to 367(±177), which was found to be significant using paired t-test [t(4)=3.188, p=0.0333]. *Zfhx3*$^{Flox/Flox}$; *Foxd1*-Cre^{+} mice displayed substantially less activity on days prior to the light pulse than controls, which could account for the apparent increase during the pulse.



Figure 3.7 | Representative actograms of behavioural response to a masking light pulse in *Zfhx3*$^{Flox/Flox}$; *Foxd1*-Cre^{+} mutants and *Zfhx3*$^{Flox/+}$ control animals. Blue shaded area denotes lights on. Locomotor activity is suppressed in *Zfhx3*$^{Flox/+}$ control mice during the light pulse, whereas the *Zfhx3*$^{Flox/Flox}$; *Foxd1*-Cre^{+} mouse continues to be active during this period.

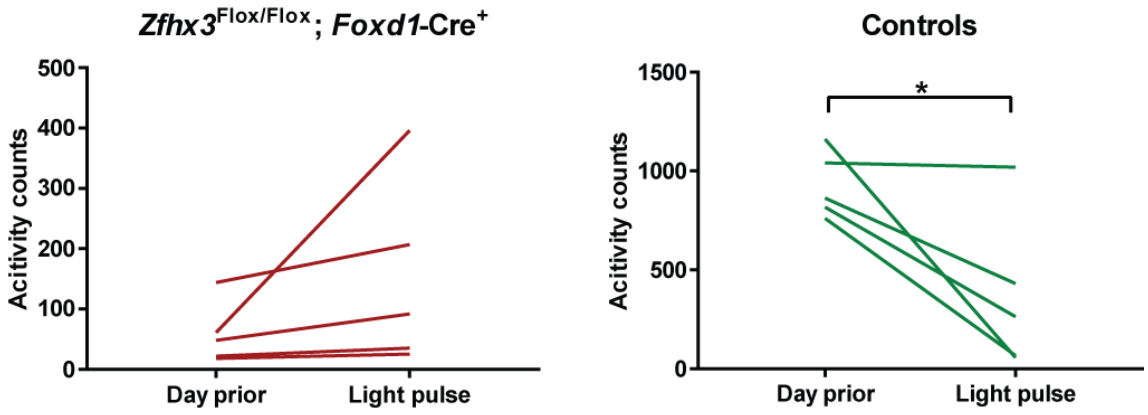


Figure 3.8 | *Zfhx3*$^{Flox/Flox}$; *Foxd1*-Cre^{+} and control mice were exposed to a 3 hour light pulse from ZT13-16. Activity counts were recorded for this 3 hour period and also the average from a corresponding 3 hour period in the 2 days prior to the light pulse. Paired t-tests were used to compare activity prior to and during the light pulse; controls showed a significant suppression of activity [t(4)=3.188, p=0.0333].

Following on from this, skeleton photoperiods were used to assess entrainment to the LD cycle in *Zfhx3*$^{Flox/Flox}$; *Foxd1*-Cre^{+} animals. Mice were housed on a standard LD cycle before being released into DD for 9 days; they were then exposed to a skeleton photoperiod, consisting of lights on at the start and end of the 'light' phase only, and their entrainment evaluated. Representative actograms for *Zfhx3*$^{Flox/Flox}$; *Foxd1*-Cre^{+} and *Zfhx3*$^{+/+}$; *Foxd1*-Cre^{+} mice are shown in **Figure 3.10**. All control [n=15] and also all *Zfhx3*$^{Flox/+}$; *Foxd1*-Cre^{+} [n=11] mice showed full entrainment to this skeleton LD cycle. Unfortunately, out of a total of 15 *Zfhx3*$^{Flox/Flox}$; *Foxd1*-Cre^{+} mice screened, 8 animals did not run enough to produce measurable entrainment data. From the remaining 7 animals, only 3 exhibited measurable entrainment. To assess entrainment, period and amplitude (**Figure 3.9**) were measured during the days in which mice were housed under the skeleton photoperiod. Period during this time was 24hr for almost all mice that displayed entrainment, this was comparable among all genotypes [H=6.097, p=0.1070]. The corresponding amplitude, however, for these

periods was found to be statistically different among genotypes [H=11.78, p=0.0082]. Multiple comparison testing revealed that *Zfhx3*$^{Flox/Flox}$ control mice had a significantly higher amplitude than *Zfhx3*$^{Flox/+}$; *Foxd1*-Cre^{+} [adjusted p=0.0200] and *Zfhx3*$^{Flox/Flox}$; *Foxd1*-Cre^{+} mice [adjusted p=0.0413]. From this data it can be concluded that *Zfhx3*$^{Flox/+}$; *Foxd1*-Cre^{+} are capable of entrainment to a standard LD cycle, however they show a reduced circadian amplitude – concurrent with their behaviour under a standard LD cycle, whereas the majority of *Zfhx3*$^{Flox/Flox}$; *Foxd1*-Cre^{+} mice do not show measurable entrainment behaviour under LD conditions.

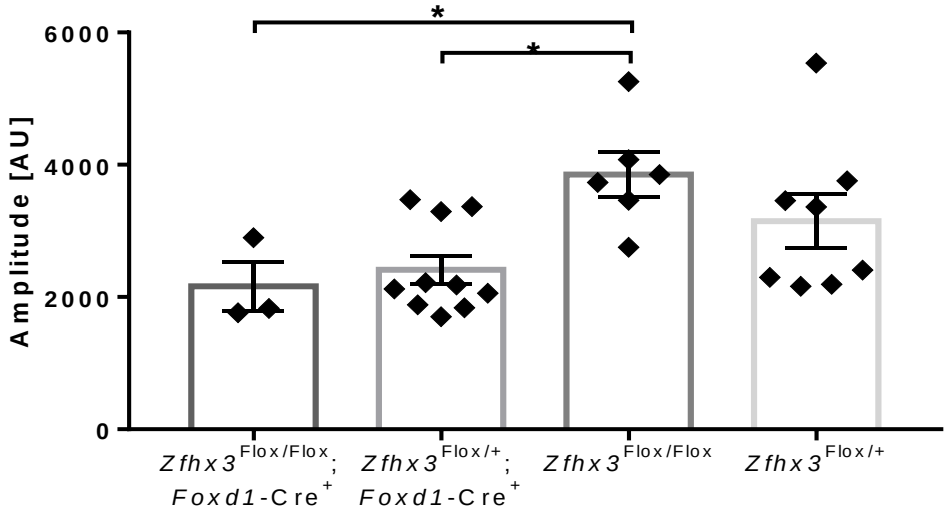


Figure 3.9 | Circadian amplitude during entrainment to skeleton photoperiods for *Zfhx3*$^{Flox/Flox}$; *Foxd1*-Cre$^{+,}$ *Zfhx3*$^{Flox/+}$; *Foxd1*-Cre$^{+,}$ *Zfhx3*$^{Flox/Flox}$ and *Zfhx3*$^{Flox/+}$ mice. * denotes significance at p<0.05.

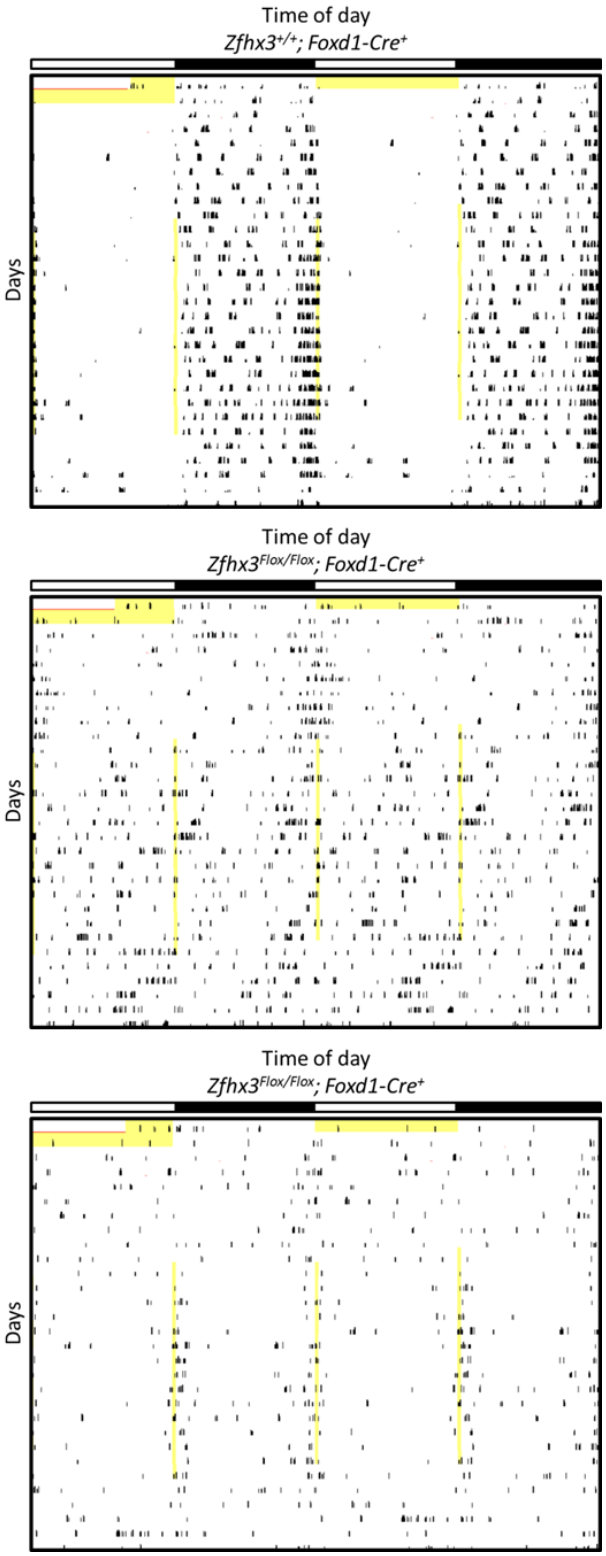


Figure 3.10 | Representative actograms for control and *Zfhx3*$^{Flox/Flox}$; *Foxd1*-Cre^{+} animals undergoing a skeleton photoperiod protocol to assess entrainment. All control mice entrained to this skeleton LD cycle compared with only 3 out of 7 *Zfhx3*$^{Flox/Flox}$; *Foxd1*-Cre^{+} mice. Yellow shading denotes lights on, first 2 days are a standard 12:12 LD cycle before release into DD, skeleton photoperiods occur from day 8 in DD.

Video tracked sleep screening of *Zfhx3*$^{Flox/Flox}$; *Six3*-Cre^{+} mice

Video tracked sleep screen analysis was used to screen for any sleep phenotypes in *Zfhx3*$^{Flox/Flox}$; *Six3*-Cre^{+} and *Zfhx3*$^{Flox/+}$; *Six3*-Cre^{+} mice; not all control genotypes could be screened in parallel with mutants and so *Zfhx3*$^{+/+}$; *Six3*-Cre^{+} mice were chosen as a representative control group for screening. Total values for parameters measured are shown in **Figure 3.11**; data was analysed using either ANOVA or Kruskal-Wallis testing followed by Tukey or Dunn's multiple comparison tests, respectively. Distance travelled in the light phase of the LD cycle was comparable between groups [H=0.4573, p=0.7956]. Distance travelled in the dark phase, however, was much reduced in *Zfhx3*$^{Flox/Flox}$; *Six3*-Cre^{+} mice when compared to both *Zfhx3*$^{Flox/+}$; *Six3*-Cre^{+} [adjusted p=0.0027] and control [adjusted p=0.0012] animals. Time spent immobile – i.e. time spent asleep, was significantly lower in the light phase for *Zfhx3*$^{Flox/Flox}$; *Six3*-Cre^{+} when compared to *Zfhx3*$^{Flox/+}$; *Six3*-Cre^{+} [adjusted p=0.0008] and control [adjusted p=0.0078] mice. In contrast, *Zfhx3*$^{Flox/Flox}$; *Six3*-Cre^{+} mice spent more time asleep in the dark phase compared to *Zfhx3*$^{Flox/+}$; *Six3*-Cre^{+} [adjusted p=0.0007] and control [adjusted p=0.0017] mice. Despite a significant decrease in total time immobile in the light phase, immobile episodes in the light were unaffected in *Zfhx3*$^{Flox/Flox}$; *Six3*-Cre^{+} mutants [F(2,28)=0.6078, p=0.5516]. However, as well as an increase in total time immobile in the dark phase, there was also a substantial increase in immobile episodes in the dark for *Zfhx3*$^{Flox/Flox}$; *Six3*-Cre^{+} mice [adjusted p<0.0001 when compared to both groups]. Taken collectively, this indicates increased sleep in the dark phase of the LD cycle in *Zfhx3*$^{Flox/Flox}$; *Six3*-Cre^{+} mice. Activity over 24 hours was also assessed in this screen (**Figure 3.12**); this was found to be significantly different between genotypes [F(46,644)=3.451, p<0.0001], with

Zfhx3$^{Flox/Flox}$; *Six3*-Cre^{+} mice showing a reduction in activity throughout the dark phase.

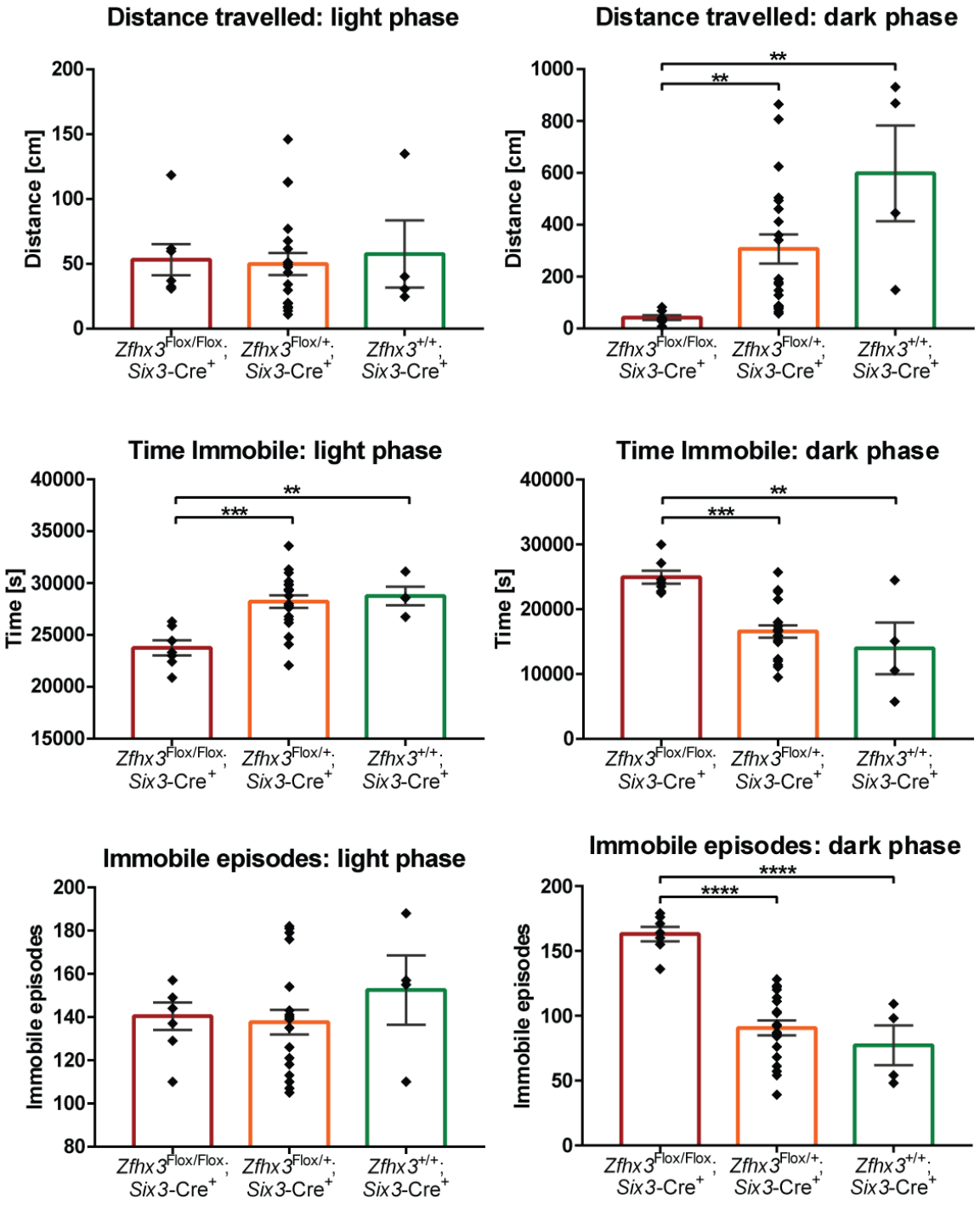


Figure 3.11 | Sleep parameters measured in *Zfhx3*$^{Flox/Flox}$; *Six3*-Cre^{+} [n=7], *Zfhx3*$^{Flox/+}$; *Six3*-Cre^{+} [n=20] and *Zfhx3*$^{+/+}$; *Six3*-Cre^{+} [n=4] mice. All measurements were over a 24 hour period of a standard 12:12 LD cycle. Error bars denote SEM of mean for group data. ** denotes significance at $p<0.01$, *** denotes significance at $p<0.001$, **** denotes significance at $p<0.0001$.

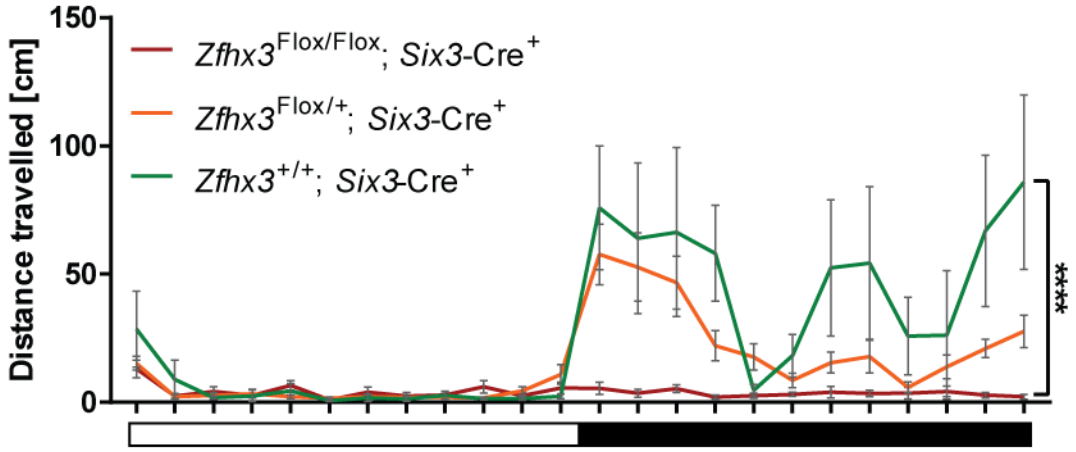


Figure 3.12 | Activity over time for *Zfhx3*$^{Flox/Flox}$; *Six3*-Cre^{+} [n=7], *Zfhx3*$^{Flox/+}$; *Six3*-Cre^{+} [n=20] and *Zfhx3*$^{+/+}$; *Six3*-Cre^{+} [n=4] mice. Lines denote average data for each genotype; error bars denote SEM of mean for group data; LD cycle indicated below graphs; **** denotes significance at $p<0.0001$.

Video tracked sleep screening of *Zfhx3*$^{Flox/Flox}$; *Foxd1*-Cre^{+} mice

Video tracked sleep screen analysis was also undertaken on the *Zfhx3*$^{Flox/Flox}$; *Foxd1*-Cre^{+} mutant line to screen for any sleep phenotypes. All parameters measured in the light phase were unaltered in *Zfhx3*$^{Flox/Flox}$; *Foxd1*-Cre^{+} animals compared to *Zfhx3*$^{Flox/+}$; *Foxd1*-Cre^{+} and *Zfhx3*$^{+/+}$; *Foxd1*-Cre^{+} control mice; namely distance travelled [H=0.3864, p=0.8243], time immobile [F(2,19)=1.153, p=0.3369] and number of immobile episodes [F(2,19)=0.0077, p=0.9924]. Conversely when analysing these parameters in the dark phase, distance travelled [H=7.617, p=0.0222], time immobile [F(2,19)=6.034, p=0.0094] and number of immobile episodes [F(2,19)=4.633, p=0.0230] were all significantly different among genotypes. Multiple testing revealed that *Zfhx3*$^{Flox/Flox}$; *Foxd1*-Cre^{+} showed a significant decrease in distance travelled in the dark compared to controls [adjusted p=0.0175]. Correspondingly, these mutants also had a greater number of immobile episodes [adjusted p=0.0271] and total time immobile [adjusted p=0.008] in the dark phase (**Figure 3.13**). Activity over 24 hours

was also statistically altered between groups [$F(46,437)=2.754$, $p<0.0001$], with *Zfhx3*$^{Flox/+}$; *Foxd1*-Cre^{+} and *Zfhx3*$^{Flox/Flox}$; *Foxd1*-Cre^{+} mutant mice both displaying a decrease in activity in the dark phase of the LD cycle (**Figure 3.14**).

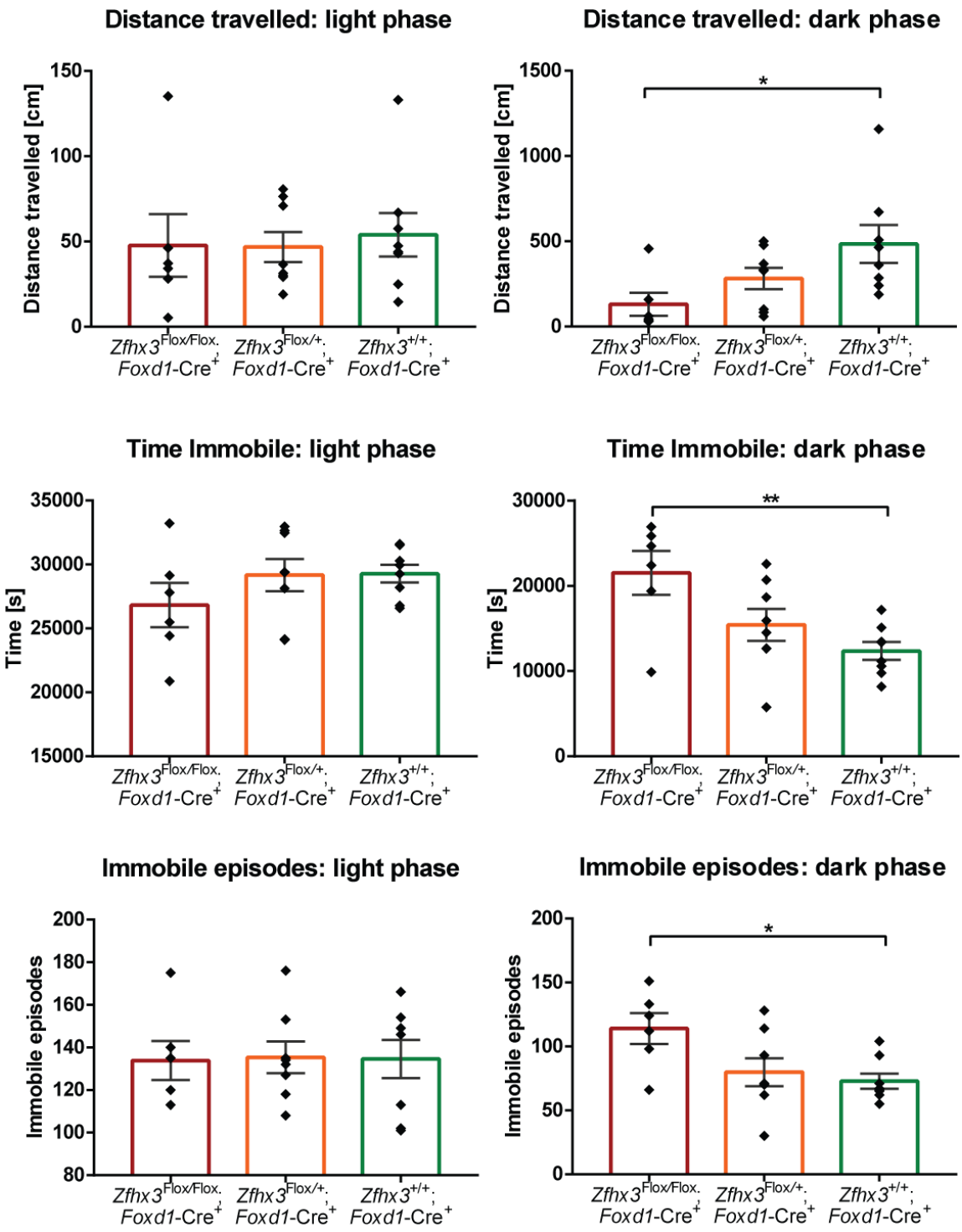


Figure 3.13 | Sleep parameters measured in *Zfhx3*$^{Flox/Flox}$; *Foxd1*-Cre^{+} [n=6], *Zfhx3*$^{Flox/+}$; *Foxd1*-Cre^{+} [n=8] and *Zfhx3*$^{+/+}$; *Foxd1*-Cre^{+} [n=8] mice. All measurements were over a 24 hour period of a standard 12:12 LD cycle. Error bars denote SEM of mean for group data. * denotes significance at $p<0.05$, ** denotes significance at $p<0.01$.

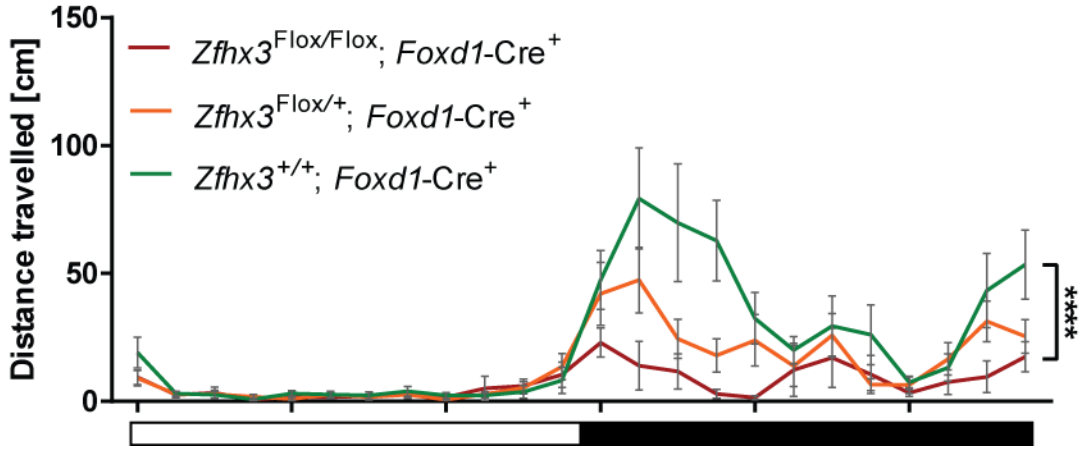


Figure 3.14 | Activity over time for *Zfhx3*$^{Flox/Flox}$; *Foxd1*-Cre^{+} [n=6], *Zfhx3*$^{Flox/+}$; *Foxd1*-Cre^{+} [n=8] and *Zfhx3*$^{+/+}$; *Foxd1*-Cre^{+} [n=8] mice. Lines denote average data for each genotype; error bars denote SEM of mean for group data; LD cycle indicated below graphs; **** denotes significance at $p<0.0001$.

Zfhx3$^{Flox/Flox}$; *Six3*-Cre^{+} mouse displays abnormal EEG sleep parameters

As well as video tracked sleep analysis, an individual *Zfhx3*$^{Flox/Flox}$; *Six3*-Cre^{+} animal underwent electro-encephalography (EEG) recording to analyse electrical sleep activity. Surgical implantation of the telemetry device to record EEG was conducted by Petrina Lau from the Neurobehavioural Genetics group at MRC Harwell. More animals are planned for recording; however this will be after the completion of this thesis. Percentage time spent in wake, rapid eye movement (REM) and non-rapid eye movement (NREM) sleep was analysed from the data recorded – 48 hours prior to and after 6 hours of sleep deprivation. Data is shown in **Figure 3.15** for this mouse, along with average data for two *Zfhx3*$^{Flox/Flox}$ mice that underwent surgery at the same time. Typically a mouse will spend a greater amount of time awake in the dark phase, as this is when nocturnal rodents are most active, and as such low amounts of REM and NREM sleep are expected in this phase in accordance. In contrast, percentage time awake is decreased in the light phase and time spent in both sleep states increased –

with slightly more time spent in NREM. The *Zfhx3*$^{Flox/Flox}$; *Six3*-Cre^{+} mouse showed no difference in percentage time awake between the light and dark phase of recording before sleep deprivation; this is in agreement with the circadian data presented previously which showed that *Zfhx3*$^{Flox/Flox}$; *Six3*-Cre^{+} mice are arrhythmic irrespective of light or dark phases. During the light phase, the homozygote mutant displays a decreased amount of time in REM sleep compared to controls. Time spent in REM is also higher during the dark phase than during the light, which is again unusual for a nocturnal species. However, the most striking finding from this data is that the *Zfhx3*$^{Flox/Flox}$; *Six3*-Cre^{+} animal spent a substantial amount of time in NREM sleep in both light and dark, and also both before and after sleep deprivation, compared to controls. Effectively, this mutant shows no 'sleep rebound' – an increase in NREM typically observed in mice following sleep deprivation protocols (Mistlberger, 2005), as it already exhibits ~40% time spent in NREM throughout the LD cycle regardless.

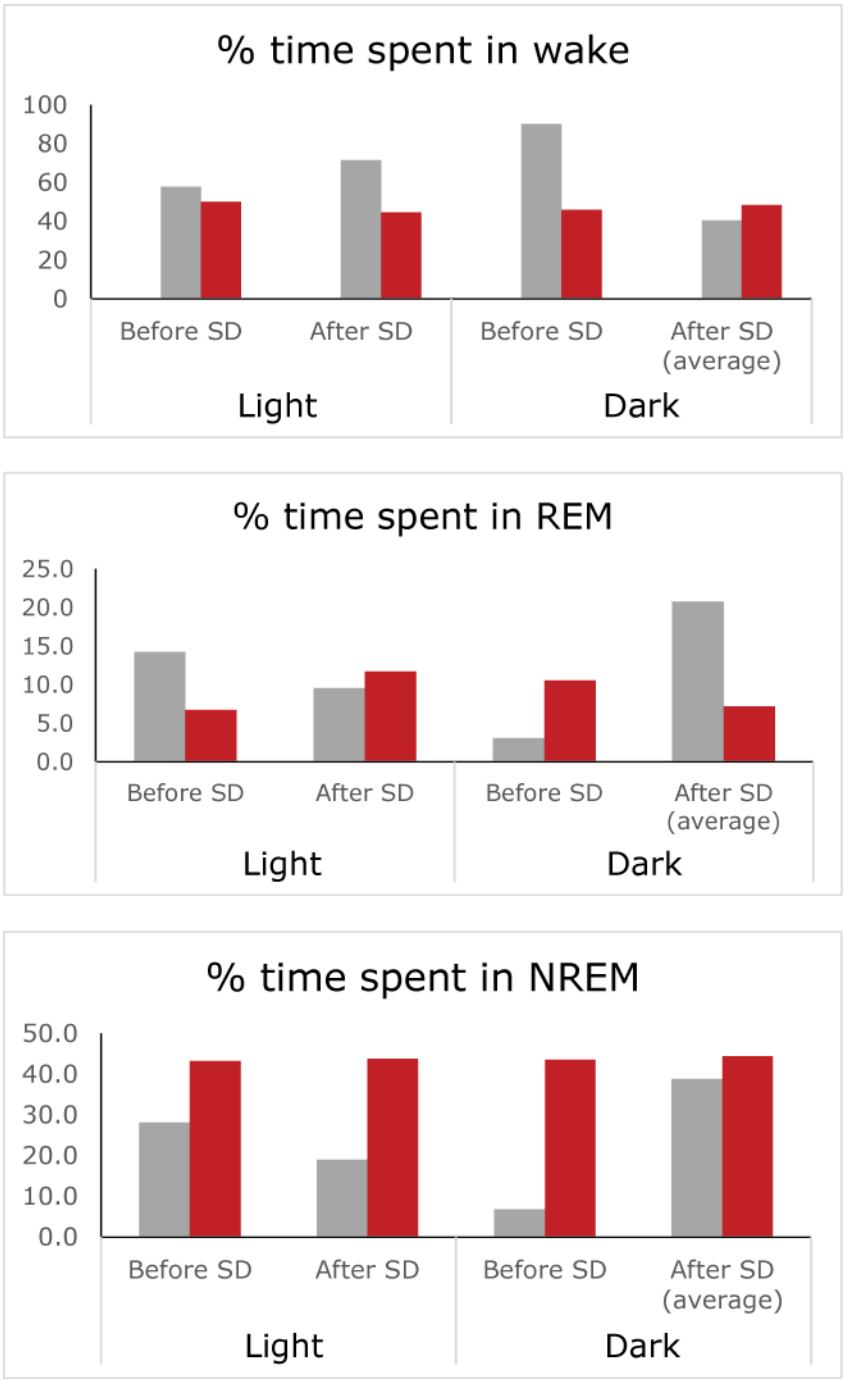


Figure 3.15 | A *Zfhx3*$^{Flox/Flox}$; *Six3*-Cre^{+} mouse was implanted with EEG recording equipment and percentage time spent in wakefulness, REM and NREM sleep analysed for 48 hours prior to and after sleep deprivation (SD). Data is shown for this individual (red bars) and also average data is shown for two *Zfhx3*$^{Flox/Flox}$ animals that also underwent recording (grey bars). SD denotes 6 hours of sleep deprivation.

Zfhx3$^{Flox/Flox}$; *Six3*-Cre^{+} mice lack SCN identity

Following circadian characterisation, *Zfhx3*$^{Flox/Flox}$; *Six3*-Cre^{+} were sacrificed and brains collected for histological examination. Sections were taken coronally through the SCN region and Nissl stained to assess morphology. **Figure 3.16** shows a series of Nissl stained sections from *Zfhx3*$^{Flox/Flox}$; *Six3*-Cre^{+} brain throughout the region that contains SCN, however there is a striking lack of SCN morphology. These images show a distinct lack of cell clustering to form the SCN; however the PVN – which is located adjacent to the SCN, is intact. An immunofluorescent image taken from the brain of another *Zfhx3*$^{Flox/Flox}$; *Six3*-Cre^{+} mutant also shows this complete lack of cell body clustering in the central region of where the SCN should reside. Scattered ZFHX3 immuno-positive cells are still present in the region.

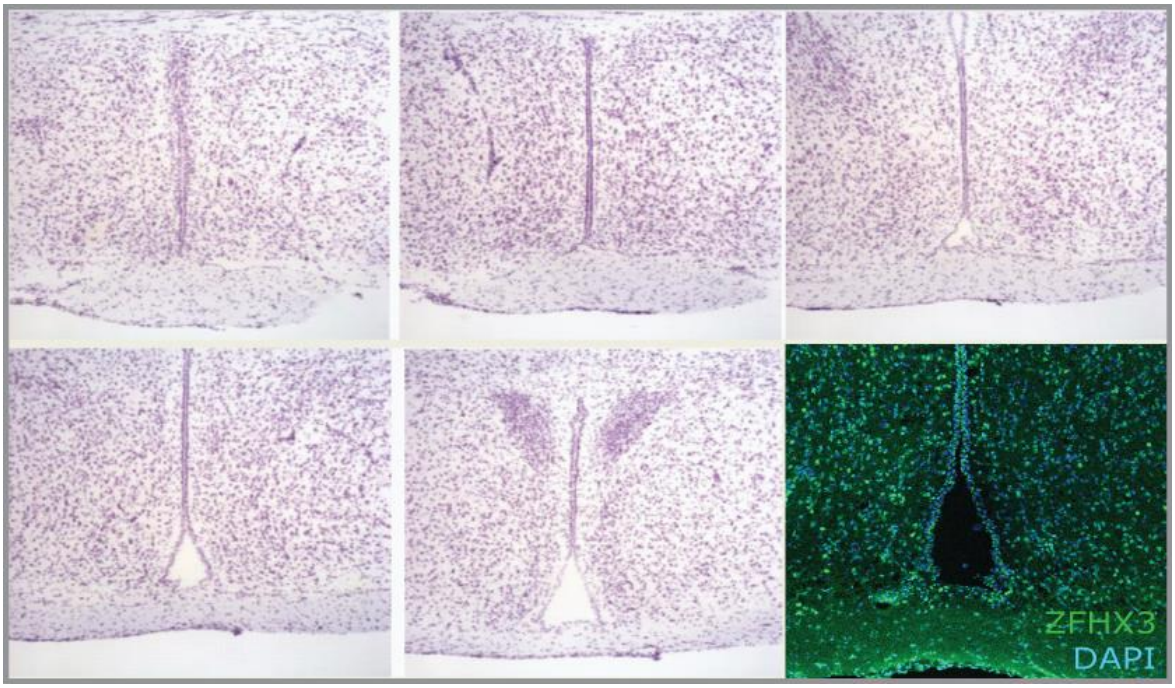


Figure 3.16 | Representative Nissl staining through the 'SCN' region of *Zfhx3*$^{Flox/Flox}$; *Six3*-Cre^{+} mutant brain and a representative immunofluorescent staining for ZFHX3 and DAPI in the central 'SCN' region of *Zfhx3*$^{Flox/Flox}$; *Six3*-Cre^{+} mutant brain. There is a distinct lack of cell clustering in the SCN region, however the PVN remains intact.

To investigate whether *Zfhx3*$^{Flox/Flox}$; *Six3*-Cre^{+} mutants had a complete loss of SCN cell identity, as opposed to a loss of structural clustering, in-situ hybridisation staining was carried out for SCN markers *Vip*, *Avp* and *Rora*. *Vip* and *Avp* are characteristically used to delineate the ventrolateral 'core' and dorsomedial 'shell' regions of the SCN respectively (Yan et al., 2007), whereas *Rora* is present throughout the nuclei (Sato et al., 2004; VanDunk et al., 2011). This work was carried out by Peter Oliver, whilst at the University of Oxford. As shown in **Figure 3.17**, there was a complete absence of staining for all three of these SCN cell markers in *Zfhx3*$^{Flox/Flox}$; *Six3*-Cre^{+} mice. *Zfhx3*$^{Flox/+}$; *Six3*-Cre^{+} showed an intermediate decrease in gene expression also.

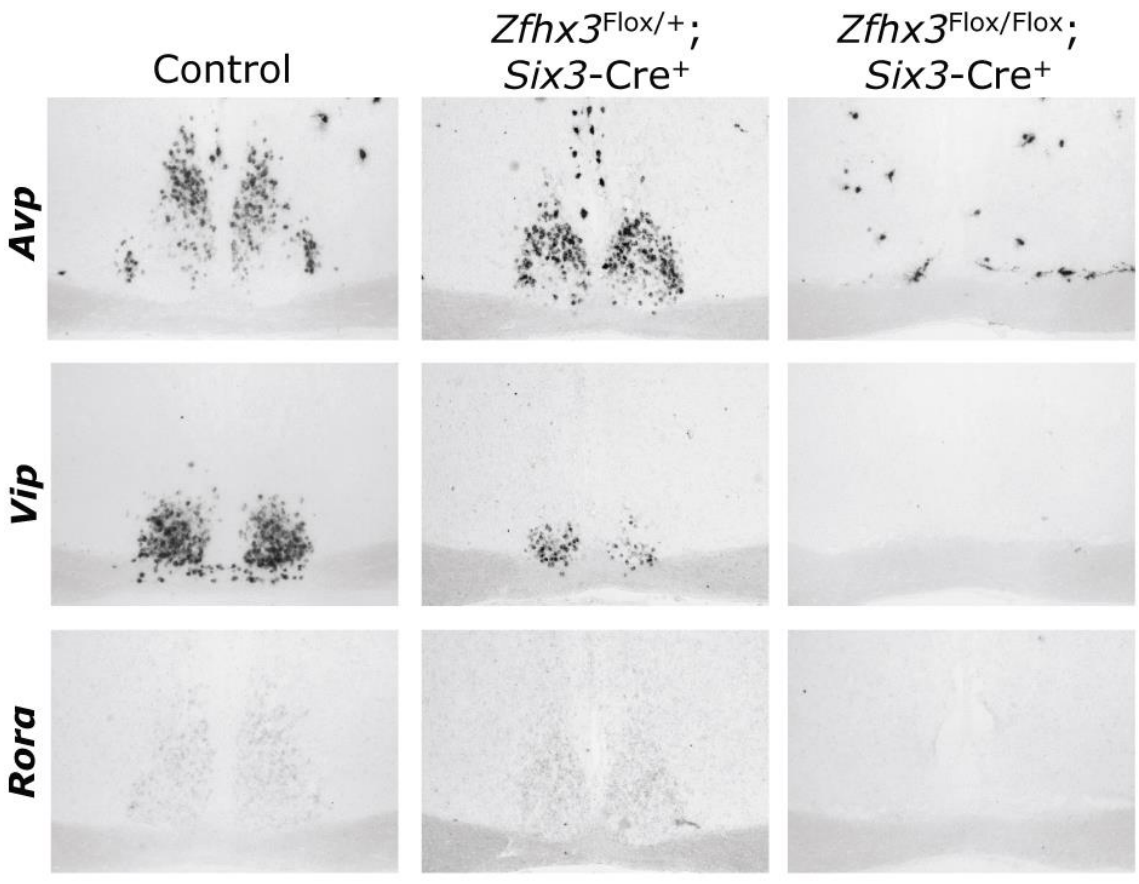


Figure 3.17 | Representative in situ hybridisation of circadian neuronal markers *Vip*, *Avp* and *Rora* on sections through SCN region of *Zfhx3*$^{Flox/Flox}$*; Six3-Cre*$^{+}$*, Zfhx3*$^{Flox/+}$*; Six3-Cre*$^{+}$ and *Zfhx3*$^{Flox/Flox}$ control mice.

Zfhx3$^{Flox/Flox}$; *Foxd1*-Cre^{+} mice retain SCN structure

Following circadian characterisation, *Zfhx3*$^{Flox/Flox}$; *Foxd1*-Cre^{+} and *Zfhx3*$^{Flox/Flox}$; *Foxd1*-Cre^{+} mice were also sacrificed and brains collected for histological examination. Brains were coronally sectioned through the SCN region and stained using either H&E or Nissl staining (**Figure 3.18**). Unlike in the *Zfhx3*$^{Flox/Flox}$; *Six3*-Cre^{+} line, cell clustering to form the SCN is evident in *Zfhx3*$^{Flox/+}$; *Foxd1*-Cre^{+} and *Zfhx3*$^{Flox/Flox}$; *Foxd1*-Cre^{+} mice. However, the SCN does appear slightly smaller in size in *Zfhx3*$^{Flox/Flox}$; *Foxd1*-Cre^{+} when qualitatively compared to *Zfhx3*$^{Flox/Flox}$ and *Zfhx3*$^{Flox/+}$; *Foxd1*-Cre^{+} images. Unfortunately in-situ hybridisation for SCN cell markers was not carried out on this line to determine whether there is any loss of SCN cell identity.

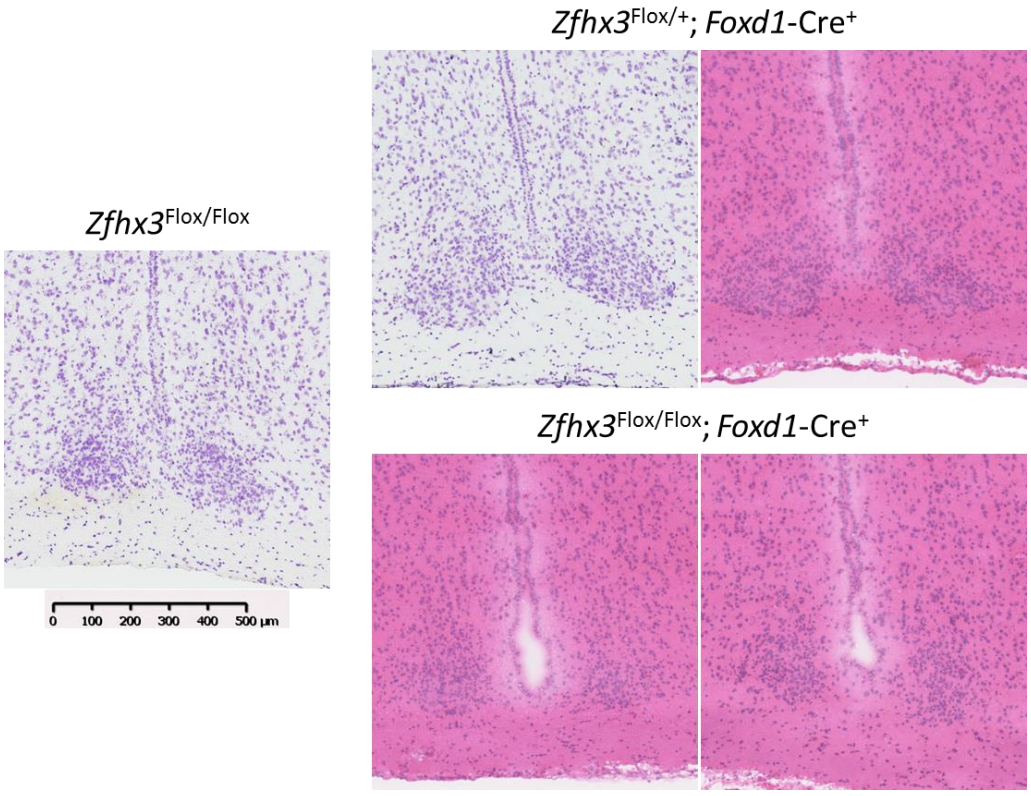


Figure 3.18 | Representative Nissl staining through the central SCN region of a *Zfhx3*$^{Flox/Flox}$ control animal; Nissl staining of a *Zfhx3*$^{Flox/+}$; *Foxd1*-Cre^{+} mutant brain and H&E staining of another *Zfhx3*$^{Flox/+}$; *Foxd1*-Cre^{+} mutant brain and also H&E staining of central SCN sections from two *Zfhx3*$^{Flox/+}$; *Foxd1*-Cre^{+} mutant brains. Increased cell density, typical of SCN morphology, is evident in all examples.

Discussion

Six3-Cre has been previously used to study eye and forebrain development in the mouse (Furuta et al., 2000a; Liu and Cvekl, 2017); similarly, *Foxd1*-Cre was originally developed to study fibrosis in the kidney (Humphreys et al., 2010). However, both *Six3* and *Foxd1* have been shown to be of critical importance in the development of the SCN (Newmann et al., 2018; VanDunk et al., 2011), thus making their corresponding Cre lines attractive candidates to drive *Zfhx3* deletion in the SCN during embryogenesis.

The data presented in this chapter on the *Zfhx3*$^{Flox/Flox}$; *Six3*-Cre^{+} line provides evidence that the transcription factor is necessary for proper development of the SCN. Not only does deletion of *Zfhx3* in this mutant cause loss of SCN nuclei formation, but there is also a complete loss of SCN cell identity. The result of this is a mouse that is behaviourally arrhythmic and unable to entrain to an LD cycle. As well as this severe circadian phenotype, these mice also exhibited unusual behaviour in video tracked sleep screening: displaying fragmented sleeping patterns across both light and dark phases. *Zfhx3*$^{Flox/+}$; *Six3*-Cre^{+} mutants appeared to display an intermediate phenotype in sleep screening – albeit not statistically significant, despite showing no circadian phenotype. *In situ* hybridisation staining images show a possible decrease in key neuropeptide expression in the SCN of these heterozygote mutants, however these were not quantified as the main focus of this line was to characterise *Zfhx3*$^{Flox/Flox}$; *Six3*-Cre^{+} animals. It would be of interest to further examine any reduction in *Avp* and *Vip* expression by a more accurate method of analysing gene expression such as qPCR, to establish whether this could be accountable for the increase in sleep time during the dark phase. Particularly as the SCN has a somewhat disputed role in the control

of sleep and wake promoting systems (Mistlberger, 2005; Stephan and Zucker, 1972). It could be that there exists a correlation between SCN cell type loss and disruption of the sleep system in these mice.

SCN ablation models have been employed many times to demonstrate that, in mice lacking an SCN, behavioural rhythmicity is abolished (Schwartz and Zimmerman, 1991). However, as the majority of SCN ablation models have been performed in adult mice, this does not confirm the role of the SCN during development in establishing the central circadian system. A previous study on *Six6*-null presented evidence for an 'SCN-less' mouse model similar to that of *Zfhx3*$^{Flox/Flox}$; *Six3*-Cre^{+}, however some of these mice displayed rhythmic locomotor activity patterns despite lacking both a discernible SCN and *Vip*/*Avp* expression (Clark et al., 2013). The authors of this work went on to assess the optic nerve morphology in these *Six6*-null mice and discovered that many displayed severe atrophy of the nerve, conversely mice with any intact remnant of the optic nerve displayed rhythmic behaviour despite an apparent lack of SCN. This led the authors to conclude that it is in-fact the optic nerve that conveys rhythmicity in the mouse circadian system and not the SCN. This is a particularly intriguing study as it appears to be the only other key experimental model for a developmental SCN lesion similar to what is presented here for *Zfhx3*$^{Flox/Flox}$; *Six3*-Cre^{+}. When dissecting *Zfhx3*$^{Flox/Flox}$; *Six3*-Cre^{+} mice, the optic nerve was indistinguishable from that of wildtype mice; although no formal characterisation was undertaken of the nerve itself, there was certainly no evidence to suggest any atrophy had taken place. Therefore, in contrast to the data presented by Clark et al, this chapter gives evidence that *Zfhx3* in the SCN is critical during development for the establishment of rhythmic locomotor activity in the mouse.

As well as confirming the role of the SCN in developing circadian activity patterns, EEG sleep phenotyping of a *Zfhx3*$^{Flox/Flox}$; *Six3*-Cre^{+} mouse suggests that the SCN is necessary for development of a normal sleep homeostat. It has been shown previously that the sleep system is controlled homeostatically without the need for an SCN in adult mice (Mistlberger et al., 1987). However, in video tracked sleep screening and also in EEG recording, *Zfhx3*$^{Flox/Flox}$; *Six3*-Cre^{+} mice display abnormal sleep phenotypes. Astoundingly, there appears to be a complete lack of sleep rebound in this mutant line. This is in stark contrast to SCN ablation models, which have been shown to still exhibit a sleep rebound following sleep deprivation despite being behaviourally arrhythmic (Easton et al., 2004; Mistlberger et al., 1983). It will be interesting to see if the high amounts of NREM and lack of sleep rebound is persistently evident in future *Zfhx3*$^{Flox/Flox}$; *Six3*-Cre^{+} EEG sleep recordings. It may also be of interest to conduct EEG recording on *Zfhx3*$^{Flox/+}$; *Six3*-Cre^{+} mice to confirm whether these mice do indeed have an intermediate sleep phenotype between controls and homozygote mutants.

A more complicated and variable phenotype was observed in *Zfhx3*$^{Flox/Flox}$; *Foxd1*-Cre^{+} animals. These mice displayed a variety of different wheel running behaviours in DD, making this line a challenge to assess phenotypically. However, all animals displayed a consistent reduction in amplitude in LD, DD and LL – indicating an overall weaker strength of circadian oscillation. This overall reduction in behavioural amplitude could be a manifestation of reduced amplitude of SCN oscillators, which can also lead to SCN neurons becoming out of phase with one another (Evans, 2016; Wang et al., 2008). This could account for the differing severity of wheel running phenotypes observed between *Zfhx3*$^{Flox/Flox}$; *Foxd1*-Cre^{+} individuals,

as coherence between oscillators could be present to differing extents – thus leading to a more or less functional circadian system as a whole. With regards to SCN formation, initial histology revealed that these mice do have an intact SCN however expression of key neuropeptides *Vip* and *Avp*, used to demarcate the nuclei was not able to be undertaken due to time constraints. Establishing whether *Vip* neurons are lost compared to *Avp* or other SCN cell types could also explain the lack of entrainment to skeletal photoperiods observed in some *Zfhx3*$^{Flox/Flox}$; *Foxd1*-Cre^{+} and equally their unresponsiveness to masking light pulses. There is much evidence from Eric Herzog's lab, for example, that *Vip* neurons and their receptors (An et al., 2012; Jones et al., 2018; Mazuski et al., 2018), are crucial for entrainment of the circadian system to light and therefore loss of these could adversely affect entrainment despite the SCN appearing to be intact visually. Another key gene for circadian coupling is Neuromedin-S (Lee et al., 2015), which has been shown to act as a pacemaker at the cellular level. It is quite possible that *Nms* expression is also altered in *Zfhx3*$^{Flox/Flox}$; *Foxd1*-Cre^{+} SCN.

As evidenced by X-Gal staining images for the *Foxd1*-Cre-R26R line, *Foxd1*-Cre appears to have a greater level of Cre expression in organs other than the brain. The circadian system is comprised of many peripheral oscillators, as well as central, all of which can contribute to changes in circadian physiology and ultimately behaviour (Brown and Azzi, 2013; Mohawk et al., 2012). This wider pattern of Cre activity, particularly in the liver – where *Zfhx3* expression continues into adulthood (Yasuda et al., 1994b), could also be contributing to the abnormal circadian behaviours in *Zfhx3*$^{Flox/Flox}$; *Foxd1*-Cre^{+} mice. As concluded in the section on Lac Z reporter characterisation in this chapter, this made *Six3*-Cre a more attractive proposition for

consistent *Zfhx3* deletion in our area of interest. Due to the consistent and striking phenotype observed in *Zfhx3*$^{Flox/Flox}$; *Six3*-Cre^{+} more efforts were undertaken to characterise this mutant line. As stated in the introduction to this thesis, both *Foxd1* and *Six3* are important genes in SCN development, therefore it may appear surprising that *Zfhx3* deletion driven by *Six3*-Cre resulted in complete SCN loss whereas *Foxd1*-Cre did not. A simple explanation for this could be that *Six3*-Cre has a greater level of overlap with *Zfhx3* in the region of the embryonic brain where the SCN forms during development or that *Six3*-Cre displays a higher efficiency of recombinase activity with the *Zfhx3*^{Flox} allele. Immunofluorescent staining for both *Zfhx3* and Cre in mutants would establish this. However, *Six3* expression has been shown to occur earlier during development than *Foxd1*, being already apparent at embryonic day 10 in the mouse brain (VanDunk et al., 2011). The majority of SCN cytogenesis has been shown to occur between E12 and E15 (Kabrita and Davis, 2008), therefore it is likely that *Zfhx3* deletion occurs before SCN formation begins in *Zfhx3*$^{Flox/Flox}$; *Six3*-Cre^{+} animals. This can be confirmed by staining for key SCN cell markers in neonates and evaluating SCN morphology during key stages in embryonic brain development. If this is indeed the case, the *Zfhx3*$^{Flox/Flox}$; *Six3*-Cre^{+} mouse can be considered a true model of a completely 'SCN-less' animal throughout its lifespan.

Results IV

Further characterisation of an 'SCN-less' mouse

Introduction

In the previous chapter (Results III), two mutant lines were discussed in which *Zfhx3* was deleted from the developing SCN region. Unexpectedly, this resulted in aberrant SCN formation in *Zfhx3*$^{Flox/Flox}$; *Six3*-Cre^{+} animals. This in turn produced a mouse model that was behaviourally arrhythmic yet otherwise viable and healthy. Results III summarised findings on the *Zfhx3*$^{Flox/Flox}$; *Six3*-Cre^{+} 'SCN-less' mouse in terms of sleep and standard wheel running circadian behaviour; in this chapter, data is presented on characterisation of further phenotypes observed in this mouse.

As well as being arrhythmic in DD, these mice also showed a complete absence of masking in LD – a remarkable circadian phenotype in itself (Rietveld et al., 1993). The closest animal model, phenotypically speaking, currently studied is that of SCN ablation. From these models, it has been shown that rhythmicity is still evident in animals as long as 25% of the SCN is remaining (LeSauter and Silver, 1999). However even in animals with complete SCN ablation, masking behaviour is still evident (Redlin and Mrosovsky, 1999). It should also be noted that ablation models only eradicate SCN input in the adult and the impact of an intact central oscillator in the SCN orchestrating the circadian system up until this point cannot be completely dismissed. In terms of genetic models, single gene knock-outs capable of abolishing rhythmic circadian activity are rare; only *Bmal1* out of the core genetic clock components has been shown to have this effect (Bunger et al., 2000). The majority of *Clock* null mutant mice also display arrhythmic activity, however this is not immediate upon release into DD (Vitaterna et al., 1994).

As *Zfhx3*$^{Flox/Flox}$; *Six3*-Cre^{+} mice were unable to entrain to the LD cycle, other Zeitgebers were assessed. One of these was entrainment to food availability, which

has been shown to be under the control of the food entrainable oscillator (FEO) (Pendergast and Yamazaki, 2018). Previous studies have shown that SCN ablation models display food anticipatory activity (FAA) comparable to wildtype animals (Davidson, 2009). Arrhythmic animals, such as homozygous Clock mutant mice, are also able to entrain to food availability (Pitts et al., 2003). However, data on FAA and its relationship to the core circadian clock is conflicting. For example, in one study FAA was shown to occur in mice lacking molecular clock function in all tissues (Storch and Weitz, 2009), however canonical clock genes *Cry1*, *Cry2* and *Bmal1* were proposed essential for FAA in another model (Takasu et al., 2012). Taken collectively, FAA and the FEO are thought to be separate to the core clock in the SCN; however, this is still under some dispute.

Studies have shown that in honeybees, the social clock is able to entrain the circadian system in animals lacking light input or time of day information (Fuchikawa et al., 2016). As *Zfhx3*$^{Flox/Flox}$; *Six3*-Cre^{+} mutants appear to be unresponsive to the LD cycle, they are a suitable model to confirm whether this is also the case in mice. Therefore, in addition to monitoring the FEO, the social clock (Paul and Schwartz, 2007) was assessed in *Zfhx3*$^{Flox/Flox}$; *Six3*-Cre^{+} mice to study whether SCN-less mutants are able to entrain to the social cues of their cagemates.

There is limited literature on genetically altered mice lacking an SCN (Newmann et al., 2018), and in studies where adult mice were actually characterised, experiments were limited to general locomotor behaviour (Clark et al., 2013). Thus, the *Zfhx3*$^{Flox/Flox}$; *Six3*-Cre^{+} mutant provided a unique opportunity to study how a mouse that developed devoid of an SCN behaves and also how the mammalian circadian system functions in the absence of its key central pacemaker.

Characterisation of visual function in *Zfhx3*$^{Flox/Flox}$; *Six3*-Cre^{+} mice

As *Zfhx3*$^{Flox/Flox}$; *Six3*-Cre^{+} mice are unable to entrain to an LD cycle and have a complete absence of masking – which is unusual, even for behaviourally arrhythmic animals (Aschoff, 1999); a logical continuation was to study their visual system. This would confirm whether it is purely SCN loss that is responsible for these deficits or whether there were defects elsewhere in the pathways responsible for light entrainment and visual function. Also, as *Six3*-Cre also displays high expression in the retina, it was vital to ensure that ablation of ZFHX3 function in the retina using this Cre line was not contributing to the circadian phenotype observed.

An initial small cohort [n=3] was used to determine whether there were any obvious abnormalities in eye structure and image forming visual function in mutants. These tests were carried out by husbandry staff at the Mary Lyon Centre, MRC Harwell. A slit lamp was used to study the morphology of the eye, allowing views of structures such as the lens, cornea and retina. Examination of mutants revealed no gross abnormalities to the eye; in fact, they were indistinguishable from their control counterparts. Optokinetic drum score, which is used to measure visual acuity, was not statistically different in *Zfhx3*$^{Flox/Flox}$; *Six3*-Cre^{+} mice when compared to heterozygous mutants or control animals (**Figure 4.1**). The results of these experiments reassured us that the image forming visual system of *Zfhx3*$^{Flox/Flox}$; *Six3*-Cre^{+} mice was likely intact.

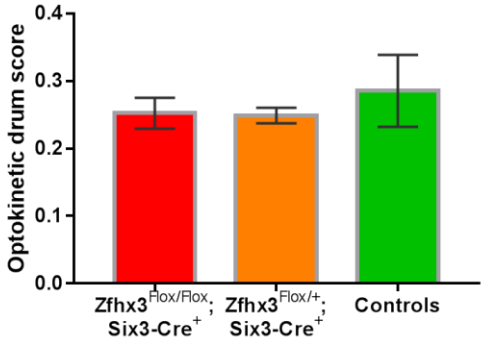


Figure 4.1 | Optokinetic drum was used to assess the visual acuity of *Zfhx3*$^{Flox/Flox}$*; Six3*-Cre^{+} [n=3], *Zfhx3*$^{Flox/+}$*; Six3*-Cre^{+} [n=3] and control mice [n=2]; no significant differences were found when analysed. Error bars denote SEM of groups.

As with previous mutant lines (*Zfhx3*$^{Flox/Flox}$; UBC-Cre^{+} and *Zfhx3*$^{Sci/-}$), pupillometry was undertaken on *Zfhx3*$^{Flox/Flox}$; *Six3*-Cre^{+} mice to assess the pupillary reflex in these animals. The protocol undertaken was the same as previously described in Results I and II pupillometry sections, however only bright (100 lux/13.4 log quanta) and dim (0.1 lux/10.4 log quanta) light was used (**Figure 4.2**). The pupillary reflex was not statistically different between *Zfhx3*$^{Flox/Flox}$; *Six3*-Cre^{+}, *Zfhx3*$^{Flox/+}$; *Six3*-Cre^{+} and *Zfhx3*$^{Flox/+}$ control mice under both bright [$F(2,23)=1.171$, $p=0.3279$] and dim [$H=0.6787$, $p=0.3279$] light intensities (**Figure 4.3**). This was the first indication that the light input pathway from the eye to the brain and the non-image forming functions of the visual system, other than entrainment to LD, were intact in these 'SCN-less' mutants.

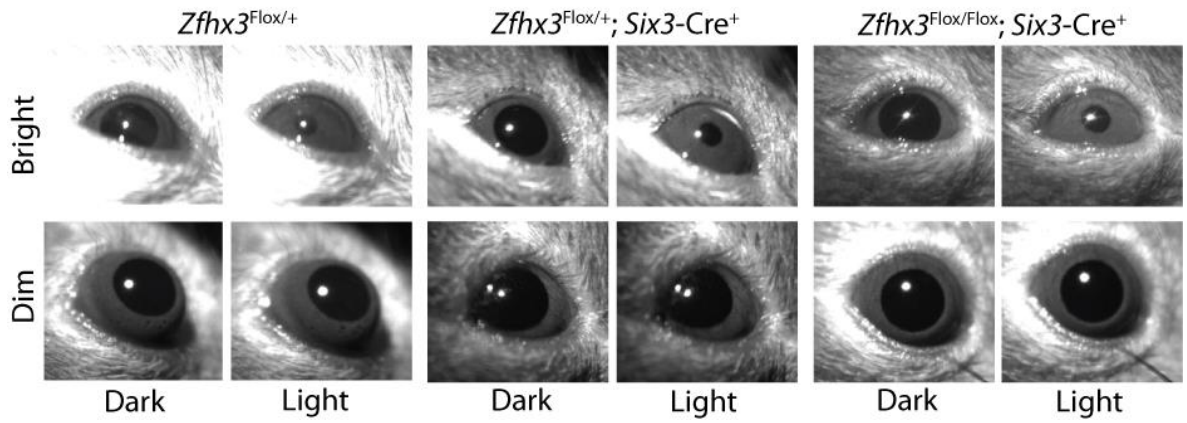


Figure 4.2 | Representative images for *Zhx3*$^{Flox/+}$, *Zfhx3*$^{Flox/+}$; *Six3*-Cre^{+} and *Zfhx3*$^{Flox/Flox}$; *Six3*-Cre^{+} mice before and after exposure to bright and dim light stimuli to measure pupillary reflex.

More in-depth retinal analysis was carried out by collaborator Steven Hughes at the Nuffield Department of Clinical Neuroscience, Oxford. This work was undertaken to study the effect of *Zfhx3* loss on light responsiveness of retinal cells. First, a B-Gal antibody was used to examine Cre expression in the *Six3*-Cre-R26R line (introduced in Results III) to determine in which retinal cell types Cre activity occurred. Co-localisation staining was then undertaken to confirm overlap of Cre with specific retinal cell types and those expressing *Zfhx3*. Unfortunately, due to the unavailability of a reliable Cre antibody, staining was not undertaken directly in *Zfhx3*$^{Flox/Flox}$; *Six3*-Cre^{+} mice. There was some co-localisation of B-Gal and ZFHX3 staining, as shown in **Figure 4.4**; however complete overlap was not observed. Co-localisation was also found between GAD67 (a marker of horizontal cells in the outer retina), Calbindin (a marker of cells in the ganglion cell layer) and B-Gal – indicating Cre expression in horizontal and ganglion cells. This indicated that some retinal disruption of *Zfhx3* expression could occur through use of the *Six3*-Cre line, however these cells did not correspond to the main *Zfhx3* expressing cells previously identified

by our group in the retina (Jess Edwards, DPhil Thesis). Therefore, from the immunofluorescence experiments it was predicted that *Zfhx3*$^{Flox/Flox}$; *Six3*-Cre^{+} mice should not have any appreciable retinal dysfunction. To confirm this, multi-electrode arrays (MEAs) were used to record electrical activity in *Zfhx3*$^{Flox/Flox}$; *Six3*-Cre^{+} retinas; principally to assess the function of intrinsically photosensitive retinal ganglion cells (iPRGs) as well as rod and cone cells. This method involved culturing retinas on an MEA and then exposing the retina to a sustained light pulse both before and after application of a rod/cone cell blocker (Lipinski et al., 2011). By doing this, the electrical activity of these three cell types responsible for the non-image forming functions (or light responsive elements) of the retina can be assessed. MEA experiments produce electroretinograms (ERGs) that consist of characteristic 'waves': the a-wave, which is due to activity of cones and rods is the initial corneal-negative deflection, whereas the b-wave is the corneal-positive deflection, derived from cells of the inner retina (Perlman, 1995). Following exposure to light after being adapted to the dark for 1 hour, *Zfhx3*$^{Flox/Flox}$; *Six3*-Cre^{+} retinas showed an a-wave activity comparable to that of control retinas with a slight attenuation of b-wave activity. This attenuation in b wave response was not seen when light exposure was timed after only 10 minutes of dark adaptation. Following application of a rod/cone blocker, substantial electrical activity was recorded from *Zfhx3*$^{Flox/Flox}$; *Six3*-Cre^{+} retina (**Figure 4.5**). Taken collectively, this data showed that the light sensitivity of the retina in *Zfhx3*$^{Flox/Flox}$; *Six3*-Cre^{+} animals was grossly unaffected as the mutant retinas showed responsiveness to light input from all cell types, thus it was concluded that the lack of masking in this mutant line was not due to any retinal deficits.

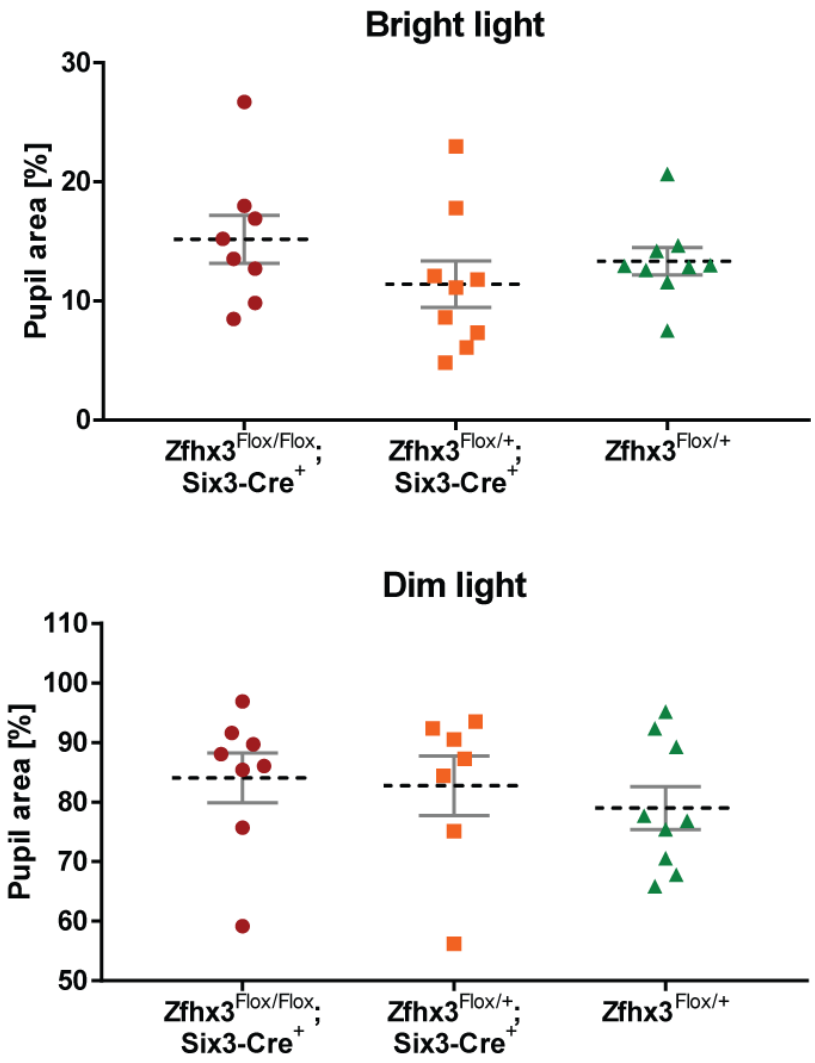


Figure 4.3 | Percentage pupil area at the point of maximal constriction (relative to dark adapted pupil size) following bright (100 lux) and dim (0.1 lux) light stimuli to the eyes of *Zhx3*$^{Flox/+}$, *Zfhx3*$^{Flox/+}$; *Six3*-Cre^{+} and *Zfhx3*$^{Flox/Flox}$; *Six3*-Cre^{+} mice. Dashed black line denotes mean of data, grey lines denote SEM of data points. No significant differences were found between groups when analysed using ANOVA (for bright light) and Kruskal-Wallis (for dim light) with α=0.05 for both tests.

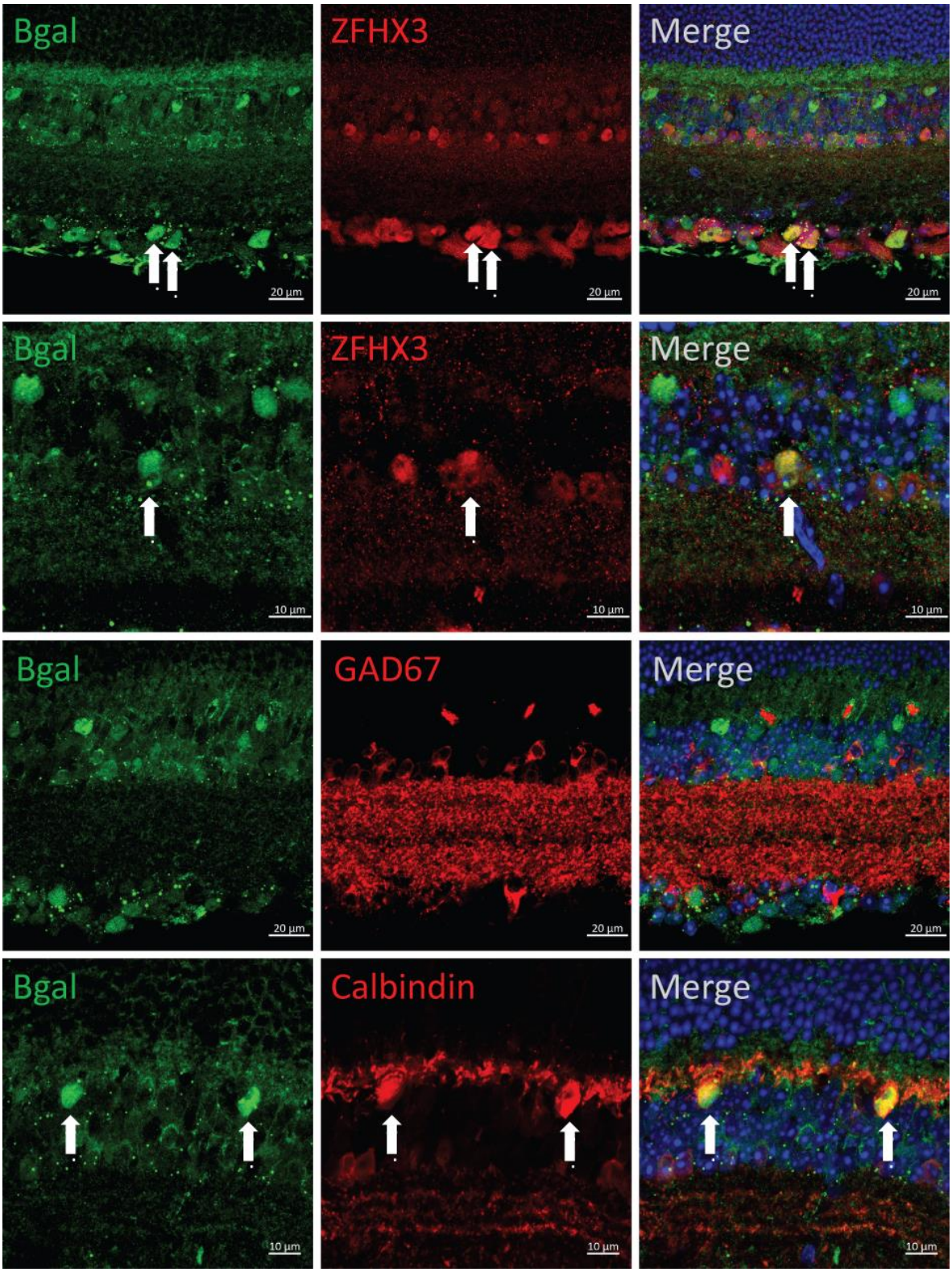


Figure 4.4 | Representative immunofluorescent staining of retinal sections from *Six3*-Cre mice for ßGal, ZFHX3, GAD67 and Calbindin. Arrows indicate cells in which co-localisation was detected.

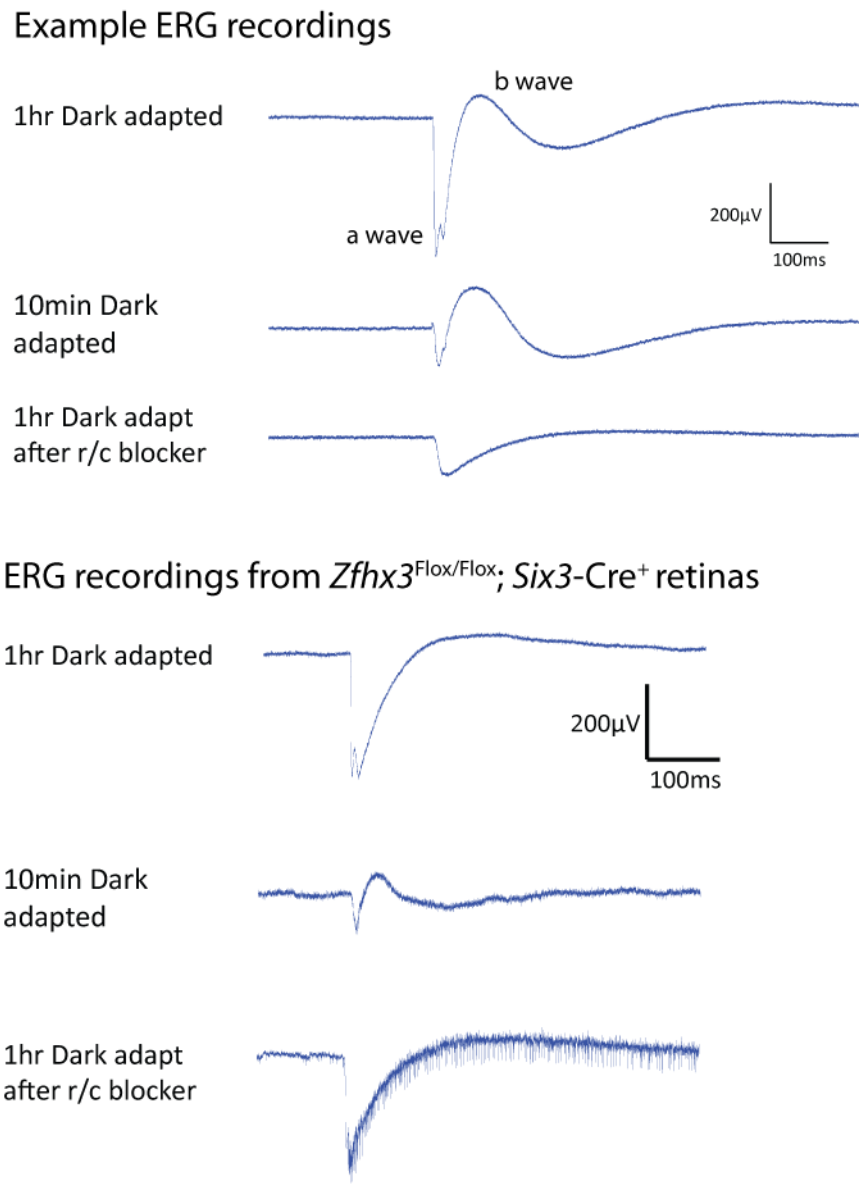


Figure 4.5 | Representative ERG recordings (above) following exposure to light after 1 hour and 10 minutes of light adaptation in wt retinas, and also after 1 hour dark adaptation after application of a rod/cone blocker. Representative ERG recordings for *Zfhx3*$^{Flox/Flox}$; *Six3*-Cre^{+} retinas are shown below.

Continuing on from this retinal work, an experiment was undertaken by another collaborator, Liz Maywood from MRC LMB Cambridge, to examine retinal targets in *Zfhx3*$^{Flox/Flox}$; *Six3*-Cre^{+} mice. As the retinas of these animals appeared functionally normal, it was important to look further downstream in case of possible

abnormalities in the neuronal targets of the retina in the brain (Fernandez et al., 2016). To study this, a fluorescent viral tracer was injected into each eye of the mouse and brains were collected after 3 days. The brains were then sectioned and imaged using confocal microscopy; note, a different fluorescent wavelength was injected into each eye, this allowed independent tracing of ipsilateral and contralateral outputs. This was a non-biased approach to trace the afferents of the RHT and assess where these retinal afferents were converging. Images through the 'SCN' region and lateral geniculate are shown in **Figure 4.6**; red staining shows afferents from the right eye, whereas green shows afferents from the left. In *Zfhx3*$^{Flox/Flox}$; *Six3*-Cre^{+} mice there was no retinal input to the region where the SCN should reside, whereas input to the geniculate appeared normal and intact. This indicates that RHT output to the SCN is compromised, most likely as there is no SCN in *Zfhx3*$^{Flox/Flox}$; *Six3*-Cre^{+} mice for neurons to converge on, but other retinal targets in the brain are unaffected in *Zfhx3*$^{Flox/Flox}$; *Six3*-Cre^{+} mice. Thus, considering all of this visual data collectively, the findings strongly suggest that it is solely the loss of the SCN itself that is responsible for the severe circadian phenotype observed in these mutants.

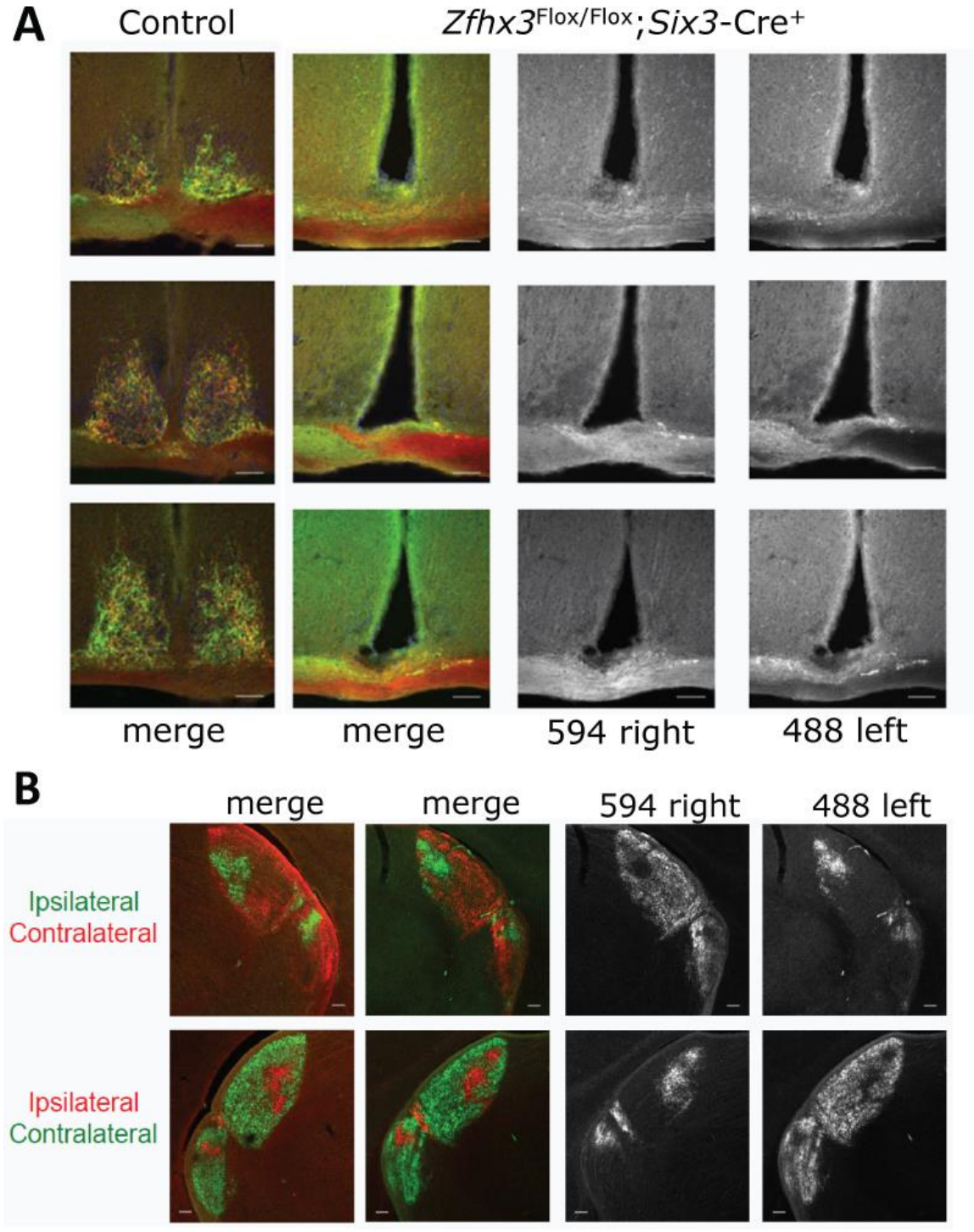


Figure 4.6 | Fluorescent tagged tracers were injected into the right (594/red) and left (488/green) eyes of *Zfhx3*$^{Flox/Flox}$*; Six3-Cre*$^{+}$, and control mice, after 72 hours mice were sacrificed and the brains harvested for imaging. **A** shows projections to the SCN region, **B** to the geniculate region (*Zfhx3*$^{Flox/Flox}$*; Six3-Cre*$^{+}$ images are shown to the right). Scale bar: 100 µm.

Zfhx3$^{Flox/Flox}$; *Six3*-Cre^{+} mice display reduced social entrainment

Home cage monitoring systems are becoming a popular way of observing changes to animal behaviour in a more natural environment, particularly any interactions that might occur between cage-mates. Recently one of these systems was developed at Harwell to monitor circadian activity of individuals in a group housed environment (Bains et al., 2016). Activity of individual animals is tracked using microchips and cages are also video recorded to monitor more subtle behaviours. From this, activity over time can be extracted – similar to data shown previously for video tracked sleep analysis. This allows us to assess how mutants behave when housed with control cage-mates, as opposed to when they are singly housed and also eliminates use of the running wheel for circadian measurements – also discussed previously (Bains et al., 2018). As shown in the previous chapter, *Zfhx3*$^{Flox/Flox}$; *Six3*-Cre^{+} mice are behaviourally arrhythmic both in running wheel and video tracked sleep screening when singly housed. Mutants in this line are also unable to entrain to the LD cycle, therefore it was of interest to assess whether their arrhythmic behaviour persisted when group housed or whether they were able to entrain to social entrainment cues from control mice in the cage.

Each cage housed three individual animals: one homozygote or heterozygote mutant and two control cage mates, and cages were recorded at 4 months and 8 months of age. **Figure 4.7** shows data for each genotype over a 24 hour period, pooled from all cages analysed. Comparable with singly housed screening methods, control animals showed little activity in the light phase at both ages screened and then high activity in anticipation of lights off and towards the end of the dark phase. *Zfhx3*$^{Flox/+}$; *Six3*-Cre^{+} also mice showed typical nocturnal activity patterns over the LD cycle. At 8

months, *Zfhx3*$^{Flox/Flox}$; *Six3*-Cre^{+} mice displayed arrhythmic activity patterns. The 8 month graph shows a reduction in distance travelled in all genotypes, this is typical for mice when screened at this older time point (Valentinuzzi et al., 1997). As was the case for singly housed circadian screening, *Zfhx3*$^{Flox/+}$; *Six3*-Cre^{+} mice displayed no overt changes to circadian behaviour compared to controls. When viewing the graphs in **Figure 4.7**, at 4 months *Zfhx3*$^{Flox/Flox}$; *Six3*-Cre^{+} mice appear to show an increase in activity at the transition between light and dark similar to that of controls and *Zfhx3*$^{Flox/+}$; *Six3*-Cre^{+} mice. This behaviour was not evident when *Zfhx3*$^{Flox/Flox}$; *Six3*-Cre^{+} were singly housed (Results III). To examine this in more detail, total distance travelled for ZT11-12 (the transition period for lights on to lights off) was measured at both 4 months and 8 months of age and compared to total activity at ZT4-5. This produced a value for percentage increase in activity at the transitionary period compared to the middle of the light phase, when mice are typically inactive. At 4 months there were no statistical differences observed between genotypes in percentage increase in activity [$H=4.777$, $p=0.0921$], indicating that *Zfhx3*$^{Flox/Flox}$; *Six3*-Cre^{+} and *Zfhx3*$^{Flox/+}$; *Six3*-Cre^{+} mice displayed an increase in activity at dark onset comparable to controls. By 8 months of age, this was no longer the case, with genotypes displaying a significantly different percentage change in activity [$H=6.21$, $p=0.0448$]. To examine this further, paired t-tests were conducted for each genotype to compare total activity increase at both 4 and 8 months of age (**Figure 4.8**). These confirmed that, at 4 months of age, *Zfhx3*$^{Flox/Flox}$; *Six3*-Cre^{+} mice display a significant increase in activity [$t(5)=4.816$, $p=0.0048$] at the onset of lights off when housed with control cagemates that they do not display when singly housed. However, this was no longer the case at 8 months of age [$t(5)=0.7867$, $p=0.4671$]. This is in contrast to

Zfhx3$^{Flox/+}$; *Six3*-Cre^{+} mice, which show significant increases at both 4 [t(4)=4.358, p=0.0121] and 8 [t(4)=4.358, p=0.0158] months of age; and also control animals ([t(25)=12.45, p=0<0.0001 at 4 months and [t(25)=6.894, p<0.0001] at 8 months).

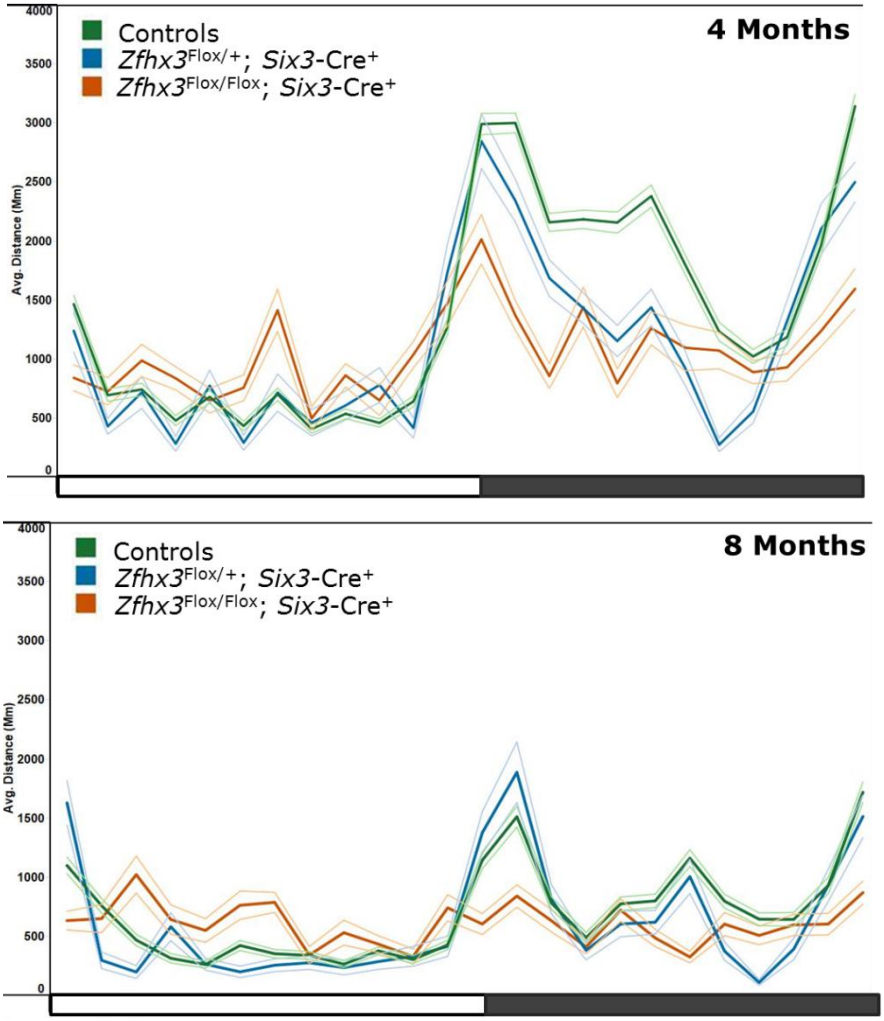


Figure 4.7 | Individual *Zfhx3*$^{Flox/Flox}$; Six3-Cre^{+} [n=6] and *Zfhx3*$^{Flox/+}$; *Six3*-Cre^{+} [n=5] mice were housed with 2 control [n=26] littermates in their home cages and their activity recorded for 24 hours at 4 months and 8 months of age. Controls were a mix of *Zfhx3*$^{+/+}$; Six3-Cre^{+} and *Zfhx3*^{Flox} animals. Average distance [cm] travelled per time bin in this time for all genotypes was pooled across cages: bold line denotes mean, faint line denotes SEM. White/black bar denotes LD cycle.

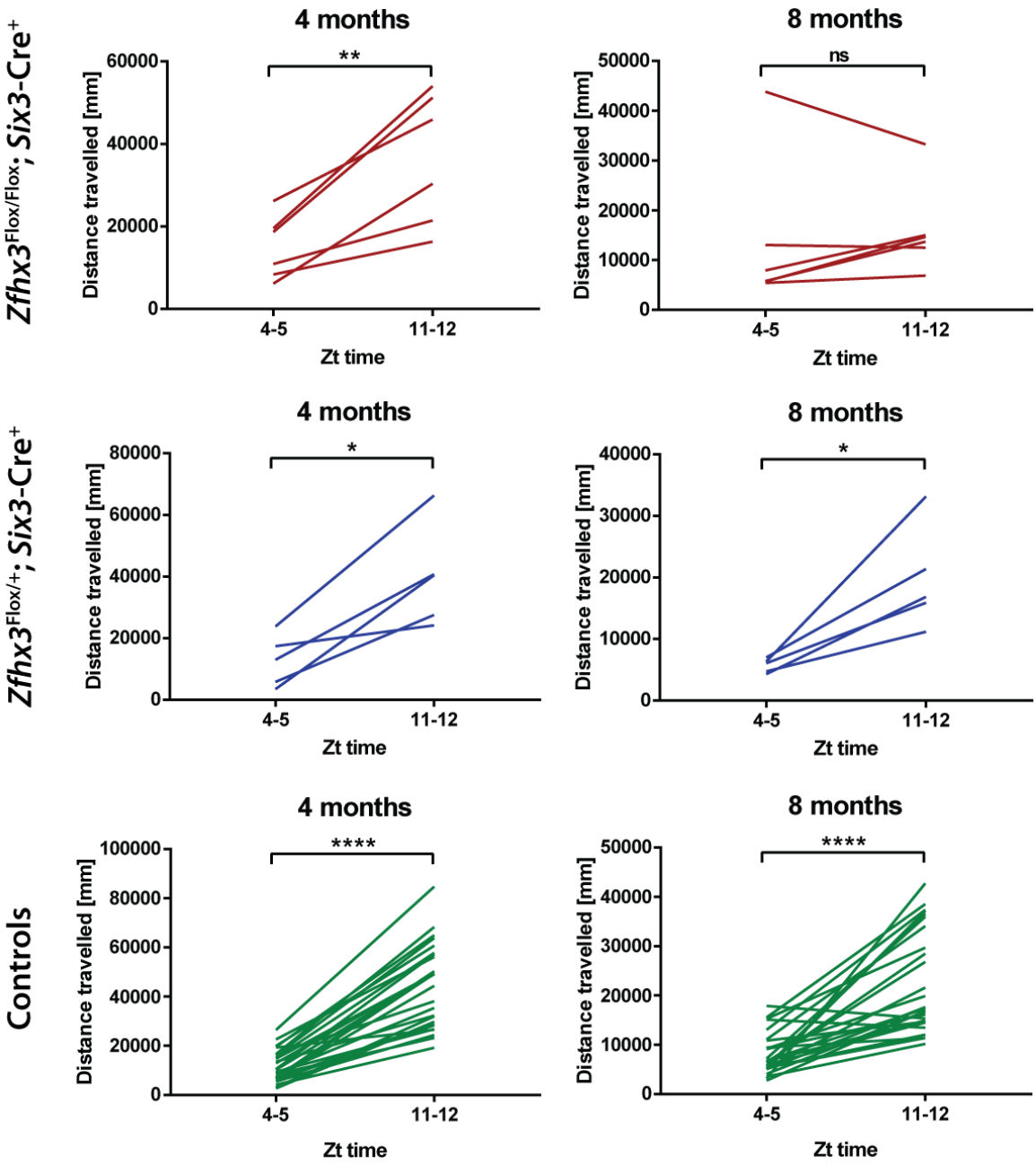


Figure 4.8 | Total distance travelled between ZT4-5 and ZT11-12 for *Zfhx3*$^{Flox/Flox}$; Six3-Cre^{+} [n=6], *Zfhx3*$^{Flox/+}$; *Six3*-Cre^{+} [n=5] and control [n=26] mice at 4 months and 8 months of age. Controls were a mix of *Zfhx3*$^{+/+}$; Six3-Cre^{+} and *Zfhx3*^{Flox} animals. * denotes significance at $p<0.05$, ** denotes significance at $P<0.01$, **** denotes significance at $p<0.0001$.

Food anticipatory activity is intact in *Zfhx3*$^{Flox/Flox}$; *Six3*-Cre^{+} mice

The data presented thus far has demonstrated the inability of *Zfhx3*$^{Flox/Flox}$; *Six3*-Cre^{+} mice to maintain entrainment to various environmental factors (LD cycle and social cues); another well studied Zeitgeber of the circadian system is food availability. Much previous work has shown that under restricted feeding conditions, mice lacking a functional molecular circadian clock and even SCN ablation models display robust food anticipatory activity (FAA) when undergoing temporal feeding regimes (Pendergast and Yamazaki, 2018). This work suggests that the food entrainable oscillator (FEO) is independent of the light entrainable oscillator in the SCN. Therefore, to assess whether the FEO was intact in 'SCN-less' mutants, *Zfhx3*$^{Flox/Flox}$; *Six3*-Cre^{+} mice underwent a timed feeding protocol, in which food availability was gradually restricted to a 6 hour window (**Figure 4.9**).

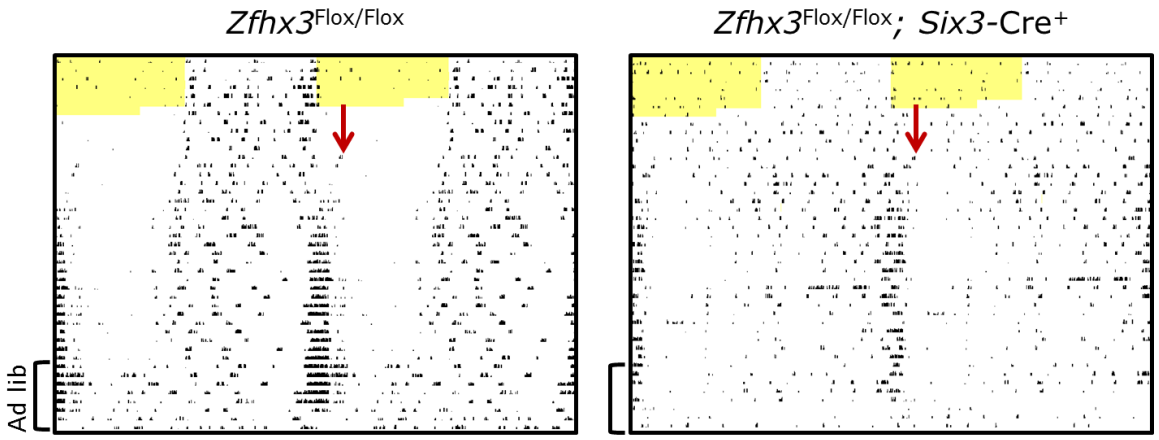


Figure 4.9 | Representative actograms for *Zfhx3*$^{Flox/Flox}$; *Six3*-Cre^{+} and control mice undergoing a timed restricted feeding protocol. Mice were maintained on ad lib food in a 12:12 LD cycle before being transferred to DD, red arrows denote when food restriction protocol began. Food was available for 12 hours a day for 3 days, followed by 8 hours a day for 3 days, and then 6 hours a day for the remainder of the protocol. Mice were then released onto *ad lib* feeding again at the time-point indicated on the figure.

Activity counts were measured for a 3 hour time window prior to food availability for the duration of the 6 hour restricted feeding schedule; for comparison, average activity for the same corresponding time in the 5 days prior to food restriction was taken. All *Zfhx3*$^{Flox/Flox}$; *Six3*-Cre^{+} mice had a significant increase in activity counts during restricted feeding [t(6)=4.01, p=0.007], thus it can be concluded that these mutants displayed FAA under restricted feeding (**Figure 4.10**). As shown in **Figure 4.9**, FAA persisted when mice were released onto ad libitum food – indicating the presence of true entrainment. There were no statistical differences in activity counts between genotypes for the time period measured prior to restricted feeding. However, anticipatory activity was significantly less in *Zfhx3*$^{Flox/Flox}$; *Six3*-Cre^{+} mice compared to *Zfhx3*$^{Flox/+}$; *Six3*-Cre^{+} [adjusted p=0.0105], *Zfhx3*$^{Flox/Flox}$ [adjusted p=0.0072] and *Zfhx3*$^{Flox/+}$ [adjusted p=0.0387] under the restricted feeding regime. This data suggests that although FAA is evident in *Zfhx3*$^{Flox/Flox}$; *Six3*-Cre^{+} mice, 'SCN-less' mutants may display less activity when entrained.

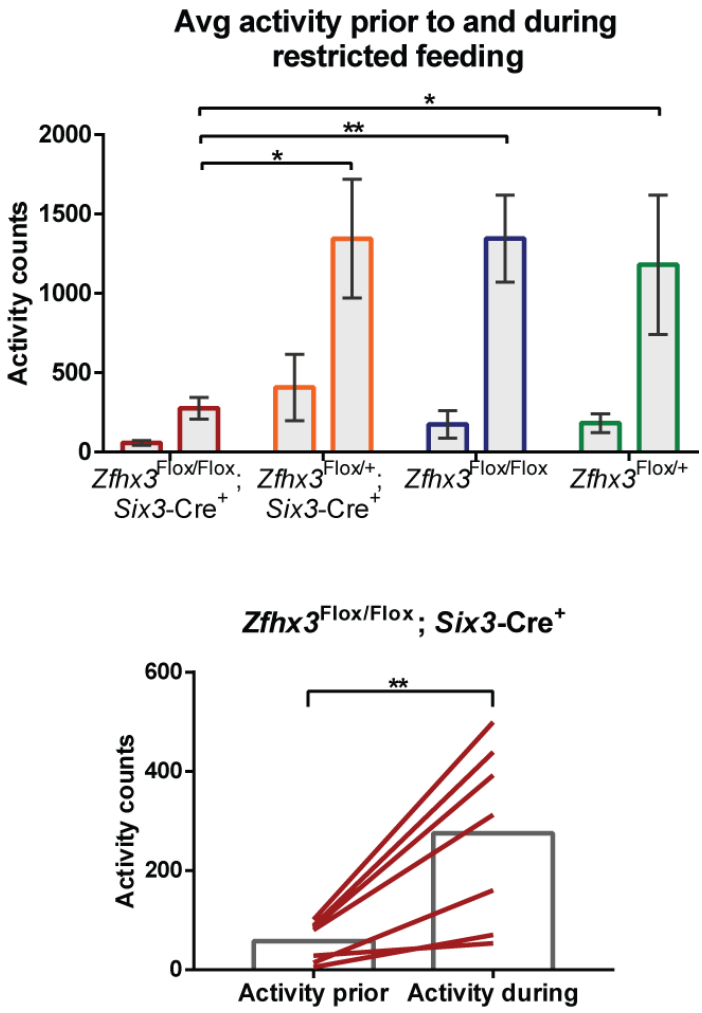


Figure 4.10 | Total activity counts for 3 hour time windows *Zfhx3*$^{Flox/Flox}$; *Six3*-Cre^{+} [n=7], *Zfhx3*$^{Flox/+}$; *Six3*-Cre^{+} [n=6], *Zfhx3*$^{Flox/Flox}$ [n=7] and *Zfhx3*$^{Flox/+}$ [n=6] mice prior to (left bars) and during (right bars) time restricted feeding. Error bars denote SEM of data sets; * denotes significance at $p<0.05$, ** denotes significance at $p<0.01$.

Zfhx3$^{Flox/Flox}$; *Six3*-Cre^{+} mice display a metabolic circadian rhythm

The circadian system compromises many hierarchical oscillators, located both centrally and peripherally. As the main central circadian oscillator was disrupted in these mutant mice, they provided a unique opportunity to assess circadian activity of peripheral oscillators in a mouse that has developed lacking an SCN. To study this, mutant mice underwent various phenotyping measures related to metabolic function to assess firstly whether factors relating to metabolic output were affected, and secondly to assess whether the metabolic system of these animals displayed a circadian rhythm.

A small age matched female cohort [n=4] underwent Echo-MRI analysis to measure lean and fat mass of *Zfhx3*$^{Flox/Flox}$; *Six3*-Cre^{+} mice compared to controls (**Figure 4.11**). This was a first step to assess whether weight and body composition was altered in these mutants compared to controls after the striking circadian locomotor phenotype was uncovered. No significant differences were apparent in body weight [$F(2,10)=0.3202$, $p=0.7332$], percentage fat mass [$F(2,10)=0.5644$, $p=0.5858$] or percentage lean mass [$F(2,10)=0.2236$, $p=0.8035$] when compared using ANOVA.

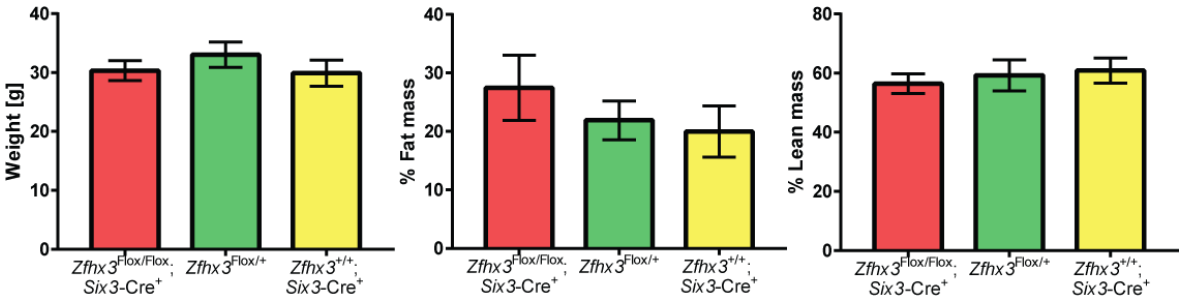


Figure 4.11 | Weight, % fat mass, % lean mass of *Zfhx3*$^{Flox/Flox}$; *Six3*-Cre^{+} [n=4], *Zfhx3*$^{Flox/+}$ [n=5] and *Zfhx3*$^{+/+}$; *Six3*-Cre^{+} [n=4] mice as measured using Echo-MRI. Error bars denote SEM of data sets. No significant differences were found between groups when analysed using one way ANOVA ($\alpha=0.05$).

A mixed sex cohort of *Zfhx3*$^{Flox/Flox}$; *Six3*-Cre^{+} mice was later used for metabolic phenotyping using a metabolic caging system. This involved mice being singly housed for a period of 3 days with access to food and water *ad libitum*; data collected during the final complete 24 hour LD period was taken for analysis. The parameters calculated were volume of O_2 consumption, volume of CO_2 production, activity/distance travelled and energy expenditure (EE). *Zfhx3*$^{Flox/+}$; *Six3*-Cre^{+} mutant mice were also tested, along with *Zfhx3*$^{Flox/+}$ and *Zfhx3*$^{Flox/Flox}$ control groups. **Figure 4.12** shows the data over time for O_2 consumption, activity and EE in *Zfhx3*$^{Flox/Flox}$; *Six3*-Cre^{+}, *Zfhx3*$^{Flox/+}$; *Six3*-Cre^{+} and *Zfhx3*$^{Flox/Flox}$ animals (only one control group is shown in this figure for simplicity and ease of viewing). Control mice in this caging system display a peak in activity prior to lights off and sustained activity throughout the dark phase, whilst little to no activity is recorded during the light phase – all characteristic traits of nocturnal animals such as mice (Bains et al., 2018). As in previous tests, *Zfhx3*$^{Flox/Flox}$; *Six3*-Cre^{+} mice show arrhythmic activity over the LD cycle in this caging system. However, unlike in previous testing, such as wheel running, in this caging system *Zfhx3*$^{Flox/+}$; *Six3*-Cre^{+} mutants appear to show no burst of activity in anticipation of lights off. Measures for oxygen consumption and energy expenditure show circadian peaks that correspond to activity in control mice, and again values for these parameters remain higher throughout the active dark phase than in the light. Surprisingly, given the extent of arrhythmic activity observed in the mutants lacking an SCN, a noticeable circadian rhythm was evident in oxygen consumption and energy expenditure – albeit with an attenuated peak compared to control mice. As well as having reduced amplitude, the peak was also delayed in *Zfhx3*$^{Flox/Flox}$; *Six3*-Cre^{+} mice compared to controls. This suggests that metabolic outputs of the circadian

system do not wholly rely on the SCN for co-ordination and control; however in the absence of an SCN the amplitude of these rhythmic outputs is dampened. *Zfhx3*$^{Flox/+}$; *Six3*-Cre^{+} mutants, who show no loss in SCN cell density, also appear to have a slightly attenuated and delayed peak of metabolic activity.

Prior to metabolic screening, this cohort underwent Dual-energy X-ray absorptiometry (DEXA) analysis to measure body composition. The results of this mirrored those seen in the early Echo-MRI experiments; there were no significant differences in body weight [$F(4,28)=0.3788$, $p=0.8218$], lean mass [$F(4,28)=1.419$, $p=0.2534$] or fat mass [$F(4,28)=0.4326$, $p=0.7838$] between genotypes (**Figure 4.13**). Therefore, any metabolic consequences due to the lack of an SCN in *Zfhx3*$^{Flox/Flox}$; *Six3*-Cre^{+} do not affect the distribution of lean and fat mass in these animals. Also, crucially, developing without an SCN and with complete behavioural arrhythmicity does not appear to cause any growth defects in mice.

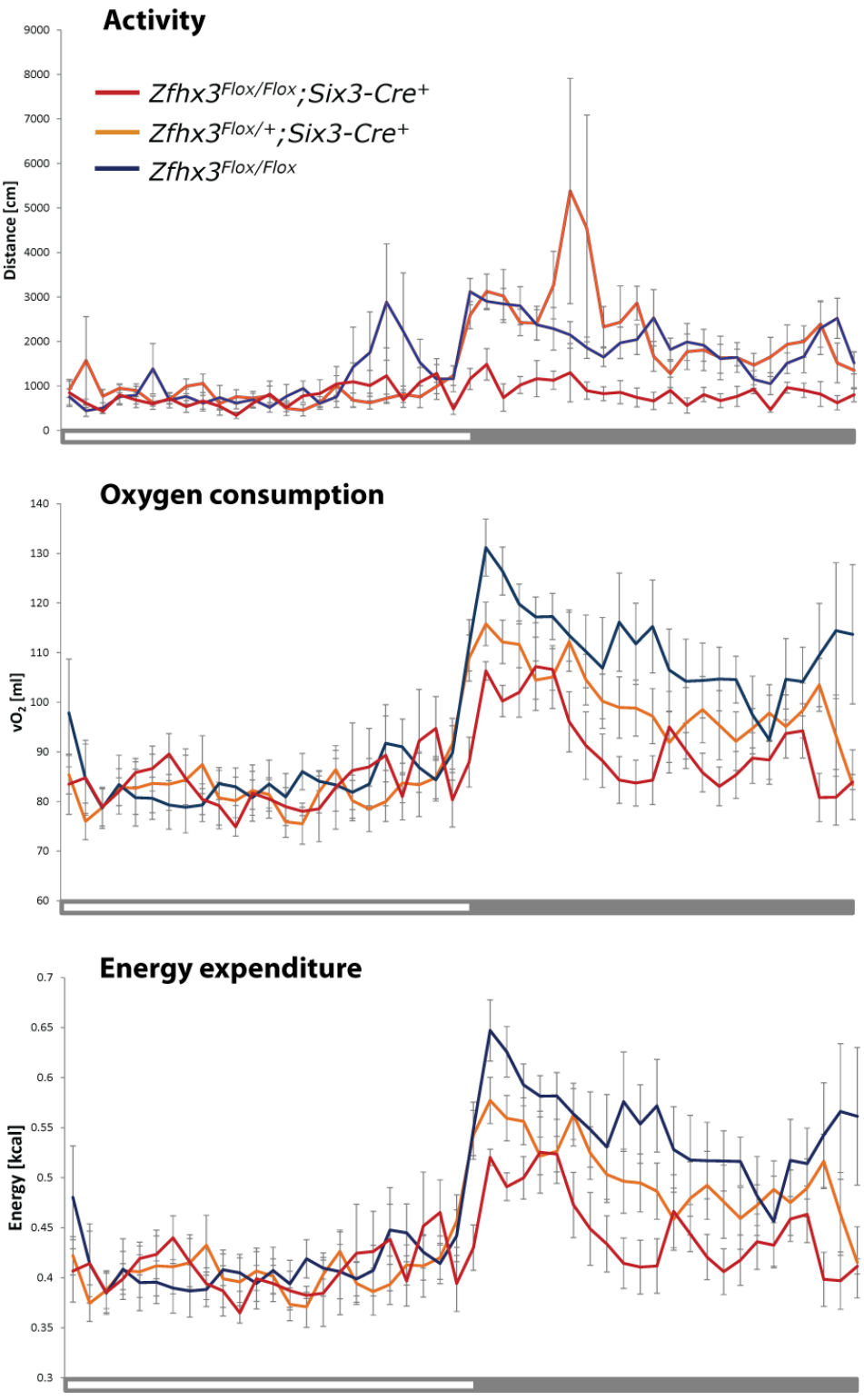


Figure 4.12 | *Zfhx3*$^{Flox/Flox}$; *Six3*-Cre^{+} [n=4], *Zfhx3*$^{Flox/+}$; *Six3*-Cre^{+} [n=8] and *Zfhx3*$^{Flox/Flox}$ [n=7] mice underwent metabolic phenotyping using metabolic caging. Shown are average line graphs for activity – measured in distance travelled [cm], oxygen consumption [ml], and energy expenditure [kcal] in these groups. Error bars denote SEM, shaded bar denotes LD cycle.

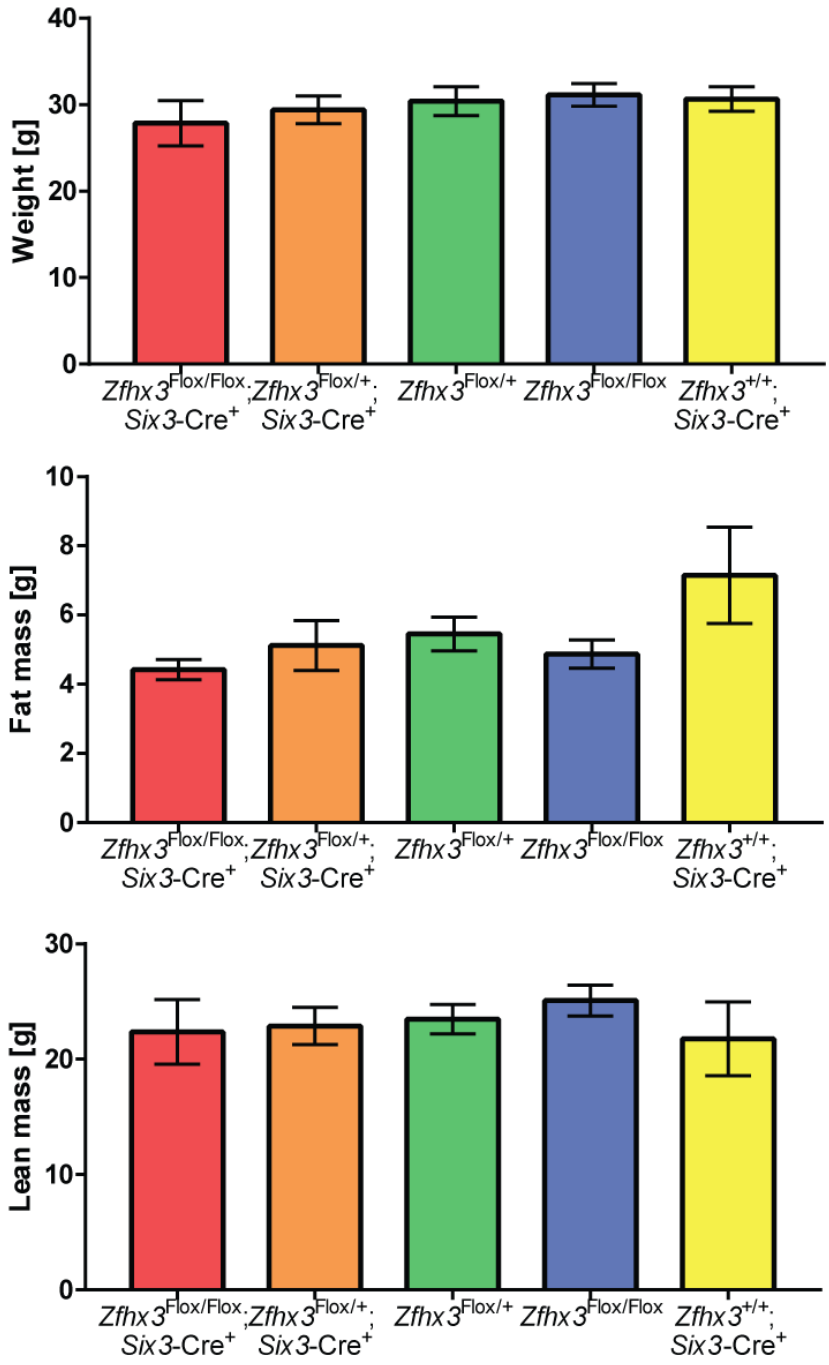


Figure 4.13 | *Zfhx3*$^{Flox/Flox}$; *Six3*-Cre^{+} [n=4], *Zfhx3*$^{Flox/+}$; *Six3*-Cre^{+} [n=8], *Zfhx3*$^{Flox/+}$ [n=11], *Zfhx3*$^{Flox/Flox}$ [n=7] and *Zfhx3*$^{+/+}$; *Six3*-Cre^{+} [n=3] mice underwent body composition measurement using DEXA. Error bars denote SEM of group data. No significant differences were found for any parameters when analysed using one way repeated measures ANOVA.

Corticosterone as a measure of HPA output in 'SCN-less' mice

Corticosterone secretion is controlled by the hypothalamic-pituitary-adrenal (HPA) axis; glucocorticoid levels display a strong circadian peak of expression due to a circadian clock present in the adrenal cortex, which receives timing input from the SCN (Pezuk et al., 2012; Son et al., 2008). Changes to this SCN regulated HPA output can result in massive downstream hormonal changes and ultimately alter metabolic and behavioural functions. As well as this, corticosterone is known to be a key synchroniser of peripheral oscillators (Balsalobre et al., 2000). Because of this, corticosterone levels over the circadian day were measured in *Zfhx3*$^{Flox/Flox}$; *Six3*-Cre^{+} mice.

The traditional method for measuring corticosterone in mice is to collect plasma from blood sampling (Kim et al., 2018); given that corticosterone is a stress related hormone and that repeated blood sampling is a very stressful procedure (Hunt and Hambly, 2006), urine collection was used for sampling instead. Corticosterone has been shown to be excreted in measurable quantities in mouse urine (Touma et al., 2003) with a delay of around 3 hours (Bamberg et al., 2001) – therefore any short term handling stress should not influence corticosterone measures in collected urine. To validate this approach, a wildtype C57B6/J mouse was used to collect urine at time-points encompassing every 4 hours throughout the LD cycle. A minimum of 24 hours was allowed between collections to allow the animal sufficient recovery time from any possible stress incurred during the collection process. Utilising this method, a rhythm of corticosterone level with a clear peak at ZT12 was observed (**Figure 4.14**). This cycling was in agreement with previous data on urinary corticosterone levels in mice (Kamakura et al., 2016).

As measurement of corticosterone from urine produced reliable cycling data in this experiment, urine was then collected from three singly housed *Zfhx3*$^{Flox/Flox}$; *Six3*-Cre^{+} male mice. These mice were all over 12 months of age and had been singly housed for the majority of their lifetime due to being used for circadian screening. Therefore, any possible social stress from cagemates prior to collection was circumvented and also corticosterone levels between individuals should have been comparable. It should also be noted that previous literature has demonstrated that singly housed male mice display comparable urinary corticosterone measures to that of group housed male mice (Hunt and Hambly, 2006). To minimise collections, urine was sampled at the peak and trough of corticosterone concentration observed in **Figure 4.14**: ZT0 and ZT12 and then values averaged for each genotype**.** As only three *Zfhx3*$^{Flox/Flox}$; *Six3*-Cre^{+} mice and two *Zfhx3*$^{+/+}$ mice were able to be used for collection, it would be deemed unsuitable to perform any statistical analysis to asses significance. However, it is evident from this pilot cohort that corticosterone levels are substantially higher at both time-points in *Zfhx3*$^{Flox/Flox}$; *Six3*-Cre^{+} mice compared to wildtypes. Also, the peak and trough of corticosterone expression appears to be inverted in these mutants – with values for ZT0 far greater than that of ZT12 (**Figure 4.14**). This could be due to a complete inversion of how corticosterone release is regulated by the circadian system or it could indicate a phase-shift in this mechanism; further data collection across 24 hours would be required to assess this.

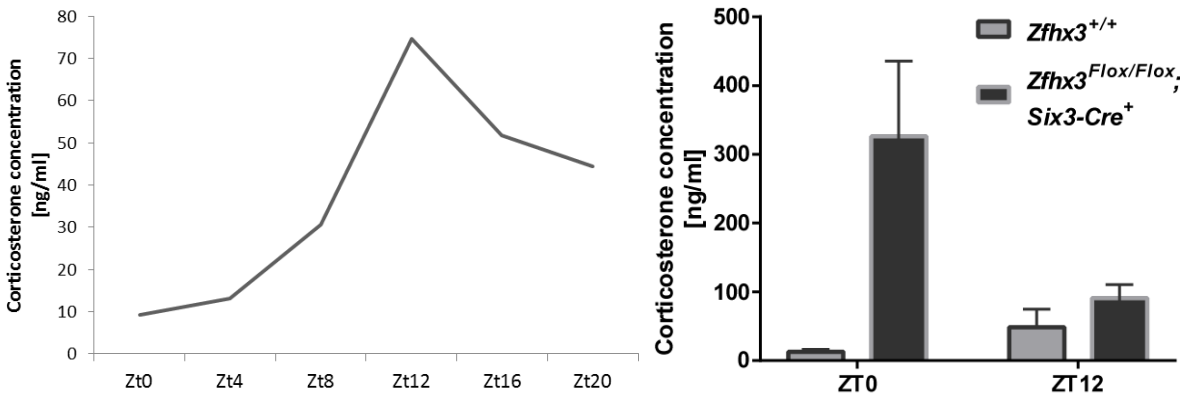


Figure 4.14 | Left: Corticosterone concentration measured from urine samples of a wildtype B6J mouse across the circadian day. The animal was kept in a standard 12:12 LD cycle with lights on at ZT0 and lights off at ZT12. **Right**: Mean corticosterone concentration measured from urine samples collected at ZT0 and ZT12 from *Zfhx3*$^{Flox/Flox}$; *Six3*-Cre^{+} [n=3] and *Zfhx3*$^{+/+}$ control mice, mice were kept under the same standard 12:12 LD cycle. Error bars denote SEM.

Activity and anxiety-related parameters are unaffected in *Zfhx3*$^{Flox/Flox}$; *Six3*-Cre^{+} mice

The key focus of this study thus far was to characterise various facets of the circadian system in *Zfhx3*$^{Flox/Flox}$; *Six3*-Cre^{+} mice; however, some more general behavioural phenotyping tests were also performed on these animals. As light and time of day cues have been shown to affect behaviour and cognition in mice (Fisk et al., 2018), these experiments were a step toward assessing whether SCN-loss would affect behaviour in *Zfhx3*$^{Flox/Flox}$; *Six3*-Cre^{+} mutants.

Open field testing was first carried out on an age matched cohort of *Zfhx3*$^{Flox/Flox}$; *Six3*-Cre^{+} mice [n=10] to assess whether their hugely disrupted circadian locomotor patterns had any effect on the general anxiety and activity in response to a novel environment. The total time animals were recorded in the arena was 20 minutes, during which time, data on frequency and total time in both the centre and

periphery of the arena was collected. Testing was carried out between ZT3-5 for all mice. The centre of the arena is deemed anxiogenic for mice; therefore, wildtype animals will typically spend more time exploring the periphery. **Figure 4.15** shows the data for this test for *Zfhx3*$^{Flox/Flox}$; *Six3*-Cre^{+} and *Zfhx3*$^{Flox/+}$; *Six3*-Cre^{+} mutants*;* due to time constraints, only *Zfhx3*$^{Flox/+}$ mice were run as a control group. The first result to note is that all groups travelled a comparable distance in the whole arena during the test [$F(2,20)=0.9665$, $p=0.3975$], this result shows that *Zfhx3*$^{Flox/Flox}$; *Six3*-Cre^{+} mice do not display noticeable hypoactivity in a novel environment. This was important to confirm, as *Zfhx3*$^{Flox/Flox}$; *Six3*-Cre^{+} mice do show reduced activity in various other screening methods presented earlier and therefore this could have confounded any further data collected. There were also no statistical differences in latency to enter the centre of the arena [$H=0.9604$, $p=0.6187$], total time in the centre [$F(2,20)=0.9478$, $p=0.4043$], frequency of entries to the centre [$F(2,20)=0.4826$, $p=0.6242$], total time spent in the arena periphery [$F(2,20)=0.8394$, $p=0.4466$] and frequency of periphery entries [$F(2,20)=0.0195$, $p=0.9807$]. From this data, it is evident that *Zfhx3*$^{Flox/Flox}$; *Six3*-Cre^{+} mice do not have any measurable differences in anxiety/stress related behaviour when analysed in a novel arena. This was a surprising result, given the high levels of corticosterone measured in these mutants.

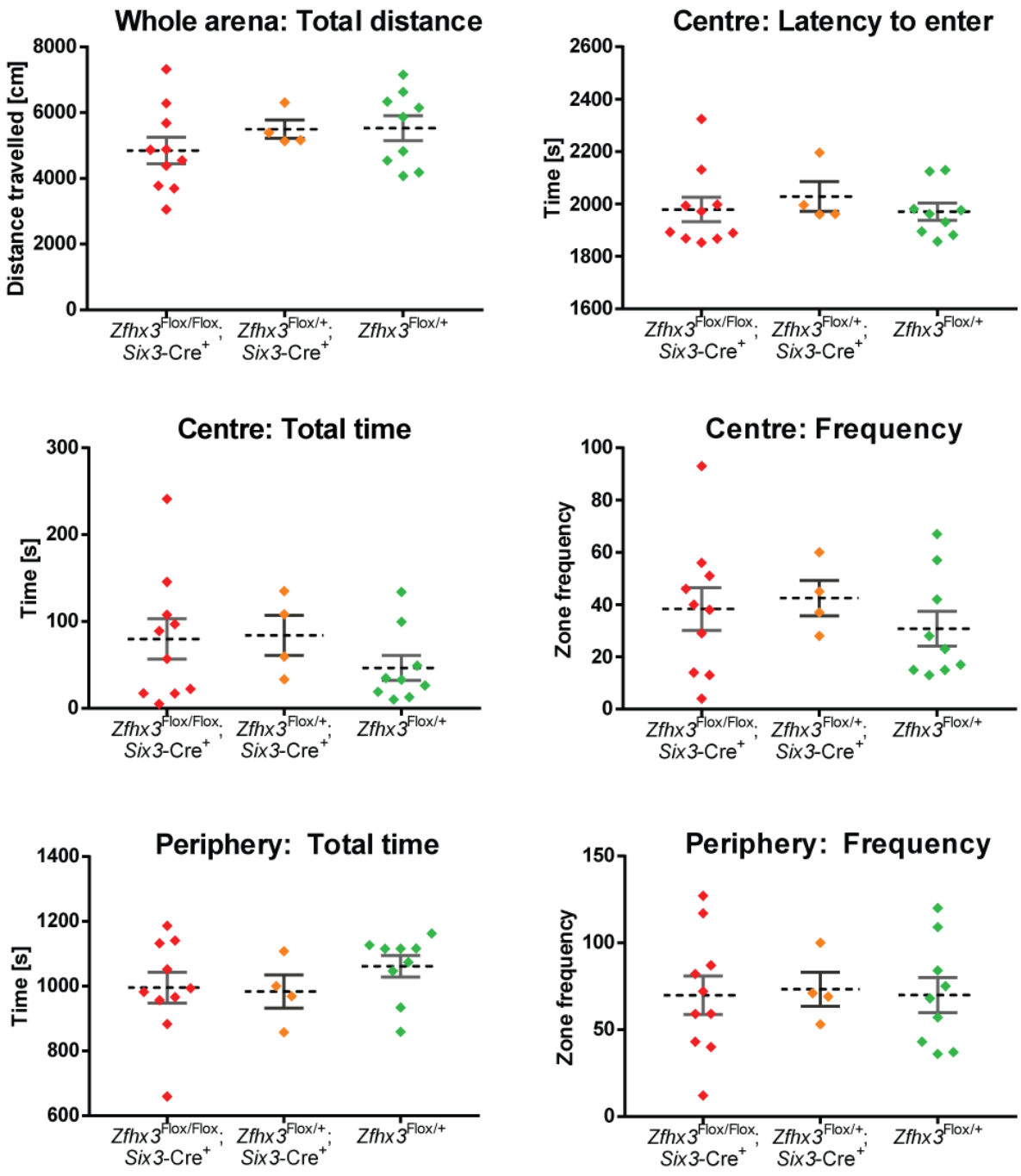


Figure 4.15 | Open field parameters measured from *Zfhx3*$^{Flox/Flox}$; *Six3*-Cre^{+}, *Zfhx3*$^{Flox/+}$; *Six3*-Cre^{+} and *Zfhx3*$^{Flox/+}$ mice. No statistical differences were found between groups in total distance travelled [$F(2,20)=0.9665$, $p=0.3975$], latency to centre [$H=0.9604$, $p=0.6187$], total time in the centre [$F(2,20)=0.9478$, $p=0.4043$], frequency of entries to the centre [$F(2,20)=0.4826$, $p=0.6242$], total time in arena periphery [$F(2,20)=0.8394$, $p=0.4466$] and frequency of periphery entries [$F(2,20)=0.0195$, $p=0.9807$]. Dashed line denotes mean of group data, error bars indicate SEM of group data.

The light-dark box is another phenotyping test used to assess a mouse's response in perceived anxiogenic areas. This test is run for a total of 5 minutes, during this time the mouse has free access to both a light (100-120 lux) a smaller dark compartment in an arena. A wildtype mouse should perceive the light area as anxiogenic and preferentially spend the majority of its time in the dark compartment. As was shown previously in Results III, *Zfhx3*$^{Flox/Flox}$; *Six3*-Cre^{+} mice display a complete absence of masking to light in a circadian context. Therefore, this experiment was also used to assess whether the behavioural response to light normally recorded in this test was also disrupted in these mutants. As is shown in **Figure 4.16**, no differences were found between *Zfhx3*$^{Flox/Flox}$; *Six3*-Cre^{+} and control mice in total time spent in the light [$t(10)=0.5466$, $p=0.5966$] and dark [$t(10)=0.5403$, $p=0.6008$] compartments of the arena. This was also the case for the number of entries to both the light [$U(10)=15$, $p=0.6970$] and dark [$U(10)=16.5$, $p=0.8485$] compartments. However, when analysing this data it became apparent that control animals spent an equal amount of time in the light and dark compartments; therefore, it could be concluded that the light compartment was not anxiogenic enough to evoke inhibitory behaviour. Thus, although mutants displayed comparable behavioural responses to light in this context as control animals, it perhaps does not confirm that this behavioural light pathway is intact in these mice – due to the possible invalidity of the test itself. Efforts were made to repeat this experiment using a higher lux level, thereby supposedly increasing the anxiogenic properties of the light compartment, however the same distribution of time spent between light and dark was observed. Therefore, the data presented here is the best available for this particular behavioural test.

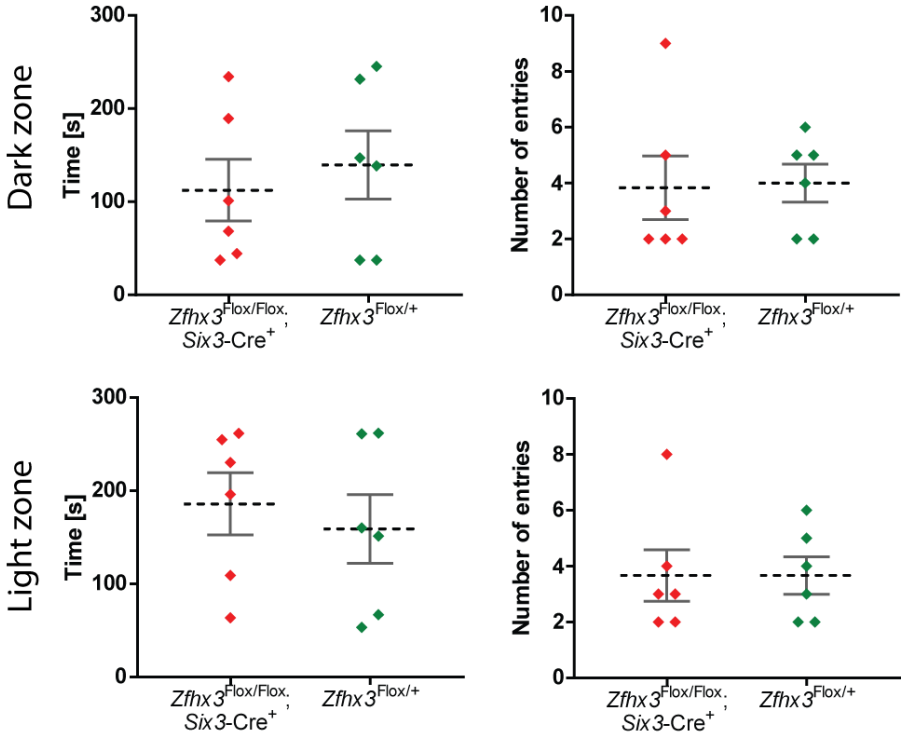


Figure 4.16 | Total time spent in and number of entries to dark and light compartments during light-dark box testing of *Zfhx3*$^{Flox/Flox}$; *Six3*-Cre^{+} and *Zfhx3*$^{Flox/+}$ mice. No significant differences were found between groups when analysed using unpaired t-tests for time and unpaired Mann-Whitney U tests for entries. Dashed line denotes mean of group data, error bars denote SEM of data.

Discussion

This chapter encompassed many different phenotyping tests to assess possible changes in behaviour and/or physiology of *Zfhx3*$^{Flox/Flox}$; *Six3*-Cre^{+} mice. These mutants provided a unique opportunity to gather data on the impact of aberrant SCN formation during development in a mouse model, thus furthering our understanding of both central and peripheral oscillators outside of the SCN.

One of the most remarkable aspects of *Zfhx3*$^{Flox/Flox}$; *Six3*-Cre^{+} mice is their inability to mask; particularly as masking behaviour is observed in SCN ablation models (Eastman et al., 1984; Gall et al., 2016; Redlin and Mrosovsky, 1999). Evidence from these published studies suggests that masking is therefore not SCN dependent. Various visual phenotyping tests were conducted on the *Zfhx3*$^{Flox/Flox}$; *Six3*-Cre^{+} line, all of which strongly suggest that these mutants retain the ability to sense and respond to light. MEA data on *Zfhx3*$^{Flox/Flox}$; *Six3*-Cre^{+} mutants suggests that the retinae of these mice are able to sense and respond to light, but this does not confirm intact light responsive pathways downstream of the eye. It has been shown that mice do not require an intact visual cortex to display masking in response to light (Redlin et al., 2003). This could explain why in *Zfhx3*$^{Flox/Flox}$; *Six3*-Cre^{+} mutants, despite a functional image-forming visual system, masking behaviour is still absent. Similarly, retained retinal input to the lateral geniculate: a key nucleus for relay between the retina and visual cortex (Weyand, 2016), also cannot be viewed as confirmation that masking should occur. There is no consensus on which particular area of the brain is responsible for behavioural masking to light (Rietveld et al., 1993). As stated previously, it had been assumed that the SCN is not necessary due to the fact that adult SCN ablation models exhibit masking behaviour. On the contrary, a study has

shown that synaptic input to the brain from ipRGCs occurs via the SCN (Fernandez et al., 2016), suggesting that perhaps the SCN serves some function in this light responsiveness pathway after all. Considering this and the data gathered thus far on *Zfhx3*$^{Flox/Flox}$; *Six3*-Cre^{+} mice, it appears that the SCN may be needed during development to form behavioural masking responses to light.

Furthering work on responsiveness to various Zeitgebers, data presented here shows that *Zfhx3*$^{Flox/Flox}$; *Six3*-Cre^{+} mutant mice display FAA, therefore the FEO in these SCN-less mutants can be considered functional. This agrees with previous work in this field on FAA in SCN ablation models, but moreover the data presented in this chapter suggests that the FEO is an entirely separate system to the SCN, from development onwards – not just in adult animals. At present, the exact location of the FEO remains elusive and results pertaining to this are inconsistent (Pendergast and Yamazaki, 2018). Various central oscillators in the brain, such as the limbic forebrain and the dorsomedial hypothalamic nucleus, have been proposed candidates; however it is likely that the FEO consists not of one specific area, but a network of interconnected brain regions and peripheral oscillators (Verwey and Amir, 2009). Silver and colleagues have also proposed that the FEO is dependent on memory and learning, and highlight the confounding effects of the light-entrainable oscillator when attempting to measure FAA (Silver et al., 2011). The *Zfhx3*$^{Flox/Flox}$; *Six3*-Cre^{+} line could be used as an invaluable tool for the study of the FEO, as there is no competing light-entrainable oscillator in the SCN during the lifetime of this mouse (Damiola et al., 2000) – allowing the study of the FEO in isolation. Moreover, *Zfhx3*$^{Flox/Flox}$; *Six3*-Cre^{+} mice still display a circadian rhythm in metabolic parameters such as energy expenditure, despite being behaviourally arrhythmic. Studies on *Vipr2*$^{-/-}$ mice, which

show reduced/less robust circadian activity but still mask to an LD cycle (Harmar et al., 2002), have shown an advance in metabolic and feeding rhythms of around 3-4 hours in LD (Bechtold et al., 2008). This data indicates that although light masks locomotor activity, feeding activity is not affected to the same extent. It would be interesting to analyse the feeding behaviours of *Zfhx3*$^{Flox/Flox}$; *Six3*-Cre^{+} mice to analyse whether feeding times are altered in these mutants who appear to live devoid of time of day cues. In addition to this, a logical next step would be to conduct indirect calorimetry on *Zfhx3*$^{Flox/Flox}$; *Six3*-Cre^{+} mice when under a restricted feeding schedule, and also on various different diet compositions – e.g. high fat diet, to assess weight gain and insulin sensitivity in mice lacking an SCN from development (Kalsbeek et al., 2014). To assess entrainment of peripheral oscillators involved in metabolism, particularly gut and liver, time-course qPCR experiments to measure genes such as *Per* and *Cry* could also be conducted on *Zfhx3*$^{Flox/Flox}$; *Six3*-Cre^{+} mice under both *ad lib* and restricted feeding schedules (Husse et al., 2014). The use of the *Per2::Luc* reporter line could also be potentially useful here to record oscillations of peripheral oscillators *ex vivo*.

There has also been a 'social' circadian clock proposed in mice (Panksepp et al., 2008) and other rodents (Castillo-Ruiz et al., 2018; Paul et al., 2014, 2015), as well as primates (Bessa et al., 2018). However, studies of this potential oscillator have been limited, most likely due to the challenges of recording activity in a group housed environment. Data presented in this chapter provides further validation for the group-housed circadian analysis conducted using caging systems at Harwell (Bains et al., 2016; Bains et al., 2018). From these studies, it was found that *Zfhx3*$^{Flox/Flox}$; *Six3*-Cre^{+} mice do display an increase in activity reminiscent of anticipatory activity in response

to lights off in the LD cycle. However, this is only apparent at 4 months of age; which is in contrast to *Zfhx3*$^{Flox/+}$; *Six3*-Cre^{+} and control animals, who display this behaviour at both 4 and 8 months of age. This data suggests that mice lacking an SCN are able to entrain somewhat to the social cues of their cagemates at younger ages, but that this dissipates with age. Previously, Schwartz and colleagues showed that when hamsters are co-housed, one hamster's τ_{DD} will adjust to that of its cagemate (Paul and Schwartz, 2007). However this data was only collected at a single age point, and a subsequent follow up study did not define the specific age when this was conducted (Paul et al., 2014). Furthering this work, the same lab has also shown that social synchrony occurs in female mice when housed in groups of five (Paul et al., 2015). This study was conducted on BALB/c mice, which have been suggested to have weaker circadian coupling than other background strains (Rosenwasser, 1990). It could be that in mice with weak circadian coupling, entrainment to weaker entrainment cues – such as social interactions, could have a greater impact than in those with a strong central circadian clock. Data presented in this chapter supports this notion; however it appears that the SCN may be necessary for this social entrainment behaviour to persist as the mouse ages. From day to day observations, there does not appear to be any overt social disruption between *Zfhx3*$^{Flox/Flox}$; *Six3*-Cre^{+} mice and their cage mates; mutants appear to nest together with controls as normal when inspecting videos from the home cage monitoring analysis system. It is also possible to collect data on proximity between cage-mates at all times from this system, which would be ideal for analysing any subtle social behaviours that are perhaps being overlooked, however analysis of this data is currently unobtainable as better analysis tools need to be developed before this can be used reliably. This would also go a step further in

characterising the social aspects of circadian entrainment, as past studies in the literature (referenced above) did not have this technology available to them.

Another surprising result of these experiments was that of the corticosterone levels in *Zfhx3*$^{Flox/Flox}$; *Six3*-Cre^{+} animals, particularly when considered in parallel with the open field data presented here. Classically, corticosterone is thought to be a major stress related hormone (Lupien et al., 2009) yet these mice display potentially higher levels of corticosterone while they display no overt stress related phenotype in open field or light dark box tests. More work could be done on measuring the levels of other glucocorticoids in an attempt to characterise how the HPA axis is affected in these animals, as the SCN has been previously shown to regulate HPA output and this regulatory system is likely absent in *Zfhx3*$^{Flox/Flox}$; *Six3*-Cre^{+} mice (Kalsbeek et al., 2012). It could be that stress response is closely linked to time of day or LD cues; therefore, if an animal has no sense of internal time, its response to stress related hormones could be considerably affected. Behavioural phenotyping of *Zfhx3*$^{Flox/Flox}$; *Six3*-Cre^{+} mice was limited due to time constraints; many more behavioural tests could be conducted on *Zfhx3*$^{Flox/Flox}$; *Six3*-Cre^{+} animals to assess both cognition and mood related phenotypes. Related to this, it has been shown that long term exposure to high corticosterone actually attenuates depression like behaviours in mice (Karten et al., 1999). Based on this finding, tests for depression-like behaviour such as the forced swim test (Bogdanova et al., 2013) could be conducted on *Zfhx3*$^{Flox/Flox}$; *Six3*-Cre^{+} animals in parallel with measurement of serotonin levels in these mutants. This data would be highly complementary to the social data collection proposed earlier, in the pursuit of further understanding of a socially entrainable oscillator in mice.

The circadian system has been historically presented as a hierarchy of oscillators, located both centrally in the brain and peripherally in other organs (Albrecht, 2012; Honma, 2018; Mohawk et al., 2012). Traditionally, the SCN is viewed as the master orchestrator of these oscillators and the key to internal timekeeping. Work presented in this chapter challenges this idea, with evidence suggesting that the SCN itself is necessary for behavioural rhythmicity in response to LD but in its absence other oscillators – such as the FEO, can potentially become the 'master clock' of the circadian system (Refinetti, 2015). Indeed, the *Zfhx3*$^{Flox/Flox}$; *Six3*-Cre^{+} line could prove to be an invaluable tool for the further study of diverse functional aspects of chronobiology.

Discussion

The data presented in this thesis builds on previous work that identified *Zfhx3* as a crucial regulator of both circadian (Parsons et al., 2015) and sleep systems (Balzani et al., 2016) in mice through study of a heterozygous missense mutation: *Zfhx3*^{Sci}. The conditional mutagenesis approach employed here facilitated further understanding of the role of *Zfhx3* in the circadian system: circumventing embryonic lethality seen in constitutive *Zfhx3* knockout mice, but also allowing the study of spatial gene function. Without this data, the characterisation of *Zfhx3* in the circadian system would be limited to what is already known about *Sci* and *Zfhx3*'s role in the development of the SCN, furthermore its function in adult circadian biology could not be verified.

Results I emphasises the temporal nature of *Zfhx3*; from the initial identification of *Zfhx3* as a novel developmental regulator of circadian rhythms via ENU mutation (Parsons et al., 2015) to confirmation that ZFHX3 is necessary in adults for stable locomotor rhythms (Wilcox et al., 2017). However, the role of *Zfhx3* in the hierarchy of circadian regulation it is still unclear, along with what co-factors the gene may be binding to in order to exert these effects. Molecular data from Parsons et al demonstrated that *Zfhx3*$^{Sci/-}$ mice had no changes in expression to canonical core clocks, but did display downregulation of key circadian related genes *Vip*, *Vipr2* and *Prokr2*. RNAseq data generated from *Zfhx3*$^{Flox/Flox}$; UBC-Cre^{+} SCN will prove to be an

invaluable resource to build on this (Results I). Analysis of this data will yield a list of genes upregulated or downregulated in adult SCN following *Zfhx3* deletion, as well as whether this expression has a differential circadian component. Comparison of this data with the aforementioned data gathered on gene expression in adult SCN in *Zfhx3*$^{Sci/+}$ mice (Parsons et al., 2015) will enable us to differentiate between genes that are altered when *Zfhx3* is disrupted developmentally versus when the gene is deleted in the adult. Analysis of gene expression differences may also reveal novel cycling genes that are altered in *Zfhx3*$^{Flox/Flox}$; UBC-Cre^{+} SCN post tamoxifen dosing. It has been shown previously that *Zfhx3* itself does not cycle (Parsons et al., 2015), therefore it is likely that targets of the gene could be cyclic – such as *Vip*, which has been shown to be previously downregulated. Alternatively, binding of *Zfhx3* to co-factors could be cyclic despite expression of the gene itself not being. This is the case for classic circadian genes CLOCK and BMAL1 (Menet et al., 2014). As *Zfhx3* is known to have a main role in cell cycle regulation (Jung et al., 2005a) and neurogenesis (Miura et al., 1995), it will be important to distinguish possible circadian related targets from genes concerned with these principal functions. One way of approaching this would be to identify genes that cycle, i.e. have differential expression across the time points collected. Cycling analysis of gene transcription in the SCN has been crucial in identifying key components of the molecular clock previously; being first applied to a mammalian circadian mutant in the *Clock/Clock* mutant mouse (Panda et al., 2002) to elucidate molecular consequences of the loss of the *Clock* gene. As *Vip* and its receptors are repeatedly implicated in maintaining rhythmicity of the core clock in adult SCN (Aton et al., 2005a; Harmar et al., 2002; Mazuski et al., 2018), it is

expected that expression of this gene will be downregulated in *Zfhx3*$^{Flox/Flox}$; UBC-Cre^{+} SCN as it was in *Zfhx3*$^{Sci/+}$ animals.

Mice where *Zfhx3* is deleted in adults display contrasting pupillary reflexes to *Zfhx3*$^{Sci/+}$ and also *Zfhx3*$^{Sci/-}$ animals (results chapters II and III); *Zfhx3*$^{Flox/Flox}$; UBC-Cre^{+} mice are less sensitive to light of all irradiances whereas *Sci* and *Zfhx3*$^{Sci/-}$ mice are more sensitive under dimmer light conditions. Rods, cones and melanopsin expressing cells have been shown to all account for pupillary light reflex in mice (Hattar et al., 2003). Immunofluorescent staining for retinal cell markers and ZFHX3 itself pre/post tamoxifen would indicate in which cell types ZFHX3 is lost and therefore whether this loss could account for the pupillometry phenotype observed. As discussed earlier, there could also be differences in gene expression changes when *Zfhx3* is knocked out in adult tissues (including retina), as opposed to when *Zfhx3* expression is altered in *Zfhx3*$^{Sci/+}$ mice. For example, it has been recently shown that a subset of retinal ganglion cells express vasopressin (*Avp*) and interestingly, these cells project predominantly to the SCN (Tsuji et al., 2017). Given that *Zfhx3* has been shown to cause changes to *Avp* expression in *Zfhx3*$^{Sci/+}$ SCN (Parsons et al., 2015), it would be unsurprising to discover changes in vasopressin expression in the retina in these animals also. As we do not yet know whether changes to *Avp* are also evident in *Zfhx3*$^{Flox/Flox}$; UBC-Cre^{+} mice, it could be there are contrasting effects on gene expression between these mutants yet to be discovered. In addition to this, a recent study revealed a link between pupillary reflex response in humans and circadian fragmentation (Bonmati-Carrion et al., 2016); therefore, elucidating the changes in pupillary reflex in these mutants could further the understanding of possible

functions of *Zfhx3* in the crucial light input pathway to the core central circadian clock in the SCN.

Progeny of many genotypes are produced when generating conditional mouse mutants and there is also a huge cost implication of housing all control genotypes for both sexes. Due to this, and the fact that other mutant lines were being generated in parallel, studies of the *Zfhx3*$^{Sci/-}$ line were particularly limited when compared to other mutant lines discussed in this thesis. Once experimental cohorts had been generated for this line, breeding was stopped in order to make space for larger cohort breeds on other mutant lines that were generating higher impact and more novel results (e.g. *Zfhx3*$^{Flox/Flox}$; *Six3*-Cre^{+}). This unfortunately led to both pre and post tamoxifen data from the same individual animals being unavailable for many mice as they had already been dosed with tamoxifen before unsuccessful circadian screening, prior to being used for passive infra-red screening. As only a finite number of animals were able to be produced in the time-frame available, a new cohort for pre tamoxifen screening was unobtainable. This meant that changes to circadian parameters could not be measured in the same mouse, which is one of the key advantages when using an inducible cre driver line. From the data presented in Results II, the exact nature of the mutation cannot be concluded; given the contrasting phenotypes of reduced circadian rhythmicity yet increased pupillary light reflex observed in *Zfhx3*$^{Sci/-}$ animals, it is likely that both loss and gain of function attributes are present in the *Sci* mutation. This is not uncommon for ENU mutants, given the complexity of mutations that ENU can induce (Acevedo-Arozena et al., 2008).

The SCN-enriched cre lines driven by *Foxd1* and *Six3* provided spatial deletion of *Zfhx3* during the development of the SCN. *Six3* expression has been shown to be

present as early as embryonic day 10 and continues into adulthood (VanDunk et al., 2011), whereas *Foxd1* expression is seen at least 1.5 days later than this at E11.5 and expression diminishes by E14.5 (Newmann et al., 2018). As SCN differentiation is known to begin between E12 and E15 and be completed 5 days prior to birth (Kabrita and Davis, 2008), this difference in expression patterns may explain the varying phenotypes observed between the *Zfhx3*$^{Flox/Flox}$; *Six3*-Cre^{+} and *Zfhx3*$^{Flox/Flox}$; *Foxd1*-Cre^{+} lines presented in this thesis. Certainly, *Zfhx3*$^{Flox/Flox}$; *Six3*-Cre^{+} mutants produced a far more robust circadian phenotype due to the complete lack of SCN morphology and cell identity in these animals. Because of this, *Zfhx3*$^{Flox/Flox}$; *Six3*-Cre^{+} mice underwent more comprehensive phenotyping than *Zfhx3*$^{Flox/Flox}$; *Foxd1*-Cre^{+} mice following circadian characterisation. Given more time, it would be ideal to study possible longitudinal neuronal cell loss in *Zfhx3*$^{Flox/Flox}$; *Foxd1*-Cre^{+} SCN as the histological staining presented in Results III appears to show a reduction in SCN size. It could be that there is a non-uniform loss of *Avp* and *Vip* expressing neurons, resulting in more core or shell of the SCN being present than usual, thus accounting for the overall instability of circadian behaviour in these animals (Aton et al., 2005a; Moore et al., 2002; Ono et al., 2016; Tokuda et al., 2018; Van der Zee et al., 1999). As well as characterisation of cellular subtypes in the SCN of *Zfhx3*$^{Flox/Flox}$; *Foxd1*-Cre^{+} animals, circuit properties could be studied using electrical recording techniques, such as MEA, on explants to give a better idea on the connectivity that remains between core and shell – as this is a key property of SCN autonomy (Azzi et al., 2017; Baggs et al., 2009b; Mohawk and Takahashi, 2011): a technique first used on mouse SCN in the 1990s by Erik Herzog, amongst others (Herzog et al., 1997). Alternatively, by crossing *Zfhx3*$^{Flox/Flox}$; *Foxd1*-Cre^{+} mice to the *Per2::Luc* reporter line (Yoo et al., 2004), real time

oscillations of neuronal sub-populations in the SCN can be recorded. This is a more popular method of observing connectivity changes in tissues *ex vivo* in circadian biology. Although an extra breeding step is required to achieve animals for recording, this method was shown to be an excellent tool to study synchronisation in the SCN in 2003 by Yamaguchi and colleagues (Yamaguchi et al., 2003) and continues to be used to the present day (Maywood, 2018). These data could then be correlated with activity phenotypes, to reveal more detailed information on how structural changes to the SCN during development may alter patterning of circadian behaviours in the adult.

The *Zfhx3*$^{Flox/Flox}$; *Six3*-Cre^{+} line proved an exciting mutant to study due to the complete loss of SCN cell identity in adult mice, generated by developmental deletion of *Zfhx3*. Not only did this confirm that *Zfhx3* is a crucial transcription factor for SCN development, but it provided an 'SCN-less' mouse that could be used to explore how the circadian system functions without the master pacemaker in the brain. Traditional SCN ablation models have been studied profusely in the past in a variety of model organisms (Berria et al., 1988; Dunn et al., 1977; Easton et al., 2004; Kafka et al., 1985; Mosko and Moore, 1979; Ruby et al., 1996). However, in all of these animals the SCN was present throughout development and therefore during critical time periods for circadian patterning of various behaviours. *Zfhx3*$^{Flox/Flox}$; *Six3*-Cre^{+} mice do not respond to typical time of day cues, such as the LD cycle, because of this it would be particularly interesting to study the cognitive functions of these mice in more depth – as cognition in rodents has been shown to have clear time of day effects (Chaudhury and Colwell, 2002; Gritton et al., 2012; Valentinuzzi et al., 2004; Winocur and Hasher, 1999). Cognition in mice can be assessed using various tests such as mazes and, for more complex learning tasks such as paired associative learning, in

operant testing chambers (Hvoslef-Eide et al., 2016). By completing this testing on *Zfhx3*$^{Flox/Flox}$; *Six3*-Cre^{+} mice at ZT time-points in the middle of subjective night and day for control animals, data can be collected on how their performance compares to wildtype mice. It could be that time of day effects on cognitive function are negated in *Zfhx3*$^{Flox/Flox}$; *Six3*-Cre^{+} mutants due to their inability to distinguish between 'day' and 'night' phases.

Previous experiments utilising the *Six3*-Cre line have been undertaken to study the circadian transcription factor *Lhx1*. In these mutant mice, despite some loss of neuropeptide expression in the SCN, rhythmicity of SCN clock gene expression and innervation of the RHT to the SCN are both preserved (Bedont et al., 2014). Despite *Lhx1* being expressed at E11.5 when SCN neurogenesis begins, gross anatomy of SCN structure remains intact – this is in contrast to what is observed in *Zfhx3*$^{Flox/Flox}$; *Six3*-Cre^{+} mutants, and suggests that *Zfhx3* is possibly upstream of *Lhx1* in this recently discovered transcriptional pathway of SCN development. As yet, SCN morphology has only been studied in adult *Zfhx3*$^{Flox/Flox}$; *Six3*-Cre^{+} animals. Neonatal brains were collected to be sectioned and stained using *in situ* hybridisation techniques carried out in Results III, however these were lost due to a freezer malfunction and so this will need to be repeated in the near future. It is expected that no SCN formation occurs at all, due to expression of *Six3*-Cre and *Zfhx3* well before SCN cytogenesis occurs. However, it is critical to confirm this in neonatal and then embryonic brain as was undertaken by Newmann and colleagues in their recent publication on early SCN formation following *Foxd1* deletion (Newmann et al., 2018). In doing this, it will be possible to establish *Zfhx3*'s position in the genetic hierarchy of SCN development.

Light is typically the main entraining factor to the circadian system via the light entrainable oscillator in the SCN. As already mentioned *Zfhx3*$^{Flox/Flox}$; *Six3*-Cre^{+} mice lack a light entrainable oscillator, therefore these animals provided an opportunity to study the role of other entrainable factors of the mammalian circadian system. Of particular interest is the food entrainable oscillator, which was shown to be still functional in Results IV. This is in agreement with previous data published on the FEO in SCN ablation and circadian mutant models, in which FAA persists despite the loss of circadian entrainment to the LD cycle (Mistlberger, 1994; Pendergast and Yamazaki, 2018), but also adds weight to these previous studies by confirming that development of the FEO is distinct from the SCN entirely. Husse and colleagues claimed to have generated a genetically ablated SCN mouse model for the study of the FEO previously (Husse et al., 2014), however their mouse model retains some SCN cell identity and does not demonstrate a complete loss of SCN structure. Despite much attention in the field, the location of the FEO remains elusive (Davidson, 2009) and it is far more likely that the FEO is not located in a discrete substructure, such as the light entrainable oscillator in the SCN, but is dispersed amongst a variety of central and peripheral oscillators (Caba et al., 2014; Gallardo et al., 2014; Olivo et al., 2017; Polidarova et al., 2013). Firstly, more in-depth study of the *Zfhx3*$^{Flox/Flox}$; *Six3*-Cre^{+} mouse brain, such as systematic characterisation of sub-regions and nuclei (e.g. arcuate and dorsomedial hypothalamus) using Nissl staining would reveal whether systems that have been previously proposed to be essential for FAA are intact. Secondly, to analyse activity in peripheral oscillators: peripheral organs such as the liver, adrenal glands and gut could be collected from *Zfhx3*$^{Flox/Flox}$; *Six3*-Cre^{+} mice that have been kept on a restricted feeding regime and also on *ad libitum* feeding, and qPCR used to validate any changes in total expression or phase of circadian related

gene expression. The aforementioned mouse model generated by Husse lacks a molecular circadian clock in the SCN despite retaining some SCN morphology, these mice continue to display peripheral circadian rhythms and so data confirming whether *Zfhx3*$^{Flox/Flox}$; *Six3*-Cre^{+} mice also display this would be a welcome complement to previously published data in the field of chronobiology. To further study whether *Zfhx3* has a role in peripheral oscillators and the control of the FEO itself, it would be interesting to conduct food restriction experiments on the adult inducible *Zfhx3*$^{Flox/Flox}$; UBC-Cre^{+} line as these mutants lack *Zfhx3* in all adult tissues – which would include any peripheral oscillators and therefore be a useful comparison to the *Zfhx3*$^{Flox/Flox}$; *Six3*-Cre^{+} data.

When *Zfhx3*$^{Flox/Flox}$; *Six3*-Cre^{+} mice are kept on *ad libitum* food, they show an attenuated circadian cycle in metabolic parameters (Results IV), this was surprising given the extent of arrhythmicity observed in locomotor rhythms. Although light does not cause behavioural masking of locomotor rhythms in these mutants, it could be providing a masking effect on metabolic circadian activity – particularly as retinal input to areas other than the SCN are intact in *Zfhx3*$^{Flox/Flox}$; *Six3*-Cre^{+} mice. Therefore, to confirm whether metabolic activity is still truly circadian in these mutants, metabolic phenotyping should be conducted in DD conditions to add to the data already presented under standard LD cycles. Much work has been conducted on the effects on glucose homeostasis and obesity in disrupted circadian systems (Kalsbeek et al., 2014), again *Zfhx3*$^{Flox/Flox}$; *Six3*-Cre^{+} mice form a suitable model to study hormonal outputs of the SCN – given they will no longer be under SCN control and to see whether mice lacking this pathway are resistant to adverse metabolic affects observed in animals kept on high fat diet challenges or under shifted circadian

paradigms (Plano et al., 2017). Previous work in this field has suggested that the SCN is necessary for maintenance of feeding rhythms in mice (Malloy et al., 2012) as well as locomotor rhythms. Data on feeding times when maintained on an *ad libitum* diet in *Zfhx3*$^{Flox/Flox}$; *Six3*-Cre^{+} mutants would further complement the metabolic circadian data generated thus far.

Current work is already ongoing to further characterise the *Zfhx3*$^{Flox/Flox}$; *Six3*-Cre^{+} mutant line that could not be included in this thesis, but will go on to further strengthen data already collected for publication. To confirm the loss of rhythmicity in the 'SCN-less' region of the brain, animals from this line have been crossed to the *Per2::Luc* reporter mouse line (Yoo et al., 2004). This will allow real-time imaging of core clock rhythms in explants from the 'SCN' region *ex vivo*, as well as other oscillatory tissues from the whole organism. In addition to this, EEG recording is currently being undertaken on more animals to strengthen the initial sleep data presented in Results III. It has been shown that aged mice display an increase in NREM sleep and a corresponding increase in sleep pressure when compared to young mice (Panagiotou et al., 2017). In the future, it would be also be fascinating to age *Zfhx3*$^{Flox/Flox}$; *Six3*-Cre^{+} mice to study how sleep architecture evolves, considering the fact that they already display a huge increase in NREM sleep at a relatively young age and also seem to display no increase in sleep pressure following sleep deprivation.

One of the major findings of this work on *Zfhx3* is that of the dual roles for the transcription factor in development of the circadian system and also maintenance of circadian rhythms in the adult mouse. This is not unique in chronobiology, with studies on the transcription factor *Lhx1* also highlighting differential roles of a transcription factor in developmental versus adult function (Bedont et al., 2014;

Hatori et al., 2014). It is likely that there are other neuronally expressed genes with undiscovered secondary functions such as those exemplified here. Many circadian related genes have been studied only using developmental knock-out or mutant models, this does not confirm that gene is needed to maintain stable circadian physiology throughout the lifespan of an animal. *Bmal1* conditional mouse mutants are a pertinent example of this, recapitulating only some of the phenotypes ascribed to constitutive nulls of the gene (Yang et al., 2016). The major conclusion of this paper was that many of the phenotypes observed in classic *Bmal1*$^{-/-}$ mice are in fact not a result of the circadian functions of the gene and have been wrongly ascribed as such. Over 10 years ago, Takashi and colleagues first generated a conditional mouse mutant in which the *Clock* gene could be switched on and off in various parts of the brain – giving both spatial and temporal mutational resolution (Hong et al., 2007). More recently, targeted deletion in NMS positive cells in the SCN has been shown to affect periodicity of mice and thus established this subset of neurons as important pacemakers of the central circadian system (Lee et al., 2015). Despite this, the uptake in conditional mutagenesis in the circadian field has been slow. Given advances in molecular biology and mutational targeting techniques since 2007, this is surprising. It is evident that there is still much to learn about the genetic control of circadian rhythms and the temporal study of currently known 'clock-related' genes seems an achievable yet fruitful endeavour.

Traditionally, the circadian system has been viewed as a hierarchical system with the SCN residing at the top of this oscillatory tree. The data presented here challenges that notion, providing evidence that other oscillators – such as the FEO, are capable of becoming the 'master oscillator' of the circadian system given the right

conditions. Moreover, these 'SCN-less' mice display no severe metabolic abnormalities, growth defects, anxiety related issues or health concerns in general – despite growing literature lauding the necessity of a functional clock in the SCN with regard to normal health and behaviour in both animal models and humans (Coomans et al., 2013; Landgraf et al., 2016; Savvidis and Koutsilieris, 2012; Truong et al., 2016; Wu et al., 2017). In the majority of this previous literature, SCN disruption has been created in animals that previously had intact circadian function. It could well be that, in animals with previous experience of being entrained to their day-night cycle, having a dysfunctional master clock is more damaging than not having one at all: a theory that was also concluded in ground breaking research conducted on Siberian hamsters (*Phodopus sungorus*) a few years ago (Fernandez et al., 2014). Of course, we do not know for sure that *Zfhx3*$^{Flox/Flox}$; *Six3*-Cre^{+} mice display a complete lack of SCN throughout early development (future studies will be undertaken to confirm this). However, these mice do show an absence of SCN throughout the entirety of their lifetime studied thus far, therefore data presented here would agree with this notion of 'no clock is better than a broken clock'.

References

Abrahamson, E.E., and Moore, R.Y. (2001). Suprachiasmatic nucleus in the mouse: retinal innervation, intrinsic organization and efferent projections. Brain Res *916*, 172-191.

Acevedo-Arozena, A., Wells, S., Potter, P., Kelly, M., Cox, R.D., and Brown, S.D. (2008). ENU mutagenesis, a way forward to understand gene function. Annu Rev Genomics Hum Genet *9*, 49-69.

Akhtar, R.A., Reddy, A.B., Maywood, E.S., Clayton, J.D., King, V.M., Smith, A.G., Gant, T.W., Hastings, M.H., and Kyriacou, C.P. (2002). Circadian cycling of the mouse liver transcriptome, as revealed by cDNA microarray, is driven by the suprachiasmatic nucleus. Curr Biol *12*, 540-550.

Albers, H.E., Walton, J.C., Gamble, K.L., McNeill, J.K.t., and Hummer, D.L. (2017). The dynamics of GABA signaling: Revelations from the circadian pacemaker in the suprachiasmatic nucleus. Front Neuroendocrinol *44*, 35-82.

Albrecht, U. (2012). Timing to perfection: the biology of central and peripheral circadian clocks. Neuron *74*, 246-260.

An, S., Tsai, C., Ronecker, J., Bayly, A., and Herzog, E.D. (2012). Spatiotemporal distribution of vasoactive intestinal polypeptide receptor 2 in mouse suprachiasmatic nucleus. J Comp Neurol *520*, 2730-2741.

Ananthasubramaniam, B., Herzog, E.D., and Herzel, H. (2014). Timing of neuropeptide coupling determines synchrony and entrainment in the mammalian circadian clock. PLoS Comput Biol *10*, e1003565.

Ansari, N., Agathagelidis, M., Lee, C., Korf, H.W., and von Gall, C. (2009). Differential maturation of circadian rhythms in clock gene proteins in the suprachiasmatic nucleus and the pars tuberalis during mouse ontogeny. Eur J Neurosci *29*, 477-489.

Antle, M.C., LeSauter, J., and Silver, R. (2005). Neurogenesis and ontogeny of specific cell phenotypes within the hamster suprachiasmatic nucleus. Brain Res Dev Brain Res *157*, 8-18.

Aschoff, J. (1999). Masking and parametric effects of high-frequency light-dark cycles. Jpn J Physiol *49*, 11-18.

Aton, S.J., Colwell, C.S., Harmar, A.J., Waschek, J., and Herzog, E.D. (2005a). Vasoactive intestinal polypeptide mediates circadian rhythmicity and synchrony in mammalian clock neurons. Nat Neurosci *8*, 476-483.

Aton, S.J., Colwell, C.S., Harmar, A.J., Waschek, J., and Herzog, E.D. (2005b). Vasoactive intestinal polypeptide mediates circadian rhythmicity and synchrony in mammalian clock neurons. Nat Neurosci *8*, 476-483.

Azzi, A., Evans, J.A., Leise, T., Myung, J., Takumi, T., Davidson, A.J., and Brown, S.A. (2017). Network Dynamics Mediate Circadian Clock Plasticity. Neuron.

Bacon, Y., Ooi, A., Kerr, S., Shaw-Andrews, L., Winchester, L., Breeds, S., Tymoska-Lalanne, Z., Clay, J., Greenfield, A.G., and Nolan, P.M. (2004). Screening for novel ENU-induced rhythm, entrainment and activity mutants. Genes Brain Behav *3*, 196-205.

Baggs, J.E., Price, T.S., DiTacchio, L., Panda, S., Fitzgerald, G.A., and Hogenesch, J.B. (2009a). Network features of the mammalian circadian clock. PLoS Biol *7*, e52.

Baggs, J.E., Price, T.S., DiTacchio, L., Panda, S., FitzGerald, G.A., and Hogenesch, J.B. (2009b). Network Features of the Mammalian Circadian Clock. Plos Biology *7*, 563-575.

Bains, R.S., Cater, H.L., Sillito, R.R., Chartsias, A., Sneddon, D., Concas, D., Keskivali-Bond, P., Lukins, T.C., Wells, S., Acevedo Arozena, A., et al. (2016). Analysis of Individual Mouse Activity in Group Housed Animals of Different Inbred Strains using a Novel Automated Home Cage Analysis System. Front Behav Neurosci *10*, 106.

Bains, R.S., Wells, S., Sillito, R.R., Armstrong, J.D., Cater, H.L., Banks, G., and Nolan, P.M. (2018). Assessing mouse behaviour throughout the light/dark cycle using automated in-cage analysis tools. J Neurosci Methods *300*, 37-47.

Balsalobre, A., Brown, S.A., Marcacci, L., Tronche, F., Kellendonk, C., Reichardt, H.M., Schutz, G., and Schibler, U. (2000). Resetting of circadian time in peripheral tissues by glucocorticoid signaling. Science *289*, 2344-2347.

Balzani, E., Lassi, G., Maggi, S., Sethi, S., Parsons, M.J., Simon, M., Nolan, P.M., and Tucci, V. (2016). The Zfhx3-Mediated Axis Regulates Sleep and Interval Timing in Mice. Cell Rep *16*, 615-621.

Bamberg, E., Palme, R., and Meingassner, J.G. (2001). Excretion of corticosteroid metabolites in urine and faeces of rats. Lab Anim *35*, 307-314.

Banks, F.D., Lobban, F., Fanshawe, T.R., and Jones, S.H. (2016). Associations between circadian rhythm instability, appraisal style and mood in bipolar disorder. J Affect Disorders *203*, 166-175.

Banks, G.T., and Nolan, P.M. (2011). Assessment of Circadian and Light-Entrainable Parameters in Mice Using Wheel-Running Activity. Current protocols in mouse biology, 369-381.

Bechtold, D.A., Brown, T.M., Luckman, S.M., and Piggins, H.D. (2008). Metabolic rhythm abnormalities in mice lacking VIP-VPAC2 signaling. Am J Physiol Regul Integr Comp Physiol *294*, R344-351.

Bedont, J.L., and Blackshaw, S. (2015). Constructing the suprachiasmatic nucleus: a watchmaker's perspective on the central clockworks. Front Syst Neurosci *9*, 74.

Bedont, J.L., LeGates, T.A., Slat, E.A., Byerly, M.S., Wang, H., Hu, J., Rupp, A.C., Qian, J., Wong, G.W., and Herzog, E.D. (2014). Lhx1 controls terminal differentiation and circadian function of the suprachiasmatic nucleus. Cell reports *7*, 609-622.

Ben-Hamo, M., Larson, T.A., Duge, L.S., Sikkema, C., Wilkinson, C.W., de la Iglesia, H.O., and Gonzalez, M.M. (2016). Circadian Forced Desynchrony of the Master Clock Leads to Phenotypic Manifestation of Depression in Rats. eNeuro *3*.

Benjamin, E.J., Rice, K.M., Arking, D.E., Pfeufer, A., van Noord, C., Smith, A.V., Schnabel, R.B., Bis, J.C., Boerwinkle, E., Sinner, M.F., et al. (2009). Variants in ZFHX3 are associated with atrial fibrillation in individuals of European ancestry. Nat Genet *41*, 879-881.

Berria, M., DeSantis, M., and Mead, R.A. (1988). Effects of suprachiasmatic nuclear ablation and melatonin on delayed implantation in the spotted skunk. Neuroendocrinology *48*, 371-375.

Bessa, Z.C.M., Melo, P.R., Goncalves, B.S.B., and Azevedo, C.V.M. (2018). Mechanisms of social synchrony between circadian activity rhythms in cohabiting marmosets. Chronobiol Int *35*, 658-672.

Bogdanova, O.V., Kanekar, S., D'Anci, K.E., and Renshaw, P.F. (2013). Factors influencing behavior in the forced swim test. Physiol Behav *118*, 227-239.

Bonmati-Carrion, M.A., Hild, K., Isherwood, C., Sweeney, S.J., Revell, V.L., Skene, D.J., Rol, M.A., and Madrid, J.A. (2016). Relationship between Human Pupillary Light Reflex and Circadian System Status. Plos One *11*, e0162476.

Brown, L.A., Hasan, S., Foster, R.G., and Peirson, S.N. (2016). COMPASS: Continuous Open Mouse Phenotyping of Activity and Sleep Status. Wellcome Open Res *1*, 2.

Brown, S.A., and Azzi, A. (2013). Peripheral circadian oscillators in mammals. Handb Exp Pharmacol, 45-66.

Brown, T.M., Hughes, A.T., and Piggins, H.D. (2005). Gastrin-releasing peptide promotes suprachiasmatic nuclei cellular rhythmicity in the absence of vasoactive intestinal polypeptide-VPAC2 receptor signaling. J Neurosci *25*, 11155-11164.

Buijs, R.M., Escobar, C., and Swaab, D.F. (2013). The circadian system and the balance of the autonomic nervous system. Handb Clin Neurol *117*, 173-191.

Bunger, M.K., Wilsbacher, L.D., Moran, S.M., Clendenin, C., Radcliffe, L.A., Hogenesch, J.B., Simon, M.C., Takahashi, J.S., and Bradfield, C.A. (2000). Mop3 is an essential component of the master circadian pacemaker in mammals. Cell *103*, 1009-1017.

Caba, M., Pabello, M., Moreno, M.L., and Meza, E. (2014). Main and accessory olfactory bulbs and their projections in the brain anticipate feeding in food-entrained rats. Chronobiol Int *31*, 869-877.

Carmona-Alcocer, V., Abel, J.H., Sun, T.C., Petzold, L.R., Doyle, F.J., 3rd, Simms, C.L., and Herzog, E.D. (2018). Ontogeny of Circadian Rhythms and Synchrony in the Suprachiasmatic Nucleus. J Neurosci *38*, 1326-1334.

Carneiro, B.T., and Araujo, J.F. (2012). Food entrainment: major and recent findings. Front Behav Neurosci *6*, 83.

Carreres, M.I., Escalante, A., Murillo, B., Chauvin, G., Gaspar, P., Vegar, C., and Herrera, E. (2011). Transcription Factor Foxd1 Is Required for the Specification of the Temporal Retina in Mammals. Journal of Neuroscience *31*, 5673-5681.

Castillo-Ruiz, A., Indic, P., and Schwartz, W.J. (2018). Time management in a co-housed social rodent species (Arvicanthis niloticus). Sci Rep *8*, 1202.

Chang, B., Hawes, N.L., Hurd, R.E., Davisson, M.T., Nusinowitz, S., and Heckenlively, J.R. (2002). Retinal degeneration mutants in the mouse. Vision Res *42*, 517-525.

Chaudhury, D., and Colwell, C.S. (2002). Circadian modulation of learning and memory in fear-conditioned mice. Behav Brain Res *133*, 95-108.

Cho, Y.G., Song, J.H., Kim, C.J., Lee, Y.S., Kim, S.Y., Nam, S.W., Lee, J.Y., and Park, W.S. (2007). Genetic alterations of the ATBF1 gene in gastric cancer. Clin Cancer Res *13*, 4355-4359.

Clark, D.D., Gorman, M.R., Hatori, M., Meadows, J.D., Panda, S., and Mellon, P.L. (2013). Aberrant development of the suprachiasmatic nucleus and circadian rhythms in mice lacking the homeodomain protein Six6. J Biol Rhythms *28*, 15-25.

Colwell, C.S., Michel, S., Itri, J., Rodriguez, W., Tam, J., Lelievre, V., Hu, Z., Liu, X., and Waschek, J.A. (2003). Disrupted circadian rhythms in VIP- and PHI-deficient mice. Am J Physiol-Reg I *285*, R939-R949.

Coogan, A.N., and Piggins, H.D. (2004). MAP kinases in the mammalian circadian system--key regulators of clock function. J Neurochem *90*, 769-775.

Coomans, C.P., van den Berg, S.A.A., Lucassen, E.A., Houben, T., Pronk, A.C.M., van der Spek, R.D., Kalsbeek, A., Biermasz, N.R., van Dijk, K.W., Romijn, J.A., et al. (2013). The Suprachiasmatic Nucleus Controls Circadian Energy Metabolism and Hepatic Insulin Sensitivity. Diabetes *62*, 1102-1108.

Damiola, F., Le Minh, N., Preitner, N., Kornmann, B., Fleury-Olela, F., and Schibler, U. (2000). Restricted feeding uncouples circadian oscillators in peripheral tissues from the central pacemaker in the suprachiasmatic nucleus. Genes Dev *14*, 2950-2961.

Davidson, A.J. (2009). Lesion studies targeting food-anticipatory activity. Eur J Neurosci *30*, 1658-1664.

Dibner, C., Schibler, U., and Albrecht, U. (2010). The mammalian circadian timing system: organization and coordination of central and peripheral clocks. Annu Rev Physiol *72*, 517-549.

Dunlap, J.C. (1999). Molecular bases for circadian clocks. Cell *96*, 271-290.

Dunn, J.D., Castro, A.J., and McNulty, J.A. (1977). Effect of suprachiasmatic ablation on the daily temperature rhythm. Neurosci Lett *6*, 345-348.

Eastman, C.I., Mistlberger, R.E., and Rechtschaffen, A. (1984). Suprachiasmatic nuclei lesions eliminate circadian temperature and sleep rhythms in the rat. Physiol Behav *32*, 357-368.

Easton, A., Meerlo, P., Bergmann, B., and Turek, F.W. (2004). The suprachiasmatic nucleus regulates sleep timing and amount in mice. Sleep *27*, 1307-1318.

El-Hennamy, R., Mateju, K., Bendova, Z., Sosniyenko, S., and Sumova, A. (2008). Maternal control of the fetal and neonatal rat suprachiasmatic nucleus. J Biol Rhythms *23*, 435-444.

Evans, J.A. (2016). Collective timekeeping among cells of the master circadian clock. J Endocrinol *230*, R27-49.

Fernandez, D.C., Chang, Y.T., Hattar, S., and Chen, S.K. (2016). Architecture of retinal projections to the central circadian pacemaker. Proc Natl Acad Sci U S A *113*, 6047-6052.

Fernandez, F., Lu, D., Ha, P., Costacurta, P., Chavez, R., Heller, H.C., and Ruby, N.F. (2014). Dysrhythmia in the suprachiasmatic nucleus inhibits memory processing. Science *346*, 854-857.

Fisher, S.P., Godinho, S.I., Pothecary, C.A., Hankins, M.W., Foster, R.G., and Peirson, S.N. (2012). Rapid assessment of sleep-wake behavior in mice. J Biol Rhythms *27*, 48-58.

Fisk, A.S., Tam, S.K.E., Brown, L.A., Vyazovskiy, V.V., Bannerman, D.M., and Peirson, S.N. (2018). Light and Cognition: Roles for Circadian Rhythms, Sleep, and Arousal. Front Neurol *9*, 56.

Fuchikawa, T., Eban-Rothschild, A., Nagari, M., Shemesh, Y., and Bloch, G. (2016). Potent social synchronization can override photic entrainment of circadian rhythms. Nat Commun *7*, 11662.

Furuta, Y., Lagutin, O., Hogan, B.L., and Oliver, G.C. (2000a). Retina- and ventral forebrain-specific Cre recombinase activity in transgenic mice. Genesis *26*, 130-132.

Furuta, Y., Lagutin, O., Hogan, B.L., and Oliver, G.C. (2000b). Retina-and ventral forebrain-specific Cre recombinase activity in transgenic mice. Genesis *26*, 130-132.

Gall, A.J., Shuboni, D.D., Yan, L., Nunez, A.A., and Smale, L. (2016). Suprachiasmatic Nucleus and Subparaventricular Zone Lesions Disrupt Circadian Rhythmicity but Not Light-Induced Masking Behavior in Nile Grass Rats. J Biol Rhythms *31*, 170-181.

Gallardo, C.M., Darvas, M., Oviatt, M., Chang, C.H., Michalik, M., Huddy, T.F., Meyer, E., Shuster, S.A., Aguayo, A., Hill, E.M., et al. (2014). Dopamine receptor 1 neurons in the dorsal striatum regulate food anticipatory circadian activity rhythms in mice. Elife *3*.

Gerkema, M.P., Van der Zee, E.A., and Feitsma, L.E. (1994). Expression of circadian rhythmicity correlates with the number of arginine-vasopressin-immunoreactive cells in the suprachiasmatic nucleus of common voles, Microtus arvalis. Brain Res *639*, 93-101.

Godinho, S.I., Maywood, E.S., Shaw, L., Tucci, V., Barnard, A.R., Busino, L., Pagano, M., Kendall, R., Quwailid, M.M., Romero, M.R., et al. (2007). The after-hours mutant reveals a role for Fbxl3 in determining mammalian circadian period. Science *316*, 897-900.

Gritton, H.J., Kantorowski, A., Sarter, M., and Lee, T.M. (2012). Bidirectional interactions between circadian entrainment and cognitive performance. Learn Memory *19*, 126-141.

Gudbjartsson, D.F., Holm, H., Gretarsdottir, S., Thorleifsson, G., Walters, G.B., Thorgeirsson, G., Gulcher, J., Mathiesen, E.B., Njolstad, I., Nyrnes, A., et al. (2009). A sequence variant in ZFHX3 on 16q22 associates with atrial fibrillation and ischemic stroke. Nat Genet *41*, 876-878.

Hall, J.C. (1990). Genetics of circadian rhythms. Annu Rev Genet *24*, 659-697.

Hardin, P.E., Hall, J.C., and Rosbash, M. (1990). Feedback of the Drosophila period gene product on circadian cycling of its messenger RNA levels. Nature *343*, 536-540.

Harmar, A.J., Marston, H.M., Shen, S., Spratt, C., West, K.M., Sheward, W.J., Morrison, C.F., Dorin, J.R., Piggins, H.D., Reubi, J.C., et al. (2002). The VPAC(2)

receptor is essential for circadian function in the mouse suprachiasmatic nuclei. Cell *109*, 497-508.

Hastings, M.H., Reddy, A.B., and Maywood, E.S. (2003). A clockwork web: circadian timing in brain and periphery, in health and disease. Nat Rev Neurosci *4*, 649-661.

Hatori, M., Gill, S., Mure, L.S., Goulding, M., O'Leary, D.D., and Panda, S. (2014). Lhx1 maintains synchrony among circadian oscillator neurons of the SCN. Elife *3*, e03357.

Hattar, S., Lucas, R.J., Mrosovsky, N., Thompson, S., Douglas, R.H., Hankins, M.W., Lem, J., Biel, M., Hofmann, F., Foster, R.G., et al. (2003). Melanopsin and rod-cone photoreceptive systems account for all major accessory visual functions in mice. Nature *424*, 76-81.

Hayter, E.A., and Brown, T.M. (2018). Additive contributions of melanopsin and both cone types provide broadband sensitivity to mouse pupil control. BMC Biol *16*, 83.

Herrera, E., Marcus, R., Li, S., Williams, S.E., Erskine, L., Lai, E., and Mason, C. (2004). Foxd1 is required for proper formation of the optic chiasm. Development *131*, 5727-5739.

Herzog, E.D., Geusz, M.E., Khalsa, S.B., Straume, M., and Block, G.D. (1997). Circadian rhythms in mouse suprachiasmatic nucleus explants on multimicroelectrode plates. Brain Res *757*, 285-290.

Hong, H.K., Chong, J.L., Song, W.M., Song, E.J., Jyawook, A.A., Schook, A.C., Ko, C.H., and Takahashi, J.S. (2007). Inducible and reversible Clock gene expression in brain using the tTA system for the study of circadian behavior. Plos Genetics *3*, 324-338.

Honma, S. (2018). The mammalian circadian system: a hierarchical multi-oscillator structure for generating circadian rhythm. J Physiol Sci *68*, 207-219.

Honma, S., Kawamoto, T., Takagi, Y., Fujimoto, K., Sato, F., Noshiro, M., Kato, Y., and Honma, K. (2002). Dec1 and Dec2 are regulators of the mammalian molecular clock. Nature *419*, 841-844.

Houdek, P., and Sumova, A. (2014). In vivo initiation of clock gene expression rhythmicity in fetal rat suprachiasmatic nuclei. Plos One *9*, e107360.

Hughes, A.T., Guilding, C., Lennox, L., Samuels, R.E., McMahon, D.G., and Piggins, H.D. (2008). Live imaging of altered period1 expression in the suprachiasmatic nuclei of Vipr2-/- mice. J Neurochem *106*, 1646-1657.

Hughes, S., Rodgers, J., Hickey, D., Foster, R.G., Peirson, S.N., and Hankins, M.W. (2016). Characterisation of light responses in the retina of mice lacking principle components of rod, cone and melanopsin phototransduction signalling pathways. Sci Rep *6*, 28086.

Humphreys, B.D., Lin, S.L., Kobayashi, A., Hudson, T.E., Nowlin, B.T., Bonventre, J.V., Valerius, M.T., McMahon, A.P., and Duffield, J.S. (2010). Fate tracing reveals the pericyte and not epithelial origin of myofibroblasts in kidney fibrosis. Am J Pathol *176*, 85-97.

Humphreys, B.D., Valerius, M.T., Kobayashi, A., Mugford, J.W., Soeung, S., Duffield, J.S., McMahon, A.P., and Bonventre, J.V. (2008). Intrinsic epithelial cells repair the kidney after injury. Cell Stem Cell *2*, 284-291.

Hunt, C., and Hambly, C. (2006). Faecal corticosterone concentrations indicate that separately housed male mice are not more stressed than group housed males. Physiol Behav *87*, 519-526.

Husse, J., Leliavski, A., Tsang, A.H., Oster, H., and Eichele, G. (2014). The light-dark cycle controls peripheral rhythmicity in mice with a genetically ablated suprachiasmatic nucleus clock. Faseb J *28*, 4950-4960.

Hvoslef-Eide, M., Nilsson, S.R., Saksida, L.M., and Bussey, T.J. (2016). Cognitive Translation Using the Rodent Touchscreen Testing Approach. Curr Top Behav Neurosci *28*, 423-447.

Ishii, Y., Kawaguchi, M., Takagawa, K., Oya, T., Nogami, S., Tamura, A., Miura, Y., Ido, A., Sakata, N., and Hashimoto-Tamaoki, T. (2003). ATBF1-A protein, but not ATBF1-B, is preferentially expressed in developing rat brain. Journal of Comparative Neurology *465*, 57-71.

Jagannath, A., Taylor, L., Wakaf, Z., Vasudevan, S.R., and Foster, R.G. (2017). The genetics of circadian rhythms, sleep and health. Hum Mol Genet *26*, R128-R138.

Jaisser, F. (2000). Inducible gene expression and gene modification in transgenic mice. J Am Soc Nephrol *11 Suppl 16*, S95-S100.

Jones, J.R., Simon, T., Lones, L., and Herzog, E.D. (2018). SCN VIP Neurons Are Essential for Normal Light-Mediated Resetting of the Circadian System. J Neurosci *38*, 7986-7995.

Jung, C.-G., Kim, H.-J., Kawaguchi, M., Khanna, K.K., Hida, H., Asai, K., Nishino, H., and Miura, Y. (2005a). Homeotic factor ATBF1 induces the cell cycle arrest associated with neuronal differentiation. Development *132*, 5137-5145.

Jung, C.G., Kim, H.J., Kawaguchi, M., Khanna, K.K., Hida, H., Asai, K., Nishino, H., and Miura, Y. (2005b). Homeotic factor ATBF1 induces the cell cycle arrest associated with neuronal differentiation. Development *132*, 5137-5145.

Kabrita, C.S., and Davis, F.C. (2008). Development of the mouse suprachiasmatic nucleus: determination of time of cell origin and spatial arrangements within the nucleus. Brain Res *1195*, 20-27.

Kafka, M.S., Marangos, P.J., and Moore, R.Y. (1985). Suprachiasmatic nucleus ablation abolishes circadian rhythms in rat brain neurotransmitter receptors. Brain Res *327*, 344-347.

Kalsbeek, A., la Fleur, S., and Fliers, E. (2014). Circadian control of glucose metabolism. Mol Metab *3*, 372-383.

Kalsbeek, A., van der Spek, R., Lei, J., Endert, E., Buijs, R.M., and Fliers, E. (2012). Circadian rhythms in the hypothalamo-pituitary-adrenal (HPA) axis. Mol Cell Endocrinol *349*, 20-29.

Kamakura, R., Kovalainen, M., Leppaluoto, J., Herzig, K.H., and Makela, K.A. (2016). The effects of group and single housing and automated animal monitoring on urinary corticosterone levels in male C57BL/6 mice. Physiol Rep *4*.

Karten, Y.J., Nair, S.M., van Essen, L., Sibug, R., and Joels, M. (1999). Long-term exposure to high corticosterone levels attenuates serotonin responses in rat hippocampal CA1 neurons. Proc Natl Acad Sci U S A *96*, 13456-13461.

Kim, C.J., Song, J.H., Cho, Y.G., Cao, Z., Lee, Y.S., Nam, S.W., Lee, J.Y., and Park, W.S. (2008). Down-regulation of ATBF1 is a major inactivating mechanism in hepatocellular carcinoma. Histopathology *52*, 552-559.

Kim, S., Foong, D., Cooper, M.S., Seibel, M.J., and Zhou, H. (2018). Comparison of blood sampling methods for plasma corticosterone measurements in mice associated with minimal stress-related artefacts. Steroids *135*, 69-72.

King, D.P., Vitaterna, M.H., Chang, A.M., Dove, W.F., Pinto, L.H., Turek, F.W., and Takahashi, J.S. (1997). The mouse Clock mutation behaves as an antimorph and maps within the W19H deletion, distal of Kit. Genetics *146*, 1049-1060.

Konopka, R.J., and Benzer, S. (1971). Clock mutants of Drosophila melanogaster. Proc Natl Acad Sci U S A *68*, 2112-2116.

Landgraf, D., Long, J.E., Proulx, C.D., Barandas, R., Malinow, R., and Welsh, D.K. (2016). Genetic Disruption of Circadian Rhythms in the Suprachiasmatic Nucleus Causes Helplessness, Behavioral Despair, and Anxiety-like Behavior in Mice. Biol Psychiat *80*, 827-835.

Lee, I.T., Chang, A.S., Manandhar, M., Shan, Y., Fan, J., Izumo, M., Ikeda, Y., Motoike, T., Dixon, S., Seinfeld, J.E., et al. (2015). Neuromedin s-producing neurons act as essential pacemakers in the suprachiasmatic nucleus to couple clock neurons and dictate circadian rhythms. Neuron *85*, 1086-1102.

Lein, E.S., Hawrylycz, M.J., Ao, N., Ayres, M., Bensinger, A., Bernard, A., Boe, A.F., Boguski, M.S., Brockway, K.S., Byrnes, E.J., et al. (2007a). Genome-wide atlas of gene expression in the adult mouse brain. Nature *445*, 168-176.

Lein, E.S., Hawrylycz, M.J., Ao, N., Ayres, M., Bensinger, A., Bernard, A., Boe, A.F., Boguski, M.S., Brockway, K.S., Byrnes, E.J., et al. (2007b). Genome-wide atlas of gene expression in the adult mouse brain. Nature *445*, 168-176.

LeSauter, J., and Silver, R. (1998). Output signals of the SCN. Chronobiol Int *15*, 535-550.

LeSauter, J., and Silver, R. (1999). Localization of a suprachiasmatic nucleus subregion regulating locomotor rhythmicity. J Neurosci *19*, 5574-5585.

Levinson, R.S., Batourina, E., Choi, C., Vorontchikhina, M., Kitajewski, J., and Mendelsohn, C.L. (2005). Foxd1-dependent signals control cellularity in the renal capsule, a structure required for normal renal development. Development *132*, 529-539.

Li, J.D., Burton, K.J., Zhang, C., Hu, S.B., and Zhou, Q.Y. (2009). Vasopressin receptor V1a regulates circadian rhythms of locomotor activity and expression of clock-controlled genes in the suprachiasmatic nuclei. Am J Physiol Regul Integr Comp Physiol *296*, R824-830.

Lipinski, D.M., Yusuf, M., Barnard, A.R., Damant, C., Charbel Issa, P., Singh, M.S., Lee, E., Davies, W.L., Volpi, E.V., and MacLaren, R.E. (2011). Characterization of a dominant cone degeneration in a green fluorescent protein-reporter mouse with disruption of Loci associated with human dominant retinal dystrophy. Invest Ophthalmol Vis Sci *52*, 6617-6623.

Liu, W., and Cvekl, A. (2017). Six3 in a small population of progenitors at E8.5 is required for neuroretinal specification via regulating cell signaling and survival in mice. Dev Biol *428*, 164-175.

Loh, D.H., Kudo, T., and Colwell, C.S. (2015). Short circuiting the circadian system with a new generation of precision tools. Neuron *85*, 895-898.

Loudon, A.S., Semikhodskii, A.G., and Crosthwaite, S.K. (2000). A brief history of circadian time. Trends Genet *16*, 477-481.

Lowrey, P.L., and Takahashi, J.S. (2011). Genetics of circadian rhythms in Mammalian model organisms. Adv Genet *74*, 175-230.

Lupi, D., Sekaran, S., Jones, S.L., Hankins, M.W., and Foster, R.G. (2006). Light-evoked FOS induction within the suprachiasmatic nuclei (SCN) of melanopsin knockout (Opn4-/-) mice: a developmental study. Chronobiol Int *23*, 167-179.

Lupien, S.J., McEwen, B.S., Gunnar, M.R., and Heim, C. (2009). Effects of stress throughout the lifespan on the brain, behaviour and cognition. Nat Rev Neurosci *10*, 434-445.

Malloy, J.N., Paulose, J.K., Li, Y., and Cassone, V.M. (2012). Circadian rhythms of gastrointestinal function are regulated by both central and peripheral oscillators. Am J Physiol Gastrointest Liver Physiol *303*, G461-473.

Maywood, E.S. (2018). Synchronization and maintenance of circadian timing in the mammalian clockwork. Eur J Neurosci.

Maywood, E.S., Reddy, A.B., Wong, G.K., O'Neill, J.S., O'Brien, J.A., McMahon, D.G., Harmar, A.J., Okamura, H., and Hastings, M.H. (2006). Synchronization and maintenance of timekeeping in suprachiasmatic circadian clock cells by neuropeptidergic signaling. Curr Biol *16*, 599-605.

Mazuski, C., Abel, J.H., Chen, S.P., Hermanstyne, T.O., Jones, J.R., Simon, T., Doyle, F.J., 3rd, and Herzog, E.D. (2018). Entrainment of Circadian Rhythms Depends on Firing Rates and Neuropeptide Release of VIP SCN Neurons. Neuron *99*, 555-563 e555.

Mendez, N., Abarzua-Catalan, L., Vilches, N., Galdames, H.A., Spichiger, C., Richter, H.G., Valenzuela, G.J., Seron-Ferre, M., and Torres-Farfan, C. (2012). Timed maternal melatonin treatment reverses circadian disruption of the fetal adrenal clock imposed by exposure to constant light. Plos One *7*, e42713.

Menet, J.S., Pescatore, S., and Rosbash, M. (2014). CLOCK:BMAL1 is a pioneer-like transcription factor. Genes Dev *28*, 8-13.

Mistlberger, R.E. (1994). Circadian Food-Anticipatory Activity - Formal Models and Physiological-Mechanisms. Neurosci Biobehav R *18*, 171-195.

Mistlberger, R.E. (2005). Circadian regulation of sleep in mammals: role of the suprachiasmatic nucleus. Brain Res Brain Res Rev *49*, 429-454.

Mistlberger, R.E., Bergmann, B.M., and Rechtschaffen, A. (1987). Relationships among wake episode lengths, contiguous sleep episode lengths, and electroencephalographic delta waves in rats with suprachiasmatic nuclei lesions. Sleep *10*, 12-24.

Mistlberger, R.E., Bergmann, B.M., Waldenar, W., and Rechtschaffen, A. (1983). Recovery sleep following sleep deprivation in intact and suprachiasmatic nuclei-lesioned rats. Sleep *6*, 217-233.

Mistlberger, R.E., and Skene, D.J. (2004). Social influences on mammalian circadian rhythms: animal and human studies. Biol Rev Camb Philos Soc *79*, 533-556.

Miura, Y., Tam, T., Ido, A., Morinaga, T., Miki, T., Hashimoto, T., and Tamaoki, T. (1995). Cloning and characterization of an ATBF1 isoform that expresses in a neuronal differentiation-dependent manner. Journal of Biological Chemistry *270*, 26840-26848.

Mohawk, J.A., Baer, M.L., and Menaker, M. (2009). The methamphetamine-sensitive circadian oscillator does not employ canonical clock genes. Proc Natl Acad Sci U S A *106*, 3519-3524.

Mohawk, J.A., Green, C.B., and Takahashi, J.S. (2012). Central and peripheral circadian clocks in mammals. Annu Rev Neurosci *35*, 445-462.

Mohawk, J.A., and Takahashi, J.S. (2011). Cell autonomy and synchrony of suprachiasmatic nucleus circadian oscillators. Trends Neurosci *34*, 349-358.

Moore, R.Y., Speh, J.C., and Leak, R.K. (2002). Suprachiasmatic nucleus organization. Cell Tissue Res *309*, 89-98.

Mosko, S.S., and Moore, R.Y. (1979). Neonatal ablation of the suprachiasmatic nucleus. Effects on the development of the pituitary-gonadal axis in the female rat. Neuroendocrinology *29*, 350-361.

Murray, S.A., Eppig, J.T., Smedley, D., Simpson, E.M., and Rosenthal, N. (2012). Beyond knockouts: cre resources for conditional mutagenesis. Mamm Genome *23*, 587-599.

Nakashima, A., Kawamoto, T., Honda, K.K., Ueshima, T., Noshiro, M., Iwata, T., Fujimoto, K., Kubo, H., Honma, S., Yorioka, N., et al. (2008). DEC1 modulates the circadian phase of clock gene expression. Mol Cell Biol *28*, 4080-4092.

Newmann, E.A., Kim, D.W., Wan, J., Wang, J., Qian, J., and Blackshaw, S. (2018). Foxd1 is required for terminal differentiation of anterior hypothalamic neuronal subtypes. Dev Biol *439*, 102-111.

Nolan, P.M., Kapfhamer, D., and Bucan, M. (1997). Random mutagenesis screen for dominant behavioral mutations in mice. Methods *13*, 379-395.

Oliver, P.L., and Davies, K.E. (2012). New insights into behaviour using mouse ENU mutagenesis. Hum Mol Genet *21*, R72-81.

Oliver, P.L., Sobczyk, M.V., Maywood, E.S., Edwards, B., Lee, S., Livieratos, A., Oster, H., Butler, R., Godinho, S.I., Wulff, K., et al. (2012). Disrupted circadian rhythms in a mouse model of schizophrenia. Curr Biol *22*, 314-319.

Olivo, D., Caba, M., Gonzalez-Lima, F., Rodriguez-Landa, J.F., and Corona-Morales, A.A. (2017). Metabolic activation of amygdala, lateral septum and accumbens circuits during food anticipatory behavior. Behav Brain Res *316*, 261-270.

Ono, D., Honma, S., and Honma, K. (2016). Differential roles of AVP and VIP signaling in the postnatal changes of neural networks for coherent circadian rhythms in the SCN. Sci Adv *2*, e1600960.

Panagiotou, M., Vyazovskiy, V.V., Meijer, J.H., and Deboer, T. (2017). Differences in electroencephalographic non-rapid-eye movement sleep slow-wave characteristics between young and old mice. Sci Rep-Uk *7*.

Panda, S., Antoch, M.P., Miller, B.H., Su, A.I., Schook, A.B., Straume, M., Schultz, P.G., Kay, S.A., Takahashi, J.S., and Hogenesch, J.B. (2002). Coordinated transcription of key pathways in the mouse by the circadian clock. Cell *109*, 307-320.

Panksepp, J.B., Wong, J.C., Kennedy, B.C., and Lahvis, G.P. (2008). Differential entrainment of a social rhythm in adolescent mice. Behav Brain Res *195*, 239-245.

Parsons, M.J., Brancaccio, M., Sethi, S., Maywood, E.S., Satija, R., Edwards, J.K., Jagannath, A., Couch, Y., Finelli, M.J., and Smyllie, N.J. (2015). The Regulatory Factor ZFHX3 Modifies Circadian Function in SCN via an AT Motif-Driven Axis. Cell *162*, 607-621.

Paul, M.J., Indic, P., and Schwartz, W.J. (2014). Social forces can impact the circadian clocks of cohabiting hamsters. Proc Biol Sci *281*, 20132535.

Paul, M.J., Indic, P., and Schwartz, W.J. (2015). Social synchronization of circadian rhythmicity in female mice depends on the number of cohabiting animals. Biol Lett *11*, 20150204.

Paul, M.J., and Schwartz, W.J. (2007). On the chronobiology of cohabitation. Cold Spring Harb Symp Quant Biol *72*, 615-621.

Pendergast, J.S., Wendroth, R.H., Stenner, R.C., Keil, C.D., and Yamazaki, S. (2017). mPeriod2(Brdm1) and other single Period mutant mice have normal food anticipatory `activity. Sci Rep-Uk *7*.

Pendergast, J.S., and Yamazaki, S. (2018). The Mysterious Food-Entrainable Oscillator: Insights from Mutant and Engineered Mouse Models. J Biol Rhythms *33*, 458-474.

Perlman, I. (1995). The Electroretinogram: ERG. In Webvision: The Organization of the Retina and Visual System. H. Kolb, E. Fernandez, and R. Nelson, eds. (Salt Lake City (UT)).

Pezuk, P., Mohawk, J.A., Wang, L.A., and Menaker, M. (2012). Glucocorticoids as entraining signals for peripheral circadian oscillators. Endocrinology *153*, 4775-4783.

Pezuk, P., Mohawk, J.A., Yoshikawa, T., Sellix, M.T., and Menaker, M. (2010). Circadian organization is governed by extra-SCN pacemakers. J Biol Rhythms *25*, 432-441.

Pittendrigh, C.S. (1960). Circadian rhythms and the circadian organization of living systems. Cold Spring Harb Symp Quant Biol *25*, 159-184.

Pitts, S., Perone, E., and Silver, R. (2003). Food-entrained circadian rhythms are sustained in arrhythmic Clk/Clk mutant mice. Am J Physiol Regul Integr Comp Physiol *285*, R57-67.

Plano, S.A., Casiraghi, L.P., Moro, P.G., Paladino, N., Golombek, D.A., and Chiesa, J.J. (2017). Circadian and Metabolic Effects of Light: Implications in Weight Homeostasis and Health. Frontiers in Neurology *8*.

Plautz, J.D., Kaneko, M., Hall, J.C., and Kay, S.A. (1997). Independent photoreceptive circadian clocks throughout Drosophila. Science *278*, 1632-1635.

Polidarova, L., Sladek, M., Novakova, M., Parkanova, D., and Sumova, A. (2013). Increased Sensitivity of the Circadian System to Temporal Changes in the Feeding Regime of Spontaneously Hypertensive Rats - A Potential Role for Bmal2 in the Liver. Plos One *8*.

Ralph, M.R., Foster, R.G., Davis, F.C., and Menaker, M. (1990). Transplanted suprachiasmatic nucleus determines circadian period. Science *247*, 975-978.

Redlin, U., Cooper, H.M., and Mrosovsky, N. (2003). Increased masking response to light after ablation of the visual cortex in mice. Brain Res *965*, 1-8.

Redlin, U., and Mrosovsky, N. (1999). Masking by light in hamsters with SCN lesions. J Comp Physiol A *184*, 439-448.

Refinetti, R. (2015). Comparison of light, food, and temperature as environmental synchronizers of the circadian rhythm of activity in mice. J Physiol Sci *65*, 359-366.

Reppert, S.M., and Schwartz, W.J. (1986). Maternal suprachiasmatic nuclei are necessary for maternal coordination of the developing circadian system. J Neurosci *6*, 2724-2729.

Rietveld, W.J., Minors, D.S., and Waterhouse, J.M. (1993). Circadian rhythms and masking: an overview. Chronobiol Int *10*, 306-312.

Rinchik, E.M. (1991). Chemical mutagenesis and fine-structure functional analysis of the mouse genome. Trends Genet *7*, 15-21.

Roenneberg, T., and Merrow, M. (2016). The Circadian Clock and Human Health. Curr Biol *26*, R432-443.

Rosenwasser, A.M. (1990). Circadian activity rhythms in BALB/c mice: A weakly-coupled circadian system? Biological Rhythm Research *21*, 91-96.

Ruby, N.F., Dark, J., Heller, H.C., and Zucker, I. (1996). Ablation of suprachiasmatic nucleus alters timing of hibernation in ground squirrels. Proc Natl Acad Sci U S A *93*, 9864-9868.

Ruzankina, Y., Pinzon-Guzman, C., Asare, A., Ong, T., Pontano, L., Cotsarelis, G., Zediak, V.P., Velez, M., Bhandoola, A., and Brown, E.J. (2007). Deletion of the developmentally essential gene ATR in adult mice leads to age-related phenotypes and stem cell loss. Cell Stem Cell *1*, 113-126.

Sato, T.K., Panda, S., Miraglia, L.J., Reyes, T.M., Rudic, R.D., McNamara, P., Naik, K.A., FitzGerald, G.A., Kay, S.A., and Hogenesch, J.B. (2004). A functional genomics strategy reveals Rora as a component of the mammalian circadian clock. Neuron *43*, 527-537.

Savvidis, C., and Koutsilieris, M. (2012). Circadian Rhythm Disruption in Cancer Biology. Mol Med *18*, 1249-1260.

Schibler, U., Gotic, I., Saini, C., Gos, P., Curie, T., Emmenegger, Y., Sinturel, F., Gosselin, P., Gerber, A., Fleury-Olela, F., et al. (2015). Clock-Talk: Interactions between Central and Peripheral Circadian Oscillators in Mammals. Cold Spring Harb Symp Quant Biol *80*, 223-232.

Schibler, U., Ripperger, J., and Brown, S.A. (2003). Peripheral circadian oscillators in mammals: time and food. J Biol Rhythms *18*, 250-260.

Schwartz, W.J., and Zimmerman, P. (1991). Lesions of the suprachiasmatic nucleus disrupt circadian locomotor rhythms in the mouse. Physiol Behav *49*, 1283-1287.

Shibata, S., and Moore, R.Y. (1987). Development of neuronal activity in the rat suprachiasmatic nucleus. Brain Res *431*, 311-315.

Shimomura, H., Moriya, T., Sudo, M., Wakamatsu, H., Akiyama, M., Miyake, Y., and Shibata, S. (2001). Differential daily expression of Per1 and Per2 mRNA in the suprachiasmatic nucleus of fetal and early postnatal mice. Eur J Neurosci *13*, 687-693.

Siepka, S.M., and Takahashi, J.S. (2005). Methods to record circadian rhythm wheel running activity in mice. Methods Enzymol *393*, 230-239.

Silver, R., Balsam, P.D., Butler, M.P., and LeSauter, J. (2011). Food anticipation depends on oscillators and memories in both body and brain. Physiol Behav *104*, 562-571.

Son, G.H., Chung, S., Choe, H.K., Kim, H.D., Baik, S.M., Lee, H., Lee, H.W., Choi, S., Sun, W., Kim, H., et al. (2008). Adrenal peripheral clock controls the autonomous circadian rhythm of glucocorticoid by causing rhythmic steroid production. Proc Natl Acad Sci U S A *105*, 20970-20975.

Srinivas, S., Watanabe, T., Lin, C.S., William, C.M., Tanabe, Y., Jessell, T.M., and Costantini, F. (2001). Cre reporter strains produced by targeted insertion of EYFP and ECFP into the ROSA26 locus. BMC Dev Biol *1*, 4.

Stephan, F.K., and Zucker, I. (1972). Circadian rhythms in drinking behavior and locomotor activity of rats are eliminated by hypothalamic lesions. Proc Natl Acad Sci U S A *69*, 1583-1586.

Storch, K.F., and Weitz, C.J. (2009). Daily rhythms of food-anticipatory behavioral activity do not require the known circadian clock. Proc Natl Acad Sci U S A *106*, 6808-6813.

Sumova, A., and Cecmanova, V. (2018). Mystery of rhythmic signal emergence within the suprachiasmatic nuclei. Eur J Neurosci.

Sun, X., Fu, X., Li, J., Xing, C., Martin, D.W., Zhang, H.H., Chen, Z., and Dong, J.T. (2012). Heterozygous deletion of Atbf1 by the Cre-loxP system in mice causes preweaning mortality. genesis *50*, 819-827.

Sun, X., Xing, C., Fu, X., Li, J., Zhang, B., Frierson, H.F., Jr., and Dong, J.T. (2015). Additive Effect of Zfhx3/Atbf1 and Pten Deletion on Mouse Prostatic Tumorigenesis. J Genet Genomics *42*, 373-382.

Sun, X., Zhou, Y., Otto, K.B., Wang, M., Chen, C., Zhou, W., Subramanian, K., Vertino, P.M., and Dong, J.-T. (2007). Infrequent mutation of ATBF1 in human breast cancer. Journal of cancer research and clinical oncology *133*, 103-105.

Tahara, Y., Aoyama, S., and Shibata, S. (2017). The mammalian circadian clock and its entrainment by stress and exercise. J Physiol Sci *67*, 1-10.

Takahashi, J.S. (2017). Transcriptional architecture of the mammalian circadian clock. Nat Rev Genet *18*, 164-179.

Takasu, N.N., Kurosawa, G., Tokuda, I.T., Mochizuki, A., Todo, T., and Nakamura, W. (2012). Circadian regulation of food-anticipatory activity in molecular clock-deficient mice. Plos One *7*, e48892.

Tataroglu, O., Davidson, A.J., Benvenuto, L.J., and Menaker, M. (2006). The methamphetamine-sensitive circadian oscillator (MASCO) in mice. J Biol Rhythms *21*, 185-194.

Thaung, C., West, K., Clark, B.J., McKie, L., Morgan, J.E., Arnold, K., Nolan, P.M., Peters, J., Hunter, A.J., Brown, S.D., et al. (2002). Novel ENU-induced eye mutations in the mouse: models for human eye disease. Hum Mol Genet *11*, 755-767.

Tokuda, I.T., Ono, D., Honma, S., Honma, K.I., and Herzel, H. (2018). Coherency of circadian rhythms in the SCN is governed by the interplay of two coupling factors. PLoS Comput Biol *14*, e1006607.

Touma, C., Sachser, N., Mostl, E., and Palme, R. (2003). Effects of sex and time of day on metabolism and excretion of corticosterone in urine and feces of mice. Gen Comp Endocrinol *130*, 267-278.

Truong, K.K., Lam, M.T., Grandner, M.A., Sassoon, C.S., and Malhotra, A. (2016). Timing Matters: Circadian Rhythm in Sepsis, Obstructive Lung Disease, Obstructive Sleep Apnea, and Cancer. Ann Am Thorac Soc *13*, 1144-1154.

Tsuji, T., Allchorne, A.J., Zhang, M., Tsuji, C., Tobin, V.A., Pineda, R., Raftogianni, A., Stern, J.E., Grinevich, V., Leng, G., et al. (2017). Vasopressin casts light on the suprachiasmatic nucleus. J Physiol *595*, 3497-3514.

Turcot, V., Lu, Y., Highland, H.M., Schurmann, C., Justice, A.E., Fine, R.S., Bradfield, J.P., Esko, T., Giri, A., Graff, M., et al. (2018). Protein-altering variants associated with body mass index implicate pathways that control energy intake and expenditure in obesity. Nat Genet *50*, 26-41.

Turner, P.V., Brabb, T., Pekow, C., and Vasbinder, M.A. (2011). Administration of substances to laboratory animals: routes of administration and factors to consider. J Am Assoc Lab Anim Sci *50*, 600-613.

Valentinuzzi, V.S., Menna-Barreto, L., and Xavier, G.F. (2004). Effect of circadian phase on performance of rats in the Morris water maze task. J Biol Rhythms *19*, 312-324.

Valentinuzzi, V.S., Scarbrough, K., Takahashi, J.S., and Turek, F.W. (1997). Effects of aging on the circadian rhythm of wheel-running activity in C57BL/6 mice. Am J Physiol *273*, R1957-1964.

Van der Zee, E.A., Jansen, K., and Gerkema, M.P. (1999). Severe loss of vasopressin-immunoreactive cells in the suprachiasmatic nucleus of aging voles coincides with reduced circadian organization of running wheel activity. Brain Res *816*, 572-579.

VanDunk, C., Hunter, L.A., and Gray, P.A. (2011). Development, maturation, and necessity of transcription factors in the mouse suprachiasmatic nucleus. J Neurosci *31*, 6457-6467.

Verwey, M., and Amir, S. (2009). Food-entrainable circadian oscillators in the brain. Eur J Neurosci *30*, 1650-1657.

Vitaterna, M.H., King, D.P., Chang, A.M., Kornhauser, J.M., Lowrey, P.L., McDonald, J.D., Dove, W.F., Pinto, L.H., Turek, F.W., and Takahashi, J.S. (1994). Mutagenesis and mapping of a mouse gene, Clock, essential for circadian behavior. Science *264*, 719-725.

Vitaterna, M.H., Ko, C.H., Chang, A.M., Buhr, E.D., Fruechte, E.M., Schook, A., Antoch, M.P., Turek, F.W., and Takahashi, J.S. (2006). The mouse Clock mutation reduces circadian pacemaker amplitude and enhances efficacy of resetting stimuli and phase-response curve amplitude. Proc Natl Acad Sci U S A *103*, 9327-9332.

Vosko, A., van Diepen, H.C., Kuljis, D., Chiu, A.M., Heyer, D., Terra, H., Carpenter, E., Michel, S., Meijer, J.H., and Colwell, C.S. (2015). Role of vasoactive intestinal peptide in the light input to the circadian system. Eur J Neurosci *42*, 1839-1848.

Vosko, A.M., Schroeder, A., Loh, D.H., and Colwell, C.S. (2007). Vasoactive intestinal peptide and the mammalian circadian system. Gen Comp Endocrinol *152*, 165-175.

Wang, J., Xu, L., and Wang, E. (2008). Robustness, dissipations and coherence of the oscillation of circadian clock: potential landscape and flux perspectives. PMC Biophys *1*, 7.

Watanabe, M., Miura, Y., Ido, A., Sakai, M., Nishi, S., Inoue, Y., Hashimoto, T., and Tamaoki, T. (1996). Developmental changes in expression of the ATBF1 transcription factor gene. Molecular Brain Research *42*, 344-349.

Weaver, D.R. (1998). The suprachiasmatic nucleus: a 25-year retrospective. J Biol Rhythms *13*, 100-112.

Webb, A.B., Angelo, N., Huettner, J.E., and Herzog, E.D. (2009). Intrinsic, nondeterministic circadian rhythm generation in identified mammalian neurons. Proc Natl Acad Sci U S A *106*, 16493-16498.

Weyand, T.G. (2016). The multifunctional lateral geniculate nucleus. Rev Neurosci *27*, 135-157.

Whitmore, D., Foulkes, N.S., and Sassone-Corsi, P. (2000). Light acts directly on organs and cells in culture to set the vertebrate circadian clock. Nature *404*, 87-91.

Wilcox, A.G., Vizor, L., Parsons, M.J., Banks, G., and Nolan, P.M. (2017). Inducible Knockout of Mouse Zfhx3 Emphasizes Its Key Role in Setting the Pace and Amplitude of the Adult Circadian Clock. J Biol Rhythms *32*, 433-443.

Wilkie, A.O. (1994). The molecular basis of genetic dominance. J Med Genet *31*, 89-98.

Winocur, G., and Hasher, L. (1999). Aging and time-of-day effects on cognition in rats. Behav Neurosci *113*, 991-997.

Wreschnig, D., Dolatshad, H., and Davis, F.C. (2014). Embryonic development of circadian oscillations in the mouse hypothalamus. J Biol Rhythms *29*, 299-310.

Wu, X.Y., Balesar, R., Lu, J., Farajnia, S., Zhu, Q.B., Huang, M.L., Bao, A.M., and Swaab, D.F. (2017). Increased glutamic acid decarboxylase expression in the hypothalamic suprachiasmatic nucleus in depression. Brain Struct Funct *222*, 4079-4088.

Yamaguchi, S., Isejima, H., Matsuo, T., Okura, R., Yagita, K., Kobayashi, M., and Okamura, H. (2003). Synchronization of cellular clocks in the suprachiasmatic nucleus. Science *302*, 1408-1412.

Yamaguchi, S., Mitsui, S., Yan, L., Yagita, K., Miyake, S., and Okamura, H. (2000). Role of DBP in the circadian oscillatory mechanism. Mol Cell Biol *20*, 4773-4781.

Yamaguchi, Y., Suzuki, T., Mizoro, Y., Kori, H., Okada, K., Chen, Y., Fustin, J.M., Yamazaki, F., Mizuguchi, N., Zhang, J., et al. (2013). Mice genetically deficient in vasopressin V1a and V1b receptors are resistant to jet lag. Science *342*, 85-90.

Yan, L., Karatsoreos, I., Lesauter, J., Welsh, D.K., Kay, S., Foley, D., and Silver, R. (2007). Exploring spatiotemporal organization of SCN circuits. Cold Spring Harb Symp Quant Biol *72*, 527-541.

Yang, G.R., Chen, L.H., Grant, G.R., Paschos, G., Song, W.L., Musiek, E.S., Lee, V., McLoughlin, S.C., Grosser, T., Cotsarelis, G., et al. (2016). Timing of expression of the core clock gene Bmal1 influences its effects on aging and survival. Sci Transl Med *8*.

Yasuda, H., Mizuno, A., Tamaoki, T., and Morinaga, T. (1994a). ATBF1, a multiple-homeodomain zinc finger protein, selectively down-regulates AT-rich elements of the human alpha-fetoprotein gene. Molecular and Cellular Biology *14*, 1395-1401.

Yasuda, H., Mizuno, A., Tamaoki, T., and Morinaga, T. (1994b). ATBF1, a multiple-homeodomain zinc finger protein, selectively down-regulates AT-rich elements of the human alpha-fetoprotein gene. Mol Cell Biol *14*, 1395-1401.

Yoo, S.H., Yamazaki, S., Lowrey, P.L., Shimomura, K., Ko, C.H., Buhr, E.D., Siepka, S.M., Hong, H.K., Oh, W.J., Yoo, O.J., et al. (2004). PERIOD2 :: LUCIFERASE real-time reporting of circadian dynamics reveals persistent circadian oscillations in mouse peripheral tissues. P Natl Acad Sci USA *101*, 5339-5346.

Zaw, K.T.T., Sato, N., Ikeda, S., Thu, K.S., Mieno, M.N., Arai, T., Mori, S., Furukawa, T., Sasano, T., Sawabe, M., et al. (2017). Association of ZFHX3 gene variation with atrial fibrillation, cerebral infarction, and lung thromboembolism: An autopsy study. J Cardiol *70*, 180-184.